Biophysical Studies of SNARE Protein-Membrane Interactions

Christina Elizabeth Turner

Department of Chemistry

Imperial College London

A Thesis Submitted for a Degree of Doctor of Philosophy

20 July 2009

DECLARATION OF AUTHORSHIP

I, Christina Elizabeth Turner declare that this thesis, and the work presented in it, is my own and that it has been generated by me as the result of my own original research.

I confirm that:

1. This work was done wholly or mainly while in candidature for a research degree at this University;

2. Where any part of this thesis has previously been submitted for a degree or any other qualification at this University or any other institution, this has been clearly stated;

3. Where I have consulted the published work of others, this is always clearly attributed;

4. Where I have quoted from the work of others, the source is always given. With the exception of such quotations, this thesis is entirely my own work;

5. I have acknowledged all main sources of help;

6. Where the thesis is based on work done by myself jointly with others, I have made clear exactly what was done by others and what I have contributed myself;

7. Either none of this work has been published before submission, or parts of this work have been published as:

ABSTRACT

SNARE (Soluble NSF (N-ethylmaleimide Sensitive Fusion) Attachment Protein Receptors) proteins have been linked to the membrane fusion mechanism since 1993 as fusion proteins and have been suggested to be the minimal machinery. The complexity of the fusion process means that many questions remain unanswered as to how SNARE proteins perform their role. The most favoured model (the stalk model) does not involve proteins directly and so the influence of the SNARE proteins on lipid properties is of interest. In this thesis, work is presented which investigates how these proteins may manipulate membrane properties in order to promote fusion.

Purified proteins solutions of His_6-VAMP2 (Vesicle Associated Membrane Protein 2), His_6-SNAP-25 (Synaptosomal-associated Protein 25) and a truncated form of Syntaxin 1A (His_6-ΔN-Syx 1A, w.t aa 181-288) were obtained following bacterial over-expression. Fluorescent versions of His_6-VAMP2 and His_6-ΔN-Syx 1A were produced by the addition of cysteine residues to the C-terminus followed by labelling using Alexa Fluor® 488-C_5-maleimide and Alexa Fluor® 555-C_2-maleimide respectively. These fluorescent proteins were used to establish that the purified protein inserted into model lipid bilayers.

The effect of SNARE protein incorporation on the relaxed curvature of bilayers was explored by examining giant unilamellar vesicles grown using electroformation. Bilayers containing either 1:300 His_6-VAMP2: DOPC or 1:1:600 His_6-SNAP-25: His_6-ΔN-Syx 1A: DOPC were smaller than pure DOPC vesicles, indicating that SNARE proteins increase the relaxed curvature of the bilayer. Analysis of these vesicles by micropipette aspiration suggested that VAMP2 lowered the bending rigidity of the membrane and a reduction in the area expansion modulus relative to the pure lipid bilayer was found. The t-SNARE sample also indicated a reduction in bending rigidity but the area expansion modulus was found to increase. These latter results are thought to be due to the formation of protein aggregates.

Lipid mixing assays were conducted to investigate how changes in the properties of liposome bilayers affected fusion rates. It was found that the addition of DOPE to DOPC bilayers increased the rate of hemifusion and this was also found for cholesterol addition, suggesting both components are fusogens. The rate of hemifusion rose continually upon DOPE addition but reached a plateau in the cholesterol study shortly after 10 mol%. Despite this, the fusion rates for the cholesterol study were generally higher than the same mol% DOPE added. The changes in fusion rates observed have been explained by considering the impact of the additives on the free energy and stored curvature elastic stress of membranes as well as the change in the energy of formation of intermediate structures.

From the findings of this thesis it is proposed that the SNARE proteins are able to soften the membranes in which they reside. This allows the membrane to be deformed with less energy input. The strength of the SNARE complex and the force applied to the membranes during its formation increases membrane tension and reduces inter-membrane separation; promoting hemfusion. Following the action potential of the neuron it is proposed that a conformational change occurs in the synaptic SNARE complex, pulling on the hemifusion diaphragm and inducing the formation of a fusion pore.

ACKNOWLEDGEMENT

I have been at Imperial College since my first day as an undergraduate in Oct 2000 and I regret that I am unable, for reasons of both length and sanity, to mention everyone who has helped and influenced me during my time here. I do however wish to convey my gratitude to everyone I have been in contact with over the years; who have taught me so much and kept my interest in science alive. More specifically, I would like to thank my supervisors Richard Templer, Paul Freemont and Oscar Ces who have given me endless hours of advice. In particular, I am indebted to Richard for getting me hooked on this subject with his third year undergraduate course. Richard and Oscar have been my supervisors since my final year undergraduate project and I will be forever grateful that they have allowed me to stay in the group for so long. I also thank the EPSRC and CBC for funding.

I thank the members of the liquid crystal and membrane biophysics groups, both old and new. As well as advice, they have all been sounding boards for ideas over the years. More importantly, I thank them for the regular supply of cakes, biscuits and goodies from foreign shores which we have always been so fortunate to enjoy. Some members should be thanked more explicitly including Gemma Shearman for teaching me a huge amount about the field of liquid crystals. Thanks to Annela Seddon for doing the same for biophysics as well as working with me on the Bede. To Nick Brooks and Xavier Mulet for building the microscopes, writing software programs and teaching me techniques; without which much of this project would not have been possible. Thanks to Beatrice Gauthé for designing and building huge amounts of the lab equipment (and fixing things when they broke). To Claire Stanley, Natalia Goehring, Dora Tang, Arwen Tyler and Jessica Knott for endless hours of entertainment at 3 am at the ESRF and giving me a helping hand whenever needed. Finally to Duncan Casey, who even now sends me links to SNARE papers!

I cannot thank the members of the division of molecular biosciences enough. In particular I would like to thank Val Pye for teaching me everything I could wish to know about biochemistry. To Ciaran McKweon and Alex Patrice for running a highly efficient lab and making experiments possible despite the group size. To Kirsten Jensen for teaching me about cloning and helping me with experiments at a time when I was probably at my most stressed. Finally, thanks go to Heidi Yeung and Patrik Kloppsteck for being great bench partners.

I am also grateful to Rumiana Dimova (of the Max Plank Institute of Colloids and interfaces) with whom I spent three weeks in Golm. Many of the techniques employed in this thesis were learnt while in her research group. I also thank Peter Petrov of Exeter University for the opportunity to collaborate on aspects of this project, extending it beyond the work published here.

I would like to thank Paula Rahman, who has been my flatmate since our first day in halls (except when she ran away to Pfizer for a year). I have never met anyone I have got on with so well, even though she defected to Kings for her PhD. She has unknowingly provided me with so much support over the years just by going through the same highs and lows as I have. I can only hope that I have done the same for her.

Finally, I am of course eternally indebted to my parents and brother. They have always been there, providing support both financially and emotionally and given me nothing but encouragement for everything I do. This thesis is dedicated to them.

TABLE OF CONTENTS

DECLARATION OF AUTHORSHIP I
ABSTRACT II
ACKNOWLEDGEMENT IV
TABLE OF CONTENTS VI
ABBREVIATIONS IX

CHAPTER 1. INTRODUCTION 1

1.1 VESICLE TRANSPORT PATHWAY 3
1.1.1 GENERAL VESICLE TRAFFICKING MECHANISM 3
1.1.2 NEUROTRANSMISSION 5
1.2 SNARE PROTEINS 7
1.2.1 NOMENCLATURE 8
1.2.2 UNIVERSAL STRUCTURAL FEATURES OF SNARE COMPLEXES 8
1.2.3 THE NEURONAL SNARE PROTEINS 10
1.3 LIPID MEMBRANE PROPERTIES 15
1.3.1 SELF AGGREGATION AND MESOPHASES 15
1.3.2 THE ENERGY OF CONSTRAINT 18
1.4 MEMBRANE FUSION 20
1.4.1 CLOSE PROXIMITY 20
1.4.2 MEMBRANE CONTACT 22
1.4.3 FROM HEMIFUSION TO FULL FUSION 25
1.4.4 THE FUSION ROLE OF SNARE PROTEINS, A SECTION SUMMARY 27
1.5 THE COMPLEXITY OF MEMBRANE FUSION *IN VIVO* 29
1.5.1 RAB PROTEINS 29
1.5.2 SYNAPTOPHYSIN 30
1.5.3 SM PROTEINS 31
1.5.4 MUNC13 31
1.5.5 TOMOSYN 32
1.5.6 NSF AND SNAP 32
1.5.7 COMPLEXIN 33
1.5.8 SYNAPTOTAGMIN 34
1.6 MINIMAL FUSION MACHINERY 35
1.7 PROTEIN-LIPID INTERPLAY 39
1.7.1 GENERAL MECHANISMS OF INTERPLAY 39
1.7.2 SNARE-MEDIATED FUSION 41
1.8 CONCLUDING REMARKS AND PROJECT AIMS 47

CHAPTER 2. PURIFICATION OF NEURONAL SNARE PROTEINS 49

2.1 PURIFICATION OF THE NEURONAL SNARE PROTEINS 50

2.1.1 PURIFICATION OF VAMP2 52
2.1.2 THE SYNTAXIN 1A/SNAP-25 CO-EXPRESSION SYSTEM 54
2.1.3 PURIFICATION OF SNAP-25 57
2.1.4 PURIFICATION OF SYNTAXIN 1A 59

2.2 FLUORESCENT SNARE PROTEINS 63

2.3 SMALL PROTEOLIPOSOMES 67

2.4 MATERIALS AND METHODS 71

2.4.1 SOLUTIONS AND BUFFERS 71
2.4.2 ANTIBODIES 75
2.4.3 PROTEIN EXPRESSION 75
2.4.4 PROTEIN PURIFICATION 77
2.4.5 VISUALISATION OF PURIFIED PROTEIN 79
2.4.6 QUANTIFICATION OF PROTEIN CONCENTRATION 80
2.4.7 CLONING 80
2.4.8 FLUORESCENT LABELLING 83
2.4.9 PREPARATION OF SEPHADEX G-25 AND G-50M COLUMNS 84
2.4.10 FLUORESCENT PROTEOLIPOSOME FORMATION 84
2.4.11 HPLC ANALYSIS 84

2.5 CHAPTER SUMMARY 85

CHAPTER 3. THE EFFECT OF SNARE PROTEINS ON LIPOSOME FORMATION 86

3.1 INTRODUCTION 87

3.1.1 VESICLES TYPES 87
3.1.2 ELECTROFORMATION MECHANISM 88
3.1.3 FACTORS INFLUENCING GUV FORMATION 90

3.2 MATERIALS AND METHODS 93

3.2.1 SOLUTIONS AND BUFFERS 93
3.2.2 FORMATION OF GIANT UNILAMELLAR VESICLES BY ELECTROFORMATION 93
3.2.3 MICROSCOPY 95
3.2.4 GUV SIZE 95

3.3 RESULTS 98

3.3.1 GUV FORMATION 98
3.3.2 PROTEIN INSERTION INTO GUVS 98
3.3.3 SNARE PROTEINS AFFECT GUV SIZE 99

3.4 DISCUSSION 104

3.5 CHAPTER SUMMARY 108

CHAPTER 4. MICROPIPETTE ASPIRATION STUDIES OF MEMBRANE PROPERTIES 109

4.1 INTRODUCTION 110

4.1.1 PRESSURE AND SURFACE AREA 110
4.1.2 MEMBRANE DEFORMATION AND TENSION 114
4.1.3 PRESSURE REGIMES 114

4.2 MATERIALS AND METHODS 116

4.2.1 MAKING MICROPIPETTES 116
4.2.2 ASPIRATION 117
4.2.3 DATA EXTRACTION 120
4.2.4 DATA ANALYSIS 125

4.3 RESULTS AND DISCUSSION 127

4.3.1 DOPC AND DI-ETHER PC MICROPIPETTE ASPIRATION STUDIES 127
4.3.2 SNARE PROTEIN MICROPIPETTE ASPIRATION STUDIES 132
4.3.3 EFFECT OF SNARE PROTEIN INCORPORATION 135

4.4 CHAPTER SUMMARY 141

CHAPTER 5. THE EFFECT OF MEMBRANE PROPERTIES ON LIPOSOME FUSION RATES 142

5.1 INTRODUCTION 143

5.1.1 LIPID MIXING ASSAYS 144
5.1.2 CONTENT MIXING ASSAYS 146

5.2 MATERIALS AND METHODS 148

5.2.1 VESICLE PREPARATION 148
5.2.2 FLUORIMETER ASSAY 149
5.2.3 DATA ANALYSIS 150

5.3 RESULTS 154

5.4 DISCUSSION 160

5.5 SUMMARY 165

5.6 IMPLICATIONS FOR SNARE-MEDIATED MEMBRANE FUSION 166

5.7 CONCLUSIONS 169

5.8 FUTURE WORK 170

APPENDICES 172
BIBLIOGRAPHY 179

ABBREVIATIONS

α-SNAP	Soluble NSF-attachment Protein
AFM	Atomic Force Microscopy
Amp	Ampicillin
ANTS	Aminonaphthalenetrisulphonic Acid
APS	Ammonium Persulphate
ATP	Adenosine Triphosphate
BAR	Bin, Amphiphysin, rvs (domain)
BSA	Bovine Serum Albumin
Cam	Chloramphenicol
CAPS	3-[cyclohexylamino]-1-propanesulphonic Acid
CMC	Critical Micelle Concentration
DAG	Diacylglycerol
DHPC	1,2-di-O-hexadecyl-*sn*-glycero-3-phosphocholine
DDM	n-dodecyl β-D-maltoside
Di-ether PC	1,2-di-O-(9Z-octadecenyl)-*sn*-glycero-3-phosphocholine
DMPC	1,2-dimyristoyl-*sn*-glycero-3-phosphocholine
DMSO	Dimethyl Sulphoxide
DNA	Deoxyribonucleic Acid
dNTP	Deoxyribonucleotide Triphosphate
DOPC	1,2-dioleoyl-*sn*-glycero-3-phosphocholine
DOPE	1,2-dioleoyl-*sn*-glycero-3-phosphoethanolamine
DPA	Dipicolinic Acid
DPPC	1,2-dipalmitoyl-*sn*-glycero-3-phosphocholine
DPX	p-xylylene bis(pyridinium) Bromide
DRM	Detergent Resistant Membrane
DTT	Dithiothreitol
E. coli	*Escherichia coli*
ECL	Enhanced Chemiluminescence
EDTA	Ethylenediaminetetraacetic Acid
EPR	Electroparamagnetic Resonance
ER	Endoplasmic Reticulum
EtBr	Ethidium Bromide
FRET	Fluorescence Resonance Energy Transfer
FPLC	Fast Protein Liquid Chromatography
GFP	Green Fluorescent Protein
GST	Glutathione S-transferase
GUV	Giant Unilamellar Vesicle
HA	Hemaglutinin
HEPES	4-(2-hydroxyethyl)-1-piperazineethanesulphonic Acid
HPLC	High Pressure Liquid Chromatography
IPTG	Isopropyl-beta-D-thiogalactopyranoside

ITO	Indium Tin Oxide
Kan	Kanamycin
LB	Luria-Bertani
LUV	Large Unilamellar Vesicle
18:1 LysoPC	1-(9Z-octadecenoyl)-sn-glycero-3-phosphocholine
NBD-PC	1-oleoyl-2-[12-[(7-nitro-2-1,3-benzoxadiazol-4-yl)amino]dodecanoyl]-sn-glycero-3-phosphocholine
NBD-PE	1-oleoyl-2-[12-[(7-Nitro-2-1,3-benzoxadiazol-4-yl)amino]dodecanoyl]-sn-glycero-3-phosphoethanolamine
NSF	N-ethylmaleimide Sensitive Fusion (protein)
OβG	Octyl β-glucopyranoside
PAGE	Polyacrylamide Gel Electrophoresis
PBS	Phosphate Buffered Saline
PBST	PBS-Tween20
PC	Phosphatidylcholine
PCR	Polymerase Chain Reaction
PDMS	Polydimethylsiloxane
PE	Phosphatidylethanolamine
PEG	Polyethylene Glycol
PH	Pleckstrin Homology
PI	Phosphoinositol
PIP_2	Phosphoinositol-4,5-bisphosphate
PKC	Protein Kinase C
PLA_2	Phospholipase A_2
PLC	Phospholipase C
PMSF	Phenylmethylsulphonyl Fluoride
POPC	1-palmitoyl, 2-oleoyl-*sn*-glycero-3-phosphocholine
PS	Phosphatidylserine
PUFA	Polyunsaturated Fatty Acid
RFU	Raw Fluorescence Unit
Rh-PE	1,2-dioleoyl-*sn*-glycero-3-phosphoethanolamine-N-(lissamine rhodamine B sulphonyl) (ammonium salt)
RRP	Ready Releasable Pool
SDS	Sodium Dodecyl Sulphate
SNAP-25	Synaptosomal-associated Protein 25
SNARE	SNAP (Soluble NSF (N-ethylmaleimide Sensitive Fusion) Attachment Proteins) Receptors
SOPC	1-stearoyl, 2-oleoyl-*sn*-glycero-3-phosphocholine
STED	Stimulated Emission Depletion
SUV	Small Unilamellar Vesicle
Tb	Terbium
TEMED	N,N,N',N'-Tetramethylethylenediamine
Tris	Tris(hydroxymethyl)aminomethane
VAMP2	Vesicle Associated Membrane Protein 2

Chapter 1.

INTRODUCTION

SNARE (SNAP (Soluble NSF (N-ethylmaleimide Sensitive Fusion) Attachment Proteins) Receptor) proteins are of central importance in membrane fusion events, in an evolutionarily conserved mechanism. Section 1.1 discusses the general mechanism by which all vesicle transport pathways operate. The SNARE proteins used in this study (Syntaxin 1A, SNAP-25b (Synaptosomal-associated Protein 25) and VAMP2 (Vesicle Associated Membrane Protein 2; also referred to as Synaptobrevin 2)) are located in neurons and therefore the neurotransmission pathway is discussed in further detail.

Membrane fusion requires lipid bilayers to be deformed and remodelled; SNARE proteins provide the energy for this to occur. Traditionally however, studies of membrane fusion have investigated protein roles and lipid contributions separately. In order to discuss both of these influences, general introductions of both are given in sections 1.2 and 1.3 respectively. Section 1.2 describes the general features of the SNARE super-family with explanations of the nomenclature and classifications used throughout this thesis. A detailed discussion of the structure of the individual SNARE proteins used, and the complex they form, is also included. The effect of aggregating lipid molecules into structures such as bilayers, and the resultant stored energy, is discussed within section 1.3. The most widely accepted theories of membrane fusion are discussed in section 1.4. This section brings together information from sections 1.2 and 1.3 to discuss the potential roles of both lipids and SNARE proteins at each stage of membrane fusion.

Sections 1.5 and 1.6 introduce the concept of minimal machinery i.e. the smallest number of components necessary for fusion to occur. First, section 1.5 highlights the complexity and highly regulated nature of membrane fusion *in vivo*. The large number of participants (even excluding lipid involvement) makes it difficult to untangle individual functions. Despite this, many studies (both *in vivo* and *in vitro*) have been conducted with the aim of establishing what the minimal machinery is. While still debated, it is commonly believed that the minimal machinery consists of lipid bilayers which contain the appropriate SNARE proteins. Section 1.6 provides a critique of the evidence provided by these studies and aims to introduce the reader to the most common criticisms of existing studies.

In recent years it has become increasingly evident that there is interplay between proteins and lipids in membrane fusion. While no phospholipid binding has been observed for SNARE proteins alone, evidence has emerged that complexes between SNAREs and regulatory proteins may be partly controlled by lipid moieties. Despite the lack of evidence that they form a pore, the transmembrane domains of SNARE proteins have also been shown to be essential for complete fusion to occur. Though briefly discussed throughout this chapter, protein-lipid interplay is predominantly discussed in section 1.7. Away from membrane fusion, there are many known examples of protein-driven changes in membrane environments. The general principles of this effect are described, with examples, in 1.7.1. Evidence for interplay in SNARE-mediated membrane fusion is discussed in 1.7.2. This section also includes a discussion of the controversy surrounding specific types of study used and the apparent link between lipid modification (including signal pathways) and the regulatory proteins discussed in section 1.5. Finally, section 1.8 provides the reader with concluding comments and outlines the rest of the thesis.

The emerging evidence of interplay in membrane fusion events shows a need to investigate the lipids and proteins involved collectively. The essential involvement of SNARE proteins in fusion makes them a prime candidate for such a study.

1.1 VESICLE TRANSPORT PATHWAY

Eukaryotic cells, unlike prokaryotes, have internal compartments. These membrane-enclosed bodies, known as organelles, allow for the segregation and regulation of cellular functions. Though single celled eukaryotic organisms exist, namely yeasts and protozoa, the majority of eukaryotes cooperate to form multi-cellular organisms such as mammals. This leads to specialised cells unable to survive independently and increased sophistication of function.

In order for eukaryotes to work efficiently there must be continual communication between the organelles (intracellular communication) and additionally, in the case of multi-cellular organisms, neighbouring cells (intercellular communication). The vesicle transport network is the primary means by which intracellular communication occurs. It is also instrumental in many intercellular communication events such as neurotransmission.

1.1.1 GENERAL VESICLE TRAFFICKING MECHANISM

Despite numerous pathways within this network, the general mechanism (Figure 1.1) remains the same[1, 2]. A vesicle, which is a small membrane body containing soluble and membrane associated cargo, buds from a donor organelle and fuses with the membrane of the target. First, adaptor proteins are recruited to the donor organelle membrane. These proteins bind to cargo receptors which define the soluble content of the vesicle. Adaptors also bind to coat proteins. There are three principal coat proteins which operate in different areas of the network. COPII between the endoplasmic reticulum (ER) and the Golgi complex, COPI between the Golgi complex and the ER and Clathrin between the Golgi complex and the plasma membrane. Despite this apparent segregation of coat proteins it is currently unclear whether they help to determine the path a given vesicle will follow. One of their functions is hypothesised to be the induction and stabilisation of high membrane curvature causing a vesicle to bud from the donor organelle[3, 4]. During the budding stage other proteins are introduced including proteins vital for vesicle function; scission of the vesicle then follows. The coat proteins are removed before Rab GTPase proteins on the vesicle bind to receptors at its destination, tethering the vesicle to the target organelle[5-10]. Interaction of a SNARE protein on the vesicle with a complimentary pair of SNARE proteins on the target membrane[11] leads to vesicle-target fusion[1, 12-18]. The docking and fusion stages of this pathway are highly regulated by a variety of proteins (see section 1.5).

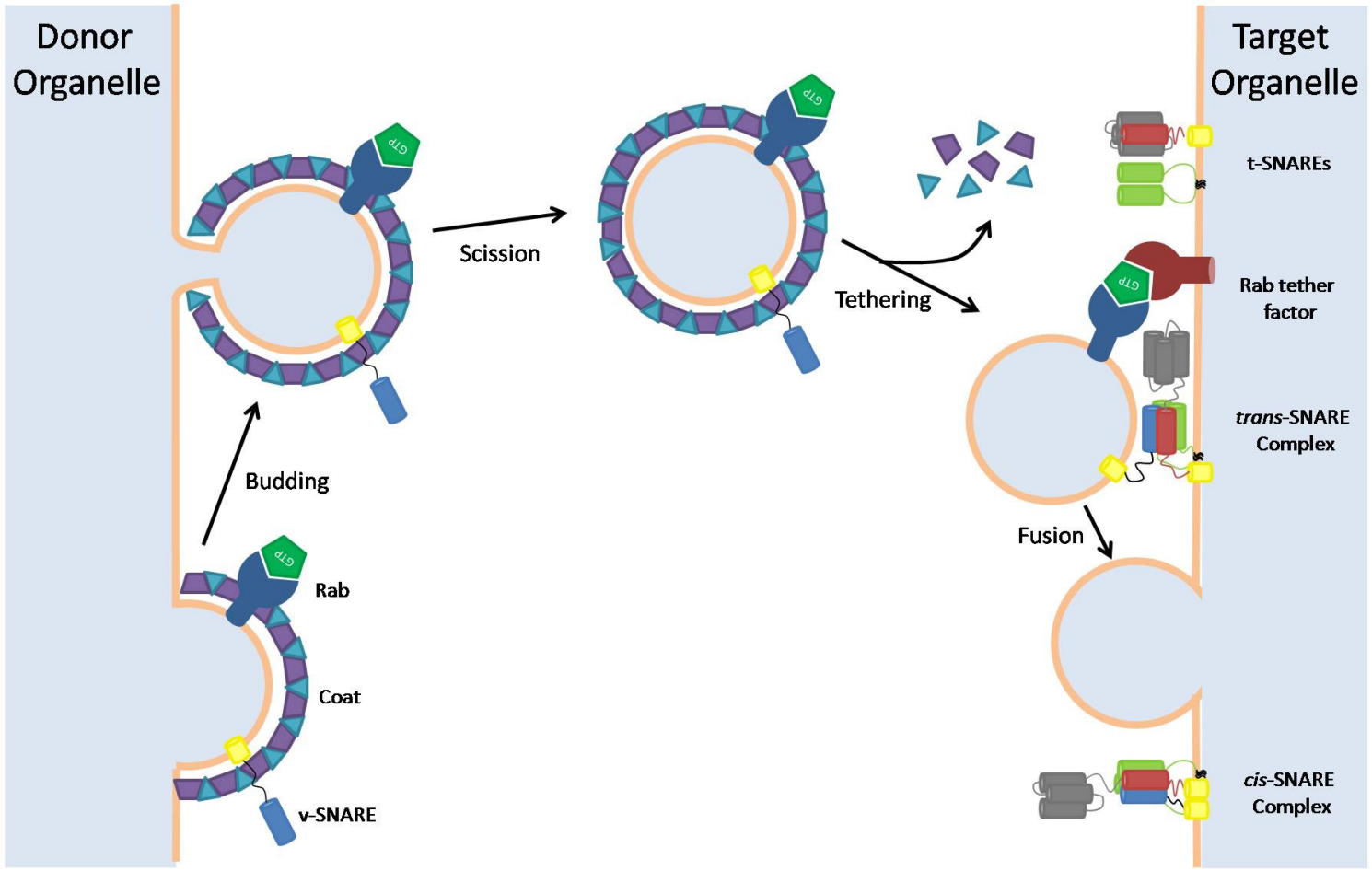


Figure 1.1. All vesicle network pathways have the same basic mechanism. Coat proteins induce local high curvature causing a vesicle to bud from the donor organelle. Coat adaptor proteins bind to both soluble and membrane-bound moieties; controlling the content of the vesicle. Once scission occurs, the vesicle is directed to the target membrane. The vesicle is tethered through the interaction of Rab proteins and their effectors which reside on opposing membranes. The v-SNARE and t-SNARE proteins form a complex bringing the vesicle close to the target membrane. The vesicle then fuses and the content released.

1.1.2 NEUROTRANSMISSION

Neurotransmission is an example of the use of the vesicle transport network for intercellular communication. Neurons pass information to neighbouring neurons through chemical signals which are released as a result of exocytosis (Figure 1.2). Neurons consist of four regions: the cell body, axon, axon terminals and dendrites. The axon terminal of one neuron forms a synapse with the dendrite of a neighbour, separated by the synaptic cleft. Vesicles containing neurotransmitters (small molecules such as dopamine, acetylcholine and serotonin) fuse to the plasma membrane at the synapse. The neurotransmitters are released into the synaptic cleft where they proceed to bind to receptors located on the dendrite of the other neuron.

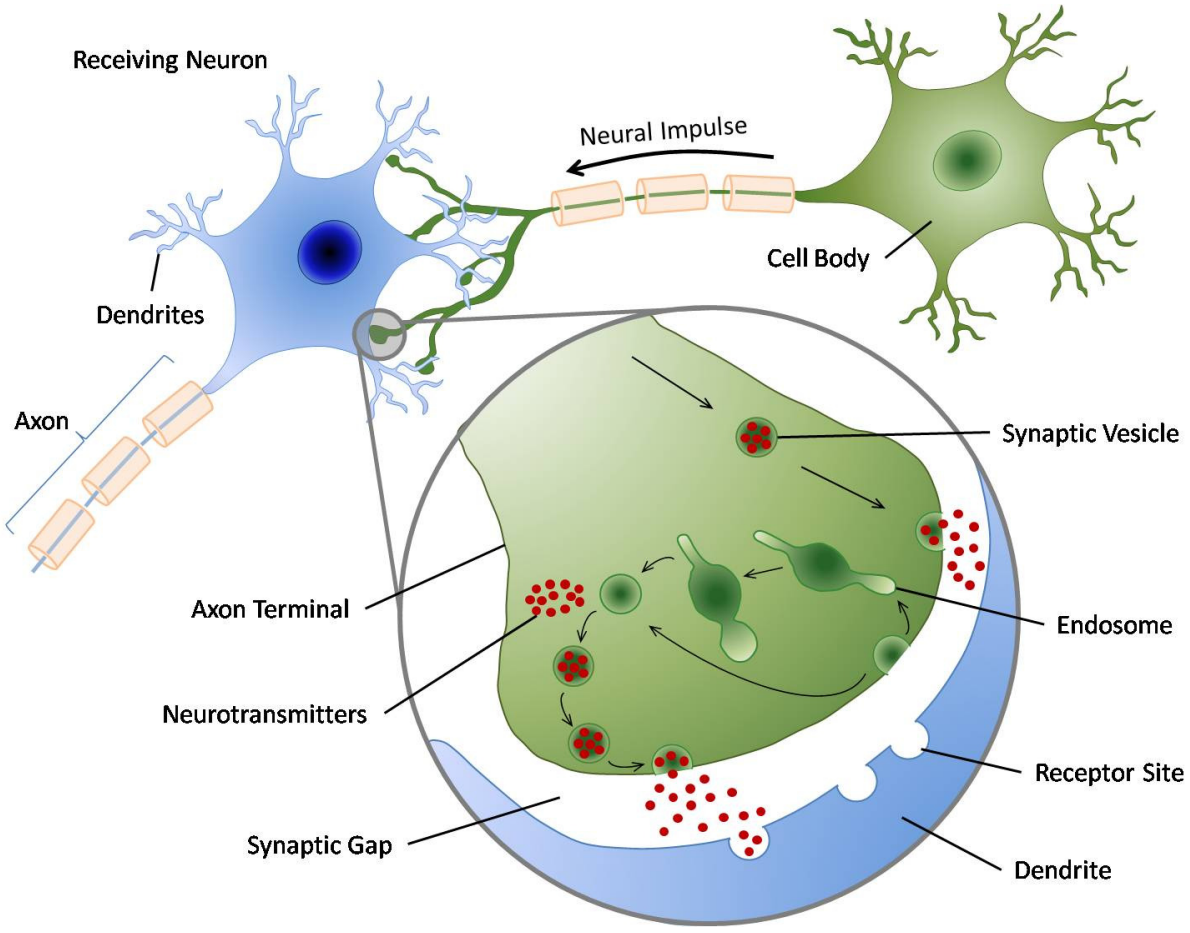


Figure 1.2. Information is passed from one neuron to another through neurotransmission. Synaptic vesicles containing small neurotransmitter molecules originate at the trans-Golgi complex and travel to the axon terminals. Upon a nerve impulse (also called an action potential) the vesicle undergoes fusion. The fusion of the vesicle with the plasma membrane releases the content of the vesicle into the synaptic cleft (or gap). Neurotransmitters bind to receptors on the receiving neuron's dendrite. The vesicle can be recycled through direct endocytosis or incorporation into an endosome. The vesicle is able to be refilled and undergo several rounds of fusion.

The vesicles that undergo this process are called synaptic vesicles[19]. They are approximately 50 nm in diameter, originate from the trans-Golgi complex and only fuse when triggered by an action potential. For these vesicles this trigger is in the form of an influx of calcium ions. Neurons must respond extremely quickly to an action potential and upon this stimulus, synaptic vesicles fuse and release neurotransmitters within 0.5 ms[20]. In order for such a fast response to be possible three vesicles pools are located in the pre-synaptic terminal[21]. First, the RRP (ready-releasable pool) contains approximately 1% of the total number of vesicles. Within this pool there is some evidence to suggest two populations of vesicles are present. The first population is of tethered vesicles and the second is of docked and primed vesicles. The second population is able to fuse almost instantaneously with the action potential. Once a vesicle has released its content it leaves the RRP and moves to the recycling pool, where it can be refilled. 10-15% of the total vesicles occupy this pool and fast exchange, recycling and trafficking is observed between it and the RRP. The third pool is rarely used despite containing 80-90% of the vesicle population. If stimulus is prolonged or intense the recycling pool can become depleted and in this situation, vesicles will transfer from the reserve pool to restore the population of the recycling pool. However, movement between them is slow. A reserve pool is necessary as axons can be up to a metre long; without it, the distance between the trans-Golgi complex and pre-synaptic terminal would inhibit intense/ prolonged stimulation.

1.2 SNARE PROTEINS

The first SNARE proteins were discovered in the 1980s[22-25] but it was not until 1993 that Thomas Söllner found them to be SNAP receptors[12], therefore linking them to membrane fusion events. Since then many proteins have been classified as SNARE proteins. Genomics has led to the identification of 36 distinct mammalian SNARE proteins[26]. These can be classified into four subfamilies; Syntaxin, SNAP-25N, SNAP-25C and VAMP, based upon homology sequencing and domain structure comparisons (Figure 1.3). The subfamilies have the alternative classification of Q_a, Q_b, Q_c and R respectively (see section 1.2.2). SNARE proteins are proposed to have some involvement in the specificity of membrane fusion events as they are localised into distinct organelles[27-29].

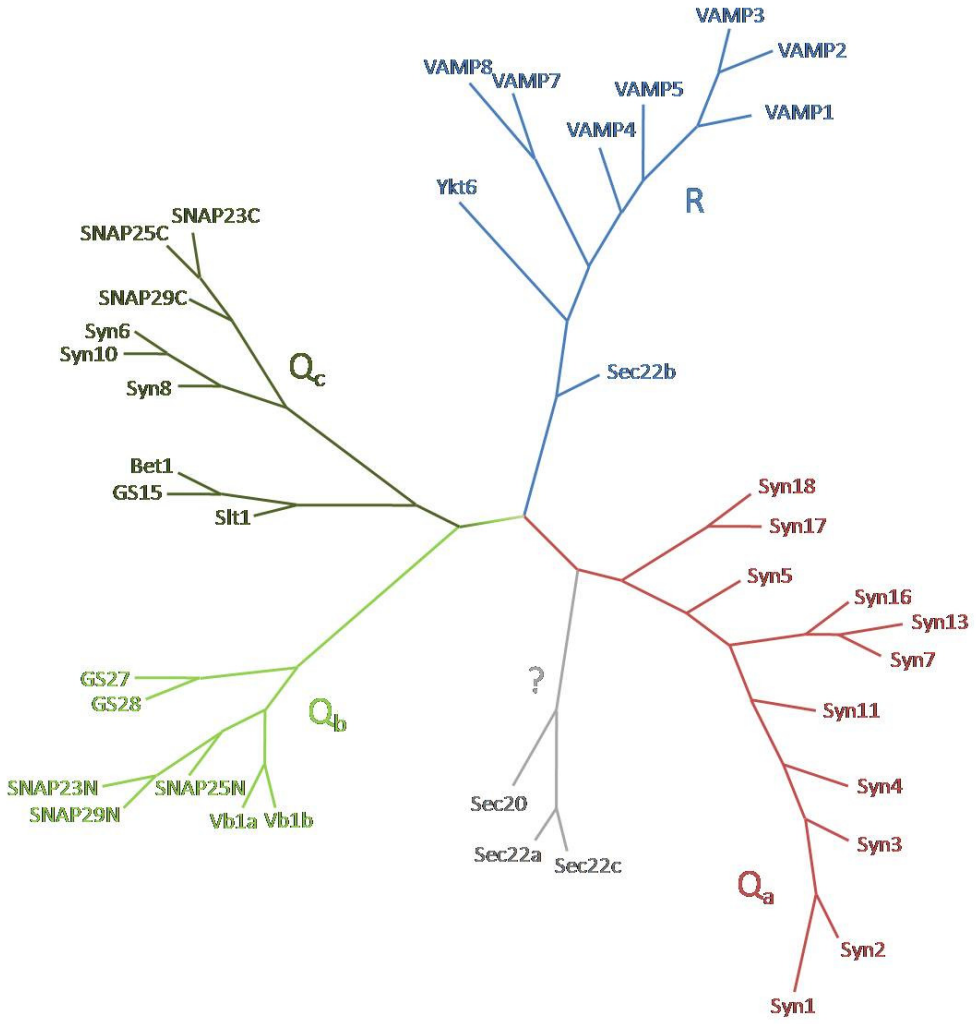


Figure 1.3. Adapted from Hong[26], the phylogenetic tree of the mammalian SNARE proteins is shown. The four branches are based upon sequence similarities within the SNARE motif. Each branch represents a SNARE subfamily: Qa/ Syntaxin (red), Qb/ SNAP-25N (light green), Qc/ SNAP-25C (dark green) and R/ VAMP (blue). Those in grey are currently unassigned to a subfamily.

To be classified as a SNARE protein several criteria must be observed[30]. These include the ability to bind to a membrane and most commonly SNARE proteins have a transmembrane domain. 31 of the 36 mammalian SNARE proteins have a single transmembrane domain[26]. The remaining SNARE proteins are SNAP-23, SNAP-25, SNAP-29, Syntaxin 11 and Ykt6. Of these, SNAP-25, Syntaxin 11 and Ykt6 have palmitoylated amino acid residues giving them lipid anchors; the remaining two have other forms of lipid anchor. Other criteria are that the SNARE proteins are relatively small proteins (typically 15-40 kDa in size) and that a large proportion of the sequence is cytosolic.

1.2.1 Nomenclature

There are two systems of nomenclature which are used when discussing SNARE proteins. The earliest describes SNARE proteins as either v- or t- SNAREs based upon their location at the start of the membrane fusion process[31]. Those SNAREs which start on the vesicle are described as v-SNAREs and most commonly are members of the VAMP subfamily. Conversely, the SNARE proteins located on the target membrane are described as t-SNAREs. The members of both the Syntaxin and SNAP-25 subfamilies are most commonly t-SNAREs. However, within the vesicle transport network recycling pathways exist; v-SNARE proteins can therefore be located on target membranes and t-SNARE proteins in vesicles. As this can lead to confusion another nomenclature system emerged[32]. Rather than location based, this nomenclature is based upon the sequence of the SNARE proteins. Throughout the SNARE super-family it has been found that some amino acid residues are conserved. At the centre of the SNARE complex (see section 1.2.2) this conserved residue is either an arginine (R) or glutamine (Q). Therefore SNARE proteins are labelled either R- or Q- SNAREs. While a few exceptions are known[26], R-SNARE proteins are usually found on vesicles and Q-SNAREs on target membranes. Therefore R-SNAREs, in most cases, can also be called v-SNAREs and Q-SNAREs called t-SNAREs. As this thesis will not discuss recycling pathways in depth the v/t- nomenclature will be used from now on.

1.2.2 Universal Structural Features of SNARE Complexes

Heptad repeats are present in the sequence of all SNARE proteins and form at least one amphipathic α-helix[18]. This helix is often called the SNARE motif or core domain and this motif is found adjacent to the transmembrane domain (in those SNARE proteins that have such a membrane anchor). In SNARE proteins with lipid anchors the motif is usually found at one, or both, of the terminal domains. *In vivo,* four of these motifs form a coiled coil structure[33] known as the core SNARE complex. Formation of the complex buries the hydrophobic faces of each α-helix within it[34-36]. It has been found that the amino acid residues within the heptad sequence can vary between SNARE

proteins. Despite this, the SNARE complexes that form have been found to be structurally highly similar[32, 33, 35]. The SNARE proteins and the complex formed by them have been shown to have similarities with viral fusion proteins and the complexes that they form[15, 37].

The SNARE complex is considered to have two states called *trans* and *cis (*Figure 1.4*)*. The *trans*-complex (also called a SNAREpin[38]) is the initial SNARE complex formed *in vivo*. The individual SNARE proteins are still localised on different membranes i.e. before full fusion has occurred. The *cis*-complex is the fully formed SNARE complex, formed after fusion. It is thought that the stability of the *cis*-complex contributes to the energy requirements of the fusion process[39, 40].

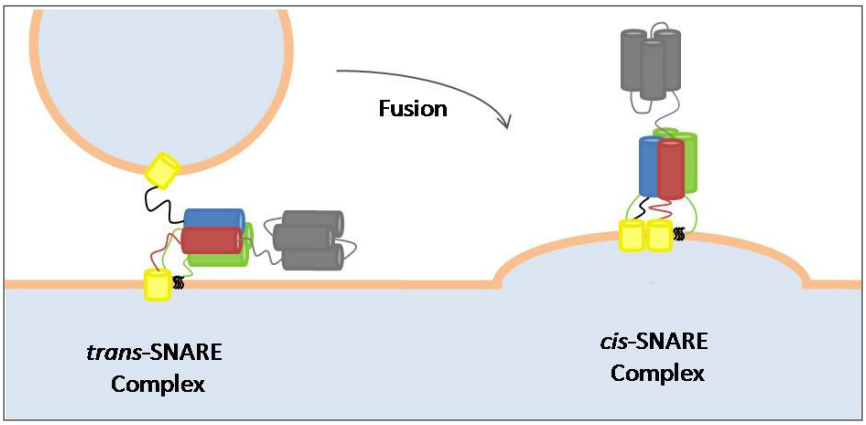


Figure 1.4. The SNARE complex exists in two states, which are presented in this figure. The trans-SNARE complex is an intermediate structure during the fusion process, with SNARE proteins located on different membranes. After fusion, the complex assembles fully to form the cis-SNARE complex, its most stable state. These two forms are a universal feature in SNARE protein function; however, some of the structural aspects represented in this figure are based upon the neuronal SNARE proteins (described in section 1.2.3).

The majority of SNARE proteins contain only one SNARE motif; formation of a SNARE complex therefore usually requires four SNARE proteins. There are three mammalian exceptions which are SNAP-23, SNAP-25 and SNAP-29 as each contains two SNARE motifs[26]. These two motifs are named based on their position. The N-terminal motif is denoted 25N and the C-terminal motif 25C. Proteins belonging to the SNAP-25 subfamily are therefore split into two further subfamilies; those with motifs homologous to 25N and those homologous to 25C. These proteins are Q-SNAREs and the motifs are sometimes referred to as light chains. An alternative notation for these motifs is Q_b for 25N motif proteins and Q_c for 25C proteins. The SNARE complex is made up of an R-SNARE (v-SNARE) motif and three Q-SNARE (t-SNARE) motifs[41, 42]. The origin of each of the α-helices in the SNARE complex structure is usually denoted R, Q_a, Q_b and Q_c (regardless of the nomenclature system in use). Q_a (the heavy chain) is the helix which originates from the Syntaxin family member and R from the VAMP family member.

1.2.3 THE NEURONAL SNARE PROTEINS

The neuronal SNARE proteins are also referred to as the synaptic SNAREs and are involved in the fusion of synaptic vesicles (see section 1.1.2). The neuronal SNARE complex is unusual as it is formed from only three SNARE proteins. A couple of isoforms of the SNARE proteins involved in this complex exist, those discussed here are those used in this study (which are also the most widely studied). These proteins are Syntaxin 1A, SNAP-25b and VAMP2 but will be referred to as Syntaxin, SNAP-25 and VAMP from now on.

1.2.3.1 Syntaxin 1A

The transmembrane domain of Syntaxin is located in the C-terminal region, adjacent to which is the SNARE motif (Figure 1.5). The N-terminus of the protein is made up of the H_{abc} domain which accounts for two thirds of the protein sequence. This domain forms three α-helices which arrange into an anti-parallel bundle[43, 44]. Structurally this N-terminal domain is highly conserved within the Syntaxin subfamily and yeast homologues. The domain is connected to the SNARE motif by a flexible linker[45] that allows Syntaxin to form a closed conformation whereby the H_{abc} domain binds to the SNARE motif. While there is evidence that the H_{abc} domain itself could be used for regulation[46, 47], the role of the four α-helix closed complex is more uncertain; though it too has been linked to regulation. The SNARE motif contains the conserved amino acid residue glutamine and therefore Syntaxin is classified as a Q-SNARE. It is also primarily located on the plasma membrane during exocytosis and is therefore also a t-SNARE protein.

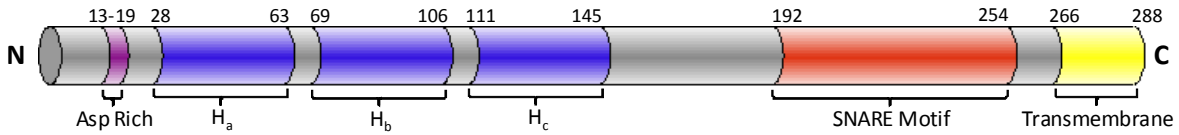


Figure 1.5. Syntaxin 1A is anchored to membranes through a transmembrane domain at its C terminus (shown in yellow) next to which is the SNARE motif (shown in red). The H_{abc} domain is located towards the N-terminal region and consists of three α-helices (each shown in blue). An aspartic acid rich domain is also present in the N-terminal region. Syntaxin is a Q- and t-SNARE protein and resides primarily on the plasma membrane, where it functions in exocytosis.

1.2.3.2 SNAP-25

This protein, like Syntaxin, is also classified as a Q- and t-SNARE protein. Unlike most SNARE proteins SNAP-25 contains two SNARE motifs. Only three SNARE proteins are required for the formation of the neuronal SNARE complex because SNAP-25 contributes both of these SNARE motifs to the SNARE complex. One of SNAP-25's motifs is located at each terminus linked by a sequence referred to as the loop or linker region (Figure 1.6). Within this loop four cysteine residues (C85, C88, C90 and C92) are palmitoylated[48-50] to provide SNAP-25 with lipid anchors rather than a transmembrane domain.

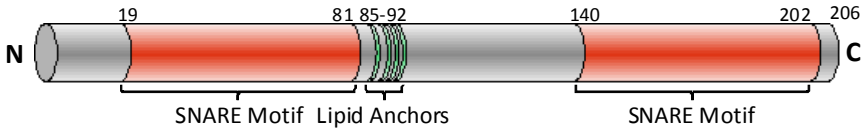


Figure 1.6. The Q- or t-SNARE protein SNAP-25 contains two SNARE motifs (shown here in red), one located at each terminus. Four palmitoylated cysteine residues provide SNAP-25 with lipid anchors (shown in green). The exact position of these anchors differs slightly between the two isoforms, a and b. It resides predominantly in the plasma membrane.

1.2.3.3 VAMP2

Also called Synaptobrevin, VAMP is located on the vesicle and as such is a v-SNARE protein. It also contains the conserved residue arginine within its SNARE motif and is therefore also classified as an R-SNARE. The N-terminal region of VAMP is made up of two domains. At the extreme end is a proline rich region, 24 amino acid residues long and ending with dibasic residues[51]. The second domain is highly conserved within the Synaptobrevin family. This domain appears to have two sequences which are highly predisposed to form α-helices. Both of these regions are thought to interact with regulatory proteins (see section 1.5). The C-terminus contains the transmembrane domain. Despite having a transmembrane domain it has been shown that VAMP is also palmitoylated[52]. VAMP only has one cysteine residue, which is located within the transmembrane domain and is therefore considered to be the site of this lipid anchor. This positions the anchor 8 residues from the membrane-cytoplasmic border and may be involved in regulation[53]. Like Syntaxin, the SNARE motif of VAMP is located adjacent to the transmembrane domain (Figure 1.7).

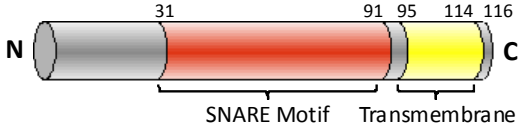


Figure 1.7. The transmembrane domain of VAMP2 is in the C-terminal region (shown in yellow). Adjacent to this membrane anchor is the SNARE motif (shown in red). VAMP2 functions mainly from synaptic vesicles in exocytosis, though it is present on other membranes due to recycling pathways.

1.2.3.4 The Neuronal SNARE Complex

The crystal structure of the core neuronal SNARE complex was determined to 2.4 Å resolution in 1998[34]. The structure was formed from the minimal fragments of Syntaxin 1A, SNAP-25b and VAMP2 required to form the complex. The complex was found to be a 4-helix twisted structure with the helices arranged parallel to each other. The overall cylindrical structure was 120 Å long with a circular cross section, though the radius of cross section changed appreciably over the length. The core SNARE complex forms 16 hydrogen bonded layers over approximately 60 residues with the layers orientated so that they are perpendicular to the bundle axis (Figure 1.8). The layers are numbered from -7 to +8 and mainly made up of side chains of hydrophobic residues. The central layer (labelled the zero layer) is made from the conserved amino acid residue (which gives the R/Q-nomenclature) in each of the SNARE proteins. As such, unlike the other layers, the zero layer is hydrophilic and is thought to be important in the disassembly of the complex once membrane fusion has occurred[54-56].

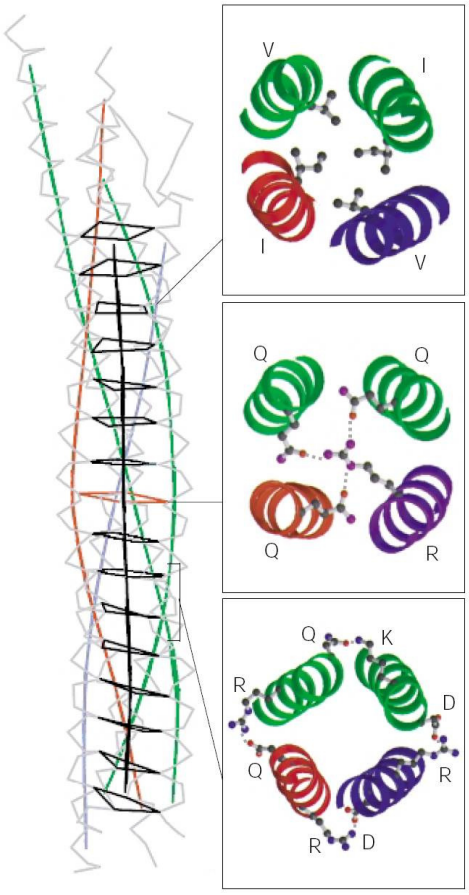


Figure 1.8. Adapted from Chen[18] the backbone of the core neuronal SNARE complex and the 16 interacting layers are shown on the left. To the right, a top down view of amino acid residue interactions is shown (VAMP in blue, Syntaxin in red and SNAP-25 in green). The zero (hydrophilic) layer, seen centre right, shows the interaction between the conserved amino acid residues found throughout the SNARE super-family.

In vitro it has been shown that no more than one arginine can be present in the zero layer but that it is possible to form a complex from four Q-SNARE proteins. *In vivo* this layer consists of one arginine and three glutamines during membrane fusion[41, 42, 57]. The central layer is surrounded by three layers (-1, -2 and +2) which show geometry and composition typical of leucine zipper protein complexes[34]. They are made from leucine, isoleucine and valine which interact in a plane. However, the remaining layers deviate significantly from classic leucine zipper models[58]. This is discussed further in the original crystallography paper[34]. The 16 layers of the complex make it extremely stable. The complex has been found to resist denaturation when exposed to the detergent SDS[59] (Sodium Dodecyl Sulphate) or heated to 90°C[60]. Proteases[59, 61, 62] and clostridial toxin[62, 63] were also shown to be ineffectual. Other SNARE protein complexes are considered to have this ladder of interacting residues, though the exact number may vary.

The end of the core complex, made from the N-terminal regions of the SNARE helices, shows interactions between Syntaxin and SNAP-25, while the C-terminus of the complex shows interactions between Syntaxin and VAMP. The surface of the complex was found to have distinct patches of hydrophobicity and hydrophilicity as well as charged regions. These, along with the highly grooved contours of the surface suggest interactions of the complex with other proteins. These interactions could be regulatory, though the surface features may also be important in membrane fusion events[34].

In July 2009 a crystal structure was published[64] for a SNARE complex including the linker and the transmembrane domains of Syntaxin 1A and VAMP2 (Figure 1.9). The protein crystal was grown by incorporating n-nonyl β-D glucopyranoside into the buffer and a resolution of 3.4 Å was achieved. This study showed that the linker and transmembrane domains of these proteins were helical, forming continuous helices from the core domain through to the C-terminus. This complex was found to be more stable than the core complex and successive removal of the membrane anchors reduced the stability. The linker regions were shown to interact through aromatic side chain contacts, forming a collar surrounded by basic residues. Using computer modelling, the complex was inserted into a lipid bilayer. This simulation suggested that the *cis*-SNARE complex sits as a rod, perpendicular to the bilayer with the linker regions of VAMP and Syntaxin buried in the upper monolayer. It was hypothesised that amino acid residues in the linker region interact with the polar headgroups of lipids in the upper monolayer.

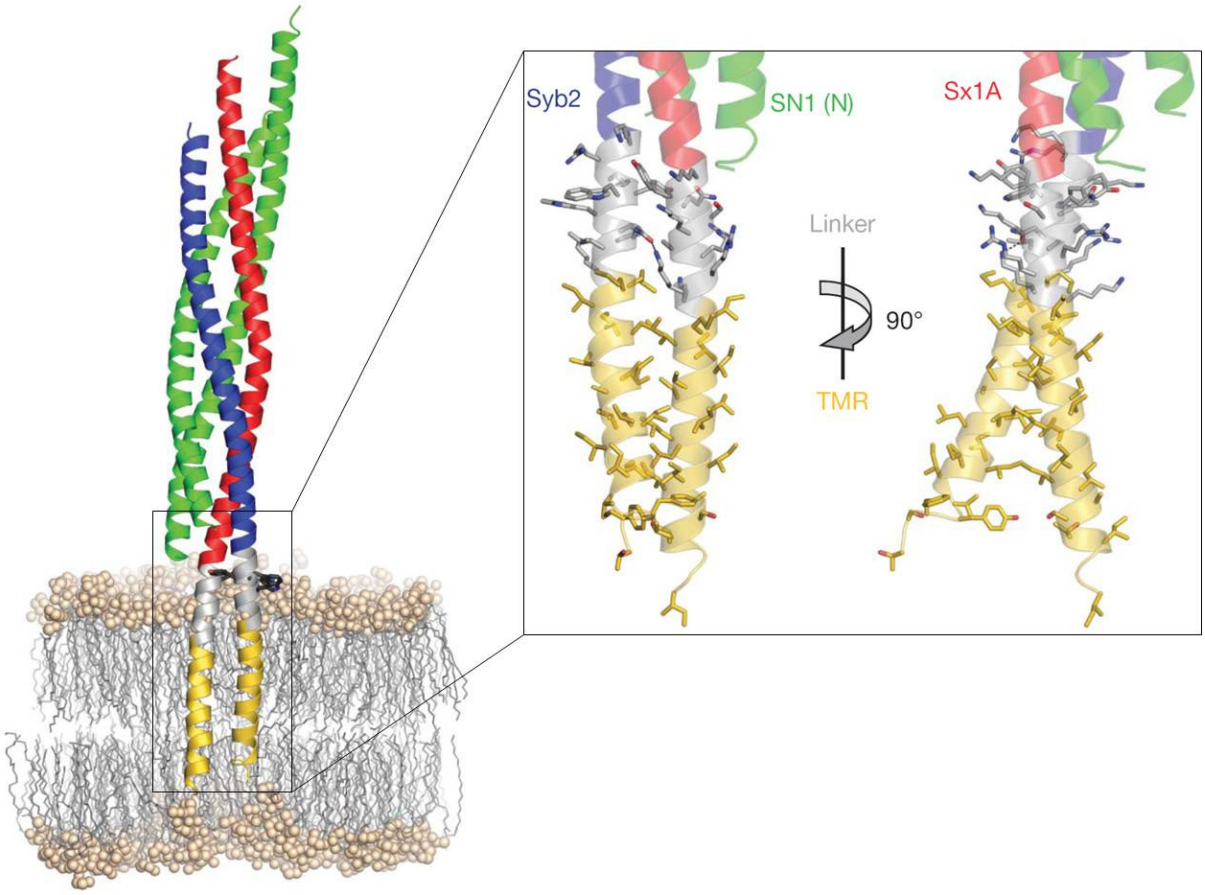


Figure 1.9 Modified from the figures of the original crystallography paper[64], the solved crystal structure of the SNARE complex with the linker and transmembrane domains of Syntaxin 1A and VAMP2 included is shown. The crystal structure reveals that Syntaxin 1A and VAMP2 form continuous helices from the beginning of the SNARE motif through to the C-terminal domains. The structure of the complex formed by the SNARE motifs is consistent with the core crystal structure found in 1998 by Sutton[34]. Beyond the core complex, the linker and transmembrane domains of Syntaxin and VAMP interact; twisting around each other. The position of the complex within a lipid bilayer was assessed using computer simulations and showed residues within the linker region interacting with the polar headgroups of the lipids.

1.3 Lipid Membrane Properties

Biological membranes are primarily composed of proteins and amphiphilic molecules called lipids. Despite the apparent role of SNARE proteins in membrane fusion, the event results in the melding of lipids from two, initially distinct, membrane structures. It is therefore important to consider the properties of lipid molecules and their possible contribution to membrane fusion events.

1.3.1 Self Aggregation and Mesophases

Lipids are amphiphiles possessing both hydrophobic and hydrophilic properties. In the presence of solvent, lipid molecules will self aggregate. Commonly, and in the case of cells, the solvent is water. The headgroup region of the lipids is hydrophilic and the aggregated structure is orientated so that this region shields the hydrophobic section (usually in the form of hydrocarbon chains) from the water.

The way in which lipids will aggregate depends on both the temperature of the system and the amount of solvent present[65]. The lipid molecular structure itself is also an important consideration. The aggregated structures formed are called mesophases. Neither solid nor liquid, the lipids within a mesophase are able to diffuse two dimensionally with respect to the surface. These mesophases are also called lyotropic liquid crystal phases.

1.3.1.1 The Lateral Pressure Profile

The aggregation of lipids is driven by the hydrophobic effect (the energetic cost of exposing the hydrocarbon chains to water). In biology, the most common aggregate structure is that of a lipid bilayer; within this structure lipids form two monolayers, which are coupled back to back. Within each monolayer forces act between individual molecules to both repel and attract them. These forces, which act within the plane of the lipid surface, can be represented by the lateral pressure profile[66-70] which shows how the lateral pressure, $\pi(z)$, varies across the depth of a monolayer (Figure 1.10).

The headgroup region of a lipid molecule is often charged or polar. Electrostatic repulsion therefore occurs when headgroups are aggregated. Steric hindrance and hydration forces can act to further increase the repulsive force at this depth. However, if headgroups are able to interact through hydrogen bonding, the lateral pressure of the headgroup region can be reduced. Within the chain region of the monolayer, collisions between chains can occur; providing a repulsive force. The ability of the chains to orientate so to avoid collisions with neighbouring chains usually increases with depth. This leads to a decrease in the repulsion over the length of the chain region. However,

introduction of chain unsaturation reduces the degrees of freedom leading to increased lateral pressure. Weak Van der Waal forces within the chain region provide some attractive force, though not sufficient to counteract the repulsive forces experienced. At the interface between the polar and non-polar regions is a highly attractive force. This force acts to keep the molecules together, shielding the chains from water (i.e. it is driven by the hydrophobic effect).

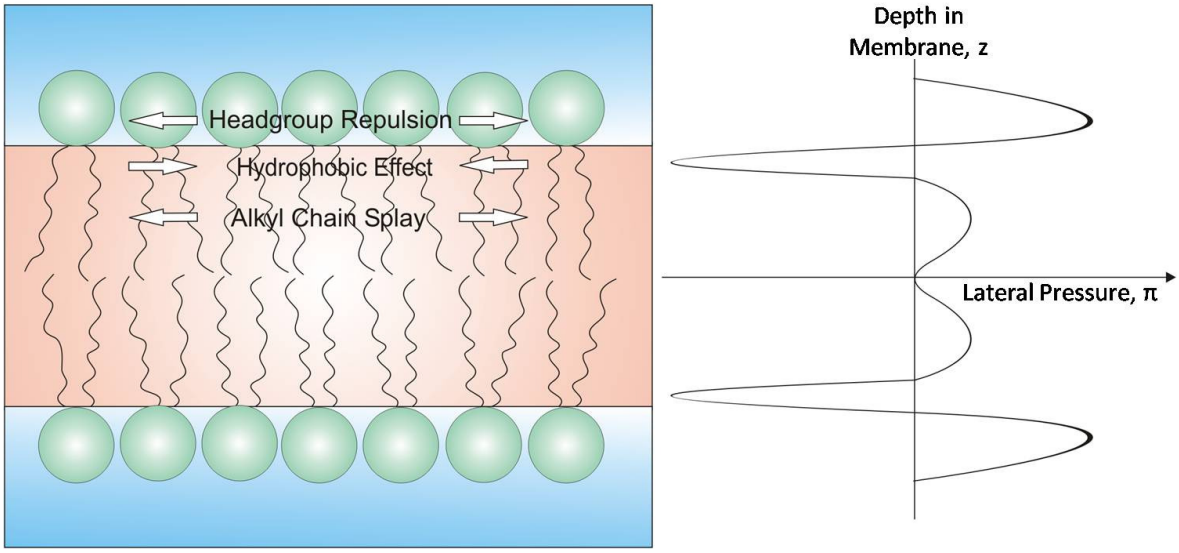


Figure 1.10. Interactions between aggregated lipid molecules lead to several forces acting within the aggregate structure. These forces (illustrated on the left of this figure) result in lateral pressure and torque tension. In this figure the lateral pressure is shown on the right, as a function of bilayer depth. Electrostatic repulsion and steric hindrance apply a repulsive force in the headgroup region. The flexibility of the lipid chains leads to collisions which introduce repulsive force within the chain region. At the interface between head and tail groups the hydrophobic effect drives the structure to shield the tail regions from polar solvent.

In order for a monolayer to reach equilibrium the lateral pressure must balance so that no net pressure acts (Equation 1.1).

$$\int \pi(z).dz = 0 \qquad \textit{Equation 1.1}$$

Integration of the moments acting at the various depths of the monolayer gives the torque tension, τ. In most cases the net torque is not zero (Equation 1.2). In these cases torque will act upon the monolayer and it will bend.

$$\tau = \int -z \cdot \pi(z).dz \neq 0 \qquad \textit{Equation 1.2}$$

1.3.1.2 Type and Curvature

The torque tension of a monolayer can be negative or positive. Therefore, the curvature that results from this non-zero torque can also be defined as negative or positive. Conventionally positive curvature is defined as surfaces which bend away from water and towards the chain region, and negative for surfaces that bend towards water (away from the chain region). Mesophases can be divided into two groups depending upon curvature. Those that possess surfaces of positive curvature are called normal phases (or type I), those with negative curvature surfaces are referred to as inverted (type II) mesophases. The classification of type is also used for individual lipids. Based on whether a single lipid component system displays positive or negative curvature the lipid molecules themselves can also be described as type I or II lipids.

For a spherical mesophase, the curvature is simply the reciprocal of the spheres radius. The surface of a sphere has the same curvature at any point but this is not the case for other surfaces. Two curvatures are needed to define the curvature of a surface at any point[71]. Two circles are drawn normal to the surface intersecting at the same point (Figure 1.11). The reciprocals of the radii give the curvatures. The two circles intersecting this point with the most negative (or most positive) curvatures are the principal curvatures c_1 and c_2 and are perpendicular to each other.

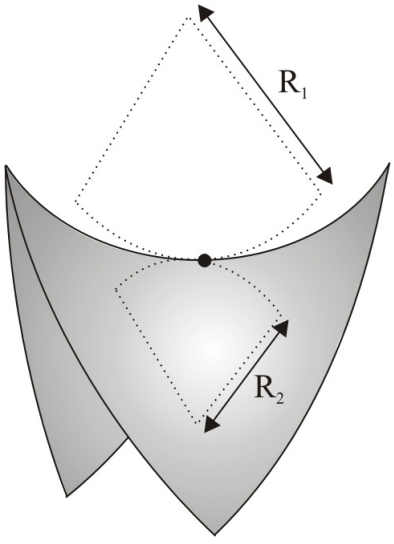


Figure 1.11. Non spherical structures usually have more than one curvature component at any given point. In order to characterise the overall curvature of a mesophase, these components must be evaluated. Circles coincident to the surface at a particular point are drawn. Those with the minimum and maximum curvature (the reciprocal of the circle radius) are defined as the principal curvatures.

As already stated, the principal curvatures of a spherical surface are equal. In a hexagonal mesophase lipids aggregate into cylinders which hexagonally pack. In this case one principal curvature will be negative or positive, depending on type, as it follows the elliptical cross section of the cylinder. The other curvature (which follows the long axis of the cylinder) will be zero. A saddle surface like the one shown in Figure 1.11 has one positive and one negative principal curvature. In a completely planar surface these curvatures are both zero.

1.3.2 THE ENERGY OF CONSTRAINT

Section 1.3.1 described how aggregation of lipids usually results in curved monolayer surfaces; defined by the two principal curvatures. In 1973 Helfrich[66] derived the free energy model for membranes. Providing that the thickness is negligible compared to the surface area, the membrane can be collapsed to a single sheet of infinitesimal thickness. The curvature free energy of the surface per unit area, g_c, can be expressed as,

$$g_c = \frac{1}{2}\kappa(c_1 + c_2 - 2c_0)^2 + \kappa_G c_1 c_2 \qquad \textit{Equation 1.3}$$

Where, κ is the bending rigidity (or splay modulus) and κ_G, the Gaussian (or saddle splay) modulus. The spontaneous curvature, c_0, is related to the torque tension[70, 72] as $\tau = -2\kappa c_0$. Equation 1.3 can be used to express the free energy of either monolayers or bilayers. However, the meaning of the moduli will be different.

The principal curvatures of a sphere are equal. By exploiting this, and differentiating Equation 1.3, it has been shown[73] that a spherical interface is at the global energetic minimum providing $-2 \leq \kappa_G/\kappa \geq 0$. The curvature of the system in this minimal energy state is the relaxed curvature, c_r, and can be related to the spontaneous curvature,

$$c_r = \frac{2\kappa}{2\kappa + \kappa_G} c_0 \qquad \textit{Equation 1.4}$$

Equation 1.3 can therefore be re-expressed based upon the relaxed, rather than spontaneous, curvature.

$$g_c = \left(k + \bar{k}\right)(H - H_r)^2 + \left(k - \bar{k}\right)(H^2 - K) \qquad \textit{Equation 1.5}$$

As with Equation 1.3, the membrane is collapsed to a minimal sheet. In this case the sheet is situated at the pivotal plane; the position where the cross sectional area does not change during isothermal bending. In Equation 1.5, H is the mean curvature and K is the Gaussian curvature and are defined as

$$H = \frac{1}{2}(c_1 + c_2)$$

$$K = c_1 c_2 \qquad \textit{Equation 1.6}$$

The moduli of Equation 1.5, k and $\bar{\kappa}$, are the bending rigidity and coupling modulus respectively. These moduli can be related to the moduli of the original Helfrich expression (Equation 1.3) providing that $-1 \leq \kappa_G/\kappa \geq 0$;

$$k = \kappa$$

$$\bar{\kappa} = \kappa + \kappa_G \qquad \textit{Equation 1.7}$$

In biology, as already stated, the principal lipid structure is that of bilayers. The coupling of two monolayers back to back means that neither monolayer can adopt its preferred curvature (unless the monolayers possess relaxed curvatures of the same magnitude but opposite sign). If both were to bend to their relaxed curvature, a vacuum within the bilayer or hydration of the chain region would be necessary; both cases are energetically highly unfavourable (Figure 1.12).

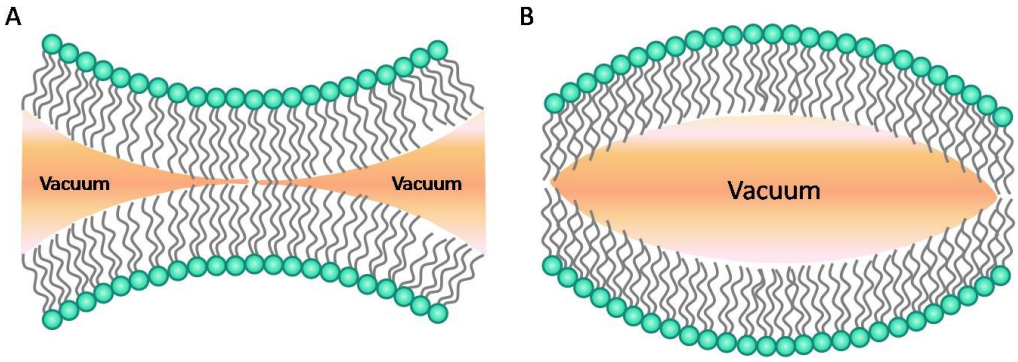


Figure 1.12. Figures A and B show monolayers which have adopted their relaxed curvature. The monolayers of A both have negative relaxed curvature and B, positive. As the figures show, if each leaflet bends to its relaxed curvature a vacuum region would form or the chain regions would be exposed to water. Both of these possibilities are energetically highly unfavourable. The leaflets of the bilayer are therefore unable to adopt the relaxed monolayer curvature.

For a bilayer made up of a single lipid component, both monolayers will have the same relaxed curvature, in both magnitude and direction. In this case the monolayers counter each other exactly and there is no overall desire to bend[74]. The relaxed curvature of the bilayer, H_r^b, is therefore equal to zero[75]. Assuming a symmetric bilayer, the bending rigidity and coupling modulus of the monolayers are related to their bilayer equivalents as follows;

$$k^b = 2k$$

$$\bar{\kappa}^b = 2\bar{\kappa} - 4\ell H_r(\bar{\kappa} + k) \qquad \textit{Equation 1.8}$$

Where, ℓ is the thickness of the monolayer.

The constraint imposed on monolayers by back to back coupling means that, relative to the relaxed state of each monolayer, there is an increase in the energy of the system. This additional energy is known as stored curvature elastic stress.

1.4 MEMBRANE FUSION

Research into membrane fusion has now been conducted for over two decades. Research has taken many forms from genetics and structural determination of proteins to theoretical modelling and lipid phase diagrams. A wealth of information has been gathered and a consensus on some aspects of membrane fusion has been reached. However, the complexity of fusion, particularly in biology, leaves much to be explained and key aspects are still debated.

1.4.1 CLOSE PROXIMITY

It is now widely believed that while the details of fusion may differ, there are general mechanisms by which two disparate membranes fuse. First, the membranes must be bought into close proximity. Neutral lipid bilayers in equilibrium can be as close as 2 nm[76]; however this is not sufficient for fusion to occur. In order to fuse, the repulsion between two membranes must be overcome; requiring energy. The fusion site itself must have an inter-membrane distance of less than 1 nm[77]. In some pure lipid systems and cells this can be achieved by dehydrating the contact area by the addition of PEG (Polyethylene Glycol)[78, 79]. Biological membranes contain proteins of many kinds as well as charged lipids. The additional steric hindrance and electrostatic repulsion increases the equilibrium inter-membrane distance and cellular membranes are typically 10-20 nm apart[71].

It is widely accepted that proteins play a key role in decreasing the membrane separation prior to fusion events. In the case of synaptic exocytosis, Rab GTPases and Rab effectors are thought to initially tether the vesicle to the plasma membrane[5]. It is hypothesised that SNARE proteins then bring the membranes closer still, providing energy to overcome repulsion. The t-SNARE proteins (Syntaxin and SNAP-25 for synaptic exocytosis) form an initial, intermediary complex[80, 81]. With the vesicle tethered to the target, the N-terminus of the v-SNARE (VAMP) interacts with that of the intermediary complex[82]. VAMP binds to a groove on the intermediary complex surface, forming the trans-SNARE complex. This coiled-coil SNAREpin zips from the N-terminal regions towards the C-terminus (and therefore the transmembrane domains); bringing the membranes close together[59, 83, 84]. The stability of the SNARE complex (even as the *trans*-complex) is thought to be sufficient to overcome repulsion and a single SNAREpin may provide enough energy to merge the proximal leaflets (the outer monolayer of each membrane)[85]. It is thought however that more than one complex is involved at each fusion site. Indeed, it has been suggested, that a ring of SNARE complexes forms around the fusion site[86, 87]. The number of SNARE complexes required has still not been proven experimentally but at least three are thought to be required for the fusion of secretory granules to the plasma membrane in PC12 cells[88].

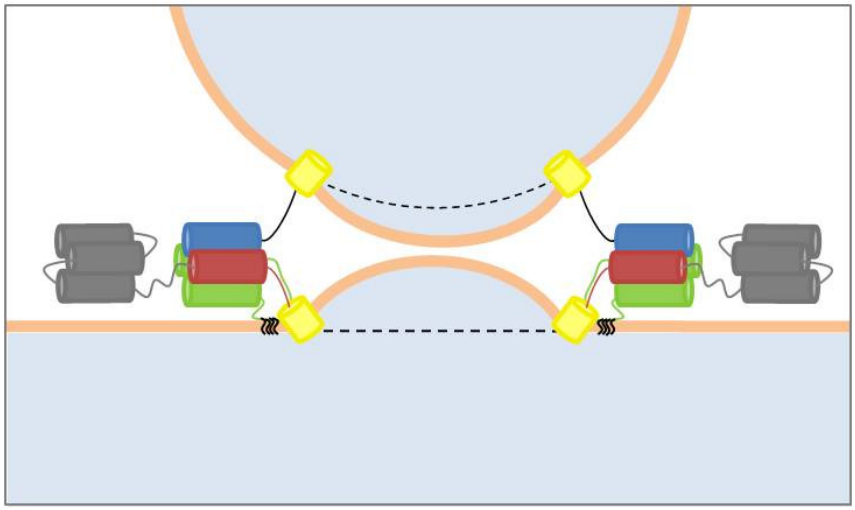


Figure 1.13. During the formation of the trans-SNARE complex, the SNARE proteins must bend. If the linker region between the transmembrane domain (shown in yellow) and the SNARE motif (red for Syntaxin and blue for VAMP) is rigid enough then the bending of the protein will apply a torque force to the membrane. This torque could force the membrane to bend locally, forming a dimple. This figure shows dimple formation on both membranes and therefore assumes that both Syntaxin and VAMP have sufficient rigidity.

When a *trans*-SNARE complex is fully formed the core SNARE complex lies between the two membranes and each SNARE protein is bent between the SNARE motif and transmembrane domain (Figure 1.13). The cross section of the core SNARE complex suggests that it may prevent the membranes coming in close enough proximity[89]. The inter-membrane distance therefore needs to be reduced further. In both VAMP and Syntaxin the transmembrane domain and SNARE motif are separated by a highly basic linker region. Studies which lengthened this linker showed that fusion was impeded[90]. The linkers have been shown to be partially embedded into the outer monolayer of the membrane in which the protein resides[89, 91, 92] and a polybasic region within the Syntaxin linker interacts with negatively charged lipids[93]. Most recently, the *cis*-SNARE complex structure has been solved including the transmembrane domains and linker regions of VAMP2 and Syntaxin 1A (see section 1.2.3.4). This also finds that the linker regions insert into the lipid bilayer and that a continuous twisted helical structure forms from the SNARE motifs through to the membrane anchors[64]. The SNARE complex is therefore unlikely to hinder close membrane proximity as much as was once thought. In addition, as the SNAREpin complex forms the proteins are forced to bend. Modelling of the Syntaxin linker suggests that this region is rigid enough that this bending applies a torque force to the membrane causing the plasma membrane to dimple towards the vesicle[94]. As VAMP contains a similar linker it is possible that the vesicle membrane is also bent (towards the plasma membrane) as the SNARE complex forms. This dimple formation would further decrease membrane separation.

Dimpling has also been suggested for viral fusion with the HA2 ectodomain of the influenza virus hemaglutinin (HA) causing dimpling of the viral membrane towards the target[95]. The same is proposed for the fusion of paramyxovirus, except that it is the target not viral membrane which bends[96]. Evidence from inflating cells has shown the importance of dimpling in the fusion process[71], however, the role of dimpling may not be to simply bring contact sites close enough together. Bending the membrane would cause the lipids of the outer monolayer to stretch and the lipids of the inner leaflet to compress. Bending the membrane in this way is likely to increase the stored curvature elastic stress of the bilayer (section 1.3.2). This is due to the lipid molecules stretching and compressing as well as bending further away from the preferred global curvature. Dimpling of the membranes towards each other gives the proximal leaflet of each membrane a positive curvature. Evidence has shown that the presence of lipids with a preferred positive curvature (e.g. lysophospholipids) inhibit the progression to the next stage of membrane fusion[97]. The inhibition of fusion at this stage could be partly due to the stabilisation of the dimple. If dimpling functioned to bring membranes into close proximity and also increase the energy of the system, then dimples which are highly stressed will drive the system to remodel in order to lower free energy. A dimple containing positive lipids in the outer leaflet would not be as unstable as one without these lipids and therefore may not have a sufficient driving force.

1.4.2 Membrane Contact

1.4.2.1 Proteinaceous Pore

Once close proximity has been established, there are two pathways which have been suggested for membrane fusion. The first of these is that proteins form a fusion pore, allowing content mixing before lipid interaction[98, 99]. However, formation of a proteinaceous pore would not explain how protein free systems fuse and would therefore imply separate mechanisms for pure lipid and biological systems. In both *in vivo* and *in vitro* experiments it has been shown that many of the same factors affect both types of system, such as the addition of specific lipid types[71]. This would suggest that the mechanism is either the same or closely related. Evidence from both systems has also shown that lipid mixing is observed before content mixing[100-103]. This indicates that membranes merge, at least partially, before pore formation. However, it is still a possibility that the pores are too small to be measured by current methods and that pore formation somehow allows lipid exchange[71].

Evidence for proteinaceous pores comes mainly from studies of the V_0 subunit of vacuolar H^+-ATPase[99]. This subunit has been shown to complex with other V_0 subunits and lipids to form a

hexameric transmembrane complex (made up of two hexamers). Triggering by calcium ions causes conformational changes in the complex. It has been suggested that a proteolipid channel radially expands opening a fusion pore[104]. Lipids would then migrate around the channel allowing lipid mixing. This hypothesis rests mainly on evidence for calcium dependent expansion and the formation of transmembrane complexes. Chernomordik[71] comments that while a pore of this nature would account for early fusion events, it is not clear how the proteolipid channel would allow the merger of the two membranes. If fusion was to occur via a proteinaceous pore before lipid mixing, the channel would have to act as a point of lipid exchange. One hypothesis is that a fusion pore is formed in each of the membranes. The edge of each pore would be partially lined with lipid and as the two pores combine the lipids would form a continuous structure[71]. The proteolipid channel would also need to allow the fusion pore to expand. The expansion of a fusion pore of this nature would require the separation of the V_0 subunits. There is currently no proposal for how these subunits would be driven to laterally separate. In considering these mechanisms, Chernomordik also casts doubt that such a structure could provide enough energy for full fusion to occur.

1.4.2.2 Lipid Stalk

The stalk model is the second proposed pathway and no direct involvement of proteins is required in the initial membrane-membrane contact. It is also hypothesised that intermediary structures are adopted before pore formation. As such, the stalk model is applicable to both pure lipid and biological systems. This model is now perhaps the most widely accepted[105, 106] and originated from theoretical modelling and examination of protein-free lipid systems.

Membranes undergo thermal fluctuations and electroporation studies have found that the maximum energy available from these fluctuations (assuming a one second timescale) is ≈40 k_BT[107, 108]. At small inter-membrane distances it has been suggested that these fluctuations allow protrusions from the outer monolayer of each membrane to interact. This would then lead to the formation of a stalk; linking the two membranes[109]. Initial studies of this hypothesis assumed a spherical area of interaction but the energy calculations based on this showed the energy barrier to be unfeasibly high[110, 111]. Several years later the stalk structure was re-modelled in various ways including tilting lipid molecules and minimising the contact area[108, 112]. This revised stalk model (Figure 1.14) was found to be energetically possible. Assuming a stalk width of 25 nm, the energy of the revised stalk model for DOPC (1,2-dioleoyl-*sn*-glycero-3-phosphocholine) was found to be 45 k_BT. For DOPE (1,2-dioleoyl-*sn*-glycero-3-phosphoethanolamine), which has a larger negative relaxed curvature than DOPC, the stalk energy was calculated to be -30 k_BT. This is consistent with studies that show pure DOPE systems can spontaneously fuse[71]. The dramatic difference in stalk energy

depending on the lipid studied highlights the importance of the lipid properties discussed in section 1.3. The structure of the stalk is such that lipids which have negative relaxed curvature (such as DOPE) can more favourably adopt the curvature required. Studies have shown that while type II lipids in the proximal leaflets promote the transition to the next stage of fusion (hemifusion, see section 1.4.3), lipids of positive curvature inhibit it[79, 97, 113]. As well as dimple stabilisation (section 1.4.1) positive curvature would affect the energy of the stalk structure, making it unfeasibly high and therefore stalk formation unfavourable.

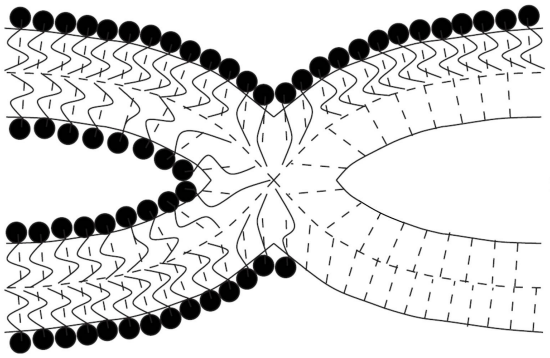


Figure 1.14. Taken from Kozlovsky and Kozlov[108] this figure shows the optimised tilt model structure of a lipid stalk. The structure was determined using a continuous approach elastic model. The stalk represents the minimal contact between two lipid bilayers and is thought to be a transient structure forming before the merging of the proximal leaflets into a hemifusion diaphragm.

Eukaryotic cells require functions to be spatially separated. The transport of content between organelles must also be tightly controlled. The complex lipid environment of biological membranes could allow the energy of a stalk structure to be equal to, or below, the energy provided by thermal fluctuations. In this situation, membranes in close enough proximity (much less than the equilibrium separation of biological membranes) could fuse spontaneously. As discussed in section 1.4.1, this could be directed by the actions of proteins. Alternatively, the energy of the stalk could be above the energy provided by thermal fluctuations. If the amount of additional energy required was not too high, membrane fusion could be perturbed until protein machinery introduced the remaining energy. This second possibility would allow even greater control of the membrane fusion process allowing proteins to bring membranes close together but only trigger fusion when it was required. It is known that vesicles in neurotransmission dock to the target membrane and fusion only occurs when triggered by an action potential (see section 1.1.2). It can be envisaged for example, that the formation of SNARE *trans*-complexes not only brings two membranes close enough together but also provides some of the energy needed, perhaps to form a stalk. The energy provided from the formation of one neuronal *cis*-SNARE complex is ≈35 k_BT[114]. While the energy released from the formation of a trans-SNARE complex would be lower it may still be sufficient, particularly if more than one SNAREpin was involved at each fusion site.

1.4.3 From Hemifusion to Full Fusion

1.4.3.1 Hemifusion

Many studies have suggested that lipid mixing occurs before content mixing[100-103] and developments have been able to show that it originates from the proximal but not distal leaflets of the membranes. These findings can be explained by the stalk model (section 1.4.2.2). The stalk is formed from only a minimal contact between the proximal leaflets which is believed to then expand into a hemifusion diaphragm[115]. The diaphragm is a single bilayer made up of the inner monolayer of each participating membrane. Its formation would cause the lipids of the proximal leaflet to mix while still keeping the content of each membrane distinct. As discussed in sections 1.4.1 and 1.4.2.2, it has been shown that the hemifusion intermediate is inhibited by the addition of type I lipids to the proximal leaflets[116-120] and there are several possible reasons for this. First, the stalk energy may be too high for a lipid composition containing a high proportion of this lipid type. Second, dimple formation would be stabilised by such lipids, giving no fusion driving force. Third, the hemifusion diaphragm is a structure where the newly merged proximal leaflets must adopt negative curvature. Therefore, the energy required to form a hemifusion diaphragm from proximal monolayers containing large amounts of type I lipids is likely to be prohibitively high. Consistent with the latter, it is has been shown that type II lipids in the outer monolayers promote hemifusion[71, 119, 121].

1.4.3.2 Fusion Pore Formation

The fusion of the distal leaflets allows content mixing to occur. The initial fusion structure is known as the fusion pore and is thought to expand out until the vesicle incorporates into the target membrane. In section 1.4.2.1 it was seen that while some evidence supports a proteinaceous pore forming after close contact, substantial evidence suggests the formation of a hemifusion diaphragm. It is still possible that a proteinaceous pore does form *in vivo*, forming after the hemifusion diaphragm[71]. As well as the evidence from vacuolar H^+-ATPase already discussed, evidence for such a pore has come from mutagenesis studies of Syntaxin[122]. Mutagenesis of the transmembrane domain showed changes in the conductance of the fusion pore. This dependence on the protein sequence was suggested as evidence for a fusion pore containing Syntaxin. Further evidence for such a pore was provided by AFM (Atomic Force Microscopy) studies where SNARE proteins on opposing bilayers were shown to cooperate to form a circular arrangement which was conductive[123].However, studies of the sequences of proteins involved in fusion, such as viral proteins, have suggested that they cannot form the types of structure associated with known channel forming proteins[104, 124].

As well as the influence seen on stalk energy and hemifusion, lipid composition has been found to affect fusion pore formation[119, 125-128]. This leads to a conclusion that the pore either contains both proteins and lipids or that the pore is lipidic. While hemifusion was inhibited by type I and promoted by type II lipids, the type I lipids added to the distal leaflets promote fusion pore formation. The affect of the lipid properties, and the capability of protein-free systems to fuse, has led to the view that a lipid-lined pore is most likely.

Modelling[113] of the hemifusion diaphragm shows the formation of a fusion pore is also promoted by lateral tension. Studies[129] of vesicles (40 nm in diameter) showed that in order for pores to form on a time-scale of seconds, a lateral tension of at least 10 mN/m was required. These studies also showed that for a set time-scale and lateral tension, the probability of pore formation increased as the area of the diaphragm was increased. The rim of the hemifusion diaphragm is believed to have a very large lateral tension[130] (≈20 mN/m). The rim is therefore considered the most likely location of fusion pore formation. A recent simulation[131] of the fusion of two protein-free vesicles also showed that membrane tension was an important factor. In this study it was observed that vesicle fusion only occurred if the membrane was stretched such that the relative area stretch was above 5%. Varying the stretch area revealed that the larger the stretch area, the shorter the time before pore formation. If we consider the stretch area to be analogous to the hemifusion diaphragm then this simulation agrees with the model previously discussed. The pore in this simulation was also shown to expand at ≈5 cm s^{-1}, in good agreement with experimental evidence[132]. The study also hypothesised that fusion is the primary pathway for the relief of membrane tension.

While proteins may not be a structural element of fusion pores, they could still have an important role in their formation. Proteins could increase the area of the hemifusion diaphragm and/or increase the lateral tension. It is likely that the membrane embedded areas of a protein would have greater influence than those areas that are not. The mutation studies of Syntaxin (discussed at the beginning of this subsection) altered the transmembrane domain. While the results were interpreted as an indication of the formation of proteinaceous fusion pores, it could have in fact altered Syntaxin's ability to affect the hemifusion diaphragm. If Syntaxin was to act on the diaphragm to increase its area or to increase the lateral tension then it would promote fusion pore formation. The mutagenesis studies could also be explained if such mutants were unable to interact with other proteins, which together act upon the diaphragm. The importance of transmembrane domains in fusion has been highlighted by studies of both viral fusion proteins and SNARE proteins where this domain was replaced by lipid anchors. The lipid anchors used spanned only the outer leaflet and in these circumstances only hemi-fused states could be achieved. These studies have

been conducted both *in vitro* and *in vivo* (reviewed in 2007[133]). They suggest that while these proteins are still able to bring membranes close enough together and aid proximal leaflet merging, the replacement of transmembrane domains prevents distal lipid mixing. The AFM study, which revealed a circular array of Syntaxins, could indicate that SNARE proteins form a ring of SNARE complexes through homotypic interactions, perhaps at the rim of the hemifusion diaphragm. The torque applied to the membrane by a ring of SNARE complexes, due to complex formation; (see discussion of dimpling in section 1.4.1) could stress the diaphragm sufficiently to induce pore formation. Rather than a proteinaceous pore, mutagenesis of the transmembrane domains could prevent the formation of a ring of SNARE complexes; reducing the induction of membrane tension and consequently inhibiting fusion.

As well as dimpling, the transmembrane domains could increase the lateral tension of the surrounding lipid bilayer due, in part, to hydrophobic mismatch. This results from a discrepancy between the length of the hydrophobic region of the protein anchor and thickness of the lipid bilayer. Lipid molecules would need to stretch and compress to accommodate the protein region; increasing the stress of the bilayer. This could further promote fusion pore formation. This would be particularly important in an area already under high tension, such as the diaphragm rim. It has been shown, by the use of synthetic peptides in *in vitro* studies[134] (of the same sequence as the transmembrane regions of VAMP and Syntaxin), that membrane fusion can be promoted by these regions alone.

1.4.4 The Fusion Role of SNARE Proteins, A Section Summary

The previous subsections have suggested roles that the SNARE proteins could play in the facilitation of membrane fusion (Figure 1.15). SNARE proteins form complexes which span two membranes. Close contact can be seen in two different stages. The initial contact where a vesicle tethers to the target membrane is not close enough for fusion to occur. SNARE complex formation would pull the two bilayers together and the complex is thought to be stable enough to overcome the repulsion between the membranes at such short inter-membrane distances. The SNARE proteins may further facilitate this close contact through dimpling the membranes as the complex forms. Dimpling the membranes would increase the stored energy of the membranes driving the fusion mechanism forward. Hemifusion results from the fusion of the outer monolayers, most likely via a transient stalk structure. The transmembrane domains of the SNARE proteins may help the diaphragm to expand and/or apply additional tension; pulling open a pore as the SNARE complex folds. Whether the SNARE proteins are enough on their own to induce fusion however is discussed in section 1.6.

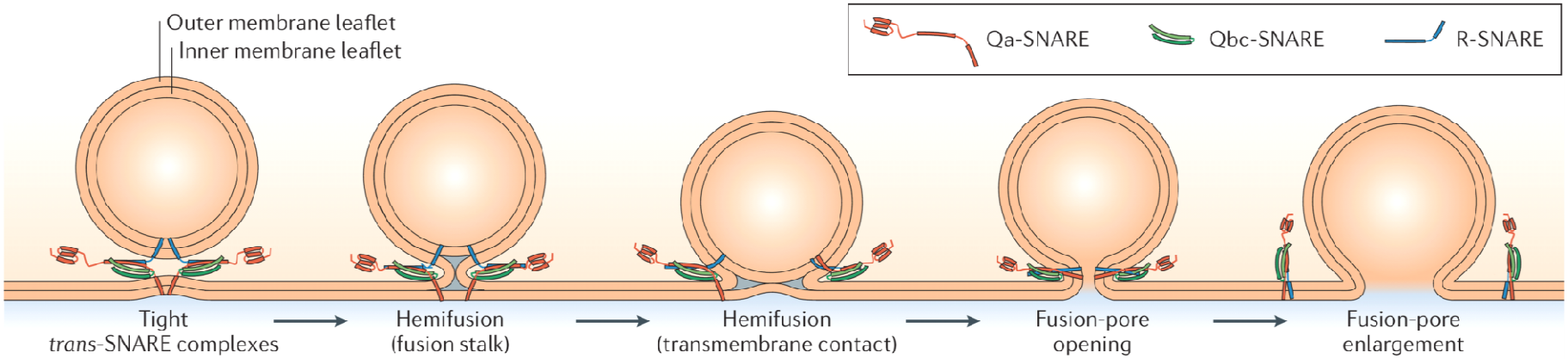


Figure 1.15. Taken from R. Jahn[16] this figure shows stalk model fusion of a vesicle to a membrane facilitated by SNARE proteins. The formation of a trans-SNARE complex (SNAREpin) brings two bilayers into close proximity. The inter-membrane distance is reduced further as the complex bends causing the membranes to dimple. A transient stalk structure is formed as point-like protrusions from each proximal leaflet interact. The stalk expands into a hemifusion diaphragm which then ruptures to form a fusion pore. Complete fusion results from expansion of the pore and the SNARE complex is rearranged into its most stable form; the cis-complex.

1.5 THE COMPLEXITY OF MEMBRANE FUSION *IN VIVO*

During the discussion of membrane fusion in section 1.4, possible roles for the SNARE proteins were proposed. While decades of study have placed SNARE proteins firmly in a centrally important role, their exact contribution has yet to be established. They may undertake one, some, or all of these roles and the difficulty in deciphering their role arises from the myriad other components involved in the *in vivo* fusion process. There are clear indications that lipids also play a role in fast and efficient fusion (this evidence has come from *in vitro* models or lipid doping of cells). *In vivo,* membranes are made up of a complex mixture of lipids containing hundreds or possibly thousands of different types and the leaflets are also asymmetric. For fusion there is then also an asymmetry in the lipid composition of the membranes undergoing this process. In the case of synaptic fusion there is further complication as it is a regulated exocytosis event and therefore fusion only occurs once a signal has been received (in this case a calcium influx). This increases the number of proteins required in the mechanism further. Evidence also points to two types of fusion process being employed[135]. The first, known as full fusion sees a fusion pore open fully and the vesicle incorporated into the plasma membrane. The second is a brief opening of a pore allowing some content to be released before the pore closes and the vesicle undocks. In this kiss-and-run process a vesicle can fuse in future fusion cycles without the need to be refilled first. SNARE proteins are therefore not the only proteins involved in the fusion process. From *in vivo* studies it is difficult to unravel the role of each protein as most show at least some interdependency and fusion is mostly a cyclic process. The additional proteins include Synaptotagmin and NSF (N-ethylmaleimide Sensitive Factor) which have been identified as key components of fusion. As with the SNARE proteins the role of these proteins is still under investigation. A brief description of these proteins and their proposed role is given in this section but most are thought of as regulatory or chaperone proteins.

1.5.1 RAB PROTEINS

When GDP-bound (the inactive state) these small GTPases are cytosolic but when GTP bound (the active state) they become bound to the membrane. They are compartment specific and over 60 isoforms have been found to be expressed in mammals[136]. These proteins are involved in tethering vesicles to target membranes through the recruitment of tether effectors. Rabs have also been shown to interact with SNARE proteins in some cases and this is believed to increase fusion specificity and fidelity[137, 138]. Rab proteins can recruit many different effectors for jobs such as cargo sorting and vesicle tethering. It is believed that the Rab proteins are instrumental in allowing fusion to proceed efficiently, creating the ideal local environment.

1.5.2 SYNAPTOPHYSIN

Synaptophysin is a membrane protein anchored by four transmembrane domains[139]. This protein resides on synaptic vesicles with both its N and C terminal regions facing the cytoplasm. It has been found to bind to VAMP[135, 139-142] and may have a role in targeting VAMP which has been newly synthesised[143]. The complex has also been shown to be dependent on cholesterol as it only forms when a high concentration of cholesterol is present[144]. The Synaptophysin-VAMP complex makes VAMP unavailable to bind to the intermediary t-SNARE complex and Synaptophysin is therefore believed to act as a regulatory protein[135, 141, 142]. Synaptophysin knock-out mice did not show significant changes in levels of neurotransmission[145]. It is thought that this could either be an indication that the role of Synaptophysin is minor or just reflects the ability of homologues (such as Synaptoporin) to substitute in its absence[26, 146].

There is some evidence that Synaptophysin can form channels in membranes[147]. Purified Synaptophysin was reconstituted into lipid bilayers and voltage-sensitive channel activity measured. This recorded an average conductance of 150 ps. Within this study cross-linking and sedimentation experiments also revealed that Synaptophysin forms hexameric homo-oligomers. Based on these findings it was suggested that Synaptophysin is a structural component of a fusion pore. If true then multiple Synaptophysin-VAMP complexes would need to come into close contact. This would allow Synaptophysin to form the hexameric complex once it dissociated from VAMP. However, this would also mean that the protein density at the fusion site would be extremely high. Each VAMP would require the two t-SNAREs to be present in its vicinity on the other membrane and other regulatory proteins (discussed within this section) would also be present. Due to the highly regulated nature of membrane fusion, particularly of neurotransmission, it is unlikely that the close contact of multiple Synaptophysin-VAMP complexes would be sufficient to dissociate them. Therefore, additional protein machinery would be necessary but no candidates for such a role have so far been identified. Additional machinery would also be required to direct the coming together of multiple Synaptophysin-VAMP complexes. The affinity of the Synaptophysin proteins would have to become greater for other Synaptophysin proteins than VAMP, in order to promote the formation of the Synaptophysin homo-complex over the Synaptophysin-VAMP complex. No studies have shown such an affinity. Together these arguments cast doubt on the involvement of Synaptophysin in a proteinaceous pore structure

1.5.3 SM PROTEINS

The SM proteins (the Sec1/Munc18 proteins) are thought to regulate membrane fusion through interactions with Syntaxin. There are seven members of the SM protein family currently known in vertebrates[81]. Munc18-1 (the SM protein linked with regulated exocytosis and therefore neurotransmission[26]) has been shown to form a tight 1:1 complex with the closed conformation of Syntaxin[148, 149]. In this complex, unlike in the SNARE complex, the linker region of Syntaxin is structured and suggests a stabilisation of the closed Syntaxin conformation. This prevents formation of the t-SNARE intermediary complex. The mutation of Munc18 to prevent Syntaxin binding showed that secretion in neuroendocrine cells was stimulated[150]. Munc18 knockout mice had only 30% the normal Syntaxin levels and died immediately after birth. Despite this, SNARE complexes were still able to form and Syntaxin was targeted correctly. However, a build up of undocked vesicles was seen[151]. This and recent studies[152] showing direct binding of SM proteins with Rab tethering complexes suggests that SM proteins are involved in the tethering of vesicles to the target membrane. Further evidence suggests that SM proteins increase the specificity of membrane fusion. Liposomes containing Syntaxin 1 and SNAP-25 were able to bind to five different v-SNAREs in an *in vitro* study. Addition of Munc18-1 allowed fusion only between the t-SNAREs and VAMP2 or VAMP8[153, 154].

1.5.4 MUNC13

This 200 kDa protein is thought to catalyze Syntaxin's change in conformation from the closed to open state through its interaction with the open confirmation (though there is currently no conclusive biophysical proof)[81]. Munc13 is believed to play an important role in priming vesicles, taking them from the tethered vesicle population to the release-ready population[17]. Inactivation of Munc13 in several organisms led to the abolishment of both spontaneous and triggered fusion[155]. Munc13-1 has been shown to contain a C1 calcium binding site which binds to DAG (Diacylglycerol)[156]. Munc13 binds to the H_{abc} domain of Syntaxin both individually[157] and as part of the intermediary t-SNARE complex[158]. The Syntaxin binding site of Munc13 and Munc18 overlap[136] suggesting they may have a mutually exclusive relationship. While Munc18 is not able to bind to the open conformation of Syntaxin, mutation of the linker region of Syntaxin (which prevents the closed confirmation from forming) also negates the need for Munc13[159]. Other proteins bind to Munc13 including Rab3 and its tether effector RIM1[160]. Munc13 may be able to bind to these two proteins at the same time as Syntaxin[135]. It is therefore proposed that an interaction cascade between the tethering proteins and Munc13 controls the switch of Syntaxin from its closed, inactive state and its open, active state[26].

1.5.5 TOMOSYN

Tomosyn is a soluble protein which is believed to act as a placeholder. As it contains an R-SNARE motif, it is able to form a complex with the t-SNAREs Syntaxin and SNAP-25[161, 162]. This complex is comparable in many ways to the neuronal SNARE complex though the surface residues differ[81]. Tomosyn occupies the same area of the complex that VAMP would. Tomosyn is therefore able to compete with VAMP, negatively regulating exocytosis. It has also been shown to dissociate Munc18 from Syntaxin[161] and therefore may be part of the machinery progressing Syntaxin from the closed to open conformation. Tomosyn appears to bind to the t-SNARE complex in a kinase dependent manner i.e. it is controlled through phosphorylation[163, 164].

Another protein similar to Tomosyn is Amisyn. This protein also forms a complex but it binds to Syntaxin specifically. Like the Tomosyn complex the Amisyn containing complex is non-fusogenic and so this protein also negatively regulates exocytosis[165].

1.5.6 NSF AND SNAP

Identified by Glick and Rothman in 1987[166] n-ethylmaleimide sensitive factor was one of the first proteins shown to be important in vesicle fusion[167, 168]. When NSF is alkylated by N-ethylmaleimide it is inactivated and it was found that vesicles were able to dock to the target membrane but fusion did not occur. It was for this reason that NSF was at first thought to be a fusion protein itself. NSF was shown to move between the cytosol and membrane and is widely distributed along the transport pathways[51] but it is incapable of binding to membranes on its own[169]. NSF has since been recognised as essential for the fusion process due to its involvement in the recycling pathways, rather than as a fusion protein itself.

In 1990 α-SNAP (Soluble NSF-attachment Protein) was found to bind to both NSF and membranes[170]. It was also observed that NSF bound to α-SNAP only when it was bound to a membrane[170, 171]. NSF does not bind directly to α-SNAP, requiring the presence of Syntaxin[81]. In addition, three SNAP molecules bind to the periphery of the SNARE complex (though only in its *cis* form)[172]. Through this the N-terminal domain of NSF is able to interact with the SNARE complex. The NSF-α-SNAP-SNARE complex is sometimes referred to as the 20S complex. The 20S complex is believed to be involved in SNARE recycling. Once membrane fusion is complete the extremely stable *cis*-SNARE complex is formed and in order for recycling to occur it must disassemble into its monomeric parts. As an ATPase, NSF provides the energy required to do this through the hydrolysis of ATP (Adenosine Triphosphate). The ATP hydrolysis also disassembles the 20S complex[31, 173]. As a hydrophilic protein, it is hypothesised that NSF interacts with the zero layer of the SNARE complex

(see section 1.2.3.4). A rotational force is appied to the complex, untwisting the coiled coil structure[54, 56]. Mutation of the conserved glutamine of Syntaxin (which contributes to this layer) results in only partial disassembly of the *cis*-SNARE complex[174]. ATP hydrolysis also results in a conformational change of Syntaxin, causing α-SNAP and VAMP to be released from the complex[175].

Regulation of this process is believed to come from various sources. Phosphorylation of Ser237 in NSF appears to affect its binding affinity for the α-SNAP-SNARE complex. Mutation of this residue to mimic phosphorylation (S237E) showed no binding of NSF to the complex, whereas another mutation (S237A; which does not mimic it) did still result in the formation of the 20S complex[176]. The function of NSF, and therefore exocytosis as a whole, is also regulated by nitrosylation[177, 178]. Further regulation is provided by β-SNAP (a protein highly homologous to α-SNAP) which is selectively expressed in neurons and is thought to regulate α-SNAP[179, 180]. Another homologue (γ-SNAP) does not bind to SNARE proteins but does bind to NSF and it is possible that this homologue acts as a recycling inhibitor by reducing the availability of NSF for formation of the 20S complex[181].

1.5.7 Complexin

Complexin (also known as Synaphin) appears to be essential for calcium dependent synaptic vesicle release, despite having no apparent calcium binding site[81]. Lack of Complexin increases the amount of spontaneous fusion but significantly reduces calcium dependent fusion[182, 183]. It is believed that Complexin may have a dual role, both stimulating and inhibiting fusion[136]. This 15 kDa soluble protein co-localises with Syntaxin and SNAP-25[26] and binds to SNARE complexes with high affinity in an anti-parallel manner[184]. It binds to the surface groove between VAMP and Syntaxin and is thought to stabilise intermediates such as the t-SNARE complex. It has been found that Complexin cannot bind to the Tomosyn-t-SNARE complex[185]. Evidence suggests that Complexin works together with another protein (Synaptotagmin; discussed in section 1.5.8) to act as a clamp, preventing the formation of the cis-SNARE complex[184, 186]. Calcium triggering in the presence of Synaptotagmin could release Complexin allowing fusion to occur[136]. Complexin has also been shown to facilitate interactions between the transmembrane domains of VAMP and Syntaxin[187] and this may aid the transition of the SNARE complex from its *trans* to *cis* conformation.

1.5.8 SYNAPTOTAGMIN

Sixteen Synaptotagmin (Syt) proteins have been identified in vertebrates[136] with SytI predominantly expressed in neuronal cells[188]. It is a small glycoprotein (65 kDa) which resides on synaptic vesicles[189, 190] and is anchored to the membrane by a single transmembrane domain. It has two calcium binding sites C2A and C2B[191] with SytI showing low affinity binding[192, 193], but is known to interact with calcium channels where ion concentrations are highest[136, 194]. Syt is essential for calcium triggered release and SytI knockout mice showed defective synchronous release but also increased spontaneous (asynchronous) release[195]. This suggests a role for Syt as a calcium sensitive regulator but also a negative regulator of spontaneous fusion[26]. Syt is able to interact with Syntaxin, SNAP-25, the t-SNARE intermediary complex and the SNAREpin complex[25, 31, 196-200]. It is believed that this interaction controls the development of the SNARE complex, holding a vesicle in a fusion-ready state[81] and allowing the full SNARE-complex to form only with the action potential.

The two fusion pathways of kiss-and-run or full fusion require different fusion pores. Kiss-and-run requires only small pores which are transient while full fusion requires pores to exist over longer time scales and to expand so that the vesicle and plasma membranes fully merge. Over-expression of SytI has been shown to increase pore opening and dilation times[201-203] and is therefore believed to be involved in determining the type of fusion event [204].

Syt also binds to acidic lipids, such as phosphatidylserine (PS), and also to PIP_2 (phosphatidylinositol 4, 5-bisphosphate)[190, 205-209]; but only in the presence of calcium. PS is present in high concentrations in synaptic vesicles (12 mol% of total lipid composition[189]), which also contain 1.5-2 mol% phosphatidylinositol lipids. PiP_2 is in high abundance in microdomains within the plasma membrane[210] and has been found to be an essential component of secretory vesicle fusion[209]. When bound to the SNARE complex the calcium and phospholipid binding sites of Syt are orientated away from the complex[81]. The interaction of Syt with acidic lipids leads to the insertion of four hydrophobic loops to a third of the depth of a single monolayer[211]. This would cause the bilayer to want to adopt a positive curvature (due to the area difference between the two monolayers caused), promoting fusion pore formation (discussed in section 1.4.3). Induction of positive curvature would be unfavourable for PS and PIP_2 as they are type II lipids. Insertion of Syt may therefore increase the stored curvature elastic stress of the system, driving fusion forward. High concentrations of PS (30%) also interfere with the Syt-SNARE complex[212]. Upon calcium release it is proposed that the C2A and C2B domains cooperatively bind calcium, Syt then penetrates the membranes through interaction with lipids and the Syt-SNARE complex dissociates allowing the SNARE complex to fully fold.

1.6 MINIMAL FUSION MACHINERY

The myriad factors that affect membrane fusion make pinpointing exact roles for the different components difficult *in vivo*. Assays employing liposomes containing purified protein allow the nature of the proteoliposomes to be controlled. The first SNARE protein-containing assay of this type was developed by Rothman and colleagues in 1998[38] and the removal of proteins and simplification of the lipid environment has provided much useful data since. In particular this method has been used in the determination of the minimal requirements for fusion, at least in terms of proteins. In the Rothman assay it was shown by lipid mixing that liposomes containing co-expressed Syntaxin and SNAP-25 were capable of fusing with liposomes containing VAMP. As lipid mixing cannot confirm full fusion, the assay was later repeated using ^{33}P labelled DNA (Deoxyribonucleic Acid) duplex formation as this reports content mixing[213]. The ability of the SNARE proteins to induce fusion was seen as evidence that they are the minimal machinery for fusion. This proposal has led to much debate[214] and criticism of the results from this type of assay[215].

Many *in vitro* assays of this type use high SNARE protein densities in order for fusion events to occur. This is particularly seen with regards to VAMP where the liposomes used have often contained as many as 750 copies of the protein in an SUV[38, 216] (Small Unilamellar Vesicle; typically 50nm diameter). This gives a protein: lipid ratio of approximately 1:33 (based upon the area of a PC (Phosphatidylcholine) headgroup of 63 $Å^2$ [217]). Physiologically, studies have shown 70 copies of VAMP are present in synaptic vesicles (also approximately 50nm diameter)[189] which is a protein: lipid ratio closer to 1:350. However, VAMP accounts for approximately only 9% of the total protein contained in a synaptic vesicle[189]. High protein densities, particularly of Syntaxin, have been shown to cause vesicle leakage. It is therefore thought that the results seen where such densities have been used may be due, more to the disruption of the lipid bilayer than the functional role of SNARE proteins. The fusion of proteoliposomes is still viewed by some as a leaky process whereas physiologically this is not a leaky event[215]. It is therefore questioned whether SNARE proteins are sufficient for fusion to occur in a physiologically relevant way.

Perhaps the most widely expressed criticism is of the time scales needed for fusion events to occur. In these assays, fusion events are often infrequent and take several minutes. The fastest *in vitro* assay measured fusion rates of 25 ms[218]. The fusion of VAMP proteoliposomes with a planar lipid bilayer containing the t-SNAREs Syntaxin and SNAP-25 was monitored using fluorescent lipid probes. Docking and full fusion were distinguished by monitoring the diffusion of the probe into the planar lipid bilayer. This assay showed that for fusion to occur both v- and t- SNAREs had to be present. Another assay, by Bowen[219], monitored fusion of SNARE containing membranes using single

molecule detection of content mixing and showed fusion rates of approximately 100ms. While these rates are a significant improvement on earlier assays they are still more than 40 times slower than physiological rates. However, it should be taken into account that these assays are simplified models and therefore do not contain regulatory proteins or complex lipid mixtures. Regulatory proteins, as discussed in section 1.5, usually leave vesicles in a fusion ready state with complexes that are already partially assembled. Physiological rates of fusion are therefore measured from a different starting point from the fusion observed in the *in vitro* assays. As a result it is perhaps overly simplistic to compare the fusion rates so directly. In a SNARE proteoliposome no Munc13, for example, is present (unless purposely added) to keep Syntaxin in its open confirmation or Tomosyn to stabilise the t-SNARE intermediary complex. The significance of this lack of additional, facilitating proteins is highlighted from studies showing that removal of the H_{abc} domain of the protein Sso1p (which belongs to the Syntaxin subfamily) greatly increases the number and speed of fusion events in these *in vitro* assays[220]. Removal of this domain prevents the protein adopting a closed confirmation. The need for Munc13 in this situation is therefore removed and Sso1p is made available to form a SNARE complex.

It is still unclear whether SNARE proteins are sufficient for full fusion or whether on their own they are capable of only docking and fusing vesicles to a hemifused state. Results from *in vitro* assays are conflicting. Some suggest full fusion can be seen[216, 221], while other studies, using PEG to bring SNARE vesicles together, suggest SNAREs are insufficient[222]. Studies of yeast SNARE proteins in a simple lipid model of only two or three lipid components suggested that the vesicles could only reach hemifusion[223]. Some studies of vacuole fusion, in which SNARE proteins are in their native environment, have also shown SNARE proteins incapable of passing hemifusion[224]. However, studies of cells with inverted (or 'flipped') SNAREs (engineered SNARE proteins which are embedded in the outermost cell membrane but stick out into the extracellular space) have shown both full and hemi-fusion occurring[225].

Evidence has been gathered from *in vitro* studies that fusion is able to occur in the absence of SNAP-25[81]. This would suggest that VAMP and Syntaxin are sufficient for membrane fusion and would cast doubt on the role of the SNARE complex. This is not to suggest that they would be sufficient physiologically but only in simple, model systems. In these assays high protein densities were required and therefore, as already discussed, this result may only reflect membrane disruption. *In vivo* studies show that changes to SNAP-25 affect neurotransmission. SNAP-25 knock-out mice died before birth and while brain structure was considered normal, other morphological deformities were seen[226, 227]. *In vivo* assays, which used neurotoxins that cleave SNAP-25, showed a reduction in

calcium sensitive fusion though spontaneous fusion was unaffected[228, 229]. SNAP-25 has been shown to have some interaction with Synaptotagmin and it is likely that SNAP-25 must be present for a fusion event triggered by calcium to occur[230].

VAMP 2 knock-out mice died immediately after birth[231]. A slight decrease in spontaneous fusion was seen while the calcium dependent fusion events were reduced 100 fold. A further study[232] showed that VAMP deletion affected fast recycling of synaptic vesicles as its absence delays the replenishing time of vesicle pools. The synaptic vesicles of these VAMP knock-out mice also had altered size and shape. Compared to wild-type vesicles the mutant vesicles were heterogeneous in size, 30% larger on average and were more elongated (20% wild type vesicle had an asymmetric ratio of >1.2 compared to over 50% of mutant vesicles). A role for SNARE proteins in coat assembly (see section 1.1.1) has been suggested for several years[233]. VAMP deletion shows the same affect on vesicle shape as mutation studies on Clathrin adaptor proteins[234, 235]. As will be discussed in section 1.7.1, the coat protein complexes are considered to be instrumental in the induction of local membrane curvature. These *in vivo* studies suggest that VAMP may not be essential for fusion events to occur but that it is important for endocytosis and recycling.

In considering whether SNARE proteins are the minimal machinery required for fusion it is important to define the system being examined. Not all fusion event pathways are as highly regulated as neurotransmission. In these cases, given the evidence from *in vitro* assays, SNARE proteins may be sufficient for fusion with additional proteins providing other input such as tethering and specificity. The neuronal SNARE proteins are a special case within the SNARE super-family. SNAP-25 is one of the few SNAREs to have a lipid anchor rather than a transmembrane domain and the SNARE complex only requires three individual proteins to form due to the dual contribution of SNAP-25. As *in vivo* synaptic fusion requires a calcium trigger, it can be argued that the minimal machinery must include all the proteins necessary for membranes to fuse in response to a calcium influx. In *in vitro* assays containing just the SNARE proteins some studies suggest that addition of calcium was not necessary for fusion to occur[218, 219]. This is thought to be because SNARE proteins do not bind to calcium and the assay lacked Synaptotagmin, a protein essential for calcium sensitive fusion. Some assays have shown an increase in fusion with the addition of Synaptotagmin and calcium to the assays[236]. Mutations of Synaptotagmin to reduce its affinity to SNARE proteins were shown to decrease lipid mixing[237]. However other assays that have been conducted have shown that Synaptotagmin incorporation showed no affect on fusion rates whether calcium was present or not[219].

The differing opinions on the definition of what a minimal machine is can lead to confusion when comparing the views of different research groups. Some consider the SNARE proteins to be merely

the motor for fusion, while other proteins are needed to correctly direct the energy provided by SNARE complex formation. Recent evidence suggests that the stabilisation energy of SNARE complex formation is ≈35 k_BT, which is one of the highest protein folding energies recorded[114]. However, Sudhof[215] comments that SNAREs may be by themselves "powerful but hapless". The most conventional definition is that the minimal machinery and therefore the fusion proteins must be "critical for fusion in a biologically relevant context and [is] sufficient to promote the merger of both the outer and inner leaflets of membranes in model systems". From this definition it is largely accepted that SNARE proteins constitute the minimal fusion machinery[238].

Clearly the determination of the minimal machinery of fusion does require further study. Most importantly, future studies need to be conducted to determine unambiguously whether SNAREs are capable of inducing full fusion or only hemifusion. It may be that the minimal machinery will not be the same for all SNARE systems, especially in the case of the neuronal SNAREs[230]. *In vitro* and *in vivo* studies often give conflicting data. *In vitro* assays may currently be too simplistic to reliably determine the minimal machinery. *In vitro* assays exploring this question are still predominantly focussed upon protein needs and do not fully consider the contribution of the lipid environment. Equally, *in vivo* data may be misleading due to the cyclic nature of fusion pathways and protein redundancy may lead to homologue proteins replacing mutated or knocked-out proteins allowing functions to occur, at least in part.

1.7 Protein-Lipid Interplay

Much of the doubt that SNARE proteins are the minimal fusion machinery has centred on *in vitro* studies. In these studies fusion was seen to be leaky and/or slow. Leaky vesicles are seen particularly at high protein concentration and as such, suggest that the SNARE proteins may influence the lipid bilayer in which they are contained. Membrane fusion *in vivo* is usually described in a proteocentric manner, despite the stalk model involving lipid remodelling[53]. Proteins are responsible for bringing membranes into close proximity, providing energy, stabilising intermediates and regulating the process. This gives the impression that lipids are passive elements. However, as has been mentioned throughout the introductory sections, lipids have been shown to affect fusion rates and components.

Biological membranes contain hundreds of lipids with different properties. Each of these components will contribute to the energy of the membrane; the membrane will therefore occupy the state giving the lowest global energy. Most importantly, bilayers *in vivo* are asymmetric and undergo dynamic changes in composition. The dynamic change in lipid composition is partly due to cellular functions that metabolise lipids. These changes in lipid species would alter the energy of the membrane. While a global property, if compositional change was fast enough the energy of the membrane would not dissipate into the entire membrane before a particular process occurred. This would result, at least fleetingly, in a local energy difference.

1.7.1 General Mechanisms of Interplay

Protein-lipid interplay is an accepted concept in several areas of molecular biology including the budding of a vesicle from a donor compartment. There are thought to be two main mechanisms (Figure 1.16) by which proteins exploit lipid properties causing local changes in membrane curvature (this has been discussed at length by Zimmerberg and Kozlov[239]). First, some proteins and protein complexes are able to bind to membrane surfaces imposing curvature upon it. This method, known as the scaffold mechanism, requires the protein moiety to be sufficiently rigid for imposition of its curvature and to have enough binding affinity to interact with the polar lipid headgroups. The energy to bend a membrane must also be lower than the energy required for the protein to bind to the membrane. Second, proteins inserting areas of their sequence into one membrane leaflet would cause a local membrane deformation. This would induce a local membrane stress and/or cause a redistribution of lipid molecules (on a time averaged basis) causing a change in the local lipid composition. This is called the local curvature method.

Dynamin and BAR (Bin, Amphiphysin, Rvs) domain containing proteins such as Endophilin[240] act as scaffold proteins to promote the formation of cylindrical membrane shapes[71]. The BAR domain has a concave face containing 12 hydrophobic amino acid residues[241] which show a strong interaction with lipid headgroups[242]. Upon binding to this face membranes are shown to adopt the curvature of this banana shaped domain. Other proteins thought to follow the scaffold mechanism include the coat proteins Clathrin, COPI and COPII[243] mentioned in section 1.1.1. Local curvature induction is seen from proteins such as Epsin[244, 245], Amphiphysin[241] (which contains a BAR domain) and Sarl[246]. All work through the insertion of an amphipathic helical domain into a single membrane leaflet. Sar1 is a core protein of the COPII coat assembly. This small GTPase is thought to insert its N-terminal α-helix into a monolayer, thereby deforming the membrane.

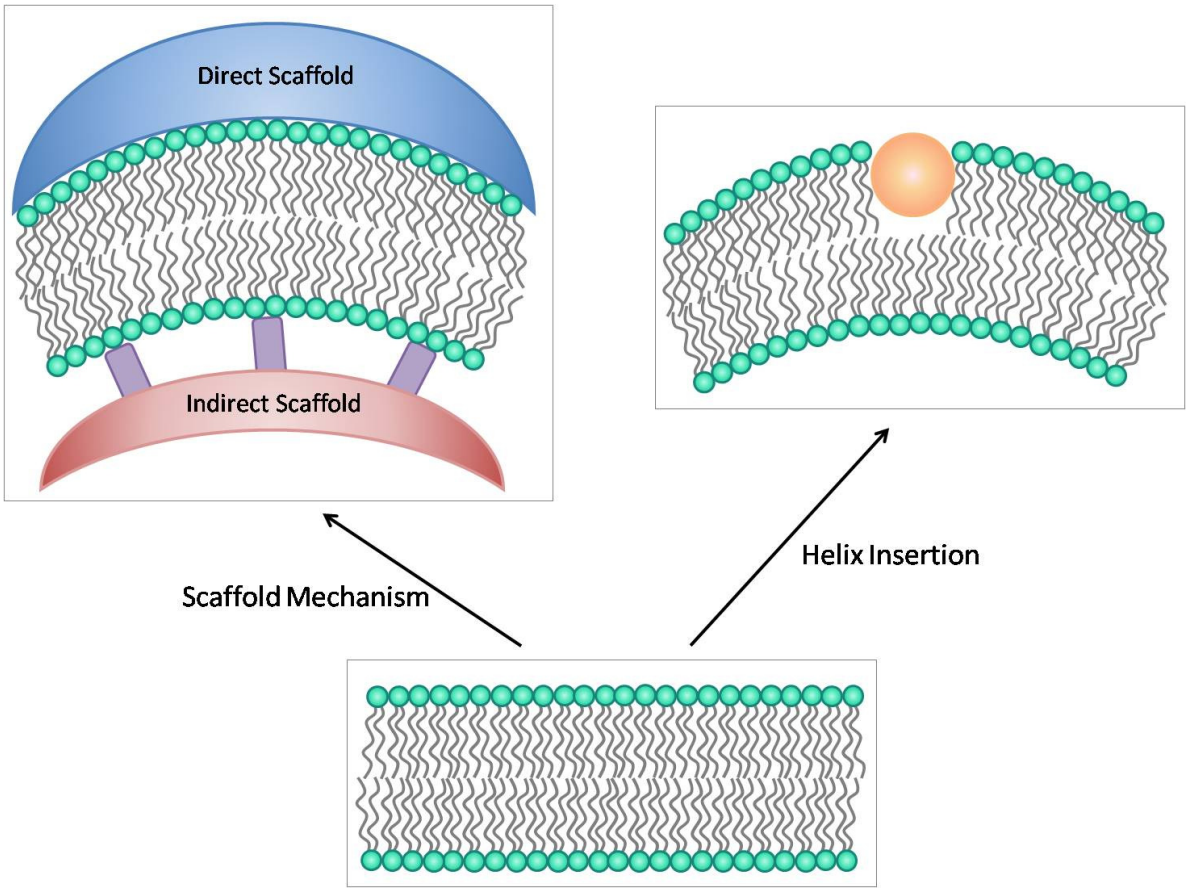


Figure 1.16. Proteins are capable of altering the local environment of lipid molecules by inducing curvature. The direct scaffold mechanism sees protein domains, such as BAR domains, bind directly to the membrane. Proteins which bind to the membrane via accessory proteins induce curvature by the indirect scaffolding mechanism. Proteins can also insert into the membrane. Insertion of an amphipathic helix into one leaflet induces curvature caused by area mismatch between the two monolayers.

In vesicle budding, Epsin and Clathrin are thought to cooperate to deform a local patch of membrane[239, 244]. Epsin induces curvature locally which is then stabilised by Clathrin. Upon polymerisation of Clathrin to form a caged complex, PIP_2 may be hydrolysed[239]. Epsin has a strong binding affinity to PiP_2[245] and is thought to bud vesicles from membrane patches rich in this lipid. Upon PIP_2 hydrolysis Epsin dissociates from the vesicle. At this point the spontaneous curvature of the membrane changes but the vesicle is unable to compensate for this change through the flow of lipids from/to the donor compartment. It is believed that this triggers coat disassembly. During the budding of a vesicle from the donor membrane, a neck is formed; this neck is then sealed, causing fission. Dynamin, Amphiphysin and Endophilin have all been shown to be important in this process and believed to induce and stabilise the formation of this neck[239-241].

1.7.2 SNARE-Mediated Fusion

1.7.2.1 Controversy

It is first important to note that the majority of evidence linking SNARE proteins to lipid properties comes from methods thought to investigate lipid rafts. There are two main methods of investigation and both are considered highly controversial. The idea of lipid rafts comes from the concept that membranes are not passive structures in which proteins diffuse but laterally highly organized[247].

The first method is known as DRM (Detergent Resistant Membrane removal) and uses detergent extraction of membrane components. It was considered that patches high in cholesterol and sphingolipids exist *in vivo*. These patches are thought to be so tightly packed that they would resist dissolution in detergent preparations. It was therefore thought that membrane patches retrieved by this method would be a reflection of physiological membrane patches. Proteins associated with these extractions would show a high affinity for these patches *in vivo*. The data that has been obtained from this method often shows large variations and conflict. This is partly due to differences in the extraction process, ranging from the use of different detergent: protein ratios to whether or not detergent was used in the size separation gradient. A consensus has since been reached that these membrane patches are not physiologically relevant and therefore while the method may prove useful, interpretation of data must be treated with extreme care[53, 247, 248].

The second method is the depletion of cholesterol, usually *in vivo*. Findings from *in vitro* studies that cholesterol and sphingolipids segregate into liquid-ordered phases[249] were thought to be evidence that these phases existed physiologically. This is now regarded as untrue[247]. Nonetheless, while not in the form of a liquid-ordered phase, it is still believed patches containing high concentrations of cholesterol and sphingolipids do exist. The effect of disrupting these patches has therefore been

investigated. This method uses various agents to deplete cholesterol including inhibiting the sphingolipid metabolism process in cells or by addition of β-cyclodextrin[248]. Cholesterol is an important molecule in many cellular processes and therefore changes seen in fusion pathways as a result of its depletion may not be directly related. It is not currently understood what affect cholesterol depletion has on cytoskeletal processes, for example. As with DRM, it is therefore unclear how results from studies employing this method should be interpreted. An alternative method would be to deplete the sphingolipids as they are considered less universally important, but this is not currently possible[247].

It is also worth noting here that the definition of a lipid raft was not universal and caused problems in comparing studies from disparate research groups. In the Keystone Symposium on Lipid Rafts and Cell Function a robust definition was decided upon. Lipid rafts have been renamed membrane rafts to reflect protein involvement. Membrane rafts are "10-100nm in size and are heterogeneous structures displaying highly dynamic sterol and sphingolipid enriched domains that have functions in compartmentalising cellular functions"[247]. Unlike lipid rafts, membrane rafts are not considered static entities and as such molecules are able to diffuse in and out of the domain. The composition of a membrane raft must therefore be considered on a time averaged basis.

1.7.2.2 Clusters

Within this subsection the results observed are mainly from studies which employed DRM and/or cholesterol depletion methodology. It is therefore unclear how physiologically relevant the finding are. Nonetheless they may prove to be a useful insight into protein-protein and protein-lipid interactions and for this reason they are still included.

Experiments suggest that Syntaxin forms clusters 170-256nm in diameter[250]. STED (Stimulated Emission Depletion) microscopy analysis of these clusters suggests that these are in fact clusters of clusters and that each individual cluster may be less than 100nm in diameter[251]. Depletion in cholesterol within the plasma membrane is shown to severely affect the integrity of these clusters[250, 252]. Syntaxin clusters are thought to be located at the plasmalemmal fusion site (for neurotransmission this would be the plasma membrane at the axon terminals) and it is proposed that vesicles fuse at this site due to interactions with these clusters[210, 250, 252]. Mutation studies of Syntaxin suggest that these clusters are formed at least in part by Syntaxin-Syntaxin interactions, mainly through the transmembrane domains[251, 253]. Studies from DRM show that Syntaxin association with cholesterol enriched domains is seen to be anywhere from 0 to 50%[250, 252, 254, 255]. The use of photo-activated cholesterol and the resultant cross-linking of Syntaxin with cholesterol suggests a close proximity of the two entities[250]. These findings have led some to consider these

Syntaxin clusters as membrane rafts, though the large variation in values cast doubt. The use of the so-called raft markers ThyI[250] and flotilin[252], which are thought to segregate into cholesterol rich domains, showed no overlap with Syntaxin clusters. It has also been shown *in vitro* that GUVs (Giant Unilamellar Vesicles) which contained liquid-ordered and liquid-disordered phases showed Syntaxin has a preference for the disordered phase[256, 257].

1.7.2.3 Palmitates

As described in section 1.2.3, SNAP-25 has four cysteine residues which are palmitoylated; providing SNAP-25 with a lipid anchor. There is some evidence however that the palmitates do not act merely as anchors.

The first consideration is that despite containing transmembrane domains, many SNARE proteins including VAMP2 and other proteins such as SytI contain palmitoylated cysteine residues[49, 52]. It is possible that these additional lipid tails help the proteins to sort properly. In addition to this it has been found that palmitoylation of VAMP2 only occurs in adult rats not embryos, suggesting up-regulation during development. The SNARE protein TlgI was shown *in vivo* to mis-sort and undergo degradation when mutated to be palmitate deficient[258]. This suggests that in addition to sorting, palmitates are important for SNARE maintenance. Studies using the DRM and cholesterol methods found that SNAP-25 associated with detergent resistant patches unless they were cholesterol depleted[252]. However, as already discussed these findings are controversial and conflicting studies have been published.

SNAP-25 has two isoforms; 25a and 25b. The difference between these is the position of the palmitoylated cysteine residues[259, 260]. Both proteins are expressed in the neurons of humans but changes in the levels of expression of each are seen during development. In embryos SNAP-25a is expressed at higher levels, upon birth the levels change and 25b is more highly expressed[259]. It has been shown that disruption of this, so that 25a expression remains high, leads to premature death[261]. It is believed that SNAP-25b is required for fast, inducible fusion which is more greatly needed post birth[259, 262] and a difference in exocytosis rates is seen between the two isoforms (SNAP-25b produces higher rates than 25a)[263]. *In vivo* studies showed that where neurotoxins had been used to abolish fusion, the system could not be rescued by addition of cysteine mutated SNAP-25, but could by wild type SNAP-25[264]. This suggests that the lipid anchor is somehow important in fusion events.

Analysis of the position of the palmitate anchors during fusion reveals that they lie next to transmembrane regions (Figure 1.17). VAMP2 contains both a transmembrane domain and

palmitoylated cysteine as does SytI, both of which reside on the synaptic vesicle. In the plasma membrane, the arrangement of the t-SNARE complex shows that the palmitate groups of SNAP-25 lie in a comparable position with respect to the transmembrane domain of Syntaxin[265]. Whether this has a functional relevance to the fusion mechanism is unclear. One suggestion is that the lipid anchors (and possibly their interaction with transmembrane domains) are needed to properly transfer the energy provided by SNARE formation into the lipid bilayer, allowing remodelling[265]. It is also possible that the ring of SNARE complexes hypothesised to form does so through interactions of the transmembrane domains and the lipid anchors.

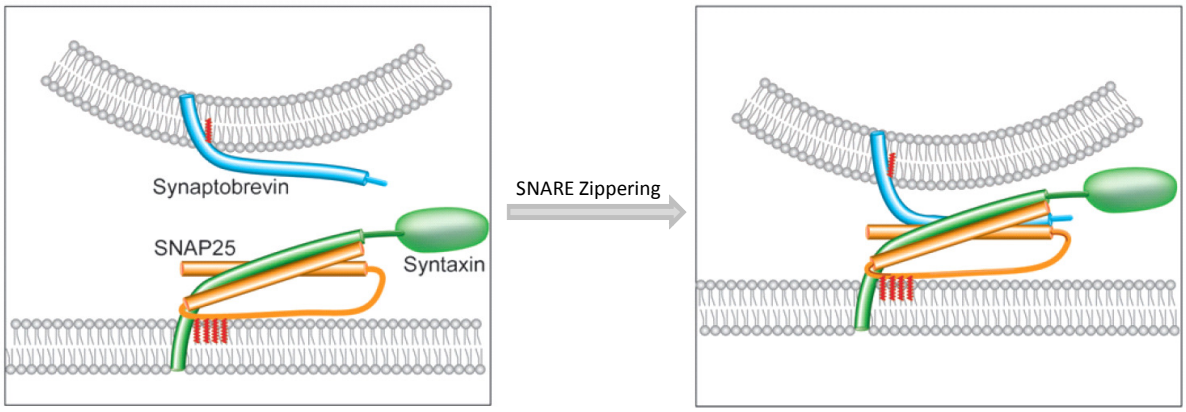


Figure 1.17. The protein VAMP2 contains palmitoylated amino acid residues despite the presence of a transmembrane domain. The lipid modification lies next to the transmembrane domain and may be important for sorting and in the fusion mechanism. The palmitate groups of SNAP-25 lie next to the transmembrane domain of Syntaxin 1 when the t-SNARE intermediary complex is formed. Figure modified from Davletov[265].

1.7.2.4 Enzymatic Lipid Modification

There is mounting evidence that some lipids may have a regulatory role in membrane fusion events *in vivo*. Already mentioned has been the dependency of the Synaptophysin-VAMP complex upon cholesterol levels (section 1.5.2) and examples of phospholipid binding, particularly the binding of Synaptotagmins to PS and PiP_2 (section 1.5.8). Studies investigating the affects of phospholipases and kinases suggest that fatty acid production and phosphorylation are also important events in fusion.

Phosphatidylinositols

Phosphatidylinositol 4, 5-bisphosphate or PIP_2 as it is better known, is implicated in both the docking and fusion of synaptic vesicles. It is highly concentrated at the plasmalemmal fusion site of the presynaptic terminals[210] and it interacts with many proteins associated with neurotransmission, suggesting an involvement in localizing synaptic vesicle fusion at this site[53]. For example, PIP_2 binds

in a calcium dependent manner to Synaptotagmin[209, 266] and Munc13[206, 209, 267] which (as discussed in sections 1.5.8 and 1.5.4 respectively) are essential regulatory proteins. Studies on chromaffin cells have shown a direct relationship between the amount of PIP_2 and the size of the ready-releasable vesicle pool[268] and it has been shown to inhibit fusion in model systems[269] in the absence of CAPS (Calcium Activated Protein in Secretion). It is also known that kinases and phosphatases (which together control the extent of phosphorylation of inositol lipids) regulate vesicle trafficking[270-272]. The DAG and PIP_3 which are generated by these processes are known to be important signal molecules. Dephosporylation of PIP_2 to PI may promote hemifusion if present in the proximal leaflets of merging membranes as PI has been shown to have type II lipid behaviour[273].

Diacylglycerol

Diacylglycerol binds to Munc13 through the C1 domain[156, 274]. This has been found to be an essential step in neurotransmission[156]. It is thought that its action may be involved in Munc13-Rab associations regulating or directing Rab effectors and other recruiter proteins to the fusion site[265]. In Drosophila melanogaster, inhibition of a protein which has strong similarities with DAG lipase results in a large decrease in neurotransmission[275, 276]. PLC (Phospholipase C) generates DAG from PIP_2. The headgroup portion is able to leave the membrane while DAG remains within the membrane. DAG is known to recruit the enzymes PKC (Protein Kinase C) and DAG lipase[265]. DAG lipase breaks DAG into arachidonic acid and monoacylated glycerol[277]. Arachidonic acid has been shown to influence neurotransmission; this will be discussed in the following paragraph. Inhibition of PLC and, by inference the fall in levels of DAG, is known to block exocytosis of synaptic vesicles[278, 279].

Fatty Acids

Phospholipase A_2, C and D (PLA_2, PLC and PLD respectively) have all been thought to be involved in fusion for many years[280]. This is partly because lysophospholipids have been shown to affect fusion rates both in *in vivo* and *in vitro* experiments. PLC followed by DAG lipase, as already discussed in the previous paragraph, produces arachidonic acid from PIP_2 which is known to bind to fusion regulator proteins. Arachidonic acid is also produced by PLA_2 from the breakdown of PC lipids along with lysoPC. Lysophospholipids, as discussed in section 1.4, are type I lipids and therefore implicated in the promotion of membrane dimple formation and fusion pores but inhibit the intermediary hemifusion structure. It has been shown that when membrane depolarization or neurotransmission occurs unsaturated fatty acids are released into the cytosol indicating a link between lipid metabolism and the fusion event[281-283]. It is unclear what the exact role of lipid metabolism may be,

but evidence from studies of snake venom (which contains PLA_2) suggests that these events act upstream of SNARE complex assembly[280, 284, 285].

There are many studies linking arachidonic acid with membrane fusion. External addition of this fatty acid enhances neurotransmission and it is able to rescue systems mutated to prevent the biosynthesis of Polyunsaturated fatty acids (PUFAs) in *C. Elegans*[286-288]. A fatty acid molecule, such as arachidonic acid, in combination with a PC lipid molecule can be considered a type II lipid[70] and as such could promote hemifusion. It would therefore be expected that external addition would facilitate fusion, at least to this stage. *In vitro* studies have also shown that arachidonic acid binds to the Syntaxin-Munc18 complex[289]. Studies of human diets rich in PUFAs such as omega 3 and 6[290] have shown that a few genes are down-regulated including the gene that controls Munc18 expression. It was thought that association of arachidonic acid with the Syntaxin-Munc18 complex promotes a change from the closed to open Syntaxin conformation. Later studies have shown however that Munc18 and Syntaxin remain bound even during t-SNARE complex formation[291]. It is now thought possible that arachidonic acid loosens the closed complex of Syntaxin enough that it is available to bind to SNAP-25. It is perhaps conceivable that once SNAP-25 is bound, Syntaxin it is not able to bind non-specifically and therefore, only once the SNAREpin complex is formed, does Munc13 catalyze the full opening of Syntaxin and removal of Munc18.

Further studies are needed to determine the exact relationship between all of these components. Lipids have been shown to be capable of inhibiting or promoting fusion without interaction with proteins. Lipid metabolism may change the lipid composition of the fusion site to take advantage of this. However, the presence of lipid binding sites in proteins linked to membrane fusion, suggest additional lipid roles.

1.8 Concluding Remarks and Project Aims

While there are still many questions about the affect of protein-protein interactions on membrane fusion, it has become clear that protein-lipid interactions must also be considered. Both experimental and simulation studies suggest that SNARE proteins may have several affects on membranes to increase the stored energy, including the stretching and compression of lipid molecules. By increasing the stored curvature elastic stress of membranes, fusion may be driven forward. In this regard, evidence that the absence of the transmembrane regions of SNARE proteins prevents a progression beyond a hemi-fused state is particularly important. Transmembrane domains, as they span both monolayers, are not considered to affect local membrane curvature, however they can result in a hydrophobic mismatch with the surrounding lipids. They may also apply a moment of force (the bending force proposed to be applied during SNARE complex formation) which would be expected to alter local curvature. A ring of SNAREpins encircling a hemifusion diaphragm would apply such a force in all directions and may lead to both an increase in the diaphragm area and its lateral tension; promoting fusion pore formation.

It is important to investigate the SNARE-lipid relationship as findings show that high protein densities lead to the formation of leaky vesicles *in vitro*. It is not clear whether SNARE proteins form clusters *in vivo.* If they do then while the copy number of a protein may be low over the whole surface (of the synaptic vesicle for example), it may in fact concentrate into one small area making the local concentration higher. A local bilayer disruption (which could be represented by leaky vesicles) may be relevant to the fusion mechanism.

In order to investigate the relationship between SNARE proteins and lipids it was necessary to develop an *in vitro* assay that was capable of measuring the affect of various factors on membrane properties. It was the aim of this project to develop such an assay in house and use it to measure the affects of SNARE proteins upon membrane properties.

- Chapter 2 discusses the purification of the neuronal SNARE proteins and their reconstitution into artificial liposomes. The use of this technique has allowed protein density and lipid composition to be controlled.
- Chapter 3 investigates the effect SNARE protein insertion has upon the size and curvature of GUVs (which are analogous in size to the outer membrane of cells) and therefore the implied affects these proteins have on the curvature free energy of the bilayer.
- Chapter 4 presents data obtained from micropipette aspiration and compares the membrane properties of a pure lipid model with SNARE proteoliposomes.

- Chapter 5 shows the general effect that the alteration of membrane properties has on liposome fusion rates and relates these findings to changes in these properties due to SNARE protein insertion. A hypothesis for how these results may impact on the membrane fusion mechanism *in vivo* is discussed. At the end of this chapter an overall conclusion is provided, with suggestions for future work.

Chapter 2.

PURIFICATION OF NEURONAL SNARE PROTEINS

This chapter describes the methods used to optimise the purity and solubility of the neuronal SNARE proteins; qualities essential in order for the proteins to be used in *in vitro* assays. The methods of SNARE protein purification vary widely between research groups and as such various methods have been employed during this study. Each method was investigated in order to ascertain which would result in the best protein solutions for use in *in vitro* assays. Contaminating proteins were of particular concern as these could compromise the results obtained.

High quality purified protein solutions of full length His_6-VAMP2 (2 ml, 46.1 µM) and His_6-SNAP-25b (1.5 ml, 43.6 µM) have been obtained (section 2.1). It was necessary to produce a truncated form of Syntaxin 1A in order to obtain a protein solution which could be used in the *in vitro* assays. This truncated form (His_6-ΔN-Syx) lacks the H_{abc} regulatory domain and consists of the amino acid residues 181-288 of wild type Syntaxin. A 1.5 ml sample of 74.0 µM concentration was obtained.

Cloning was carried out to produce modified His_6-VAMP2 and His_6-ΔN-Syx (section 2.2.1.1). In this work additional cysteine residues were added to the C-terminal region of each protein. In one cloning step, it was possible to add two cysteine residues to His_6-ΔN-Syx but only one to His_6-VAMP2. These new proteins, His_6-VAMP2-Cys and His_6-ΔN-Syx-CysCys were also purified and high quality protein solutions obtained. Following the purification of His_6-VAMP2-Cys and His_6-ΔN-Syx-CysCys, fluorescent labelling of these proteins was carried out (section 2.2.1.2). The labels chosen were the small molecule dyes Alexa Fluor® 488-C_5-maleimide and Alexa Fluor® 555-C_2-maleimide. As these are thiol reactive dyes they only labelled His_6-VAMP2-Cys and His_6-ΔN-Syx-CysCys at the C-terminal cysteine residues, which had been added by cloning. These fluorescent probes can act as FRET (Förster (or Fluorescence) Resonance Energy Transfer) partners and the production of these proteins allows future development of this project through the use of this property. His_6-VAMP2-488 was obtained at 30.6 µM with a protein: dye molar ratio of 1:1.2 while the concentration of His_6-ΔN-Syx-555 was 35.3 µM with a ratio of 1:3.

Liposomes were produced with SNARE protein incorporated (section 2.3). Analysis of these proteoliposomes by western blot confirmed protein insertion, while HPLC (High Pressure Liquid Chromatography) showed complete detergent extraction. It was also determined that SNAP-25 incorporation was as a direct result of its ability to bind to ΔN-Syx.

2.1 PURIFICATION OF THE NEURONAL SNARE PROTEINS

The initial constructs for full length His_6-VAMP2, His_6-SNAP-25, GST-Syntaxin 1A and the co-expression system His_6-SNAP-25/GST-Syntaxin 1A used in this project were generously provided by Dr G. Schiavo of Cancer Research UK. A truncated version of the Syntaxin 1A (ΔN-Syx) protein was cloned and purified in the course of this project; this is discussed in section 2.1.4.2. A schematic of the constructs is shown in Figure 2.1.

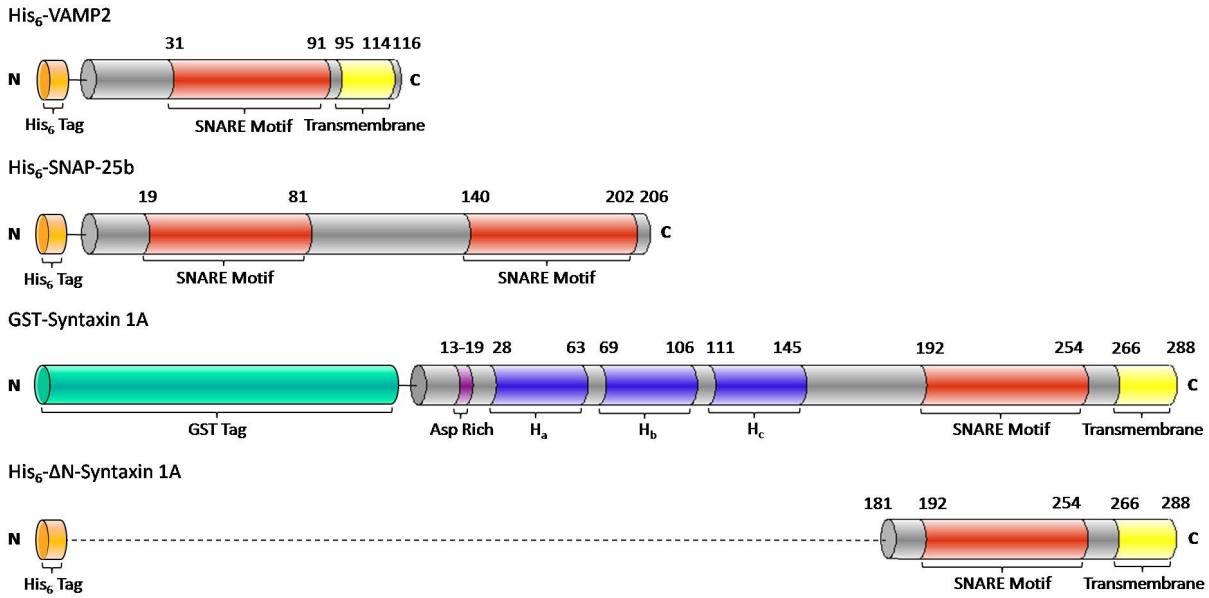


Figure 2.1. The protein constructs for the SNARE proteins used in this project are shown. The expression systems for the His_6-VAMP2, His_6-SNAP-25b and GST-Syntaxin 1A constructs were supplied by Dr. G. Schiavo. The final construct, shown at the bottom of the figure consists of the C-terminal portion of Syntaxin 1A with the N-terminal GST tag replaced by a His_6 tag and was cloned from the GST-Syntaxin 1A construct.

All of the expression vectors were transformed into Rosetta™ cells. Rosetta™ cells are an engineered BL21 strain of *E. coli* developed to improve the expression of eukaryotic protein. Expression trials were conducted to establish the best colonies and growth media in terms of levels of expression and proteins solubility. Part of this work was conducted in the fulfilment of an MRes degree[(292)].

It should be noted that the lipid anchors of SNAP-25 and VAMP2 would be added as a post-synthetic modification *in vivo*. As a result of expression in *E. coli,* these anchors are not present in the purified protein solutions obtained in this study. VAMP2 is still able to associate with membranes as it contains a transmembrane region. SNAP-25 however does not have another form of membrane attachment. In this study SNAP-25 is added only in the presence of Syntaxin 1A (which has a transmembrane domain). Association of SNAP-25 to membranes is therefore only seen as a result of complex formation with Syntaxin.

While a detailed description of the materials and methods used throughout this chapter can be found in section 2.4, a general overview of the purification procedure followed can be seen in Figure 2.2.

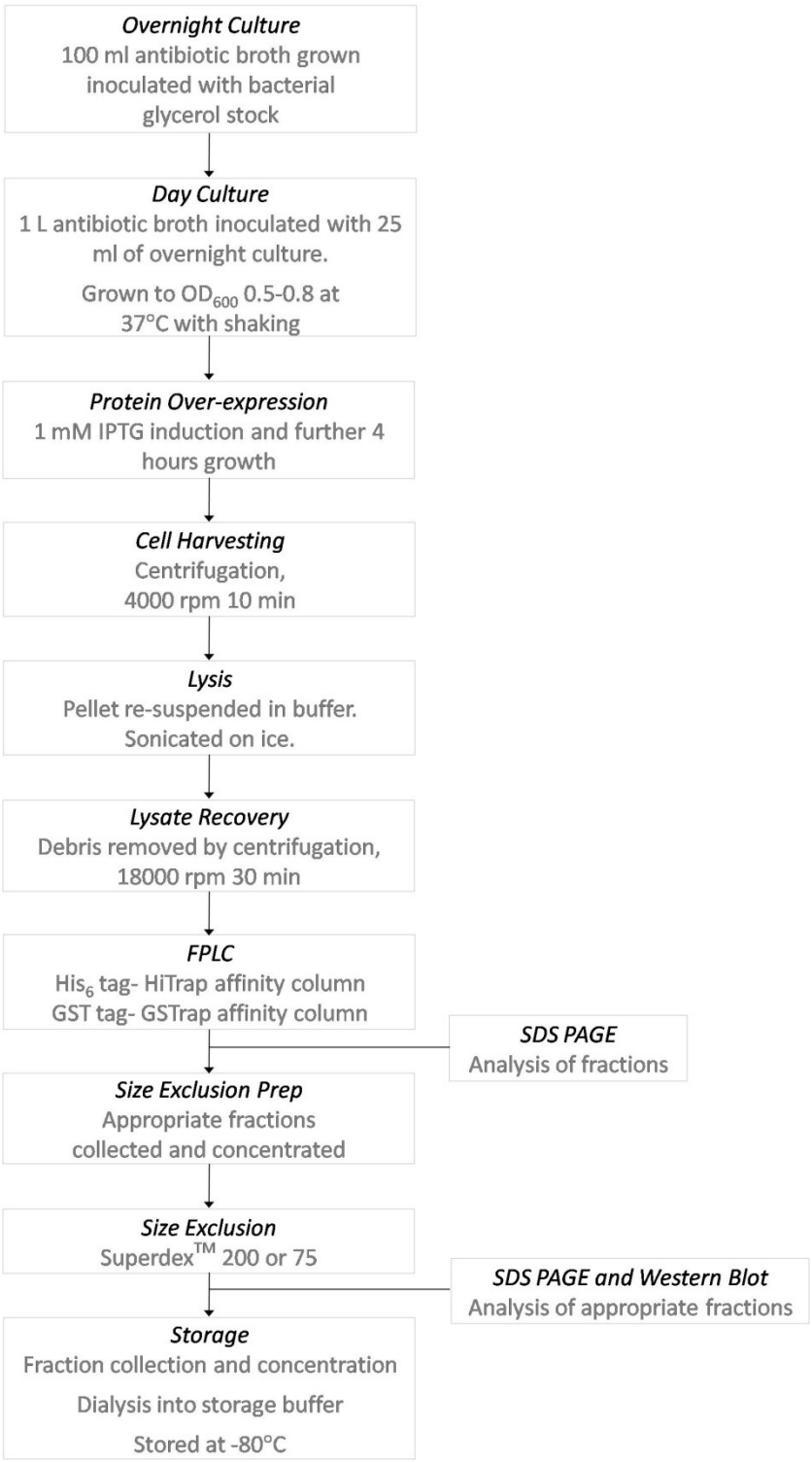


Figure 2.2. This figure aims to provide the reader with an overview of the stages followed during the purification of the neuronal SNARE proteins. Detailed protocols for each step can be found in the materials and methods section of this chapter.

2.1.1 PURIFICATION OF VAMP2

VAMP2 is the smallest of the neuronal SNARE proteins and runs on SDS PAGE to ≈18 kDa. The expression vector pET-16b inserts an N-terminal His_6 tag to the VAMP2 sequence, this was used for purification. The initial purification methodology employed FPLC using an affinity column followed by size exclusion (also known as gel filtration) with the buffers HiTrap 1a, 1b and NaHEPES respectively. This protocol resulted in all detectable VAMP2 protein eluting in the void volume of the gel filtration column. As the column used has a globular protein exclusion limit of 1300 kDa, the presence of VAMP2 in the void volume indicated it had formed large aggregates.

In an attempt to reduce any aggregation caused by non-specific binding, the cell lysate was incubated with K-elution buffer prior to purification. The presence of ATP in this buffer provided energy for *E. coli* proteins to correctly fold. The purification protocol described above was then repeated, with a greater quantity of soluble protein detected. SDS PAGE analysis identified an 18 kDa band in later (lower molecular weight) gel filtration fractions. This band was confirmed to be VAMP2 through western blot analysis. However, in addition to this band many other protein bands were detected. The western blot revealed that these bands, largely, did not contain VAMP2.

VAMP2 is believed to be largely unfolded *in vivo* unless bound to other proteins such as Synaptophysin or other SNARE proteins. Approximately 60% of the protein sequence is cytosolic and VAMP2 contains only one membrane-spanning domain (which has been modelled as an α-helix[34]). These domains usually refold spontaneously in the presence of a membrane environment or detergent. For these reasons it was considered possible to denature the cell lysate proteins without detrimentally affecting future work. The purification protocol was therefore repeated with the addition of 4 M urea to each of the purification buffers (renamed in section 2.4.1 as Urea HiTrap 1a, b and Urea NaHEPES for clarity). The amount of soluble protein was vastly increased and the cell lysate was diluted two-fold in Urea HiTrap buffer 1a to reduce viscosity. SDS PAGE analysis of the gel filtration fractions revealed a much cleaner purification (Figure 2.3).

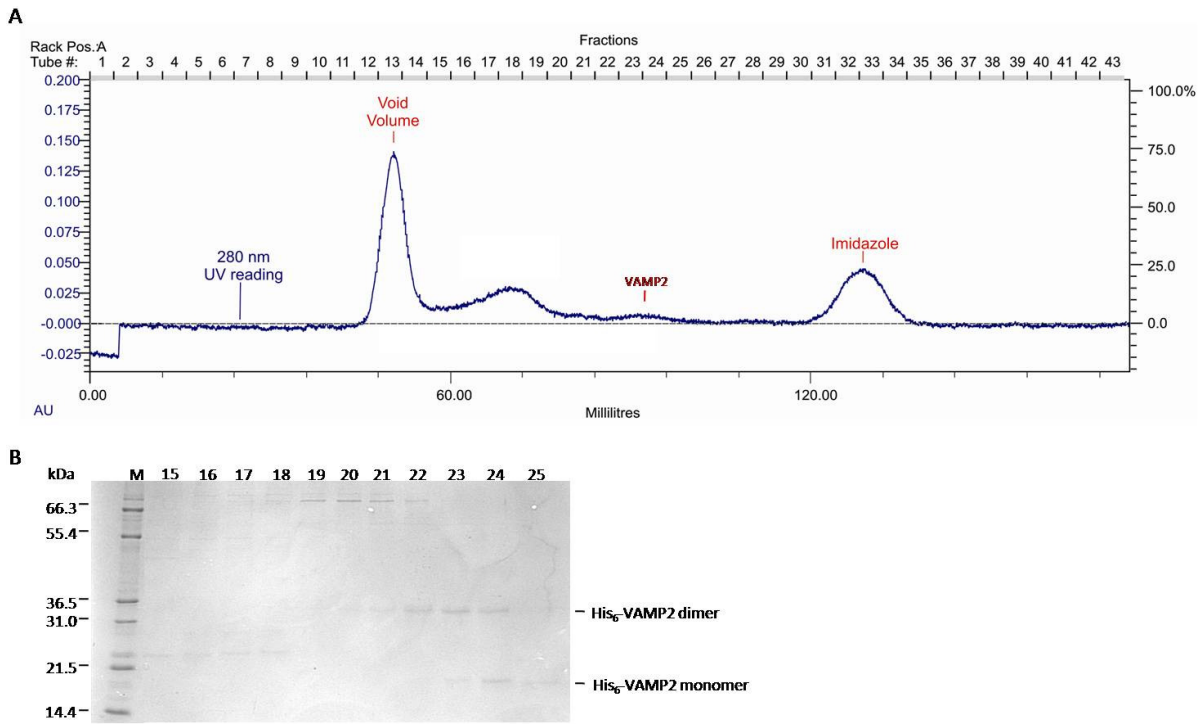


Figure 2.3. In this figure the size exclusion profile of VAMP2 in Urea NaHEPES is shown (A) with the corresponding SDS PAGE gel (B). The amount of VAMP2 is small in comparison to other proteins eluted. However, the analysis clearly shows an 18 kDa band in the presence of only one other visible band and that these proteins are well separated from other protein bands detected.

The later fractions contained only two detectable bands; at 18 and 36 kDa respectively. Western blot ascertained that both of these fractions contained VAMP2. It is believed that these bands represent VAMP2 monomer and dimer (Figure 2.4). Western blot analysis is often more sensitive than SDS PAGE and the western blot detected more than these two bands. These were of higher molecular weight and consistent with higher order VAMP2 oligomers (i.e. ≈54 kDa). The appropriate fractions were collected and concentrated before the protein was dialysed with storage buffer. This buffer contained no urea and had added detergent. The use of this buffer would improve the stability of VAMP2 whilst in storage at -80°C. After extensive dialysis the protein solution was concentrated further. It was seen that protein precipitated out of solution at relatively low concentrations. The highest concentration achieved was a 2 ml solution at 0.83 mg/ml (46.1 µM).

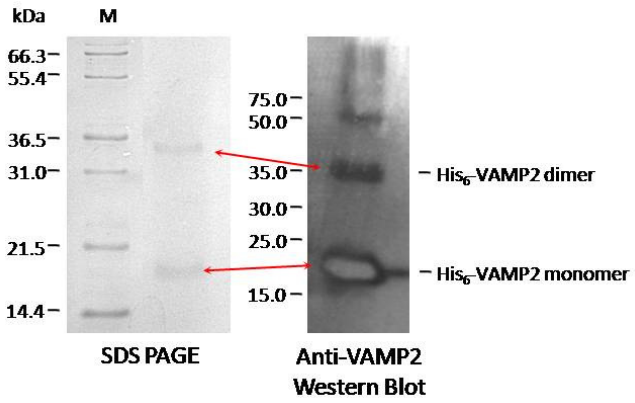


Figure 2.4. The concentrated protein solution from VAMP2 purification using urea was analysed by SDS PAGE and anti-VAMP2 western blot. This figure shows the result of these on the left and right of the figure respectively, with the molecular weight in kDa shown. Only two bands are visible on the SDS PAGE gel and are at approximately 18 and 36 kDa. The western blot shows these bands contain VAMP2 and are believed to be the VAMP2 monomer and VAMP2 dimer. The western blot shows additional bands at higher molecular weights consistent with higher order VAMP2 oligomers.

2.1.2 The Syntaxin 1A/SNAP-25 Co-expression System

A co-expression construct was provided by Dr Schiavo, who commented that the expression level of both proteins was higher in this system than when separately expressed. He also saw that the t-SNARE intermediary complex was easier to form from this system (Dr G. Schiavo; personal communication). The lack of membrane anchor in purified SNAP-25 solutions meant that SNAP-25 could only added to *in vitro* assays in the presence of Syntaxin. Attempts to purify the t-SNARE proteins therefore began with the co-expression construct.

The differences between un-induced and induced cell culture were clearly visible by SDS PAGE (Figure 2.5) with large additional protein bands seen in the induced culture at ≈31 kDa and 55 kDa. These were assigned as SNAP-25 and Syntaxin respectively which was confirmed by separate anti-SNAP-25 and anti-Syntaxin western blots.

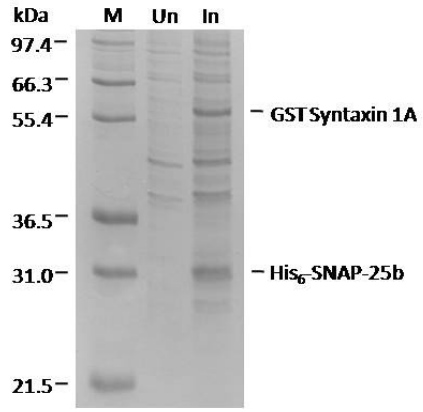


Figure 2.5. This figure shows the SDS PAGE analysis of both un-induced (Un) and induced (In) bacterial cultures containing the co-expression vector. From comparison of the two samples the over expression of GST-Syntaxin (55 kDa) and His_6-SNAP-25 (31 kDa) can be clearly seen.

The initial purification protocol exploited the N-terminal His_6 tag of SNAP-25 and its affinity to Syntaxin. The cell lysate was incubated with K-elution buffer (as this was shown to be successful for VAMP2 purification) and then FPLC was performed with a HiTrap affinity column (HiTrap buffer 1a and b); this was followed by size exclusion (NaHEPES buffer). Analysis of the collected fractions by SDS PAGE showed SNAP-25 and Syntaxin to be present only in large aggregates as they eluted in the column void volume. A large number of additional protein bands were also seen on the gel. It is desirable to have a 1:1 ratio of the t-SNARE proteins as both the t-SNARE and SNARE complex have a 1:1 ratio of these proteins *in vivo*. The results of this purification showed that the expression of SNAP-25 was far above that of Syntaxin (Figure 2.6). It was therefore necessary to modify the purification procedure.

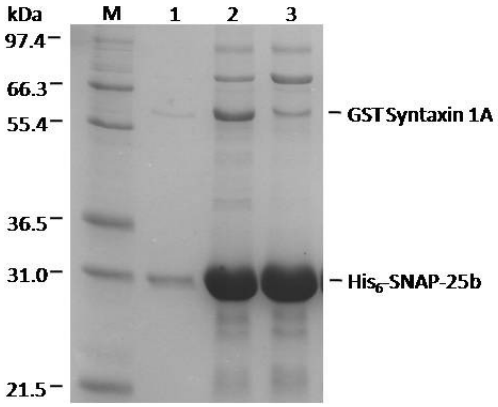


Figure 2.6. An SDS PAGE gel of the void volume fractions from size exclusion purification is shown. These fractions contain proteins of a molecular weight higher than the exclusion limit of the column used (1300 kDa). These proteins are therefore highly aggregated during purification. Proteins other than those of interest are detected on the gel and the fractions show that His_6-SNAP-25 is in large excess of GST-Syntaxin, which is undesirable.

Rather than a His_6 tag, Syntaxin has an N-terminal GST tag. Following cell lysate incubation with K-elution buffer, FPLC was therefore first performed using a GST affinity column (GSTrap buffer 1a and 1b). Rather than the elution buffer (GSTrap buffer 1b) simply being GSTrap buffer 1a with the addition of reduced glutathione, an elution buffer was chosen which allowed the eluting protein solution to be loaded immediately onto a HiTrap affinity column. Thus, any excess SNAP-25 or Syntaxin would be removed through the combination of these two FPLC steps. The addition of the HiTrap FPLC step also removed free GST from the sample. SDS PAGE analysis of the final elution fractions showed only three visible protein bands; these ran to 31, 35 and 55 kDa. Western blot analysis confirmed the lower and upper band to be SNAP-25 and Syntaxin respectively. The middle band was not detected by either western blot and was therefore considered to be contaminating protein (Figure 2.7).

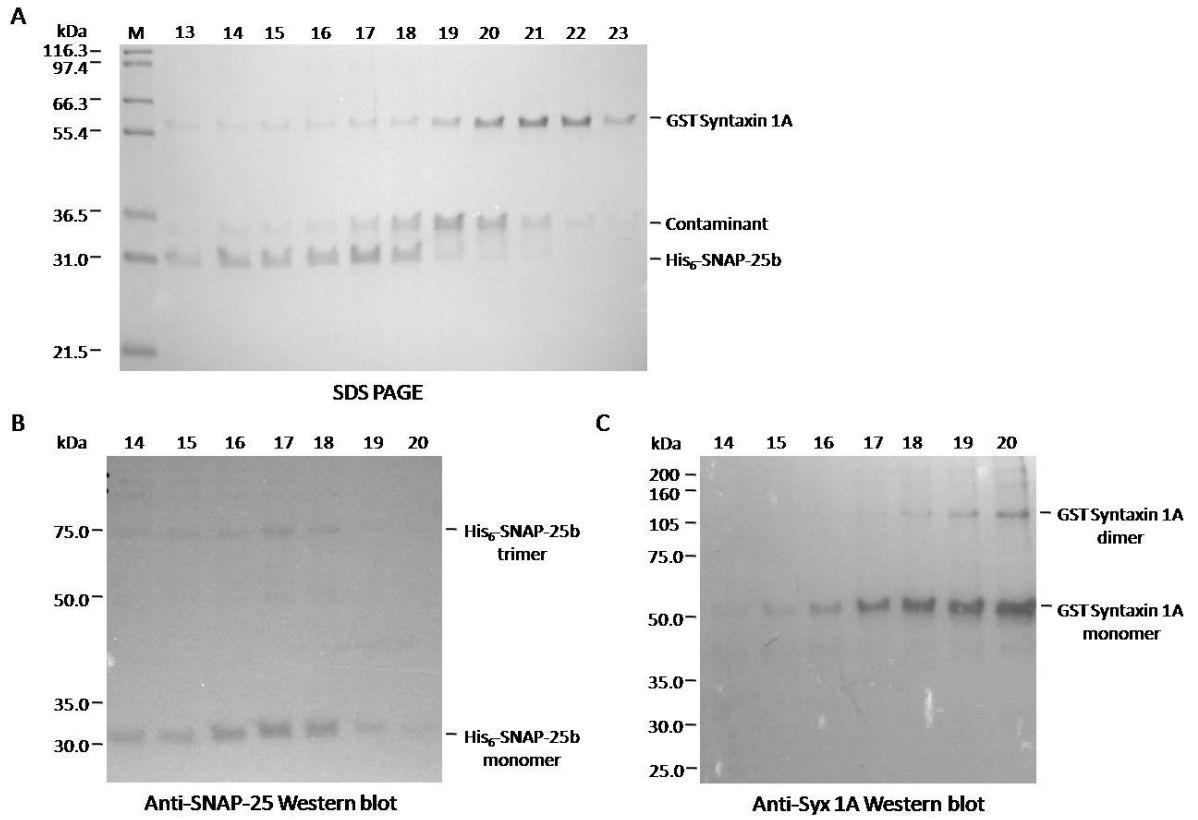


Figure 2.7. Figure A shows the SDS PAGE gel from the size exclusion purification step. Three protein bands can be seen at 31, 35 and 55 kDa. An anti-SNAP-25 western blot (B) and anti-Syxntaxin 1A western blot (C) identify the 31 kDa band as SNAP-25 and 55 kDa as GST-Syntaxin. However, neither blot shows these proteins to be present in the 35 kDa protein band.

The initial attempt to remove the contaminating protein used size exclusion (NaHEPES buffer). The weights of SNAP-25 and the contaminant were close and also of relatively low molecular weight, this step was therefore performed using a Superdex 75 column. Analysis of the fractions revealed that despite its lower monomer molecular weight, SNAP-25 was eluted first from the column. This was followed by the contaminant and then Syntaxin. The gel showed that the separation of SNAP-25 and the contaminant was not sufficient and that SNAP-25, as expected from the elution profile, was present mainly as oligomers. Gel filtration was repeated under various conditions. A high salt buffer, high pH and low pH buffer were tried but the contaminant protein could not be removed. The overlapping elution profile of all three proteins and the stability of this profile, even under such harsh conditions, led to the conclusion that the contaminant must bind with high affinity to SNAP-25 and/or Syntaxin. The SDS gel revealed the three proteins to be in an approximate 1:1:1 ratio. It is possible that the three proteins formed a SNARE-like complex structure.

The *in vitro* assay could not be used with such a large amount of a contaminating protein. It was therefore decided that the co-expression system would not produce acceptable protein solutions and focus moved to the purification of separately expressed t-SNARE proteins.

2.1.3 Purification of SNAP-25

Like VAMP2, the expression vector (pQE-30) of the construct provided by Dr Schiavo inserted an N-terminal His_6 tag to the SNAP-25 sequence. The first purification protocol was based upon published work by Ernst[199] though guanidine was replaced by urea. This method lyses the cell pellets with a buffer containing the denaturant agent (breaking buffer 1). As with VAMP2, SNAP-25 is believed to be largely unfolded in the absence of binding proteins and SNAP-25 does not contain a folded transmembrane domain like VAMP2. It was therefore concluded that denaturation of SNAP-25 during purification would not be detrimental. The denatured cell lysate was purified using FPLC with a HiTrap affinity column. In addition to the protocols described in section 2.4, a wash step was added before the use of HiTrap buffers 2a and 2b. In this step the column was washed with 10-column volumes of HiTrap wash buffer, which contained urea. A large number of protein bands were visible on the SDS PAGE gel of the FPLC fractions. Size exclusion, using NaHEPES buffer, was therefore added but revealed SNAP-25 to be highly aggregated, with elution in the column void volume.

The Ernst protocol was repeated with modifications; 4M urea was added to the HiTrap buffers (renamed urea HiTrap 2a and b) and urea NaHEPES buffer was used. The purification was much cleaner and SDS PAGE analysis detected only two protein bands, at 25 and 30 kDa. Western blot analysis identified the 25 kDa but not the 30 kDa band as containing SNAP-25 (Figure 2.8). The western blot also detected a higher molecular weight band at 75 kDa, consistent with a SNAP-25 trimer.

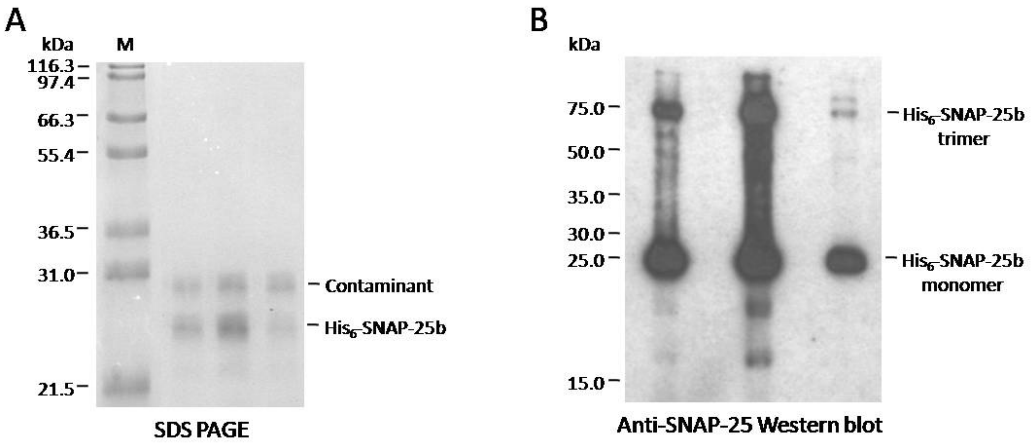


Figure 2.8. On the left is shown an SDS PAGE gel of size exclusion fractions where Ernst methodology with additional urea was used at each purification step. Two protein bands are visible on this gel at 25 kDa and 30 kDa. The 25 kDa band was confirmed as SNAP-25 monomer by anti-SNAP-25 western blot (shown on the right). This blot also revealed higher order oligomers (weight consistent with a SNAP-25 trimer) which were not visible on the SDS PAGE gel. The 30 kDa was not detected on the blot.

The best purification was achieved using the same buffers and protocols employed in the final purification of His_6-VAMP2. The cell pellet was lysed in urea HiTrap 1a and then FPLC with HiTrap affinity column (urea HiTrap 1a and 1b) and size exclusion (urea NaHEPES buffer). The analysis of the fractions by SDS PAGE detected a double band at approximately 25 kDa, both of which were confirmed by western blot as SNAP-25 containing bands (Figure 2.9). SNAP-25 is known to produce a double band, with the lower one representing some C-terminal degradation[38]. As with previous western blots, higher oligomers were detected including a SNAP-25 dimer and trimer at 50 and 75 kDa respectively. The appropriate elution fractions were collected and concentrated. The solution was then dialysed with storage buffer and stored at -80°C. A protein solution of approximate volume 1.5 ml was obtained with a concentration of 1.09 mg/ml (43.6 µM).

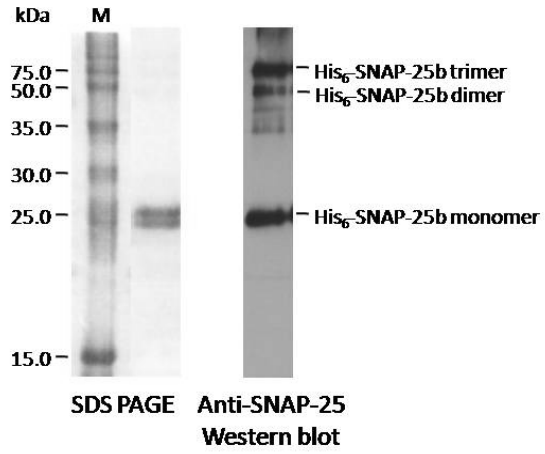


Figure 2.9. This figure shows the SDS PAGE gel (left) and corresponding anti-SNAP-25 western blot (right) with the molecular weights in kDa indicated. Only the SNAP-25 protein band is visible by SDS PAGE while the more sensitive western detects homo dimers and trimers at 50 and 75 kDa respectively.

2.1.4 PURIFICATION OF SYNTAXIN 1A

2.1.4.1 Full length Syntaxin 1A

Full length Syntaxin 1A was expressed containing an N-terminal GST tag. In Ernst's paper purification of GST-tagged proteins was achieved using denaturing agents. Unlike VAMP2 and SNAP-25, Syntaxin has a large folded region (the H_{abc} domain) and it was therefore undesirable to denature Syntaxin due to concerns that it would not re-fold properly. The initial purification attempt instead used buffers and protocols based on the published method of Weber[38]. This method uses detergent rather than denaturation, to reduce aggregation and improve purity. The cell pellet was first lysed in breaking buffer 2. This buffer differs slightly from the published buffer with no PMSF (Phenylmethylsulphonyl Fluoride) added and the substitution of 10 mM β-mercaptoethanol with 2 mM DTT. FPLC was conducted using a GSTrap affinity column which had been pre-equilibrated with 1% Triton X-100 wash buffer. The cell lysate was loaded onto the column and a 10-column volume wash step preformed with 1% Triton X-100 wash buffer before purification by GSTrap buffer 2a and 2b. Appropriate fractions (as assessed by SDS PAGE) were collected and size exclusion performed in detergent NaHEPES buffer (like Weber, the detergent OβG was used). The analysis of the gel filtration profile showed that Syntaxin was eluted in the column void volume and as such indicated the formation of large aggregates. The purification was repeated with the substitution of the detergent OβG with DDM; however this gave the same result.

GST is capable of forming homo-dimers and it was believed that this contributed to the formation of large protein aggregates. The expression vector pGEX-4T-2 contains a Thrombin cleavage site and so the cleavage of this tag was attempted (following the non-specific wash step of FPLC). SDS PAGE analysis of the eluted protein did not detect a protein band at the molecular weight of a Syntaxin monomer (33 kDa). Western blot analysis showed that only the bands at 55 and 66 kDa contained Syntaxin. This suggested that a large amount of the Syntaxin remained uncleaved (the 55 kDa band is GST-Syntaxin). An increase in the Thrombin incubation time caused non-specific cleavage of the protein. It is possible that the large aggregates formed prevented much of the Thrombin accessing the cleavage sites. The band at 66 kDa is consistent with a tag-free Syntaxin dimer. *In vivo,* the H_{abc} domain of Syntaxin folds down to bind to the SNARE motif; *in vitro* it is possible that two Syntaxin molecules could interact in a head-tail manner to form a stable dimer. Chain formation due to aligned interaction between proteins could also been envisaged, leading to the formation of very large aggregates (Figure 2.10). Therefore even if full GST cleavage was successful it could result in a purified protein sample containing mainly SDS stable homo-dimers and large aggregates. A truncated version of Syntaxin 1A (ΔN-Syx, 181-288) was therefore produced.

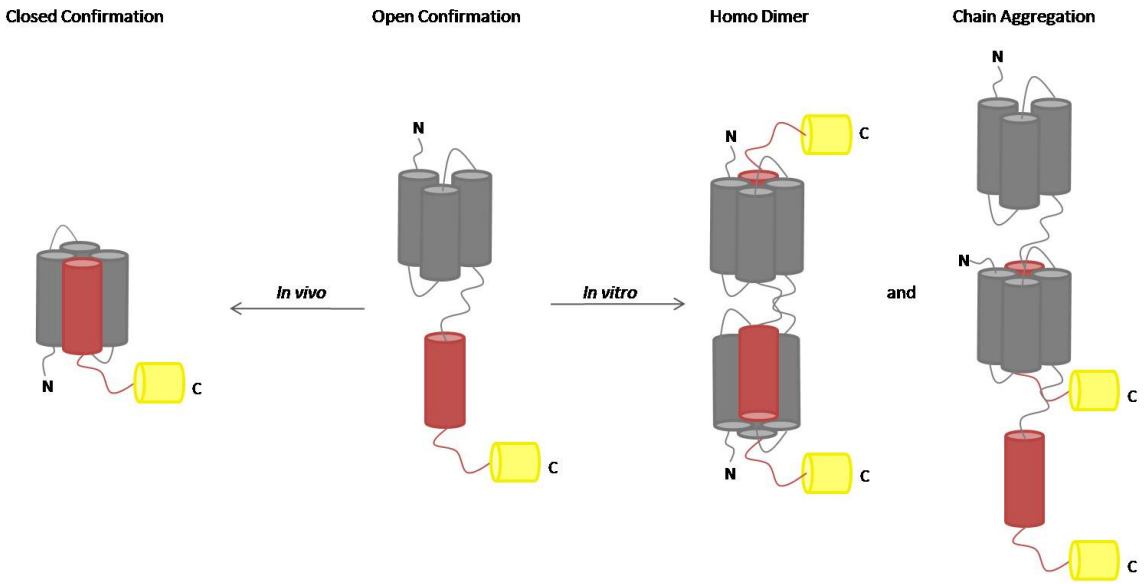


Figure 2.10. In vivo the H_{abc} domain of Syntaxin (shown here in grey) folds down to form a complex with the SNARE motif (red) allowing Syntaxin to occupy two states; the open and closed conformations (shown on the left of this figure). In vitro regulatory proteins are not present and so multiple Syntaxin molecules can interact. Two Syntaxin molecules interacting in a head-tail fashion could form a homo dimer as the H_{abc} domain of each binds to the SNARE motif of the other (centre right). Chain aggregates could also form if head-head interactions occurred. In this situation the H_{abc} domain of protein one would bind to the SNARE motif of protein two, the H_{abc} domain of protein two would then bind to the motif of a protein 3. This could repeat indefinitely, forming large aggregate structures.

2.1.4.2 ΔN-Syntaxin 1A

Due to the H_{abc} domain of Syntaxin, it was not possible to use denaturation methods in the purification protocol. However, denaturation had proved to give high quality protein solutions for both SNAP-25 and VAMP2. As discussed in sections 1.2.3.1 and 1.5.4, *in vivo* Syntaxin forms a closed conformation as part of membrane fusion regulation. It has also been shown that removal of the H_{abc} domain improves fusion rates in *in vitro* assays, due to the formation of the closed confirmation being prevented[159]. Therefore, the removal of the H_{abc} domain would potentially improve *in vitro* assays. As discussed in 2.1.4.1, this domain also contributed significantly to the highly aggregated nature of the purified protein; therefore, its removal could also improve the quality of the protein solution obtained. There were therefore several advantages associated with the production and use of ΔN-Syx when compared with wild type Syntaxin. As well as the potential reduction in aggregation just from its removal, the lack of the H_{abc} domain would also allow purification to include denaturing agents as the remaining sequence is structurally similar to VAMP2.

ΔN-Syx was cloned into a new vector, pPROEX-HTb (the vector map is supplied in the appendix, see page 176) which inserts an N-terminal His_6 tag rather than a GST tag. The sequence based predicted weight of full length Syntaxin 1A is 33 kDa, while GST is a 26 kDa protein. A full length Syntaxin protein molecule is therefore almost doubled in weight by this tag. The SNARE complex forms starting at the N-terminal regions of the SNARE proteins and the use of such a large tag at this terminus could impede future assays (a GST tag at the C-terminus instead would impede membrane insertion). ΔN-Syx had the H_{abc} domain removed and therefore contained the amino acid residues 181-288 of full length Syntaxin. The sequence based predicted weight of ΔN-Syx was therefore ≈15 kDa. It was thought ill-considered to use a protein tag (GST) so much larger than the protein of interest, particularly when located at the N-terminal, as already discussed. For these reasons a vector was chosen to add a much smaller purification tag.

The cloning protocol is described in detail in section 2.4. However briefly, the custom-made synthetic oligonucleotides (primers) Synt.c-ter 5' and Synt.c-ter 3' were designed to read the Syntaxin sequence only between amino acid residues 181-288. PCR amplification produced high levels of the ΔN-Syx fragment when an annealing temperature of 54°C and extension temperature of 68°C were used. The PCR fragments and pPROEX-HTb vector were cut using the restriction enzymes BamHI and HindIII followed by purification using standard kits. The His_6-ΔN-Syx expression vector was produced through ligation and was then transformed into XL1-Blue cells from which single colonies were selected. The DNA of these colonies was extracted, compared to pure pPROEX-HTb vector and the DNA sequence checked for ΔN-Syx insertion (Figure 2.11).

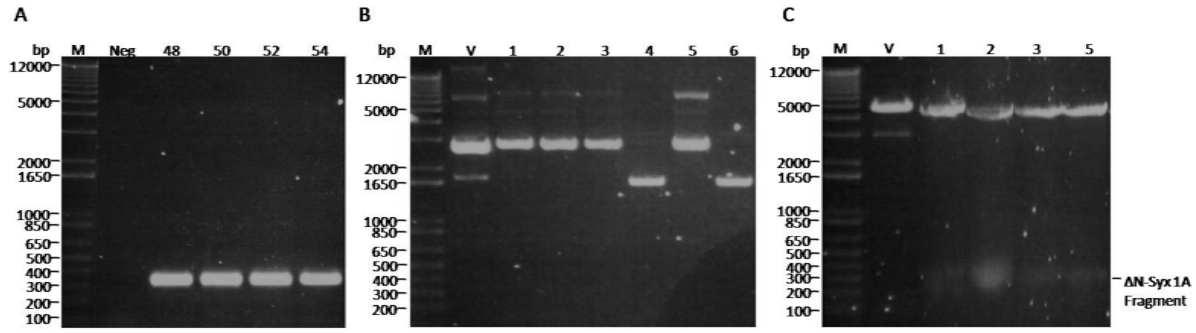


Figure 2.11. All three parts of this figure show agarose gels with base pair markers (M). Figure A shows the amplification of the ΔN-Syx fragment where the top ledger shows the negative control and temperature of each sample (°C). Figure B shows DNA extracted from XL1-Blue colonies (1-6) which had been transformed with ΔN-Syx pPROEX-HTb ligation product. These were compared to the empty vector (V). Figure C shows the digestion of the DNA from colonies 1-3 and 5 using the restriction enzymes HindIII and BamHI. The fragment seen at approx. 350 bp corresponds to the PCR fragment weight, indicating successful fragment insertion.

Once sequencing was confirmed, the DNA was transformed into Rosetta™ cells and expression trials conducted to optimise cell growth and protein expression. The one disadvantage of H_{abc} removal was that the epitope for the antibodies against Syntaxin is located in this domain. Western blot analysis of His_6-ΔN-Syx purification was therefore conducted using anti-His_6. The protein was purified using the method established for both His_6-VAMP2 and His_6-SNAP-25 i.e. FPLC purification using urea HiTrap 1a and 1b followed by size exclusion using urea NaHEPES. SDS PAGE analysis detected a protein band at approximately 15 kDa which was also detected by anti-His_6 western blot (Figure 2.12). As with His_6-VAMP2 and His_6-SNAP-25, His_6-ΔN-Syx containing fractions were concentrated and the solution dialysed into storage buffer. By this method a 1.5 ml solution containing 1.11 mg/ml (74.0 µM) His_6-ΔN-Syx was obtained.

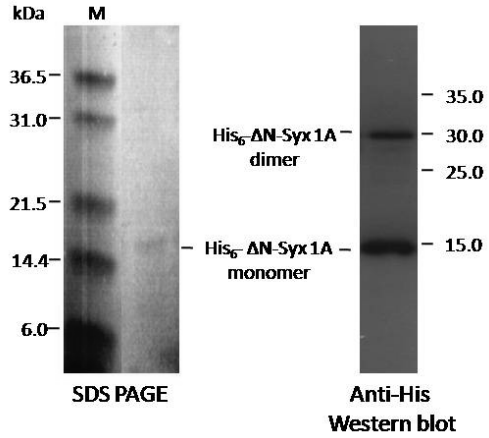


Figure 2.12. The SDS PAGE gel and anti-His western blot of purified deltaN-Syx protein solution are shown on the left and right of this figure respectively. Only one protein band is visible by SDS PAGE at approx. 15 kDa. This band and another at 30 kDa were detected by western blot. These bands represent deltaN-Syx monomer and dimer.

2.2 FLUORESCENT SNARE PROTEINS

Fluorescent labelling of the SNARE proteins allowed protein insertion into a simple lipid model to be confirmed (see Chapter 3). The Alex Fluor® dyes (Invitrogen) were chosen for labelling. These dyes have high molar extinction coefficients and are small molecule dyes. A biochemical alternative would have been to use fluorescent protein tags such as GFP (Green Fluorescent Protein) and its modifications (Red FP, Cyan FP etc). However, these proteins are large (GFP is 26.9 kDa) and would therefore pose the same problems as GST (discussed in section 2.1.4). The small molecule nature of the Alexa dyes would not interfere with SNARE complex formation or membrane insertion.

As the purified SNAP-25 protein was incapable of binding to membranes independently, it was decided that only VAMP2 and ΔN-Syx would be labelled. These two proteins were labelled with different Alexa Fluor® dyes so that the proteins could be distinguished. The labels could also act as FRET partners allowing future development of this project. In order to control the site of labelling, a maleimide form of the Alexa Fluor® dyes was chosen. This dye reacts with thiol groups and therefore reacts with the amino acid residue cysteine. Wild type Syntaxin 1A contains three cysteine residues; of these, one is found in the H_c helix (C145) and the other two (C171 and C172) are in the transmembrane region. VAMP2 only has one cysteine residue which is located in its transmembrane domain (C103). The cysteine residues within the membrane anchors are unavailable for labelling provided that the protein is in a membrane environment or in the presence of detergent. For Syntaxin, the use of the truncated form ΔN-Syx removed the remaining cysteine residue. It was therefore unnecessary to mutate the wild type cysteine residues.

2.2.1.1 Cysteine Clones

To provide available cysteine residues the proteins VAMP2 and ΔN-Syx were cloned to add cysteine residues to the C-terminal end. The C rather than N-terminal region was chosen so that, by FRET, monitoring of the formation of SNARE complexes would be possible in future studies. Custom-made synthetic oligonucleotides (primers) were designed so that the 3' (reverse or antisense) primer contained the additional cysteine residues. The initial primers were designed to add two cysteine residues to the protein sequence. As with the production of ΔN-Syx, the vector pPROEX-HTb was used to provide each protein with an N-terminal His_6 tag, for the use in purification.

ΔN-Syx-CysCys

The primers Synt.c-ter 5' and Synt.c-ter 3' Cys were used for the production of ΔN-Syx-CysCys PCR fragments. The amplification of the ΔN-Syx-CysCys fragment by this method was successful when a temperature gradient of 50-56°C (2 degree interval) was used with an extension temperature of 68°C (Figure 2.13). The 56°C PCR product was used for subsequent steps.

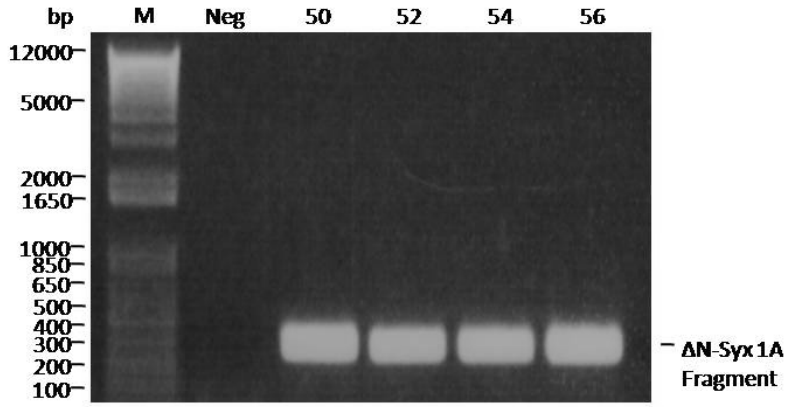


Figure 2.13. In this figure the results of PCR amplification of the ΔN-Syx-CysCys fragment is shown on agarose gel. A base pair marker (M) was loaded into the first lane followed by a negative control and each sample from the temperature gradient (50-56°C).The DNA was visualised by ultra violet light.

Once transformed into XL1-Blue *E. coli* cells, the DNA was checked for fragment insertion by a restriction enzyme double digest (HindIII and BamHI) as well as DNA sequencing. Following sequence confirmation, His_6-ΔN-Syx-CysCys was transformed into Rosetta™ cells from which expression trials were conducted followed by large scale expression and purification using the same protocol described for His_6-ΔN-Syx (section 2.1.4.2).

VAMP2-Cys

The initial primers used were VAMP-2-5' and VAMP-2-3' Cys. Despite many variations in the temperature cycling protocol (such as changes to the annealing and extension temperatures), amplification of the PCR fragment was not detected by agarose gel. New synthetic oligonucleotides were therefore designed. VAMP-2-3' Cys B was a modification of VAMP-2-3' Cys so that two cysteine residues would be added but the annealing backbone of the primer was increased. VAMP-2-3' 1Cys was a modification such that it's sequence was that of VAMP-2-3' Cys but with only one cysteine residue added and VAMP-2-3' 1Cys B was a combination of these modifications giving this primer only one cysteine residue but a longer annealing backbone. To accompany the 3' primers with longer annealing backbones a new 5' primer had to be designed which has been named VAMP-2-5' B. Details of primer sequences can be found in section 2.4.7.1.

Each possible combination of primers was trailed using the temperature gradient 48-54°C and 52-58°C (again with 2 degree intervals). Only one combination showed PCR fragment amplification which used the primers VAMP-2-5' and VAMP-2-3' 1Cys (Figure 2.14). The VAMP2 protein would therefore contain one, rather than two, additional cysteine residues. The 58°C PCR product was carried forward to subsequent cloning steps. Fragment insertion was confirmed by DNA sequencing and a double digest assay by the restriction enzymes HindIII and BamHI. Once sequencing was confirmed, the DNA was transformed into Rosetta™ cells, the expression optimised and His_6-VAMP2-Cys protein purified in the same manner as His_6-VAMP2.

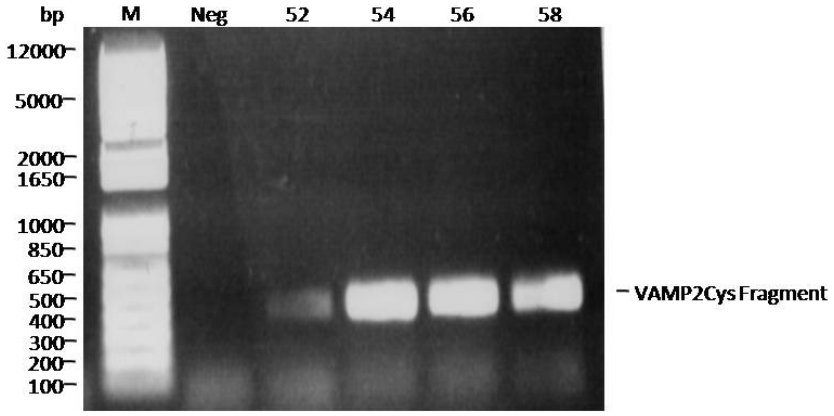


Figure 2.14. In this figure the results of PCR amplification of the VAMP2-Cys fragment is shown on agarose gel. A base pair marker (M) was loaded into the first lane followed by a negative control and each sample from the temperature gradient (52-58°C).The DNA was visualised by ultra violet light.

2.2.1.2 Fluorescent Labelling

The purified protein solutions of His_6-ΔN-Syx-CysCys and His_6-VAMP2-Cys were labelled with Alexa Fluor® 555 C_2-maleimide (MW ≈1250 g/mol) and Alexa Fluor® 488 C_5-maleimide (MW 720.66 g/mol) respectively. The protein solution was in storage buffer which already contained 1.5% sodium cholate and therefore dialysis or addition of detergent was unnecessary. Following the labelling protocol of Invitrogen, each protein was fluorescently labelled and excess dye removed using a desalting column and extensive dialysis. Protein solutions were then assessed for the degree of labelling (Equation 2.1).

$$\frac{A_x}{\varepsilon} \times \frac{MW\ of\ protein}{mg\ protein/ml} = \frac{moles\ of\ dye}{moles\ of\ protein} \qquad \textit{Equation 2.1}$$

Where A_x is the absorption of the dye at the absorption maximum wavelength and ε is the molar extinction coefficient of the dye.

Alex Fluor® dye	**λ at A_x, nm**	**ε M^{-1} cm^{-1}**
Alexa Fluor® 488 C_5-maleimide	493	72000
Alexa Fluor® 555 C_2-maleimide	556	158000

Table 2.1

From Equation 2.1 it was determined that a 0.5 ml sample of His_6-VAMP2-488 at a concentration of 0.55 mg/ml (30.6 µM) had been obtained with a protein: dye molar ratio of 1:1.2. For His_6-ΔN-Syx-555, a 0.5 ml sample of 0.53 mg/ml (35.3 µM) concentration was obtained with a protein: dye molar ratio of 1:3. In both cases the ratio was slightly higher than expected (1:1 for His_6-VAMP2-488 and 1:2 for His_6-ΔN-Syx-555 would be expected, based on the number of cysteine residues) this is most likely due to incomplete removal of free dye. However, as discussed in 2.3, all free dye is removed in subsequent steps.

2.3 SMALL PROTEOLIPOSOMES

Proteoliposomes were formed by mixing protein solution, detergent and lipid together followed by detergent extraction. The addition of lipid was such that the protein: lipid ratio was either 1:60 or 1:300 prior to detergent extraction. The detergent: protein ratio used was 8:1. After the mixture was incubated at 4°C for 1 hour the detergent was extracted using a PD-10 desalting column packed with Sephadex G-50m matrix material. The absorption of each collected fraction was measured at 280 nm as well as the wavelength of maximum absorption if any fluorescent dye was incorporated (either fluorescent lipid probes or fluorescent protein). Elution profiles showed two peaks; the first peak showing elution of proteoliposomes in the void volume of the column and the second, elution of detergent, lipid monomers and free fluorescent dyes (Figure 2.15). The void volume fractions were collected and the proteoliposomes pelleted by ultra centrifugation.

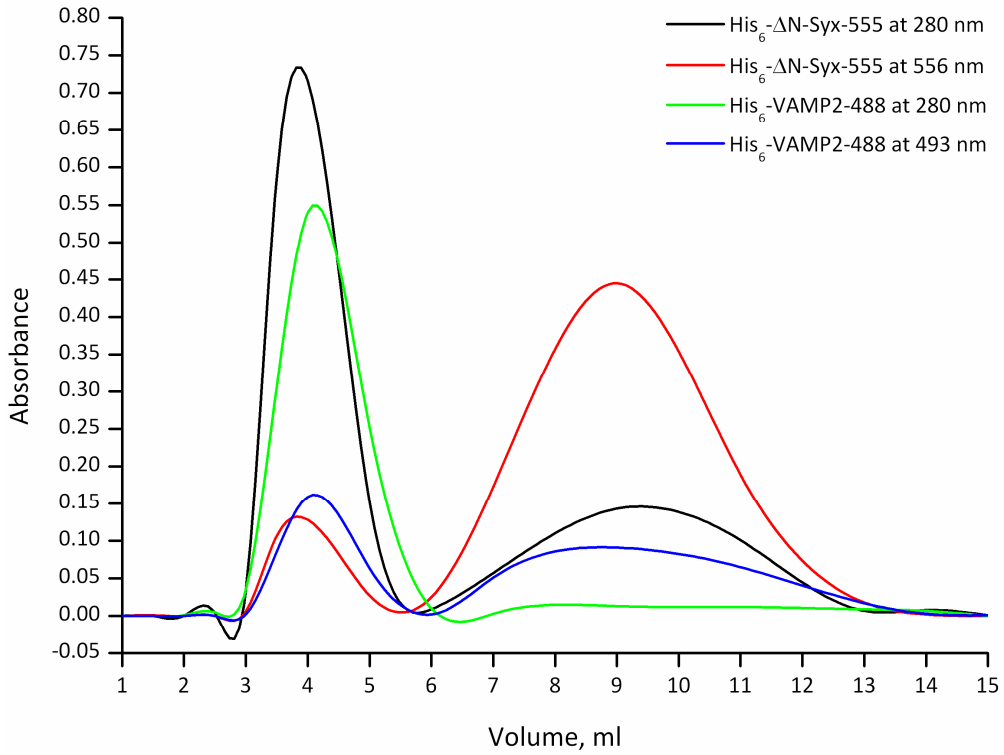


Figure 2.15. This figure shows the elution profile of two proteoliposome samples. Both samples are made from the lipid DOPC with one sample containing the fluorescent protein His_6-ΔN-Syx-555 and the other His_6-VAMP2-488. The protein: lipid molar ratio before detergent extraction was 1:300. Each fraction was analysed at 280 nm and the wavelength for maximum absorption of the fluorescent label. For His_6-VAMP2-488 this is at 493 nm and at 556 nm for His_6-ΔN-Syx-555. Proteoliposomes were eluted in the column void volume (3-5 ml). Free dye along with detergent and lipid monomers are eluted in the second, broad peak (6-13 ml).

2.3.1.1 Western Blot Analysis

Proteoliposomes containing His_6-VAMP2, His_6-SNAP-25 or His_6-ΔN-Syx were formed and analysed by western blot (Figure 2.16). The blots confirmed the presence of His_6-VAMP2 or His_6-ΔN-Syx in proteoliposome samples. As had been expected, due to its lack of membrane anchor, no SNAP-25 was detected when added independently to liposomes. Proteoliposomes were then produced containing both His_6-ΔN-Syx and His_6-SNAP-25. In this case separate anti-His_6 and anti-SNAP-25 blots confirmed the presence of both proteins. It was therefore shown that SNAP-25 does not non-specifically associate with liposomes and that the protocol does not affect ΔN-Syx/SNAP-25 complex formation.

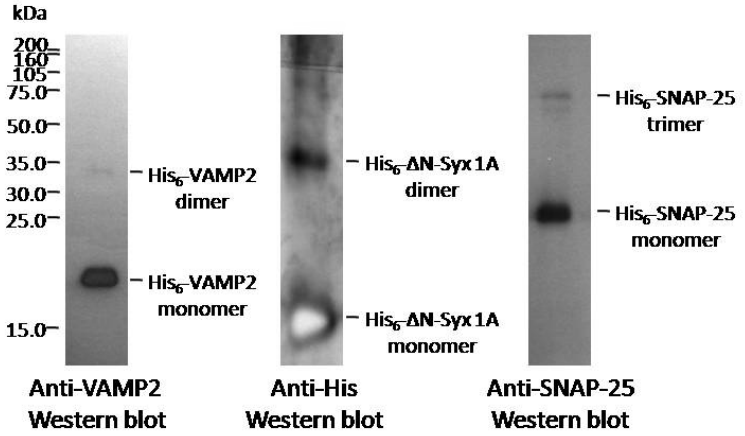


Figure 2.16. Proteoliposomes formed from DOPC and SNARE protein were analysed by western blot. His_6-VAMP2 liposomes were analysed using anti-VAMP2 (left) and His_6-ΔN-Syx liposomes by anti-His (centre). To check for SNAP-25 incorporation, the SNARE proteins His_6-SNAP-25 and His_6-ΔN-Syx were co-mixed to form t-SNARE liposomes, these were analysed by anti-SNAP-25 (right). All three western blots show protein insertion and though present, higher order oligomer bands are weaker than in the corresponding purified protein solutions.

From this analysis, it can also been seen that higher order oligomer bands are weaker. The combination of high detergent concentration during proteoliposome formation and the membrane environment provided by lipids following detergent extraction seems to break down these oligomers so that the vast majority of the protein exists in its monomeric state.

2.3.1.2 HPLC Analysis

It was important to establish the quantity of detergent still present in proteoliposomes as this would affect future *in vitro* assays. The pellets were therefore analysed by HPLC. The retention time of DOPC (≈14 min) and sodium cholate (5.3-6 min) was determined for the solvent conditions used. A calibration curve was produced for sodium cholate and a calibration curve for DOPC, produced under the same conditions, was provided by a current PhD student Duncan Casey (Figure 2.17).

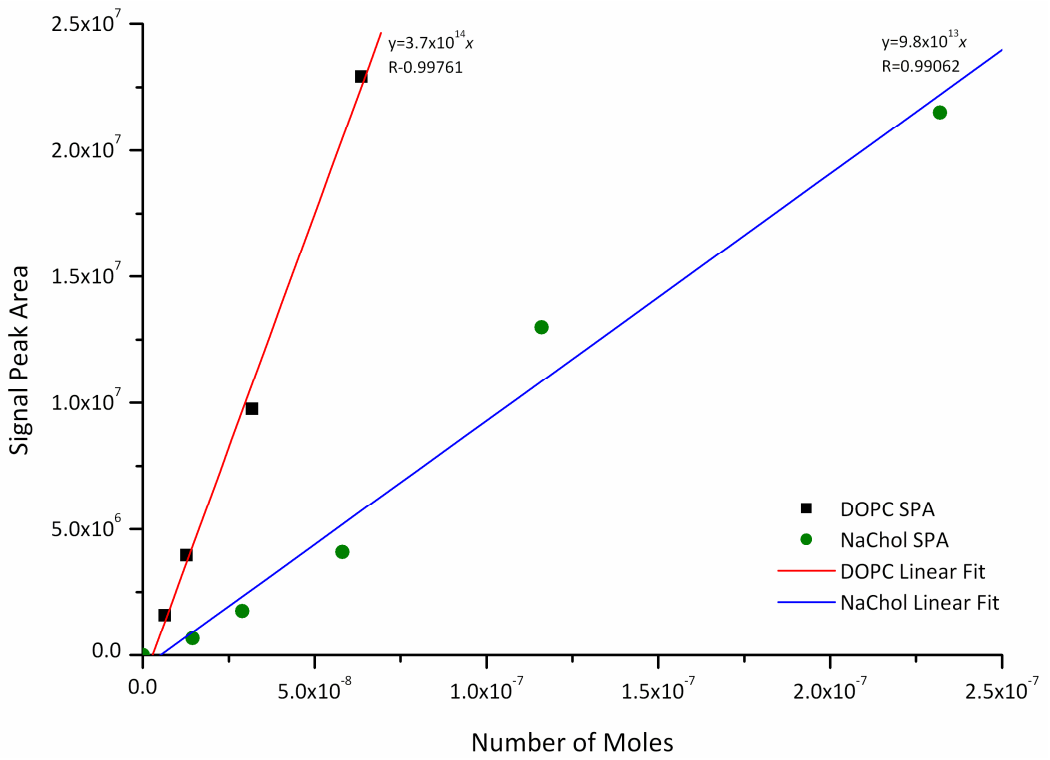


Figure 2.17. HPLC calibration curves were determined for the lipid DOPC and the detergent sodium cholate (NaChol) for the solvent regime to be used during analysis of proteoliposomes. The calibration curve for DOPC was obtained from D. Casey and is shown in red. The calibration curve for NaChol is shown in blue.

Two samples of His_6-VAMP2 DOPC proteoliposomes and two samples of t-SNARE (1:1 His_6-ΔN-Syx: His_6-SNAP-25) DOPC proteoliposomes were analysed by HPLC (Figure 2.18). Within the background error, no detergent was detected. The amount of DOPC present was also established from the calibration curve. On the assumption that all the protein had inserted into liposomes and been eluted into the void volume during detergent extraction it was seen that the final protein: lipid ratio was 1:30 ±10 (regardless of whether a 1:60 or 1:300 protein: lipid ratio had been used). It was therefore necessary to add further lipid to proteoliposome samples prior to use in *in vitro* assays.

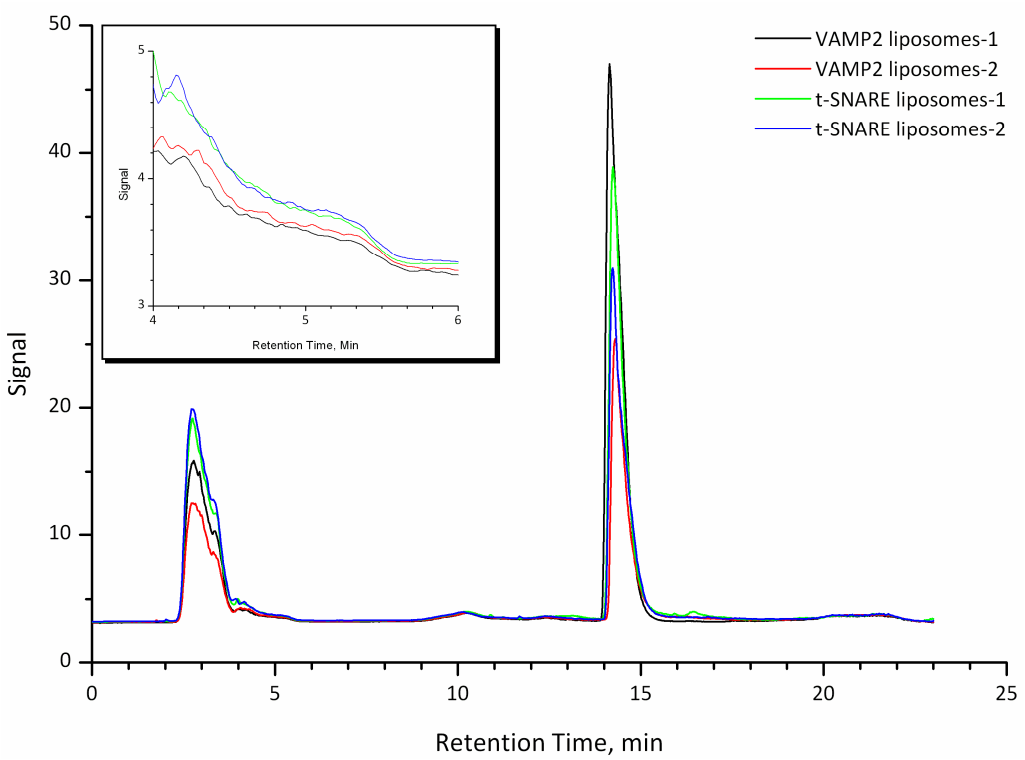


Figure 2.18. The HPLC profiles of two VAMP2 and two t-SNARE liposome samples are shown. The large peak at 14.5 minutes shows the elution of DOPC from the column. The inset graph shows the region between 4 and 6 minutes. The retention time of sodium cholate is 5.5 minutes; within background error no detergent is detected. The elution peaks seen between 2 and 4 minutes are due to residual storage buffer components.

2.4 Materials and Methods

2.4.1 Solutions and Buffers

2.4.1.1 Growth Media

LB (Luria-Bertani) broth	Purchased from Molecular Dimensions Limited (MDL) 10 g/L Casein Hydrolysate (tryptone), 5 g/L Yeast Extract, 0.5 g/L NaCl
Superior broth	Purchased from MDL, developed by AthenaES proprietary medium formulation
Power broth	Purchased from MDL, developed by AthenaES proprietary medium formulation
LB-Agar	Purchased from MDL, developed by AthenaES proprietary medium formulation

2.4.1.2 Antibiotics

Ampicillin (Amp)	10% (w/v) in 50% EtOH (ethanol)
Kanamycin (Kan)	3.5% (w/v) in d.H_2O
Chloramphenicol (Cam)	3.5% (w/v) in 95% EtOH

2.4.1.3 Purification Buffers

Dialysis Buffers

Storage Buffer	20 mM HEPES (4-(2-hydroxyethyl)-1-piperazineethanesulphonic Acid) pH 7.4, 100 mM KCl, 1.5% (w/v) sodium cholate

Breaking and incubation Buffers

K-elution buffer	50 mM Tris (Tris(hydroxymethyl)aminomethane) pH 7.4, 10 mM $MgSO_4$, 2 mM ATP
Breaking buffer 1	50 mM Tris pH 8.2, 4 M urea, 10 mM imidazole
Breaking buffer 2	50 mM Tris pH 8.0, 300 mM KCl, 10% (w/v) glycerol, 2 mM DTT (Dithiothreitol) 5% (v/v) Triton X-100 4 EDTA-free protease inhibitor tablets

His_6 Affinity Column Buffers

HiTrap buffer 1a	25 mM HEPES pH 8.0, 500 mM KCl, 20 mM imidazole, 5% (v/v) glycerol
HiTrap buffer 1b	HiTrap buffer 1a with 500 mM imidazole
Urea HiTrap buffer 1a	HiTrap buffer 1a + 4 M urea
Urea HiTrap buffer 1b	HiTrap buffer 1b + 4 M urea
HiTrap wash buffer	50 mM Tris pH 8.2, 4 M urea, 20 mM imidazole
HiTrap buffer 2a	20 mM Tris pH 7.7, 300 mM NaCl, 20 mM imidazole
HiTrap buffer 2b	HiTrap buffer 3-a with 250 mM imidazole
Urea HiTrap buffer 2a	HiTrap buffer 2a + 4 M urea
Urea HiTrap buffer 2b	HiTrap buffer 2b + 4 M urea

GST (Glutathione S-Transferase) Affinity Column Buffers

GSTrap buffer 1a	PBS (Phosphate Buffered Saline) + 5% (v/v) glycerol
GSTrap buffer 1b	50 mM Tris pH 8.0, 10 mM reduced glutathione, 5% (w/v) glycerol, 0.05% Tween20
1% Triton X-100 wash	Breaking buffer 2 with 1% (v/v) Triton X-100
GSTrap buffer 2a	50 mM Tris pH 8.0, 100 mM KCl, 10% (v/v) glycerol, 0.8% (w/v) OβG (Octyl β-glucopyranoside) or DDM (n-dodecyl β-D-maltoside)
GSTrap buffer 2b	GSTrap 2a + 10 mM reduced glutathione
Binding buffer	20 mM sodium phosphate, pH 7.5 0.15 mM NaCl
High salt wash	Binding buffer with 1 M NaCl

Size Exclusion Buffers

NaHEPES buffer	20 mM HEPES pH 7.4, 300 mM NaCl, 5% (w/v) glycerol, mM DTT
Urea NaHEPES buffer	NaHEPES buffer + 4 M urea
High salt NaHEPES buffer	NaHEPES buffer 1, pH 9.0
High pH NaHEPES buffer	NaHEPES buffer 1 with 4M NaCl
Low pH buffer	20 mM Sodium Citrate pH 4.0, 300 mM NaCl, 0.1 mM DTT, 5% (w/v) glycerol
Detergent NaHEPES	NaHEPES buffer + 0.8% (w/v) OβG or DDM

Detection

Tris-Acetate-EDTA (TAE) running buffer (50x)	2 M Tris-acetate pH 8.3, 0.05 M EDTA (Ethylenediaminetetraacetic Acid)
DNA Agarose gel	1% (w/v) Agarose in TAE 6.34 fM EtBr (Ethidium Bromide)
DNA gel loading buffer	0.25% (w/v) bromophenol blue, 40% (w/v) sucrose
SDS resolving gel	0.39 mM Tris pH 8.8, 15% (v/v) acrylamide mix, 0.1% (w/v)SDS, 0.1% (w/v) APS (Ammonium Persulphate), 0.04% (v/v) TEMED (NNN'N'Tetramethylethylenediamine)
SDS stacking gel	0.065 mM Tris pH 6.8, 4% (v/v) acrylamide mix, 0.1% (w/v) SDS, 0.1% (w/v) APS, 0.04% (v/v) TEMED
SDS loading buffer	200 mM Tris pH 8.8, 8% (w/v) SDS, 20% (v/v) glycerol, 1 mM bromophenol blue, 20 mM DTT

SDS gel running buffer (10x)	250 mM Tris, 2 M glycine, 0.4% (w/v) SDS
Native gel	0.39 mM Tris pH 8.8, 10% (v/v) acrylamide mix, 0.1% (w/v) APS, 0.04% (v/v) TEMED
Native gel loading buffer	200 mM Tris pH 8.8, 20% (v/v) glycerol, 1% (w/v) bromophenol blue
Native running buffer (10x)	250 mM Tris, 2 M glycine
Lysis buffer	10 mM Tris pH 8.0, 0.1 M NaH_2PO_4, 8 M urea
PAGE Coomassie Blue stain solution	30% (v/v) EtOH, 10% (v/v) acetic acid, 0.05% (w/v) Brilliant Blue R™
PAGE de-stain solution	30% (v/v) EtOH, 10% (v/v) acetic acid
Western Blot blocking solution	2.5% (w/v) skimmed milk powder (Sainsbury's Basic) in dH_2O
CAPS transfer buffer (100x)	1 M CAPS (3-[cyclohexylamino]-1-propanesulphonic acid) pH 11.0
PBS	10 mM NaH_2PO_4 pH 7.4, 1.8 mM K_2HPO_4, 140 mM NaCl, 2.7 mM KCl
PBST (PBS-Tween20)	PBS + 0.05% (v/v) Tween20

HPLC Solvents

HPLC Solvent A	101/21/2/0.1 (w/w) n-hexane/isopropanol/acetic acid/triethyl amine
HPLC Solvent B	155/17.5/2/0.1 (w/w) Isopropanol/water/acetic acid/triethyl amine

2.4.2 ANTIBODIES

Antigen	Antibody	Description	Source	Application
VAMP2	Anti-VAMP2	Mouse monoclonal clone 69.1	Synaptic Systems (SYSY)	1:10000
SNAP-25	Anti-SNAP-25	Mouse monoclonal clone 71.1	SYSY	1:10000
Syx 1A	Anti-Syx 1A	Mouse monoclonal clone 78.3	SYSY	1:10000
His_6	Anti-His_6	Mouse monoclonal clone 4A12E4	Invitrogen	1:5000
Mouse Ig	Goat Anti-Mouse Ig	Goat polyclonal	DAKO	1:2000

Table 2.2

2.4.3 PROTEIN EXPRESSION

The GST-Syntaxin 1A / His_6-SNAP-25b co-expression system and His_6-VAMP2 system were grown in Power media, the His_6-SNAP-25b single expression system in LB with the addition of 1% glycerol and the GST-Syntaxin 1A system in Superior broth.

2.4.3.1 Expression Vectors

The vector maps and amino acid sequences of the proteins below can be found in the appendices.

Construct	UniProt Accession	Vector	Resistance	Bacteria	Source*
His_6-VAMP2	P63045	pET-16b (Novagen)	Amp	Rosetta™	Dr G Schiavo
His_6-SNAP-25b	P60881	pQE-30 (Qiagen)	Amp	Rosetta™	Dr G Schiavo (Prof JE Rothman)
GST-Syx 1A†	P32851	pGEX-4T-2 (GE Healthcare)	Amp	Rosetta™	Dr G Schiavo (Dr RH Scheller)
GST-Syx 1A/ His_6-SNAP-25b		pGEX KG/pET	Amp/Kan	Rosetta™	Dr G Schiavo
His_6-ΔN-Syx-1A (a.a 181-288)		pPROEX-HTb (Invitrogen)	Amp	Rosetta™	-

Table 2.3

2.4.3.2 Production of Glycerol Stocks

10 ml of LB (containing antibiotic solution at 1 µl/ml) overnight cultures were grown of each bacterial system provided by Dr Giampietro Schiavo (or later transformed Rosetta cells). 1 ml of overnight culture was pelleted by centrifuge in an eppendorf at 4000 rpm for 10 min at room temperature. The bacteria pellet was gently re-suspended in LB glycerol (10% glycerol (v/v)) and stored at -80°C for later use.

* The original source is shown in brackets.
† Syntaxin 1A.

2.4.3.3 Isolation of Plasmid DNA

The QIAprep MiniPrep kit and protocol were used to obtain small amounts of DNA from 5ml of LB Amp (or LB Amp/Kan) overnight cultures, according to the manufacturer's instructions. DNA preparations were re-suspended in 50 µl ddH_2O and then stored at -20°C. For larger quantities (predominantly for cloning), 100 ml cultures were grown and the QIAprep MidiPrep kit used.

2.4.3.4 Transformation of E. coli

50 µl electro-competent Rosetta™ (Novagen, Rosetta 2 (DE3), strain F^- *ompT hsdS*$_B$(r_B^- m_B^-) *gal dcm* (DE3) pRARE2 (Cam^R)) or XL1-Blue competent cells (Stratagene, strain *recA1 endA1 gyrA96 thi-1 hsdR17 supE44 relA1 lac* [F'*proAB lacI*^{q}*ZΔM15 Tn10* (Tet^r)]) were thawed on ice. 2 ng of DNA was added and then the cells transferred to a pre-chilled 0.1cm gap cuvette. The cells were transformed using a BioRad Gene Pulsar (1.67 V, 25 µF, 200 Ω). Cells were then re-suspended in 200 µl LB and incubated with shaking at 37°C for one hour. 20 µl, 50 µl and 100 µl were then plated on LB agar (containing antibiotic solution (1 µl/ml)) and incubated at 37°C overnight.

2.4.3.5 Protein Expression Trials

5 ml of LB (with additional antibiotics 1 µl/ml) was inoculated using cells from glycerol stocks and then shaken overnight at 37°C. 20 ml of Broth with antibiotics (1 µl/ml) was inoculated with 2 ml of the overnight culture and grown at 37 or 32°C with shaking to an OD_{600} 0.5-0.8. The culture was induced by addition of 1 mM IPTG (isopropyl-beta-D-thiogalactopyranoside) and incubation continued for four more hours. Cells were harvested by centrifugation at 4000 rpm for 10 min and stored at -80°C. Pellets were defrosted, re-suspended in 5 ml HiTrap buffer 1a and then lysed by ultrasound for 2 minutes (with 1 second pulses) at amplitude 15. 1 ml was pelleted by centrifuge at 13000 rpm for 10 min. The supernatant was kept (soluble protein fraction) and the pellet re-suspended in 1 ml lysis buffer (insoluble protein fraction).

2.4.3.6 Large Scale Protein Expression

<u>His_6-VAMP2, His_6-SNAP-25b, GST-Syntaxin 1A and His_6-ΔN-Syntaxin 1A Systems</u>

150 ml of broth (with added antibiotics (1 µl/ml)) was inoculated using cells from glycerol stocks and then shaken overnight at 37°C. 6 x 1L of antibiotic broth were each inoculated with 25 ml of the overnight culture and grown at 37°C with shaking to an OD_{600} 0.5-0.8. 1 mM IPTG was added to each litre and incubation continued for four more hours. Cells were harvested by centrifugation at 4000 rpm for 10 min and the pellets stored at -80°C.

Co-expressed GST-Syntaxin 1A / His_6-SNAP-25b System

150 ml of broth (with added antibiotics (1 µl/ml)) was inoculated using cells from glycerol stocks and then shaken overnight at 37°C. 6 x 1L of antibiotic broth were inoculated with 25 ml of the overnight culture and grown at 37°C with shaking to an OD_{600} 0.5-0.8. 1 mM IPTG was added to each litre and incubation continued for four more hours. Cells were harvested by centrifugation at 4000 rpm for 10 min and the pellets stored at -80°C.

2.4.4 Protein Purification

2.4.4.1 His_6 Tag Purification

Pellets of harvested cells were defrosted on ice and re-suspended in HiTrap buffer a, at 10 ml per 1L of culture grown. Sonication of the suspension on ice at amplitude 15 for 2 x 6 min (1 second pulses, suspension stirred vigorously in between time periods) lysed the cells. Cellular debris was removed by centrifugation at 18000 g for 30 min at 4°C. A HiTrap affinity column (5 ml, Amersham Bioscience) was used for purification of proteins with His_6 tags (and those proteins that bind to His_6 tagged proteins). The supernatant was loaded onto a Ni^{2+} charged HiTrap affinity column pre-equilibrated with HiTrap buffer a. Unbound protein was washed out with 10 column volumes of HiTrap buffer a and non-specific bound protein removed by a volume step of 8 column volumes of 10% HiTrap buffer b. A gradient from 10- 100% buffer b over 8 column volumes eluted the SNARE proteins. 4 ml fractions were collected over the buffer b gradient region. The purification was conducted at 4°C on a BioRad DuoFlow FPLC (Fast Protein Liquid Chromatography) system.

2.4.4.2 GST Tag Purification

A GSTrap affinity column (5 ml, Amersham Bioscience) was used for initial purification of proteins with GST tags (and those proteins that bind to GST tagged proteins). Pellets of harvested cells were defrosted on ice and re-suspended in breaking buffer or GSTrap buffer a (20 ml per 1L of culture grown; see section 2.1). Sonication on ice of the suspension at amplitude 15 for 2 x 6 min (1 second pulses, suspension stirred in between time periods) lysed the cells. Cellular debris was removed by centrifugation at 18000 g for 30 min at 4°C.

The Supernatant was loaded overnight at 0.5 ml/min using a peristaltic pump onto a GSTrap affinity column (5 ml, Amersham Bioscience) pre-equilibrated with breaking buffer or GSTrap buffer a. The column was then mounted to a BioRad DuoFlow FPLC system where unbound protein was washed out with 10 column volumes of GSTrap buffer a. Non-specific bound protein was removed by a volume step of 8 column volumes of 10% GSTrap buffer b. A gradient from 10-100% buffer b over 8

column volumes eluted the GST tagged protein (and binding partners). 4 ml fractions were collected over the buffer b gradient region. The purification was conducted at 4°C.

2.4.4.3 GST Cleavage

The protocol described in section 2.4.4.2 was followed up to and including the non-specific wash step. Rather than a gradient step the column was then washed with 3 column volumes of GSTrap buffer a. 20 µl of 1 µg/µl Thrombin stock was added to 4.98ml PBS and loaded onto the GSTrap affinity column. The flow-through was discarded and the column incubated for 12 hours at room temperature. A benzamidine column (1 ml, GE Healthcare) pre-equilibrated with binding buffer was connected to the GSTrap affinity column. The columns were then washed with 4 column volumes of binding buffer and the flow through collected in 1 ml fractions. The columns were washed further with 4 column volumes of high salt wash and the flow through collected in 1 ml fractions.

2.4.4.4 Size Exclusion

Dilute protein preparations obtained from affinity column purification steps were concentrated in a centrifugal concentrator (20 ml iCON™, 9k MW cut off, Pierce) at 4000 rpm and 4°C. The concentrated fractions were assessed on SDS-PAGE gels to see if further purification was required. If required, proteins were purified further by size exclusion using a Superdex 200 column (Amersham Bioscience, void volume ≈38 ml, globular protein exclusion limit 1300 kDa). The column was equilibrated overnight with 1.5 column volumes of NaHEPES buffer. The concentrated protein solution was loaded into a static loop which had been washed with flow-through from the protein concentration step. The protein solution was loaded onto the column with additional NaHEPES (50% of loop volume). 100% NaHEPES over 1 column volume eluted the proteins. 4 ml fractions were collected over the entire run. This purification was run on a BioRad FPLC system at 4°C.

2.4.4.5 Concentration of Dilute Protein Preparations

Protein solutions were concentrated as described in section 2.4.4.4. The concentrated fractions were assessed on SDS-PAGE gels to see if further purification was required.

2.4.5 Visualisation of Purified Protein

2.4.5.1 Denaturing Polyacrylamide Gel Electrophoresis (SDS PAGE)

These were used throughout, during both expression and purification steps. Gels were made from 5 ml resolving gel topped with 1 ml stacking gel. Each protein sample was added to 5 µl SDS loading buffer and then denatured at 95°C for 5 minutes. Between 10 and 20 µl of each sample was then loaded onto the gel. 5 µl of Mark12™ Unstained Standard (Invitrogen) was also loaded into one lane. The gel was run at 180 V, 30 mA or 200 V, 50 mA for 1 hr 12 min for one and two gels respectively. Gels were stained with Coomassie stain then de-stained to visualise protein bands.

2.4.5.2 Western Blot and Chemiluminescent Detection

Proteins were separated by size using SDS-PAGE as described above but using 10 µl full range rainbow marker (GE Healthcare) rather than Mark12™ marker. Proteins were transferred to HyBond ECL (Enhanced Chemiluminescence) nitrocellulose membrane using a Hoefer SemiPhor protein transfer tank and the semi-dry procedure according to the manufacturer's protocol. In brief this protocol is as follows:

6 pieces of 3 mm chromatography paper (Anachem) and 1 piece of HyBond ECL nitrocellulose membrane (GE Healthcare) were cut to the size of the gel (usually 9.5 x 7 cm). The chromatography paper was soaked in 30 ml CAPS transfer buffer. The HyBond membrane was placed on top of the acrylamide gel and then sandwiched between triple layers of the CAPS soaked chromatography paper; this was placed in the transfer tank. The current needed was calculated from the dimensions of the acrylamide gel using a simple equation (amps = width (cm) x length (cm) x 0.8) and in most cases gave a current of 53 mA. With the power set to 100 W protein transfer proceeded for 1 hour.

After transfer the nitrocellulose membrane was placed in a Petri dish with 50 ml block solution and rocked at room temperature for 60 min before being stored at 4°C overnight. The next day the membrane was left rocking at room temperature for at least 30 min before it was incubated (with rocking) with the primary antibody (1:10000 in 10 ml block solution) for 1-1½ hours, again at room temperature. The membrane was then washed with PBS, PBST and then PBS again for ten minutes each. Incubation (with rocking) with the secondary antibody (1:2000 in 10 ml block solution) then took place for 45 min. Again the membrane was washed with PBS, PBST and finally PBS.

Protein bands were detected using an ECL Advance Western Blotting Detection Kit and Hyperfilm ECL (both from GE Healthcare) as recommended by the manufacturer. The membrane was exposed to the film for between 30 seconds and 1 hour.

2.4.6 Quantification of Protein Concentration

The Beer Lambert law (λ=εcl) was used to determine protein concentrations (c). The absorbance of the protein solution at 280 nm (λ) was found after dilution in 6 M guanidinium hydrochloride, 20 mM phosphate buffer (pH 6.5); three readings were taken. Based on the known sequence of each of the proteins, plus any tags, the molecular weights and extinction coefficients (ε) were calculated using the ExPANSy ProtParam tool*.

Protein	Predicted Molecular Weight, Da	Extinction Coefficient†, $M^{-1}cm^{-1}$
His_6-VAMP2	13513.6	13980
His_6-SNAP-25	24137.9	7210
GST-Syntaxin 1A	58985.5	47440
His_6-ΔN Syx	15633.0	10555

Table 2.4

2.4.7 Cloning

2.4.7.1 Synthetic Oligonucleotides

Synthetic oligonucleotides for PCR (Polymerase Chain Reaction) and mutagenesis were obtained from Eurofin MWG Operon (Ebersberg, Germany).

Primer DNA Sequences

Primer stock solutions of 1 µg/µl were made from the lyophilised primer by addition of ddH_2O. The proteins ΔN-Syx, ΔN-Syx-CysCys, VAMP2 and VAMP2-Cys were all cloned in pPROEX-HTb.

The restriction site for the enzyme BamHI was added to the 5' fragments and the restriction site for the enzyme HindIII to the 3' fragments. The predicted melting temperature (T_m) for the whole fragment and that of the annealing backbone (T_{an}) is also shown. Where cysteines have been introduced into the protein sequence, these are indicated in **orange**.

Synt.c-ter 5'

5'- CGG GAT CCA TCA TCA TGG ACT CCA GC -3' T_m 68°C, T_{an} 53.7°C

Synt.c-ter 3'

5'- CCC AAG CTT CTA TCC AAA GAT GCC CC-3' T_m 66.4°C, T_{an} 52.9°C

Synt.c-ter 3' Cys

* http://us.expasy.org/tools/protparam.html
† At 280 nm assuming all cysteine residues to be half residues due to DTT use in purification steps.

5’- CCC AAG CTT CTA ACA GCA TCC AAA GAT GCC CCC G-3’ T_m 73.1°C, T_{an} 54.3°C

VAMP-2-5’

5’- CGG GAT CCA TGT CGG CTA CCG CTG-3’ T_m 69.6°C, T_{an} 54.3°C

VAMP-2-5’B

5’- CGG GAT CCA TGT CGG CTA CCG CTG C-3’ T_m 71.2°C, T_{an} 57.0°C

VAMP-2-3’ Cys

5’- CCC AAG CTT TTA GCA GCA AGT GCT GAA GTA AAC GAT G-3’ T_m 70.6°C, T_{an} 52.4°C

VAMP-2-3’ 1Cys

5’- CCC AAG CTT TTA GCA AGT GCT GAA GTA AAC GAT G-3’ T_m 68.3°C, T_{an} 52.4°C

VAMP-2-3’ 1CysB

5’- CCC AAG CTT TTA GCA AGT GCT GAA GTA AAC GAT GAT G-3’ T_m 69.5°C, T_{an} 56.5°C

VAMP-2-3’ CysB

5’- CCC AAG CTT TTA GCA GCA AGT GCT GAA GTA AAC GAT GAT G-3’ T_m 71.5°C, T_{an} 56.5°C

2.4.7.2 DNA Sequence Amplification

PCR was used to amplify specific DNA sequences and in all cases a RoboCycler Gradient 40 Temperature Cycler (Stratagene) was used.

PCR samples (25 µl)

17.5 µl dH_2O
2.5 µl PFU buffer (10 mM stock)
200 µM dNTP (Deoxyribonucleotide Triphosphate)
1 µl Forward (5’) primer (100 ng/µl)
1 µl Reverse (3’) primer (100 ng/µl)
1 µl DNA (5 ng/µl or water for negative control)
1 µl 50% DMSO (Dimethyl Sulphoxide)
0.5 µl PFU Turbo polymerase (2.5 units/µl stock)

A negative control plus four samples underwent temperature cycling, where the following protocol was used:

Temperature °C	Time, sec	Cycles
95	30	1
95	30	
Gradient	60	10
68	30	
95	30	
65	60	20
68	30	
68	300	1

The final temperature gradients that were used were 48-54°C (2 degree interval) for ΔN-Syx, 50-56°C for ΔN-Syx-CysCys and 52-58°C for VAMP2-Cys. The products were analysed by agarose gel and the highest temperature sample in each case (showing amplification) was then used.

2.4.7.3 Agarose Gel Electrophoresis

1% Agarose was dissolved in TAE buffer by heating in a microwave. When hand-hot the gel was poured into a mould and 50 ng/ml ethidium bromide solution added (to give ethidium bromide concentration of 6.34 fM). Once DNA sample was added, the gels were run in TAE buffer at 100 V and 70 mA. DNA was visualised under ultraviolet light by Gene Genius (Syngene).

2.4.7.4 Restriction Digestion

Vector DNA and PCR fragments were digested through the use of restriction enzymes. The primers were made to include the restriction sites of the enzymes BamHI and HindIII so that these could be used to digest PCR fragments. These enzymes were also used to cut the pPROEX-HTb vector.

PCR fragment digestion	10.3 µl dH_2O
	2 µl 10x Enzyme buffer
	2 µl BSA (Bovine Serum Albumin; 500 µg/ml stock)
	0.7 µl HindIII (10 units/µl stock)
	0.5 µg PCR product

The PCR fragments were digested overnight with the restriction enzyme HindIII by incubation at 37°C. The enzyme was inactivated through heating (65°C for 20 minutes). The restriction enzyme BamHI was then added (7 units) and the sample incubated at 37°C for a further 2 hours. This enzyme was then inactivated through heating, as above, and the PCR fragment cleaned using a QIAprep PCR purification kit.

Vector digestion	2 µl 10x Enzyme buffer
	2 µl BSA (500 µg/ml stock)
	0.7 µl HindIII (10 units/µl stock)
	0.7 µl BamHI (10 units/µl stock)
	2 µg Vector
	Made to 20 µl with dH_2O

The vector was cut and cleaned in the same manner as PCR fragments with the exception that the enzymes were added together. Incubation at 37°C proceeded for two hours before enzyme inactivation by heating, followed by purification using the QIAprep PCR purification kit.

2.4.7.5 DNA Fragment Ligation

To prevent self-ligation, the vector was first dephosphorylated.

Dephosphorylation	1 µl 10x Dephosphorylation buffer 1 µl Shrimp Alkaline phosphatase (1 unit/µl stock) 1 µg Vector 7 µl dH_2O

The reaction mixture was incubated at 37°C for 10 minutes followed by deactivation at 65°C for 20 minutes. Ligation of the PCR fragment and vector was achieved using a T4 ligase.

Ligation	100 ng Dephosphorylated vector Fragment (or water for negative control) 1 µl 10x T4 Ligase buffer 1 µl T4 Ligase (5 unit/µl) Made to 10 µl with dH_2O

Purified fragment solution was added so that the vector to fragment molar ratio was approximately 1:3 (as assessed by agarose gel). This was then incubated at 16°C overnight.

2.4.7.6 Fragment Insertion Verification

XL1-Blue cells were transformed with ligation product (see transformation protocol, section 2.4.3.4) and grown on LB-Agar plates. Single colonies were chosen and grown in 5 ml LB broth. The DNA was extracted using a QIAprep MiniPrep kit. The DNA was analysed by agarose gel and compared to a sample of pure vector. Cultures from colonies containing DNA of the correct weight were then grown in 100 ml LB broth. DNA was extracted using a QIAprep MidiPrep kit and double digested using both the HindIII and BamHI restriction enzymes. The digestion products were checked, by agarose gel, for a fragment of correct weight. DNA sequence analysis was also used for further confirmation.

2.4.8 Fluorescent Labelling

Alexa Fluor® 488 C_5-maleimide and Alexa Fluor® 555 C_2-maleimide were used to fluorescently label purified protein solutions of His_6-VAMP2-Cys and His_6-ΔN-Syx-CysCys respectively (Invitrogen). The thiol-reactive probes protocol (provided by Invitrogen) was followed but is described briefly below.

The following was conducted in the dark and using foiled covered vessels to minimise light exposure. 500 µl of purified protein solution was stirred using a magnetic stirrer. A 10 mM solution of Alexa dye was made by dissolving the lyophilised dye product in DMSO. The dye solution was then added to the protein solution drop-wise to give a dye: protein molar ratio of between 10:1 and 20:1. The solution was incubated, with stirring, overnight at 4°C. 0.2 mg/ml reduced glutathione dissolved in

the storage buffer (the buffer of the protein solution) was then added, in excess of the dye. The solution was passed through a Sephadex G-25 packed PD-10 desalting column (GE Healthcare) followed by extensive dialysis to remove glutathione and excess dye.

2.4.9 Preparation of Sephadex G-25 and G-50m Columns

Columns were prepared as instructed by the manufacturer (GE Healthcare). Sephadex G-25 or G-50m matrix material (GE Healthcare) was soaked in ddH_2O overnight at room temperature. The matrix was poured into PD-10 columns with the tip closed. The matrix was allowed to settle overnight at 4°C. Excess water was removed and the column washed through and packed with 10 column volumes of water under gravity flow. When not in use, columns were stored upright in 20% ethanol at 4°C.

2.4.10 Fluorescent Proteoliposome Formation

1.5 µmol lipid DOPC (Avanti Polar Lipids, USA) was suspended in storage buffer containing 10% (w/v) sodium cholate such that the lipid: detergent molar ratio was 1:8. In the dark, fluorescent protein (His_6-VAMP2-488 or His_6-ΔN-Syx-555) was added to give a protein: lipid molar ratio of 1:300. The detergent was removed from the sample using a pre-packed, equilibrated Sephadex G-50m PD-10 desalting column and storage buffer. 0.5-1 ml fractions were collected to a total of 15 ml. The absorption of each fraction was measured at 280 nm and the maximum absorption wavelength for the dye used (see Table 2.1). Fractions from the column void volume (which contain proteoliposomes) were collected. The proteoliposomes were concentrated by ultra centrifugation at 200000 g for 90 min (Beckman Coulter, 1 ml tubes) followed by re-suspension in 10 µl storage buffer. The lipid concentration and protein: lipid ratio of the pellet were assessed by HPLC.

2.4.11 HPLC Analysis

HPLC was used to analyse proteoliposome content. HPLC was conducted using a Waters 626 HPLC pump via a 150 x 4.6 mm nitrile column (Varian Inc, Yarnton, UK). Samples were dissolved in 1 ml absolute ethanol and analysed by evaporative light scattering with an ESA 301 detector (baseline noise +/- 0.4%, evaporation temperature 80°C, drift tube 45°C). The mobile phase ran from HPLC solvent A to HPLC solvent B over an 18 minute gradient at a flow rate of 1 ml/min. 5 ml HPLC solvent A was run after each sample to allow equilibration.

2.5 CHAPTER SUMMARY

This chapter has described the purification methods used to obtain high quality protein solutions of all the proteins used in this project. Cloning work has been conducted to both improve purification and allow fluorescent labelling. Once purified, membrane incorporation of the SNARE proteins into simple membrane models was established. The particular fluorescent labels were specifically chosen for their ability to act as FRET partners allowing this project to be developed in the future. For example, the use of this property would allow the formation of the *cis*-SNARE complex to be monitored.

From HPLC, it was seen that the final protein: lipid molar ratio was lower than expected (≈1:30) and that additional lipid was required for final proteoliposome samples to be used in *in vitro* assays. The insertion of SNARE proteins into GUVs (Giant Unilamellar Vesicles) made from these samples has been confirmed through the use of the fluorescent proteins produced in this chapter. This is discussed in Chapter 3.

Chapter 3.

THE EFFECT OF SNARE PROTEINS ON LIPOSOME FORMATION

In this chapter, data is presented that shows SNARE protein incorporation into giant unilamellar vesicles (section 3.3.2). This investigation used fluorescent SNARE proteins prepared by Alexa Fluor® dye labelling (discussed in Chapter 2). The microscopy images of GUVs show the homogeneous distribution of the proteins His_6-VAMP2-488 and His_6-ΔNSyx-555 throughout the DOPC lipid bilayer (protein: lipid molar ratio 1:300).

The affect of protein on liposomes has been investigated through analysis of the mean radius and size distribution of GUVs of both protein-free vesicles and proteoliposomes (section 3.3.3). The liposome compositions used varied in both the total protein: lipid molar ratio and the amount of protein able to membrane-associate. All liposome compositions were seen to contain two vesicle populations. For DOPC liposomes these populations were found to have a mean radius of 17.4 ± 2.58 μm (40% total number of vesicles) and 10.1 ± 0.12 μm (60% total number of vesicles). The addition of small amounts of the transmembrane anchored protein VAMP2 (1:600 protein: lipid molar ratio) had no significant affect on either the mean radius or occupancy of these two populations (within experimental error). Further addition of VAMP2 (protein: lipid molar ratio 1:300) gave populations with mean radii of 9.60 ± 1.39 μm and 4.88 ± 0.05 μm with the latter distribution occupied by 92% of the total number of vesicles. The increase in membrane curvature in this case has been attributed to the hydrophobic mismatch between the VAMP2 transmembrane domain and the preferred thickness of the DOPC bilayer.

It was also shown however, that protein could influence liposome formation even when there is no obvious means of direct membrane association. A t-SNARE liposome sample was prepared with a 1:300 protein: lipid ratio containing a 1:1 ratio of the transmembrane anchored protein ΔN-Syntaxin and the anchorless protein SNAP-25. Despite this, a large population of proteoliposomes (47% total number of vesicles) occupied a distribution with a mean radius of 4.98 ± 0.03 μm. It is believed that this is due in part to the ability of SNAP-25 to influence membrane curvature even without a formal membrane anchor. As will be discussed in the subsequent chapter, the findings of chapter 4 suggest that protein aggregate structures may also have affected GUV formation in the t-SNARE sample.

A detailed discussion of these results can be found in section 3.4.

3.1 INTRODUCTION

3.1.1 VESICLES TYPES

Vesicles are enclosed structures made from lipid bilayers and take various forms (Figure 3.1). Simple liposome models can be prepared by various techniques, where the method of choice depends on the type of vesicle required. Liposome type is usually separated by size and morphology. The size range definition varies from group to group[293] but generally small liposomes have a diameter ≤50 nm, large liposomes between 100 nm and 1 µm and giant liposomes have a diameter ≥1 µm. Vesicles made of a single bilayer are also described as unilamellar; those made of a number of bilayers are multilamellar vesicles (for small numbers of bilayers they are sometimes referred to as oligolamellar vesicles i.e. bi-lamellar, tri-lamellar). During the formation of vesicles it is possible to trap other vesicles inside; these structures are referred to as multi-vesicular.

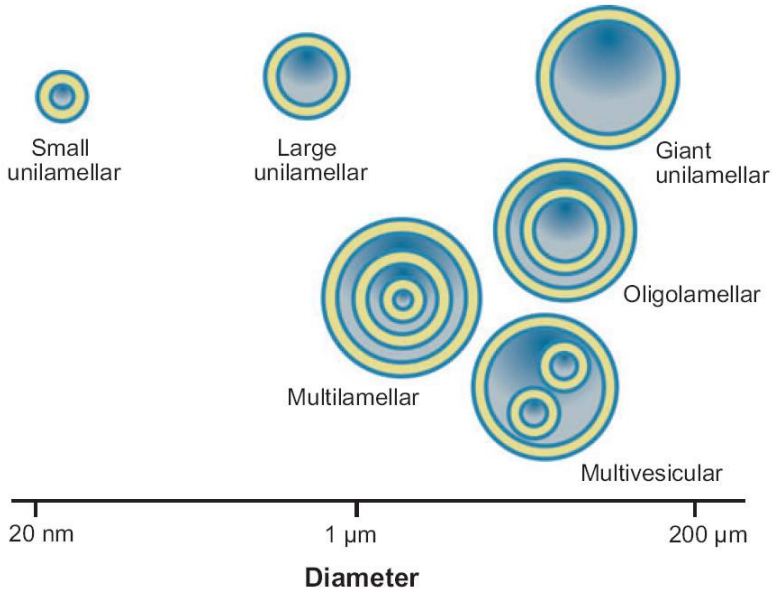


Figure 3.1. Small vesicles have a diameter below 50 nm, large vesicles are typically between 100 nm and 1 µm in size and giant liposomes have diameters above 1 µm. Unilamellar vesicles contain only one bilayer. As such these vesicles can be classified as small, large or giant unilamellar vesicles (SUV, LUV or GUVs), defining both size and morphology. Liposomes can also be made from multiple bilayers and are called multilamellar or oligolamellar vesicles. Multivesicular structures are formed when vesicles become trapped inside larger vesicles. Figure taken from Jesorka[294].

3.1.2 ELECTROFORMATION MECHANISM

GUVs are popular as *in vitro* models for cells, with the bilayer of the GUV considered to be a model for the plasma membrane. This is because the size of a GUV and cell (and therefore the global membrane curvature) is of the same order. Their size also means that they can be observed using optical microscopy.

One of the most popular methods for producing GUVs is electroformation. A lipid film deposited onto an electrode is subjected to an *ac* electric field. While the precise mechanism is still not known, it is thought that liposome formation proceeds through three basic steps; 1) the separation of interacting bilayers, 2) induction of instability and 3) bilayer bending and closure[(295)]. A lipid film deposited on a surface consists of stacked layers containing multiple bilayer domains and defects. Once a hydrating solution is added, the hydration force drives the solution through the layers (possibly through the defects) and the lipid film swells. This process is considered to be very fast with the inter-bilayer separation increasing from 0 to 10 Å in less than 10^{-4} seconds. Above this separation, the electrostatic repulsion between bilayers drives the inter-bilayer distance to increase. The application of an alternating current alters the electrostatic force, as well as van der Waals bilayer-substrate and bilayer-bilayer interactions, increasing the separation further to ≈0.1 μm. At defects, the hydrophobic regions of lipid molecules become exposed to water when the lipid film is hydrated. The defects therefore become areas of high energy and line tension occurs in the lipid layer; coupled with repulsive forces, bending instability results. The application of an alternating electric field may also apply a mechanical stress. This is caused by the electrophoretic motion induced in the lipid molecules and solute. This causes bilayers to rupture, forming bilayer fragments of different sizes. The energetic cost of exposing the edges of these fragments to water (referred to from now on as the edge energy) is large and so (provided the energetic cost of bending the membrane is not larger) a fragment is driven to bend and form a closed structure. There are thought to be two main mechanisms by which closed structures are formed (Figure 3.2); these are bilayer fusion (where two bilayer fragments fuse to form one structure) and scission (where a vesicle bud seals at its neck in a manner akin to endocytosis).

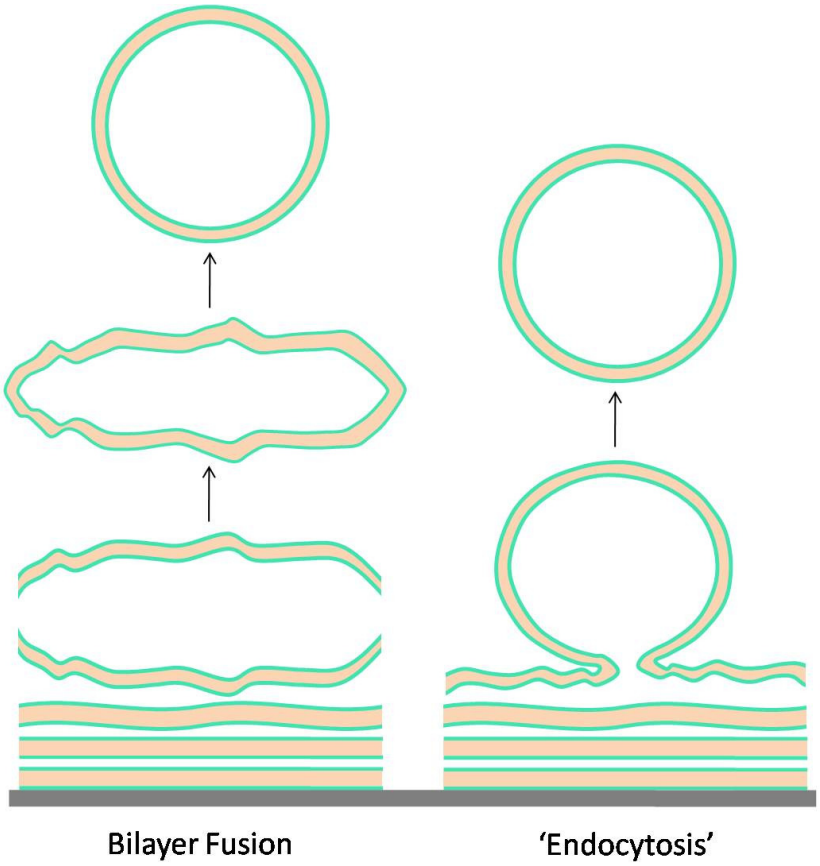


Figure 3.2. Bilayer fusion, shown on the left, is one mechanism by which liposomes may form. Two fragments, formed by mechanical stress (induced by an electric field), eliminate edge energy (the energy associated with exposure of the hydrophobic regions of the edge lipid molecules to water) by fusing together to form a closed structure. In doing so, some of the external solution is trapped within the vesicle. Another possible mechanism is not dissimilar to endocytosis in vivo. An area of a bilayer bulges out due to osmotic effects, the combination of mechanical stress and tension at the neck region causes fission of this area, resulting in the formation of a vesicle (shown on the right).

3.1.3 FACTORS INFLUENCING GUV FORMATION

As a result of electroformation, GUVs are metastable rather than thermodynamically stable structures. However, they are able to remain in these metastable states for many hours, even days. Many factors affect both the size and number of GUVs that are produced by the electroformation method. Some of these can be controlled including the electric field (type (*ac* or *dc*), voltage, frequency and function type (square wave, sinusoidal)) and buffer parameters (temperature, osmolarity and ionic strength). High salt concentration in the buffer for example, reduces both the size and number of vesicles formed and can inhibit formation completely[296]. This is thought to be due to charge screening, which reduces the electrostatic repulsion between bilayers.

Other factors include the thickness of the lipid film, which can be roughly controlled by using consistent lipid concentrations, volumes and deposition methods. The exact structure of the lipid film will however differ between experiments. Recently, research groups have used spin coating (a technique often used to produce supported lipid bilayers[297]) in an attempt to obtain more reproducible lipid films of uniform thickness[298]. However, even with this development, the lipid-lipid and lipid-substrate interactions will depend on the individual lipid properties resulting in differences between the lipid film composed of one lipid type and that of another.

3.1.3.1 GUV Curvature Free Energy

As would be expected, the need for a bilayer to bend and stretch during the formation of a liposome means that the properties of the bilayer itself (see section 1.3) are important variables. It has been shown for example that the addition of cholesterol to an egg lecithin sample inhibits liposome formation[296]. It is possible to speculate that in this example, the addition of cholesterol prevents vesicle formation by increasing membrane rigidity[299, 300]. In both the case of the fragment fusion mechanism and the endocytosis-like mechanism it can be seen that increasing the membrane rigidity increases the energy required to form GUVs. Addition of sufficient levels of cholesterol would make the energy required to form membrane buds unfeasible, inhibiting the endocytosis mechanism. Similarly, increasing the bending energy to be higher than the edge energy would inhibit the fragment fusion mechanism. It has also been shown that negatively charged lipid films can only form vesicles in the presence of an electric field (when deposited on the cathode). This may be explained by the ability of these lipids to form hydrogen bonds. In the absence of an electric field and upon hydration, a hydrogen-bonded bridge involving two negatively charge headgroups and one water molecule could form (Figure 3.3), increasing the energy required to separate bilayers. An electric field would disrupt the hydrogen-bond network, allowing vesicle formation to take place.

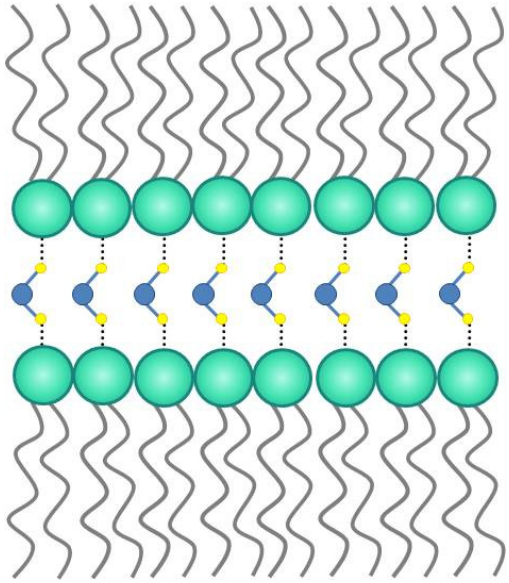


Figure 3.3. Strong bilayer-bilayer repulsion would be expected for bilayers made from a high composition of negatively charged lipids, due to electrostatic repulsive forces. The inability of these compositions to form liposomes without electric currents may be due to hydrogen bonding. A highly organised lattice of water molecules can form a hydrogen-bonded network with lipid headgroups; bridging bilayers. This would increase the energy required to separate the bilayers, which is required for vesicle formation. Application of an electric field would disrupt such hydrogen bonding and apply additional electrostatic force, allowing vesicle formation to occur.

These examples reflect the importance of considering the lipid properties and therefore the curvature free energy of the system (introduced in section 1.3.2). Electroformation creates metastable liposomes that occupy local energy minima. While not the thermodynamic energy minimum of the system (which would have a relaxed mean curvature H_r), the local energy minimum can be considered to have a local relaxed curvature (H_r'). The curvature free energy of a surface can be expressed by Equation 1.5:

$$g_c = \left(\mathrm{k} + \bar{k}\right)(H - H_r)^2 + \left(\mathrm{k} - \bar{k}\right)(H^2 - K) \qquad \textit{Equation 1.5}$$

As g_c is the curvature free energy per unit area, the total curvature free energy (G_c) of a vesicle can be expressed as the summation of the individual energy contributions of the two monolayers:

$$G_c = A^i g_c^i + A^o g_c^o \qquad \textit{Equation 3.1}$$

Where A is the surface area and the suffix i and o distinguish between the inner and outer monolayer. Assuming a vesicle is spherical with a radius R and bilayer thickness 2ℓ, Equation 3.1 can be re-expressed as:

$$G_c = 4\pi\left(k + \bar{k}\right)\left[(R - \ell)^2\left(H_r + \frac{1}{(R - \ell)}\right)^2 + (R + \ell)^2\left(H_r - \frac{1}{(R + \ell)}\right)^2\right] \qquad \textit{Equation 3.2}$$

From this, it can be seen that the free energy of the vesicle is quadratic with respect to the vesicle radius and that the minimal energy for each monolayer occurs when its radius (R ± ℓ) is equal to $1/H_r$. Therefore, as with this thermodynamic minimum, it can be expected that the local relaxed curvature, H_r', of each vesicle grown will be reflected by its radius.

3.1.3.2 Micelle and GUV Size Dispersion

The aggregation of amphiphilic molecules into micelles is governed by the hydrophobic effect. Above the CMC (Critical Micelle Concentration) it becomes more energetically favourable for molecules to aggregate together rather than to exist as monomers. The chemical potential of an aggregate that contains N molecules μ_N^0 can be expressed in terms of the interfacial tension, γ, and the cross sectional area of the amphiphile headgroup, a, at the hydrophilic/hydrophobic interface:

$$\mu_N^0 = 2\gamma a_0 + \frac{\gamma}{a}(a - a_0)^2 \qquad \textit{Equation 3.3}$$

Where a_0 is the optimum cross sectional area and $2\gamma a_0$ is equal to $\mu_{<N>}^0$where <N> is the mean number of molecules. From Equation 3.3, the mole fraction of an N-mer aggregate, X_N, can be written:

$$X_N = \left(\frac{X_{<N>}}{<N>}\right) e^{\frac{-<N>\Lambda(\Delta N)^2}{K_B T}} \qquad \textit{Equation 3.4}$$

Where Λ is equal to $\gamma a_0/9<N>^2$ and $\Delta N = N - <N>$. Equation 3.4 shows that the size of aggregates is expected to follow a Gaussian distribution. If we consider GUV formation to be analogous to micelle formation it should be expected that the size dispersion of GUVs will also follow a Gaussian distribution.

3.2 Materials and Methods

3.2.1 Solutions and Buffers

Storage Buffer	20 mM HEPES pH 7.4, 100 mM KCl, 1.5% (w/v) sodium cholate
Sucrose Solution	300 mM Sucrose ddH_2O
Glucose Solution	300 mM Glucose ddH_2O

3.2.2 Formation of Giant Unilamellar Vesicles by Electroformation

3.2.2.1 ITO Glass Preparation

ITO (Indium Tin Oxide) coated (single-sided coat, 5-10 Ω) glass slides measuring 50 x 75 x 0.7 mm were purchased from Diamond Coatings, Halesowen, UK. Conductive tape (3M, UK) was added to the ITO coated side of each slide to allow connection to a function generator by means of crocodile clips. Two glass slides were cleaned thoroughly using several cleaning steps; first using detergent followed by ethanol, distilled water and finally chloroform. Glass slides were dried under vacuum for 30 minutes. This procedure was followed prior to all experiments.

3.2.2.2 Liposome Sample Preparation

Analysis of proteoliposomes (see section 2.3) showed that pellets (following detergent extraction) contained protein and DOPC at an average molar ratio of 1:30. Before electroformation, liposome samples were made to a protein: lipid molar ratio of 1:53 and 1:267 by addition of further DOPC. Samples were then diluted with storage buffer to give a lipid concentration of 1mg/ml. Pure DOPC liposome samples were also prepared to a concentration of 1mg/ml by the same method. DOPC was purchased as a lyophilised powder from Avanti Polar Lipids, USA.

3.2.2.3 Electroformation

To prepare GUVs, a thin lipid film was first deposited onto the glass surface to allow greater surface wetting by the aqueous samples. 0.5 µl DOPC (in chloroform at 0.5 mg/ml) was deposited onto the ITO side of one glass slide and dried under vacuum for 20 minutes. 2 µl of liposome sample was deposited on top of this dry lipid film and the slide dried for a further 10 minutes under vacuum. With the addition of the initial lipid film the total protein: lipid molar ratio was 1:60 or 1:300 for proteoliposome samples.

An electroformation chamber was formed by sandwiching the dried lipid film between two ITO glass slides separated by a PDMS (Polydimethylsiloxane) spacer (Figure 3.4). The ITO coated sides of each slide formed the cell interior. Mini binder clips were used to make the cell water tight.

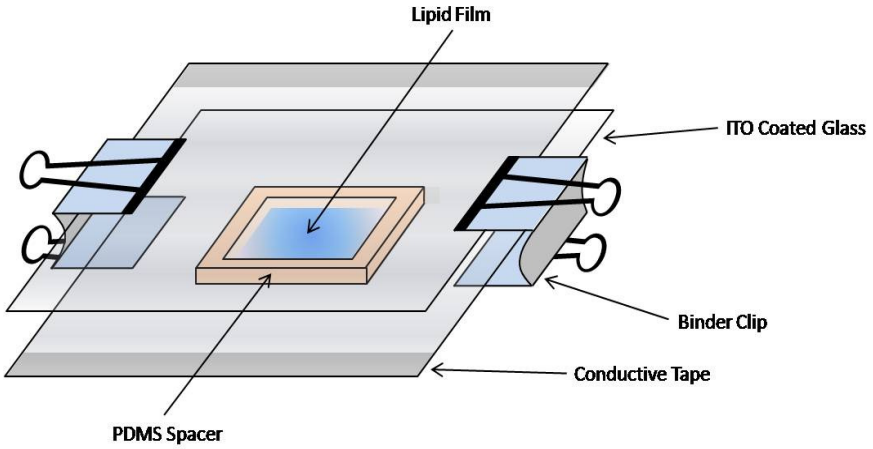


Figure 3.4. This figure shows the electroformation chamber used to produce GUV samples. A lipid film surrounded by a PDMS spacer is sandwiched between two ITO coated glass slides and sealed with binder clips. Following addition of buffer, the chamber is connected to a function generator by attachment of crocodile clips to the conductive tape adhered to each glass slide.

A needle was inserted through the PDMS into the cell chamber to allow air release. The cell chamber was then filled (using a syringe and needle) with 0.2 µm filtered sucrose solution until all air was removed. After the needles were removed the cell was placed onto a hotplate (pre-heated to 40°C) with the lipid film slide in contact with this heat source. The cell was connected to a function generator and a square wave *ac* current passed across the cell for a total of four hours.

The following procedure was used:

10 Hz, 1.2 V for 3 hours

4 Hz, 1.5 V for 30 min

2 Hz, 1.5 V for 15 min

1 Hz, 1.5 V for 15 min (voltage is the potential across the cell, as measured by voltmeter)

The hotplate was then switched off and allowed to reach room temperature before the cell was removed. The cell was carefully disassembled and the sucrose GUV solution collected. The sample was stored at room temperature in a clean glass vial and diluted five-fold with 0.2 µm filtered iso-osmotic glucose solution, just before use. GUV solutions were not kept for more than 24 hours.

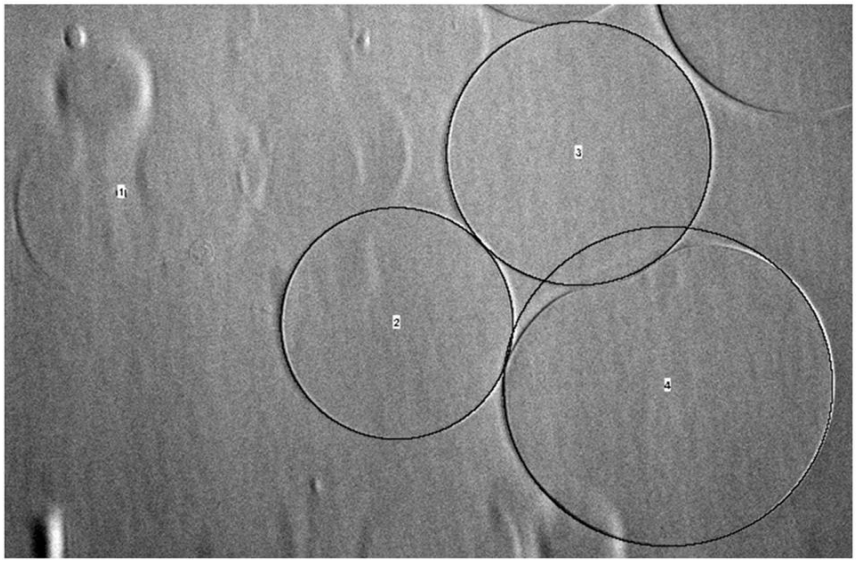
3.2.3 MICROSCOPY

A 200 µl droplet of diluted GUV sample was deposited on a glass cover slide and the sample observed. The microscope used was developed by Dr. Xavier Mulet (former PhD student) with modifications made by Dr. Nicholas Brooks (current postdoctoral reseracher). Based upon an inverted Nikon TE2000-E microscope, it is fitted with a motorised stage. A CCD camera (Hamamatsu Photonics KK., Japan) allows image acquisition. Hoffman modulation optics with Plan Fluor optic lenses (x20 and x40 magnification) were used and an arc Xe lamp provides stable fluorescence illumination. A LabView (National Instruments) based program developed by Dr. Brooks controls functions such as the light source (type, illumination levels and exposure times) and a motorised filter wheel.

3.2.4 GUV SIZE

3.2.4.1 Image Analysis

Several images at each position were taken at different focal depths so that each GUV could be analysed in full focus. Using the software Image J[(301)] each GUV (which is observed as a circle) was sized individually using the manual elliptical selection tool. Only GUVs in focus within a particular image were selected and each was labelled with an identification number to ensure it was only counted once. The measure application within Image J then gave the pixel area of the GUV (Figure 3.5). In some cases a GUV would be pressed up to a neighbouring GUV, leading to deformation of the surface. In these circumstances the ellipse that best fit the GUV edge as a whole was used, usually leading to an over-estimation of the area. A micro-ruler was used during image acquisition to allow the pixel area determined by Image J to be converted into μm^2.



Particle	Pixel Area
1	176
2	111640
3	144568
4	218508

Figure 3.5. The left of this figure shows a brightfield image obtained from a t-SNARE liposome sample (1:300 protein: lipid and 1:1 SNAP-25: ΔN-Syx molar ratio). Each GUV (in focus) was manually selected with an elliptical selection tool and assigned a label. Where a vesicle was deformed (Vesicle 4 is an example), an ellipse which best fit the edge of the vesicle as a whole was chosen, leading to an over-estimation of the area.

3.2.4.2 Error Analysis

In order to establish the mean radius and size distribution, the vesicles were grouped into area classes of 50 μm^2 size in the 0 to 13000 μm^2 range. The population of each class was then determined. The error incurred by manual selection was calculated by the repeated selection of particular vesicles chosen from a randomly selected image (Table 3.1).

Measurement	Vesicle 1	Vesicle 2	Vesicle 3
1	20880	9500	812
2	20880	8992	812
3	20612	9336	960
4	20360	9336	908
5	20612	9176	912
6	20612	9336	960
7	20880	9300	912
8	20636	9336	1020
9	20612	9176	860
10	20636	9500	860
Average	20672	9318.8	901.6
Standard Deviation	164.698	165.783	67.177
% Error	0.797	1.779	7.451

Table 3.1

As expected, the percentage error of the pixel area increased as vesicle size decreased. An exponential decay curve was found to best fit the data and the equation of this curve was used to evaluate the error associated with each of the vesicle areas measured (Figure 3.6). Using this data, the smallest and largest area calculated for each vesicle was obtained and the population of each class recalculated, giving the population error.

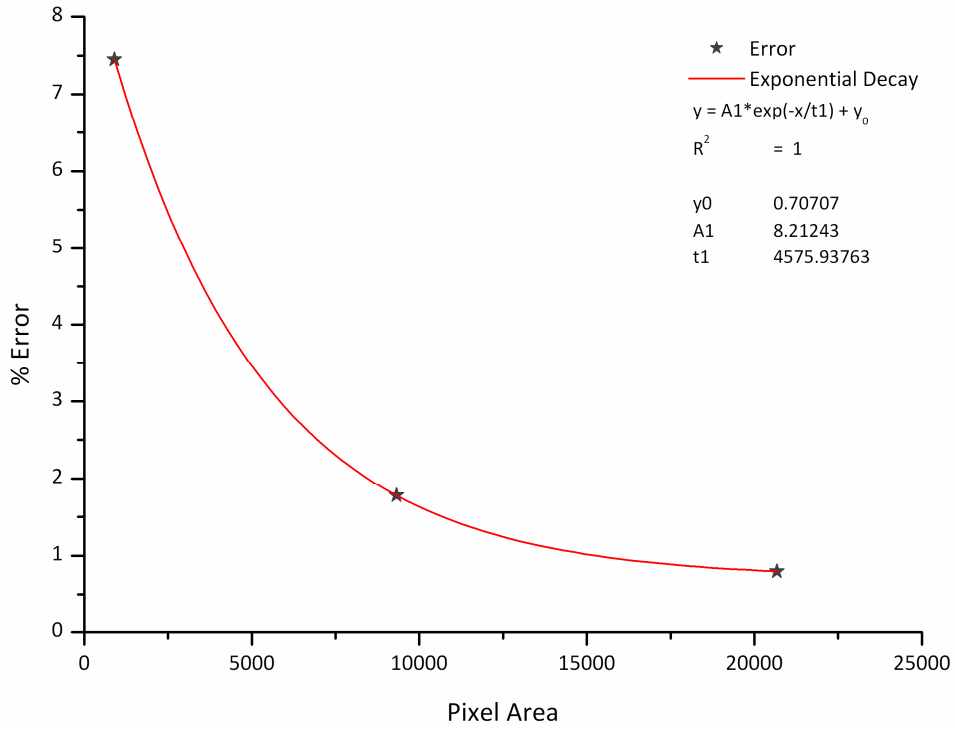


Figure 3.6. This figure shows how the percentage error of liposome area alters with vesicle size. An exponential decay curve was fit to the data and the equation of this curve used to assess the error of the area for each vesicle measured.

3.3 RESULTS

3.3.1 GUV FORMATION

The small proteoliposomes formed from detergent extraction (discussed in Chapter 2) were suspended in the protein storage buffer. This buffer contains the salt potassium chloride and therefore deposition of a lipid film would result in high concentrations of salt when the lipid solution was dried. It was first necessary to find an electroformation protocol which would allow GUV formation in these conditions. It was established that the addition of warm (40°C) sucrose solution at a relatively high concentration (300 mM) was sufficient for GUVs to form at a frequency of 10 Hz. It is likely that the use of warm sucrose solution dissolved and dispersed the salt within the lipid film, thereby reducing the salt concentration sufficiently to allow vesicle formation. The use of a high concentration of sucrose (and therefore also glucose) has the added advantage that it increases the contrast between vesicle and background under the microscope. However, GUV formation was only seen for the 1:300 protein: lipid preparations. Despite several different electroformation regimes being attempted, no GUVs were formed by the 1:60 protein: lipid preparation, suggesting protein influence on the lipid film (see section 3.4). As discussed in section 1.6, high protein densities are believed to create leaky vesicles. Therefore the lipid film of the 1:60 preparation may not have been stable enough to form GUVs during electroformation with the alternating current causing them to rupture.

3.3.2 PROTEIN INSERTION INTO GUVS

The insertion of the neuronal SNARE proteins into small proteoliposomes was established in Chapter 2. However, during electroformation these proteoliposome preparations were dried to form a lipid film and subjected to electric fields. It was not clear whether, during electroformation, protein would incorporate into forming vesicles or whether it would remain adhered to the glass substrate. This was of particular concern when it was found that the 1:60 proteoliposomes were incapable of forming GUVs. It was possible that the 1:300 samples only grew due to the addition of large amounts of DOPC to proteoliposome pellets and that the GUVs produced did not in fact contain protein. Therefore, to check that this procedure would not affect protein insertion, 1:300 proteoliposome samples containing either the fluorescent SNARE protein His_6-VAMP2-488 or His_6-ΔN-Syx-555 were produced and electroformation undertaken.

A FITC filter (Nikon, excitation 465-495 nm, emission 505 nm) was used for His_6-VAMP2-488 samples and a Texas Red filter (Nikon, excitation 540-580 nm, emission 595 nm) for His_6-ΔN-Syx-555 samples. The fluorescent images obtained clearly show the incorporation of neuronal SNARE proteins into GUVs prepared by this method (Figure 3.7). The images also show the protein to be homogenously distributed within the lipid bilayer (within the resolution of the microscope). Bright spots and patches seen on the images correspond to additional membrane moieties attached to, or trapped within, the primary GUV.

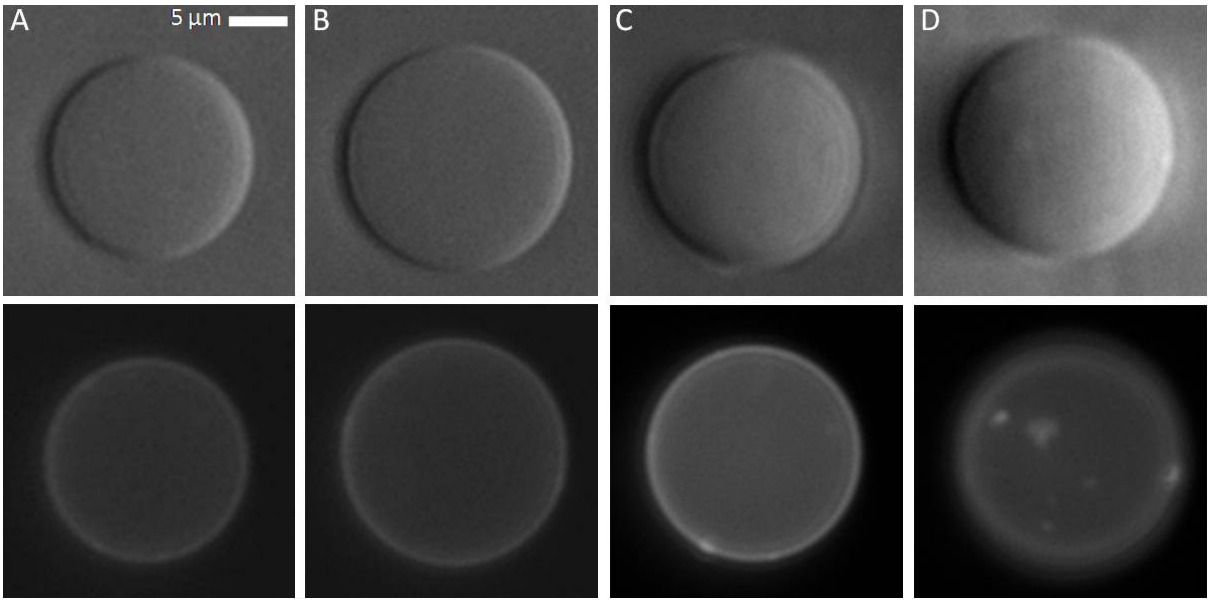


Figure 3.7. The top row of this figure shows the brightfield images of fluorescent SNARE GUVs grown by electroformation; the corresponding fluorescence images are shown underneath. Figures A and B show the incorporation and homogenous distribution of His_6-VAMP2-488 into DOPC GUVs at a protein: lipid molar ratio of 1:300. Figures C and D, show the incorporation of His_6-ΔNSyx-555 (also at a ratio of 1:300).

3.3.3 SNARE PROTEINS AFFECT GUV SIZE

The size of GUVs, varying in composition, has been analysed. While many factors affect the size and number of liposomes obtained (see section 3.1.3), the experiment was conducted so that, within reasonable error, the composition (with respect to protein type and protein: lipid molar ratio) was the only variable. The electroformation chamber described in section 3.2.2.3 was used with a modified PDMS spacer. This spacer was created so that it contained four separate chambers, allowing four lipid films to be deposited and grown at the same time without cross contamination. This method allowed many variables such as the drying and growing times, temperature, frequency and voltage to be eliminated during data analysis.

Proteoliposome samples containing either His_6-VAMP2 and DOPC or His_6-SNAP-25, His_6-ΔN-Syx and DOPC were prepared with a total protein: lipid molar ratio of 1:300; for the latter (t-SNARE) proteoliposomes the molar ratio of SNAP-25: ΔN-Syx was 1:1. As the purified SNAP-25 does not have means to attach directly to membranes (it contains no lipid anchors or transmembrane domain), the t-SNARE sample contained only half as many membrane anchors as the VAMP2 sample. A proteoliposome sample of His_6-VAMP2 and DOPC was therefore also prepared to a ratio of 1:600, allowing the influence of the transmembrane domains of VAMP2 and ΔN-Syx to be compared.

On the assumption that each vesicle was spherical the radius of each vesicle was calculated and plotted against population frequency. As discussed in section 3.1.3.2, the size dispersion was expected to fit to a Gaussian distribution; this was therefore used in order to determine the mean size of each GUV sample (Figure 3.8, Figure 3.9, Figure 3.10 and Figure 3.11). In each case it was found that two Gaussian distributions best fit the data.

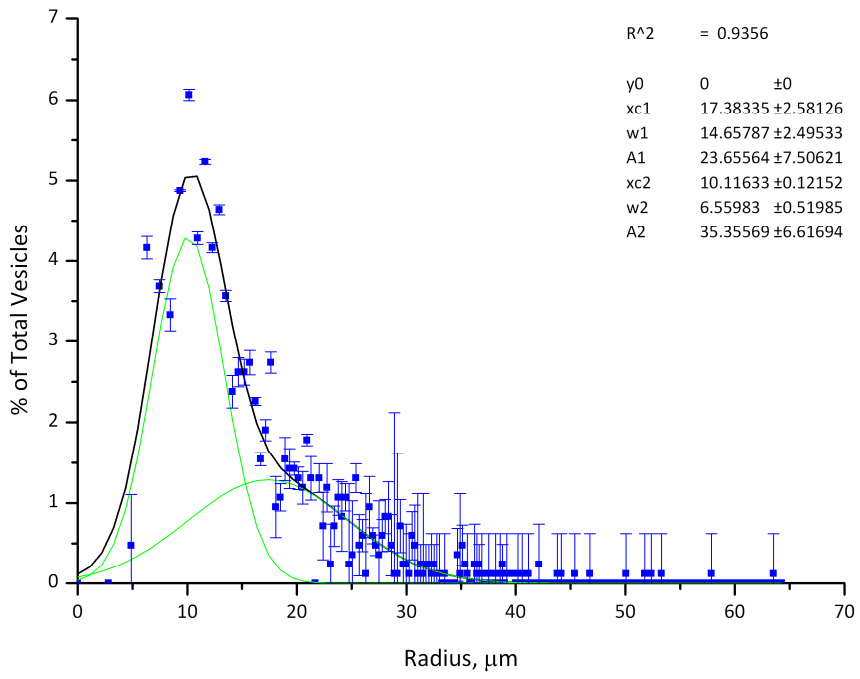


Figure 3.8. The population distribution of DOPC liposomes is shown as a function of vesicle radius. A multiple-peak Gaussian distribution has been fit to the data where the individual peaks are shown in green and the peak total is shown in black. From the distributions it can be considered that two vesicle populations exist, one with a mean size of 10 µm and the other with a mean size of 17 µm.

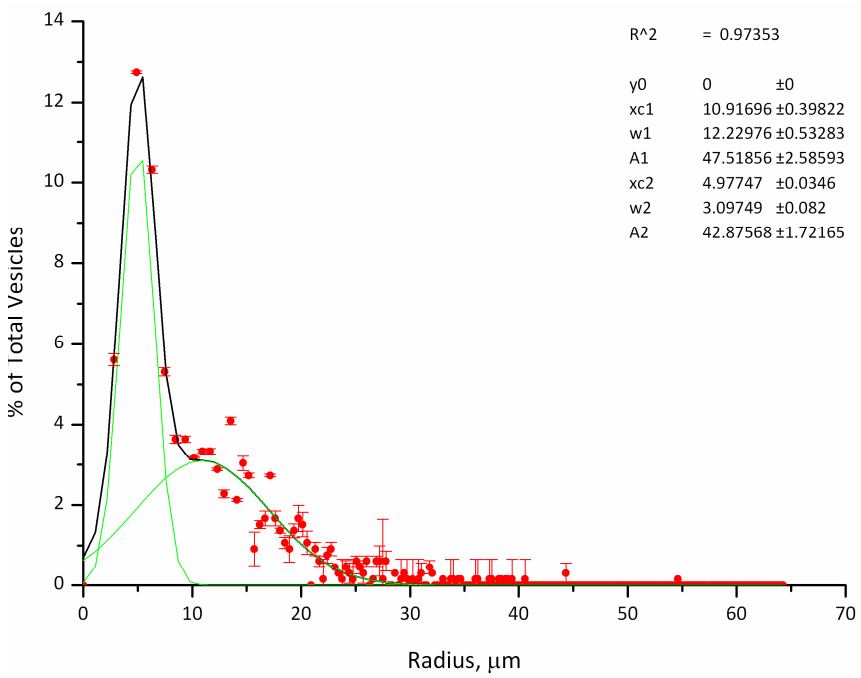


Figure 3.9. A graph showing the population distribution of t-SNARE DOPC liposomes as a function of vesicle radius is shown. The liposomes were made with a protein: lipid molar ratio of 1:300 and a SNAP-25: ΔN-Syx molar ratio of 1:1. A multiple-peak Gaussian distribution has been fit to the data where the individual peaks are shown in green and the peak total is shown in black. From the distributions it can be considered that two vesicle populations exist, one with a mean size of 11 µm and the other with a mean size of 5 µm.

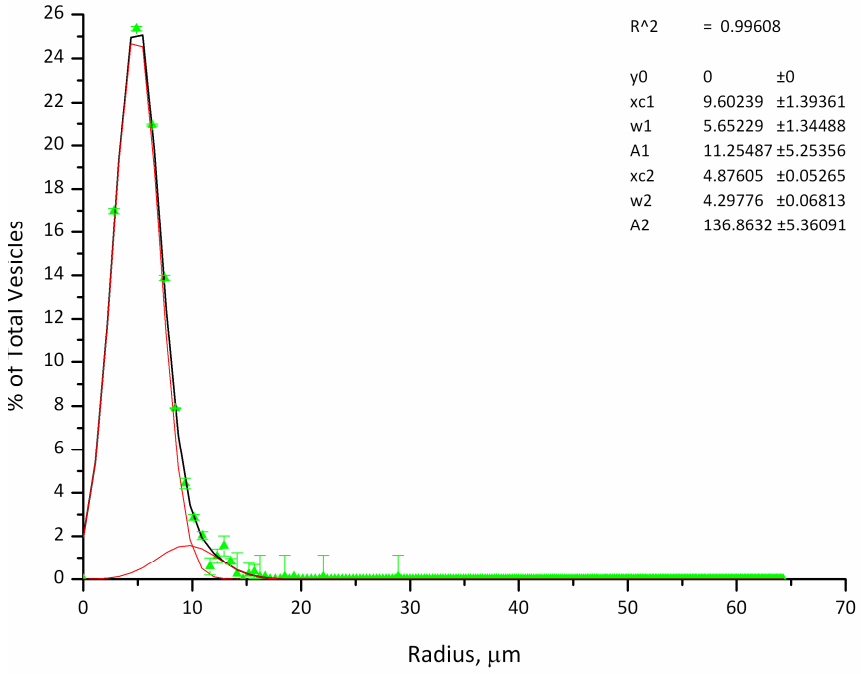


Figure 3.10. A graph showing the population distribution of VAMP2 DOPC liposomes as a function of vesicle radius is shown. The liposomes were made with a protein: lipid molar ratio of 1:300. A multiple-peak Gaussian distribution has been fit to the data where the individual peaks are shown in red and the peak total is shown in black. From the distributions it can be considered that two vesicle populations exist, one with a mean size of 10 µm and the other with a mean size of 5 µm.

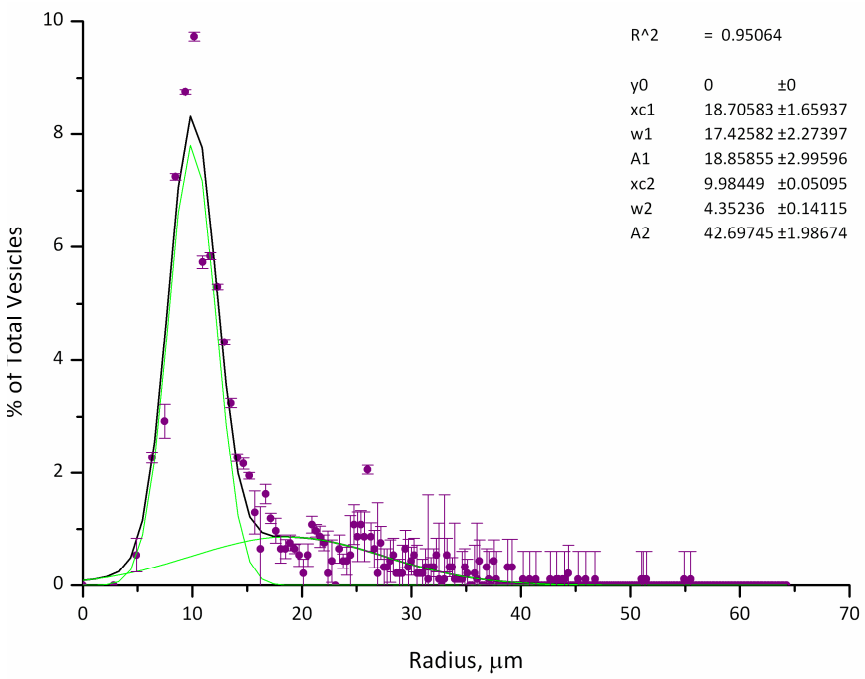


Figure 3.11. A graph showing the population distribution of VAMP2 DOPC liposomes as a function of vesicle radius is shown. The liposomes were made with a protein: lipid molar ratio of 1:600. A multiple-peak Gaussian distribution has been fit to the data where the individual peaks are shown in green and the peak total is shown in black. From the distributions it can be considered that two vesicle populations exist, one with a mean size of 10 µm and the other with a mean size of 19 µm.

Table 3.2 gives a summary of the mean size and standard deviation of each Gaussian distribution for the liposome compositions studied, based upon the multiple-peak Gaussian curve that was fit to each data set. For each composition it has been found that two vesicle populations existed. The relative occupancy of each population was calculated using the peak areas.

Composition	DOPC	t-SNARE: DOPC 1:300	VAMP2: DOPC 1:300	VAMP2: DOPC 1:600
Sample Size	841	859	836	875
Peak 1 Occupancy %	59.9 ± 11.2	52.6 ± 2.86	7.60 ± 3.55	69.4 ± 3.23
Mean Radius (µm, 3sf)	10.1 ± 0.12	10.9 ± 0.40	9.60 ± 1.39	9.98 ± 0.05
S.D (3sf)	3.28 ± 0.26	6.11 ± 0.27	2.83 ± 0.67	2.18 ± 0.07
Peak 2 Occupancy %	40.1 ± 12.7	47.4 ± 1.90	92.4 ± 3.62	30.6 ± 4.86
Mean Radius (µm, 3sf)	17.4 ± 2.58	4.98 ± 0.03	4.88 ± 0.05	18.7 ± 1.66
S.D (3sf)	7.33 ± 1.23	1.55 ± 0.04	2.15 ± 0.03	8.71 ± 1.14

Table 3.2

A visual comparison is provided in Figure 3.12 where the Gaussian fit from each of the data sets has been combined graphically. The results show that the presence of protein in liposomes affects both the vesicle radius and the relative occupancy of the vesicle populations which exist. Compared to pure lipid vesicles, the addition of a membrane-anchored protein at a 1:600 ratio (VAMP2: DOPC)

seems to have had little affect. A comparison of the two vesicle populations within these samples shows that the mean size and occupancy of each be considered equal within error. Increasing the amount of VAMP2 protein to a ratio of 1:300 (VAMP2: DOPC) altered both the mean size and occupancy of the two Gaussian distributions. A population was still seen with a mean radius at approximately 10 µm but its occupancy was reduced to only 7.6% (compared to ≈60% for DOPC). However, the second distribution of the VAMP2 sample (which accounts for 92.4% of the vesicles) has a mean size of approximately 5 µm compared to the DOPC sample with a second distribution with a mean radius at ≈18 µm. This result shows a significant decrease in the liposome size overall as a result of VAMP2 addition at this protein: lipid ratio. Surprisingly, the t-SNARE liposomes also had a large population of vesicles with a mean radius of ≈5 µm, despite having only half the number of membrane-anchored proteins as the VAMP2 1:300 sample. The second population, as with all other compositions, is seen to have a mean radius of approximately 10 µm and has an occupancy level similar to that of the DOPC sample. A discussion of these results can be found in section 3.4.

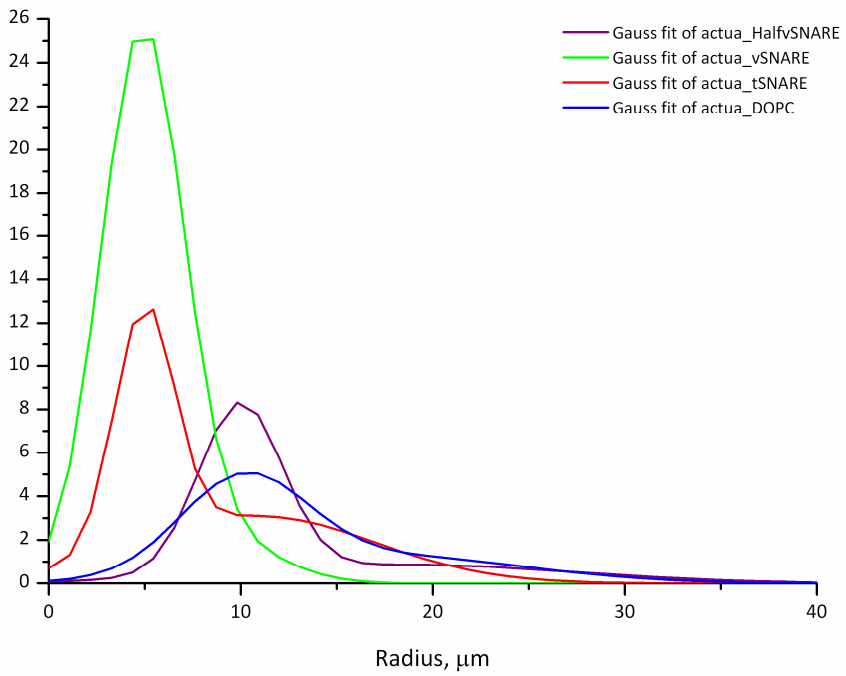


Figure 3.12. The Gaussian distribution fit to the data of each liposome population is shown. It can be seen that the size of the DOPC liposomes (blue) is comparable to the VAMP2 DOPC liposomes where the protein: lipid molar ratio is 1:600 (purple). The 1:300 VAMP2 DOPC liposome sample (green) is shown to have approximately half the mean radius of the 1:600 sample. Despite having the same number of membrane anchors, the t-SNARE DOPC liposome sample (red) also has a large population with a mean radius of approximately 5 µm, though a significant proportion still exhibit a mean radius comparable to that of the DOPC and 1:600 VAMP2 samples.

3.4 DISCUSSION

The fluorescence imaging of GUVs containing either the fluorescent SNARE protein His_6-VAMP2-488 or His_6-ΔN-Syx-555 has established that the electroformation of GUVs formed from small proteoliposome preparations (created by detergent extraction) does lead to protein insertion into these simple lipid bilayer models.

The use of a simultaneous electroformation technique has allowed data to be obtained where differences in the size of GUVs can be attributed to the presence of protein. As discussed in section 3.1.3, it was expected that if the size dispersion was analogous to that of micelles the data would follow a Gaussian distribution. Fitting the data to such a distribution required the use of a multiple-peak fitting method where two Gaussian peaks were used in each case. Employing this method gave variances higher than 93% in all cases. A comparison of the mean radii of the DOPC sample with either the VAMP2 or t-SNARE (ΔN-Syx and SNAP-25) samples shows a decrease in the radius (i.e. an increase the local relaxed curvature H_r') due to protein addition. For VAMP2 this can be explained by the effect of hydrophobic mismatch.

When a transmembrane domain is inserted into a bilayer the lipid molecules are forced to stretch and compress in order to accommodate it. This occurs when the transmembrane region and the preferred lipid bilayer thickness differ. The larger the discrepancy, the greater the hydrophobic mismatch and the higher the stored energy of the bilayer becomes. The transmembrane region of VAMP2 has been modelled as α-helical[34]. By definition[19], an α-helix is a right-handed helix with a pitch of 5.4 Å, each turn containing 3.6 amino acid residues (Figure 3.13A). The transmembrane domain sequence of VAMP2 is 20 amino acid residues long and is therefore calculated to be 30 Å long. Experimentally a pure DOPC bilayer has been found to be ≈35 Å thick[302]. The anchor of VAMP2 is therefore significantly shorter than the preferred thickness of a DOPC bilayer. As a result of this mismatch the lipid chains surrounding the anchor are required to compress, thinning the bilayer at the lipid-protein interface to prevent any exposure to water. However, a reduction in bilayer thickness can be achieved more favourably by bending the bilayer as the increase in energy can be evenly distributed throughout the system. The hydrophobic chains of lipid molecules on one leaflet are able to splay, reducing the thickness of that monolayer (Figure 3.13B) and the bilayer overall. It can therefore be seen that the addition of VAMP2 causes an increase in H_r'. It was not possible to grow GUVs that contained VAMP2 at a protein: lipid ratio of 1:60. The level of hydrophobic mismatch due to the presence of so much protein is likely to have prevented stable GUV formation.

This may provide an explanation for why vesicles containing this protein at high protein densities have historically been found to be leaky (section 1.6).

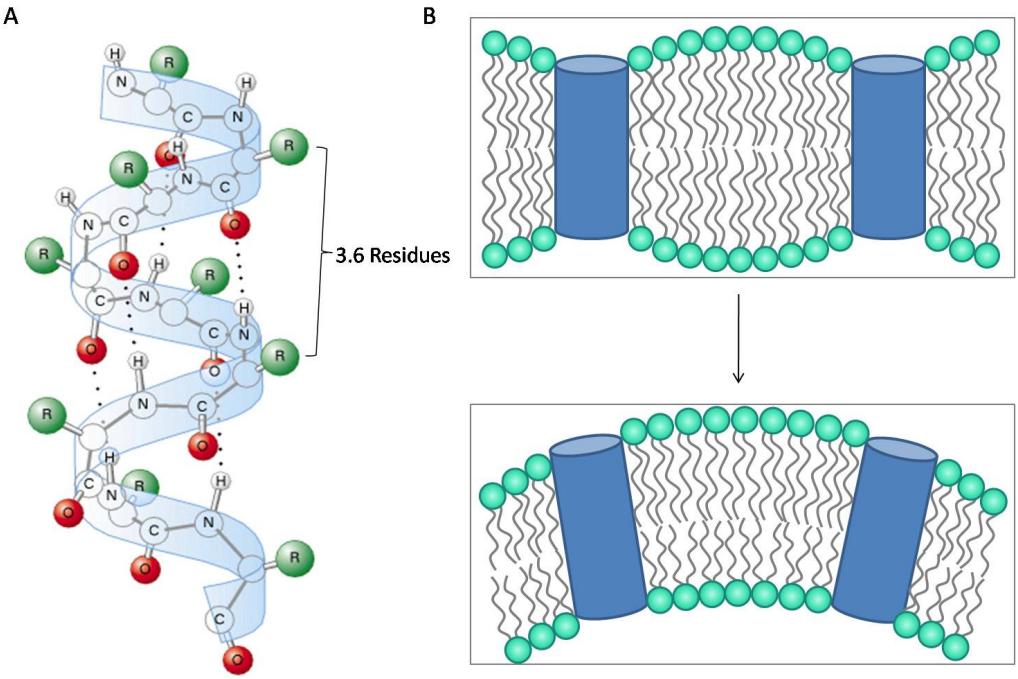


Figure 3.13. Figure A on the left shows an α-helix which is a common secondary protein structure. This right-handed helix contains 3.6 amino acid residues per turn and has a pitch of 5.4 Å (1.5 Å translation per residue). Figure B shows the consequences of hydrophobic mismatch. A hydrophobic insertion (such as a protein's membrane anchor) into a lipid bilayer forces the bilayer away from its preferred thickness if the anchor is too large or small (the latter is shown here). In order to thin the bilayer, at the lowest energetic cost, the bilayer bends allowing some lipids to splay.

The hydrophobic mismatch between the VAMP2 transmembrane domain and lipid bilayer may only be a peculiarity of the chosen model system. The membranes of cells *in vivo* are highly complex, containing thousands of lipid species. A discrepancy between transmembrane length and bilayer thickness may therefore not exist in the biological context, though an influence of the local lipid composition would be expected. However, hydrophobic mismatch is thought to be relevant *in vivo* particularly where the transmembrane anchors are larger than the bilayer thickness[303]. In these cases the domain tilts in order to accommodate itself in the membrane[304]. So if it does occur, how could hydrophobic mismatch affect the membrane fusion process?

During membrane fusion, VAMP2 is located on synaptic vesicles which are approximately 50 nm in diameter. These highly curved membrane bodies may have relatively thin bilayers and so the short anchor of VAMP2 may not have a mismatch in this environment. However, VAMP2 also resides at the trans-Golgi complex and plasma membrane at other stages of the fusion process. These membranes are flatter than synaptic vesicles and may also be thicker so that in these locations

VAMP2 would have a hydrophobic mismatch. In both of these membranes VAMP2 is recruited to vesicles as they bud. If hydrophobic mismatch does exist in these membranes, lipids surrounding the anchor would be more prone to bend and may partially determine the site of vesicle budding. Alternatively, when a membrane bud begins to form it would be energetically favourable for VAMP2 to locate at these areas of higher curvature. The anchor may therefore have a role in the recruitment of VAMP2 into these buds. As discussed in section 1.4.3, hydrophobic mismatch may play an important role in increasing the membrane tension of the fusion site, for example the hemifusion diaphragm. Such tension is hypothesised to be essential for fusion pore formation and therefore the length of the VAMP2 anchor may be important for VAMP's role in the fusion mechanism.

Considering the 5 Å difference between the size of the VAMP2 transmembrane region and the preferred thickness of the DOPC bilayer, it is surprising that the addition of this protein at a ratio of 1:600 had little or no affect. The result for the t-SNARE DOPC liposome sample is also unexpected. This liposome population contained protein at a total molar ratio of 1:300, but only half of this protein (ΔN-Syx) has a membrane anchor. On this basis alone it would be expected that the data would be similar to that of the 1:600 VAMP2 liposome population. Another consideration is any hydrophobic mismatch between the ΔN-Syx transmembrane domain and the DOPC bilayer. The residue sequence of the ΔN-Syx membrane anchor is 23 amino acid residues long and like VAMP2, has been modelled as an α-helix[34]; the transmembrane region of ΔN-Syx is therefore predicted to be 34.5 Å long. This anchor would be expected to have little mismatch with the lipid bilayer and therefore have less of an influence on H_r' than VAMP2. However, the presence of the t-SNARE proteins has been seen to affect proteoliposome size significantly.

As well as through transmembrane regions, Syntaxin 1A has been shown by EPR (Electroparamagnetic Resonance) to partially insert another part of its sequence (amino acid residues 261-265) into the membrane[92]. This sequence is situated next to the transmembrane anchor (the linker region) and is thought to insert into one monolayer, eliminating any gap between vesicle and plasma membrane bilayers during SNARE-mediated fusion. A similar basic amino acid-rich region has been identified in VAMP2 and is therefore also thought to partially insert into the membrane. As discussed in section 1.7.1 this would be expected to increase curvature by altering the area of the monolayer upon insertion of the linker.

Despite lacking the ability to membrane associate in this study, the influence of the SNAP-25 protein needs to be considered. It is possible that SNAP-25, which has lipid anchors *in vivo*, also has short amino acid residue sequences that partially insert into the membrane. As discussed in section

1.2.3.2, the anchors of SNAP-25 take the form of four palmitoylated cysteine residues at sequence numbers 85, 88, 90 and 92 for homologue b. Using the Kyte-Doolittle hydropathy plot[305] ProtScale program from Expasy*, it can be seen that the amino acid residue sequence from 81-95 is the most hydrophobic region of the protein (Figure 3.14). The hydrophobicity of this region suggests that as well as the lipid anchors in this region, these amino acid residues partially insert into the bilayer. As discussed in the previous paragraph, this would increase the area of one monolayer and consequently the curvature of the bilayer. Unlike the VAMP2 1:300 sample, the t-SNARE sample can be seen to have two vesicle populations of similar occupancy. The inability of SNAP-25 to bind to membranes in this study may have led to vesicle forming with different protein densities. The population with a mean radius of ≈10 µm may reflect vesicles with little SNAP-25 present (making the composition similar to the VAMP2 1:600 sample) while the other (with a mean radius ≈5 µm) may contain much more SNAP-25 resulting in liposomes similar in size to the VAMP 1:300 sample. Alternatively, as will be discussed in chapter 4, the higher curvature may result from protein aggregate structures. These would restrict the growth of GUVs as additional energy would be required to break the aggregate to allow the vesicles to form.

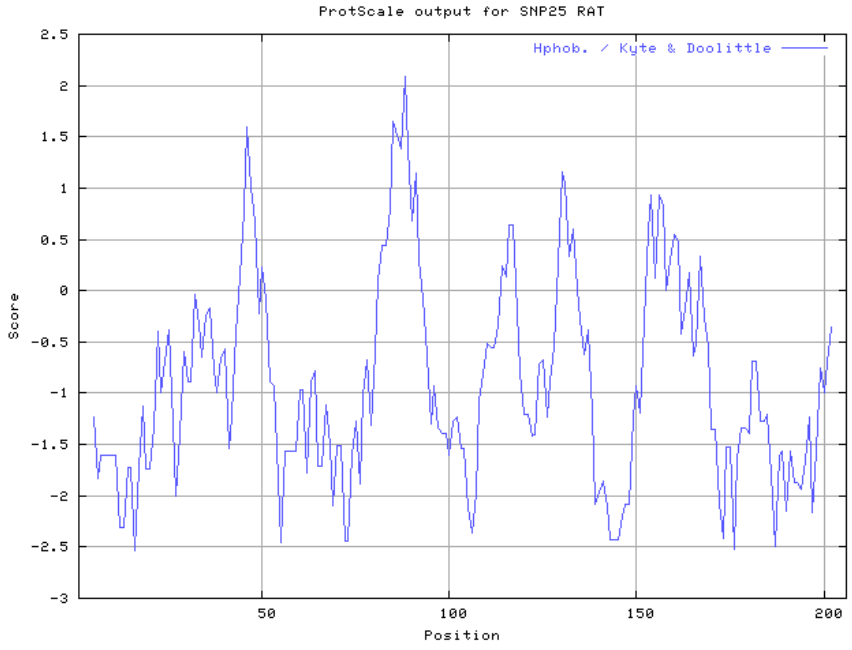


Figure 3.14. Produced using the Expasy ProtScale program, the Kyte-Doolittle hydrophobicity plot of the full wild-type SNAP-25 sequence (1-206) is shown. A window size of 7 has been used. Values above 1.6 are considered to be areas of hydrophobicity and such a region can be seen for the sequence at residues 81-95. This area contains the four cysteine residues (C85, C88, C90 and C92) which become palmitoylated post-synthetically in vivo, forming lipid anchors. It is therefore expected that this protein region would be close to the lipid bilayer. As well as lipid anchors in vivo, the hydrophobicity of this area may indicate partial insertion of these residues into the proximal membrane leaflet.

* *www.expasy.ch/tools/protscale.html*

3.5 CHAPTER SUMMARY

In this chapter it has been shown, through the use of fluorescently labelled protein, that the SNARE proteins can be incorporated and formed in giant unilamellar vesicles. The proteins were also seen to distribute evenly throughout the membrane surface.

The sizes of liposomes, produced by electroformation, have been analysed and reveal that the incorporation of protein affects this property. Insertion of VAMP2 led to the formation of liposomes with a higher curvature relative to the pure lipid system. This has been attributed to hydrophobic mismatch between the transmembrane anchor and the preferred thickness of the model lipid bilayer used. VAMP2 may have evolved to have such a short anchor due to the high curvature of synaptic vesicles. In the flatter environment of the plasma membrane or Golgi complex this mismatch may partially determine sites of vesicle budding and/or aid the recruitment of VAMP to the buds. However, this phenomenon may only be a symptom of the choice of model lipid system and therefore further investigations using more complex lipid mixtures should be conducted. For the t-SNARE liposomes, changes in size are more difficult to explain. It is possible that the linker region of these proteins partially inserts into the bilayer, altering curvature properties. As will be discussed in chapter 4 the change may also be due to the formation of aggregate structures.

In this chapter the influence of the SNARE proteins upon the curvature of bilayers has been investigated. During membrane fusion the bilayers must deform and therefore the ability of these proteins to manipulate the elastic properties of the membrane is also of interest. In order to quantitatively evaluate the changes in the membrane properties of GUVs as a result of SNARE protein insertion, an investigation using micropipette aspiration was undertaken. This technique and the data obtained by its use are discussed in Chapter 4.

Chapter 4.

MICROPIPETTE ASPIRATION STUDIES OF MEMBRANE PROPERTIES

In this chapter, a micropipette aspiration study of giant unilamellar vesicles is presented. This technique has been employed to provide quantitative data of the effect that SNARE protein incorporation has upon the membrane properties of these model membranes.

A comparative study of DOPC and di-ether PC (ether-linked DOPC; 1,2-di-O-(9Z-octadecenyl)-*sn*-glycero-3-phosphocholine) vesicles found that the DOPC vesicles had a bending rigidity (κ) of 13.4 ± 2.00 k_BT (3sf) and an area expansion modulus (K_a) of 147 ± 22.3 mN/m (3sf). The literature values for a DOPC bilayer are 0.85 ± 0.1 x10^{-19} J (≈21 ± 2.5 k_BT) and 265 ± 18 mN/m respectively[306]. While the bending rigidity found compares well, K_a is significantly lower. This has been attributed to lipid degradation as a result of the formation of the vesicles using the electroformation method. Further interpretation of the data allowed vesicles with significant degradation to be excluded. The remaining DOPC vesicles had an area expansion modulus of 248 ± 9.77 mN/m, comparing favourably with the literature value. The bending rigidity of this group was found to be 14.9 ± 3.57 k_BT (3sf). With the ester linkages replaced by ether groups, di-ether PC is not able to degrade in the same way. The overall bending rigidity of the di-ether PC vesicles was found to be 14.6 ± 4.68 k_BT (3sf) with an area expansion modulus of 232 ± 25.5 mN/m (3sf). From this study it is concluded that where possible, a swelling method should be used to produce GUVS; in preference to electroformation.

The effect of incorporating the SNARE protein VAMP2 was examined using a 1:300 protein: DOPC molar ratio. Micropipette aspiration revealed both moduli were decreased compared with pure DOPC vesicles with an area expansion modulus of 143 ± 7.06 mN/m (3sf) and a bending rigidity of 5.32 ± 0.81 k_BT (3sf). The hypothesis proposed in chapter 3, that VAMP2 causes bilayer thinning due to hydrophobic mismatch, is consistent with these findings. The insertion of the t-SNARE proteins SNAP-25 and Syntaxin 1A into DOPC GUVs (0.5: 0.5: 300 molar ratio) led to an increase in the area expansion modulus to 366 ± 37.1 mN/m (3sf). The overall bending rigidity was found to be 8.13 ±1.42 k_BT (3sf). As with the DOPC study, the data required further interpretation due to the effects of electroformation. Removal of multilamellar vesicles and those containing degraded lipid products led to a selective population average of 493 ± 6.00 mN/m (3sf) for K_a , with a bending rigidity of 8.30 ± 1.15 k_BT. The increase in K_a may reflect the ability of the t-SNARE proteins to interact with each other, forming an interconnected aggregate structure.

4.1 INTRODUCTION

The mechanical properties of GUVs have been investigated for several decades, principally by shape fluctuation analysis[307-310] and micropipette aspiration[306, 311, 312]. In this chapter, the latter technique has been employed to study the consequences of SNARE protein insertion on the membrane properties of a DOPC lipid bilayer.

Data from Chapter 3 led to postulation that SNARE proteins affect lipid membranes by increasing the relaxed curvature. Micropipette aspiration has allowed in influence of these proteins on deformation energies to be assessed quantitatively. The two properties explored by the aspiration method are the bending rigidity, κ, and the area expansion modulus, K_a (also referred to as the area compressibility modulus). The bending rigidity is a measure of the force required to bend the membrane while K_a is the force required to stretch or compress the membrane.

The following section introduces the theory of micropipette aspiration based upon work published by Henriksen in 2004[300] with the exception of the surface area equations, which were provided by Dr. Nicholas Brooks (personal communication) based upon a publication by Heinrich[313].

4.1.1 PRESSURE AND SURFACE AREA

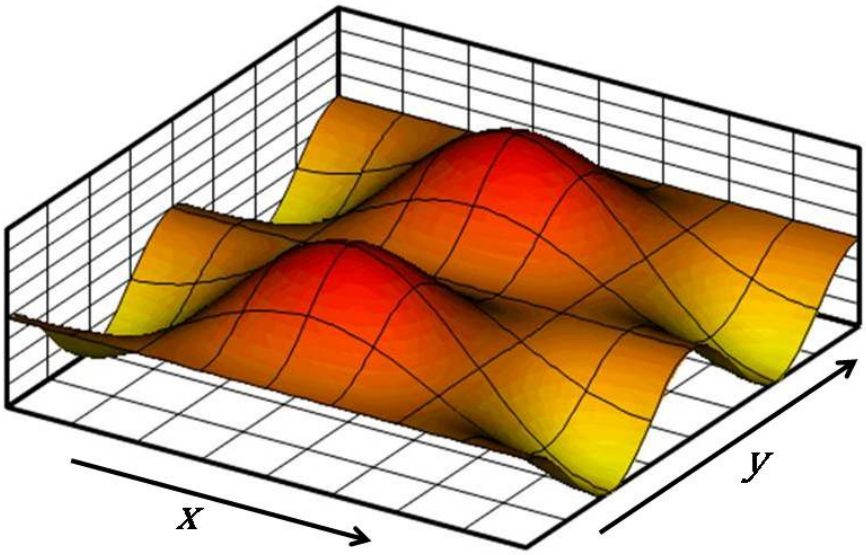


*Figure 4.1 It can be seen from this figure that though the membrane fragment fits into a frame area (A_p) of x*y, the undulations of the surface result in the actual surface area (A) being far greater. The optical resolution of a microscope is not sufficient to detect the undulation of the surface and therefore appears smooth. As a result, only A_p can be determined directly from microscopic images. Reproduced with the permission of HydeSoft Computing.*

Under a microscope, the membrane surface of a vesicle looks smooth; however, below the optical resolution the membrane is undulated (Figure 4.1). There is therefore a discrepancy between the observable area of the vesicle, A_p (referred to as the frame area) and the actual microscopic surface area, A; with $A_p < A$. Micropipette aspiration uses external pressure to pull a vesicle into a pipette of a radius much smaller than the vesicle radius. In doing so the undulations are pulled out and the microscopic surface area becomes optically resolved. At higher pressures, the surface area increases as the membrane is stretched away from the equilibrium area per lipid molecule a_0. By applying the following theory it is possible to determine the bending rigidity and area expansion modulus of the GUV membrane from the experimental data gathered during aspiration.

4.1.1.1 Pressure

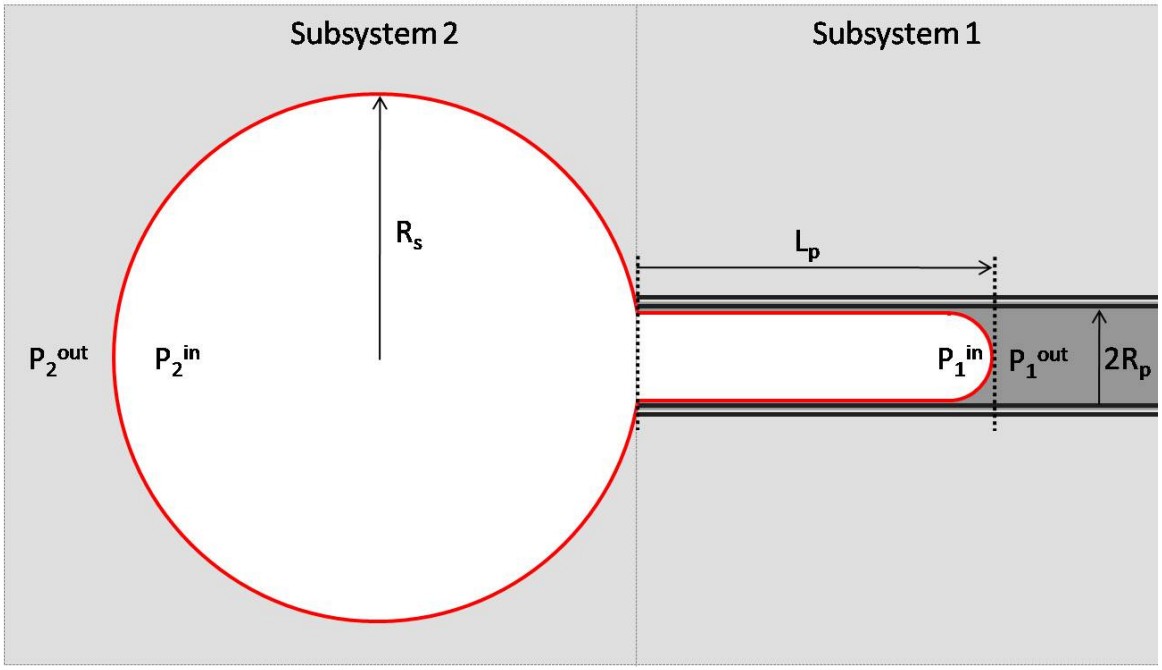


Figure 4.2 In order to describe the pressure and shape of the whole system, it must be split into two subsystems. Subsystem 1 is the portion of vesicle that has entered the micropipette; which has a radius R_p. The amount of insertion is measured by the projection length; L_p. Subsystem 2 describes the spherical section of the vesicle (radius R_s) which has remained external to the pipette. Due to continuity, the internal pressure of the vesicle in each subsystem is equal ($p^1_{in}=p^2_{in}$), however, the external pressures differ and are denoted P^1_{out} and P^2_{out}.

An aspirated vesicle can be split into two subsystems (Figure 4.2). Subsystem 1 is the proportion of the vesicle membrane which has projected into the glass pipette upon exertion of pressure. Subsystem 2 represents the membrane portion that remains external to the pipette. The pressure difference between the outside and inside of the vesicle can be used to determine the force being applied. The total pressure difference, Δp, is the summation of the pressure difference of each subsystem. As the continuous nature of the vesicle results in the internal pressure of each subsystem being equal; the pressure can be expressed as the difference between the outside pressures of the subsystems:

$$\Delta p_i = \Delta p_i^{in} - \Delta p_i^{out}$$
$$\Delta p = \Delta p_1 - \Delta p_2 = p_2^{out} - p_1^{out} \qquad \textit{Equation 4.1}$$

Where i indicates the subsystem.

4.1.1.2 Surface Area

A vesicle under zero pressure is assumed to be spherical with a radius R_0. The volume of this vesicle is therefore:

$$V_0 = \frac{4}{3}\pi {R_0}^3 \qquad \textit{Equation 4.2}$$

A vesicle under aspiration deforms as it enters the pipette. Two different shapes are used to calculate the deformation of the vesicle depending on how far it has been pulled into the pipette (Figure 4.3).

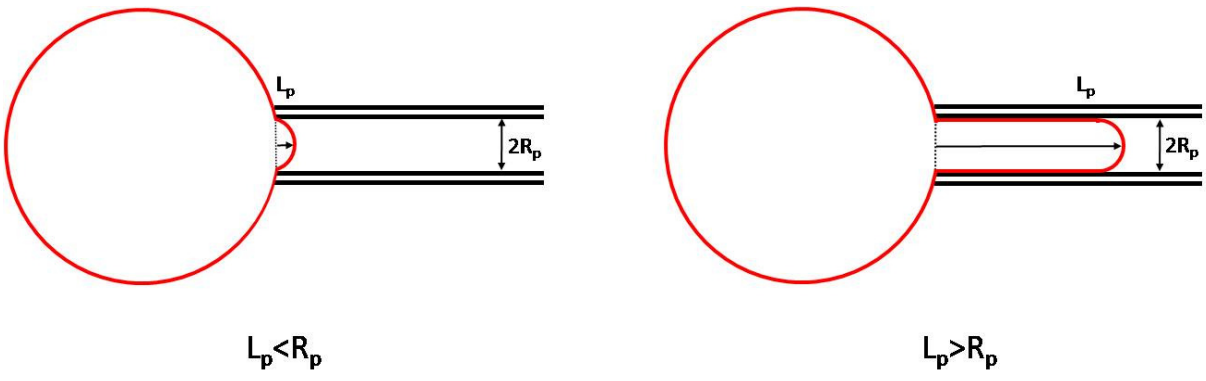


Figure 4.3. When a vesicle begins to enter the micropipette the projection length L_p is less than the radius of the pipette R_p. In this situation the vesicle can be modelled as a sphere (external to the pipette) with a spherical projection cap. As the vesicle is pulled further into the pipette L_p becomes larger than R_p and the vesicle must be modelled as an external sphere with a hemi spherically capped cylinder projecting into the pipette.

When at a projection length, L_p, below the pipette radius, R_p, the vesicle can be modelled as a sphere (radius R_s) external to the pipette, with a spherical cap projection. The volume and surface area of this shape can be calculated from

$$V_{L_p<R_p} = \frac{4}{3}\pi {R_s}^3 + \frac{1}{6}\pi L_p\left(3{R_p}^2 + {L_p}^2\right);$$
$$A_{L_p<R_p} = 4\pi {R_s}^2 + \pi {L_p}^2 \qquad \textit{Equation 4.3}$$

As the vesicle projects further into the pipette the projection length becomes greater than the pipette radius. The membrane within the pipette must now be modelled as a cylinder with a hemispheric cap, while the membrane external to the pipette remains spherical. The volume and surface area in this case can be expressed as follows:

$$V_{L_p>R_p} = \frac{4}{3}\pi {R_s}^3 + \pi {R_p}^2 L_p - \frac{1}{3}\pi {R_p}^3;$$
$$A_{L_p>R_p} = 4\pi {R_s}^2 + 2\pi R_p L_p - \pi {R_p}^2 \qquad \textit{Equation 4.4}$$

As the external sphere projects into the pipette entrance this membrane area is counted twice. The final term of this equation provides a correction for this.

The radius of the external sphere, R_s, cannot be accurately measured experimentally. However, the volume of the vesicle can be assumed to be constant and therefore it is possible to use the condition $V_0 = V_{L_p<R_p} = V_{L_p>R_p}$ to express R_s (and therefore the surface area) in terms of R_0, R_p and L_p, which can be accurately obtained.

$$R_s = R_0 \qquad \text{under zero tension}$$
$$R_s = \sqrt[3]{{R_0}^3 - \frac{1}{8}{L_p}^3 - \frac{3}{8}L_p{R_p}^2} \qquad \text{when } L_p<R_p$$
$$R_s = \sqrt[3]{{R_0}^3 + \frac{1}{4}{R_p}^3 - \frac{3}{4}L_p{R_p}^2} \qquad \text{when } L_p>R_p \qquad \textit{Equation 4.5}$$

It should be noted that these measurements are obtained from microscopy and therefore these surface area calculations represent the frame area, A_p.

4.1.2 Membrane Deformation and Tension

The deformation of a membrane following the application of pressure is assessed by the relative area change, α;

$$\alpha = \frac{A_p - A_p^{in}}{A_p^{in}} \qquad \textit{Equation 4.6}$$

Where A_p^{in} is the frame area at an initial (arbitrarily chosen) state and A_p is the frame area of the vesicle under the current aspiration pressure. By assuming that the volume of the vesicle is constant Equation 4.6 can be re-expressed:

$$\alpha_\gamma = \left[\frac{1}{2}\left(\frac{R_p}{R_s^{in}}\right)^2 \frac{\Delta L}{R_p} + \left(1 - \frac{3}{4}\left(\frac{R_p}{R_s^{in}}\right)^3 \frac{\Delta L}{R_p}\right)^{\frac{2}{3}} - 1\right]\gamma \qquad \textit{Equation 4.7}$$

$$\gamma = 1 - \frac{2R_p L_p^{in} + {R_p}^2}{4\left(R_s^{in}\right)^2} \qquad \textit{Equation 4.8}$$

Where $\Delta L = L_p - L_p^{in}$, γ is a geometric correction factor and R_s^{in} is the spherical radius at A_p^{in}.

Due to the optical resolution, the actual microscopic membrane surface area and the resolvable (frame) area are different. This is also true of membrane tension, giving rise to a surface tension, σ, and a frame tension, τ. The frame tension can be measured directly from micropipette aspiration using the following relationship;

$$\tau = \frac{\Delta p R_p}{2\left(1 - \frac{R_p}{R_s}\right)} \qquad \textit{Equation 4.9}$$

4.1.3 Pressure Regimes

4.1.3.1 Flaccid Regime

The flaccid or low pressure regime has a pressure range of 0-10^2 Pa (tension 0-10^{-1} mN/m) and in this regime the relative area change is due to the smoothing of membrane undulations. As a result, the difference between the true membrane surface area, A, and the frame area, A_p, decreases. At this pressure range, the total membrane surface area is considered to remain constant. Therefore:

$$\alpha \simeq \frac{1}{8\pi\kappa_A\beta} ln(\tau) \qquad \textit{Equation 4.10}$$

Where β is $1/\mathrm{k}_B T$.

Using this regime it is possible to evaluate κ_A(the bending rigidity; assuming A is constant) by use of a linear fit of α vs. $ln(\tau)$.

4.1.3.2 Tense Regime

Under a high pressure regime (10^3-10^4 Pa, tension 1-10 mN/m) the relative area change is governed by membrane stretching (an increase in the area per lipid molecule relative to the equilibrium value) and is therefore dependent on the area expansion modulus. As experiments measure A_p rather than A, this modulus also relates to A_p and is represented by $\overline{K_a}$ to provide distinction.

$$\alpha \simeq \frac{\tau}{\overline{K_a}} \qquad \textit{Equation 4.11}$$

Using this relationship, $\overline{K_a}$ can be calculated from a linear fit of α vs. τ.

4.1.3.3 Full Pressure Regime

It is experimentally difficult to obtain data from the flaccid regime and though the formal cross-over region between the flaccid and tense regimes occurs in the 10^2-10^3 Pa pressure range, in reality, the relative area change of the flaccid regime does have a contribution from membrane stretching. Henriksen has combined the two regimes into a single equation allowing the full pressure range to be analysed.

$$\alpha \simeq \alpha_0 + \frac{1}{8\pi\kappa_{A0}\beta} ln(\sigma) + \frac{\sigma}{\nu K_a} \qquad \textit{Equation 4.12}$$

The molecules of the membrane have an equilibrium area, a_0; the equilibrium membrane area, A_0, is therefore Na_0 where N is the number of molecules in the membrane. In Equation 4.12, ν is the ratio of the initial frame area and the equilibrium membrane area ($\nu = A_p^{in}/A_0$). By including this term, the bending rigidity at A_0 and K_a (rather than $\overline{K_a}$) can be found. It should be noted that the tension in Equation 4.12 is the surface tension (σ) rather than the frame tension.

Assuming that $A_p^{in} = A_0$, $\nu = 1$; this assumption also allows the frame tension to be identified with the surface tension (which cannot be determined experimentally). It is further assumed that A_0 remains constant throughout the experiment.

4.2 Materials and Methods

4.2.1 Making Micropipettes

Pipettes were prepared from thin walled borosilicate glass tubing (#1B100 (152mm length, 1mm outer diameter, 0.58mm internal diameter), World Precision Instruments, Stevenage, UK) using a Narishige PN 30 pipette puller. The main magnet was set to 48.0, sub magnet to 23.3 and the heater to 80.6 to produce fine, long tipped pipettes. Two pipettes can be formed from each glass tube.

Following pulling, the tip of each pipette was cleaved and polished using a Narishige MF 900 microforge. The forge consists of a platinum filament onto which a small soda-lime glass ball was melted and visualised under a x10 lens. The pipette was mounted into a pipette holder and its position controlled with micromanipulator dials. The filament heater was initially set to 40%. The filament was heated and the pipette tip bought into contact with the edge of the molten glass bead. Capillary action pulled soda-lime glass into the pipette and when the molten glass reached the required pipette diameter the heat was turned off. Retraction of both the filament and the glass bead as it cooled caused the pipette to snap, producing a straight end at the desired diameter.

The pipette end was polished to ensure no sharp edges would burst vesicles during aspiration. The filament heater setting was increased to 70% and the pipette (in the holder) moved as far away from the filament as possible. With the heat turned on, the pipette was then bought slowly towards the filament until the pipette end just melts to become smooth, but not closed.

The end region of the pipette must be long enough to allow sufficient aspiration of the vesicle and this region should be in the same focal plane. The pipette was therefore bent using the microforge. The angle of the pipette holder was changed to approximately 30% above the horizontal. The pipette was positioned so that the middle of the section to be bent was above the glass bead. The filament heater was set to 60% and, with the heat turned on; the pipette was bought slowly towards the filament, causing the pipette to bend.

Before each experiment, a pipette was backfilled with 300mM glucose solution using a MicroFil syringe needle (World Precision Instruments, Stevenage, UK) and a high pressure syringe. Buffer was forced into the pipette until a droplet was formed at the pipette tip and then the needle was slowly extricated while continually adding buffer to prevent air bubbles. The pipette tip was then soaked in a 0.2 µM filtered BSA solution (1% w/v BSA in 300mM glucose) for 30 minutes to prevent vesicles adhering to the glass during aspiration. The pipette was washed thoroughly in 300mM glucose solution to remove excess BSA just prior to aspiration experiments.

4.2.2 ASPIRATION

4.2.2.1 Microscope Set-Up

The microscope used was based around an inverted Nikon TE2000-E microscope and modified by Dr. Xavier Mulet and Dr. Nicholas Brooks. As described in chapter 3, the microscope has a CCD camera for image acquisition and uses Hoffman modulation optics. A schematic of the microscope components can be seen in Figure 4.4.

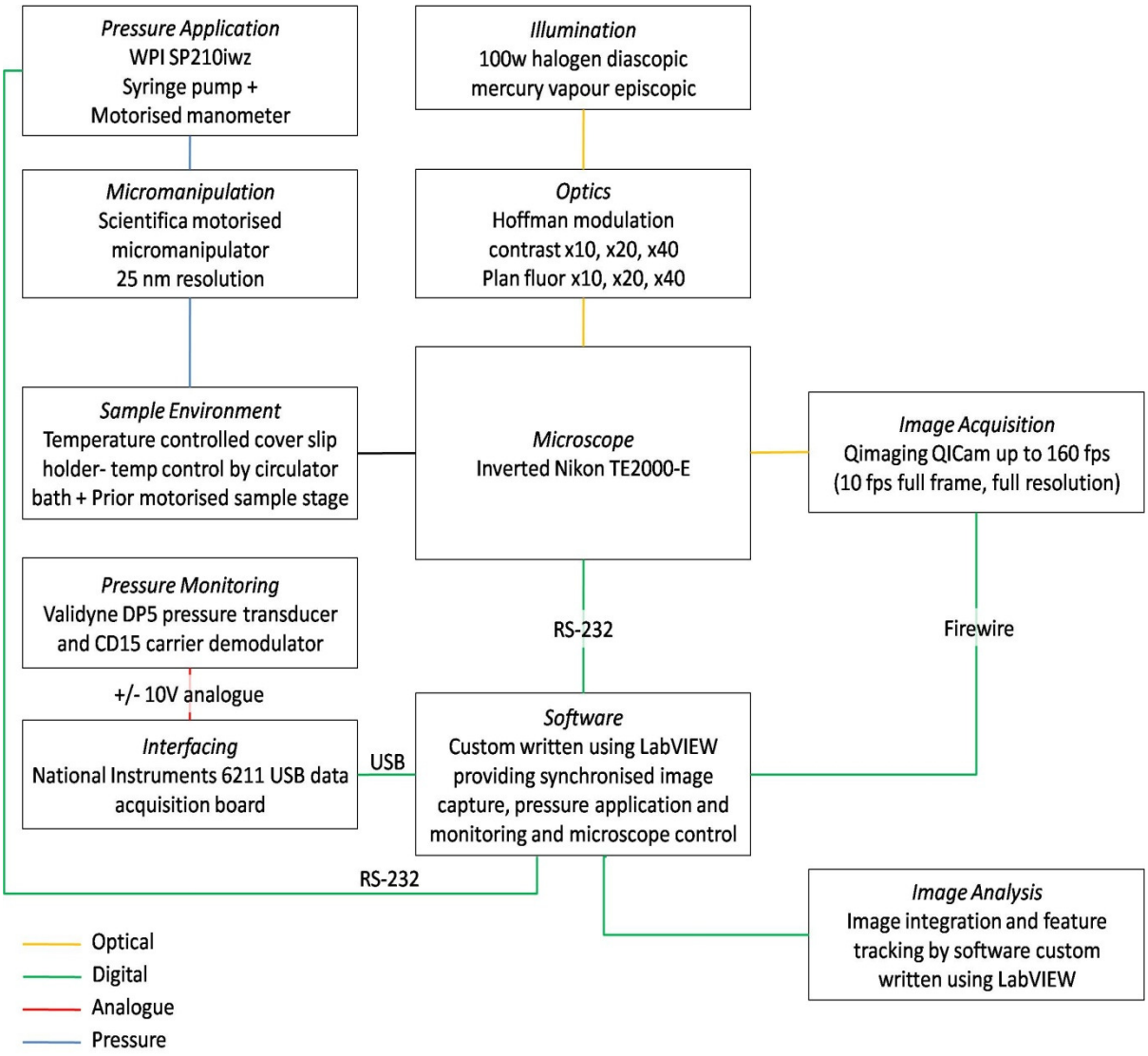


Figure 4.4 Provided by Dr Nicholas Brooks, a schematic of the microscope components used during micropipette aspiration studies is shown.

The pressure manometer, designed and built in-house, was connected to a micropipette holder (MPH4, World Precision Instruments). The holder was filled with water and any air bubbles excluded. With a water meniscus present on the holder and a buffer solution meniscus on the back opening of the micropipette, the pipette was inserted into the holder. The holder was tightened and checked to make sure there were no air bubbles before the holder was mounted onto a stage micromanipulator unit (three axis water hydraulic manipulators MHW-3, Narishige, Japan). This unit allowed the movement of the micropipette to be controlled in 3 directions through use of a joystick.

4.2.2.2 Aspiration Procedure

Setting Pressure

The pressure manometer consists of two reservoirs on separate unislides; the reference reservoir, which is open to air and the aspiration reservoir, which is closed. Initially, two different pressures must be considered; the system pressure and the sample pressure. The system pressure results from the difference in height between the reference and aspiration reservoirs. The sample pressure results from the height difference between the two reservoirs and the microscope stage. A LabView based software program developed by Dr. Brooks was used to control the position of the reservoirs and to measure the system pressure.

Before aspiration can begin, both the system and sample pressures must be set to zero. First, to ensure the system pressure was correctly calibrated, the pressure was set to zero using the LabView based program which set the two reservoirs to the same height. A manual dial on the manometer moves the level of both reservoirs in unison. Using this dial, the position of both reservoirs was altered so that they were positioned above the height of the microscope stage (resulting in positive sample pressure). The micropipette was moved to the surface of a glass cover slide, inside a 200 µl droplet of GUV sample (All lipids were purchased from Avanti Polar Lipids, USA and giant unilamellar vesicles were prepared as described in section 3.2.2.3.). The aspiration reservoir was opened to the reference reservoir and the dial of the demodulator adjusted so that the pressure read by the software (the system pressure) was zero. The aspiration reservoir was then closed to the reference reservoir and the software used to re-adjust the pressure to zero once again. This procedure was repeated three times to ensure the system pressure was measured as accurately as possible.

The sample pressure was then set to zero. With the system pressure still set to zero, the height of the reservoirs was adjusted using the manual dial of the manometer. The micropipette was bought up to a vesicle with a diameter smaller than that of the pipette, allowing it to enter the pipette unhindered. The height of the reservoirs was adjusted until it was observed that the vesicle was

under neither positive nor negative pressure. As the experiment is extremely sensitive to pressure and is seen to fluctuate, a zero sample pressure is defined as the pressure at which a vesicle is seen to oscillate at the pipette mouth.

With the system and sample pressure now equal, the aspiration pressure of the micropipette becomes the system pressure, as controlled by the LabView pressure program. At this point, it should be noted that the pressure reading is opposite to the pressure sign i.e. a positive reading indicates negative pressure and therefore a positive aspiration pressure will pull a vesicle into the micropipette.

Vesicle Aspiration

With the aspiration pressure set to zero, the sample was allowed to settle for 10 minutes so that the vesicles could sink to the cover slide surface (due to their internal content of 300 mM sucrose). A vesicle was then selected for aspiration based upon several criteria; the vesicle must:

1) Fluctuate, indicating it may be unilamellar;
2) Be at least twice the pipette diameter, in order for the vesicle to aspirate effectively;
3) Be free of inclusions;
4) Be free of membrane tethers.

The pressure software allows the aspiration pressure to be altered as either a step or ramp function. When the step function was used, it was found that the pressure change occurred too quickly and that a vesicle under aspiration would rupture at relatively low pressures. The ramp function was also found to be unsuitable, on its own, as the vesicle was unable to equilibrate fast enough at higher pressures for ramp rates of 0.5 Pa/s or above. Therefore, accurate projection lengths could not be measured by this method. Slower ramp rates were attempted but caused pressure oscillations, causing the vesicle projection edge to oscillate substantially. This would destabilise the vesicle, either disrupting the projection edge or causing the vesicle to rupture. The ramp function was therefore used with equilibration steps added.

First, an image of the chosen vesicle was taken with the CCD camera. At zero aspiration pressure, the pipette was then bought up to the vesicle and the aspiration pressure increased to 1 or 2 Pa so that the vesicle became ‘stuck’ in the pipette mouth. The vesicle was then left for 2 minutes to equilibrate and another image taken. Using a pressure ramp of 0.5 Pa/s the pressure was increased by 1 Pa. Following a one minute delay, to allow the vesicle to equilibrate, an image was taken and the pressure increased again using a pressure ramp. With one minute equilibration steps, images were taken at 1 Pa intervals in the 1-20 Pa pressure range. For pressures between 20 and 100 Pa,

images were taken every 5 Pa with the equilibration time increased to two minutes; over 100 Pa, an equilibration time of three minutes was used with images taken every 10 Pa. The experiment was continued until the vesicle ruptured.

Upon rupture, the aspiration pressure was set to -50 Pa, to expel membrane fragments. Before another vesicle was selected, the aspiration pressure was set to zero and the sample pressure adjusted back to zero if necessary. Another vesicle was then aspirated as above. Due to potential complications arising from evaporation, no more than two vesicles were aspirated from a single droplet.

4.2.3 Data Extraction

A suite of programs has been developed by Dr Nicholas Brooks to extract the data on the vesicle area and tension from the microscope images taken during an aspiration experiment. These programs were all written using LabView 8.5 and Vision 8.5 (National Instruments). The image acquisition software of the microscope produces a text file containing both the image filename and the pressure at the time the image was recorded. Using the first of Dr. Brooks' programs, the Tiff image files and the text file for a given vesicle were converted into one avi movie file.

This movie file was then analysed using the second program; called BMM Integration. With this program, a horizontal and vertical region is selected from one movie frame, along with the pipette edge. Five aspects of an image are evaluated by this method (Figure 4.5). Integration of the vertical region of the image shows the position of the top and bottom of the external vesicle sphere, the pipette edge region accounts for pipette movement during the experiment and the horizontal integration tracks the back edge of the vesicle and the projecting vesicle edge.

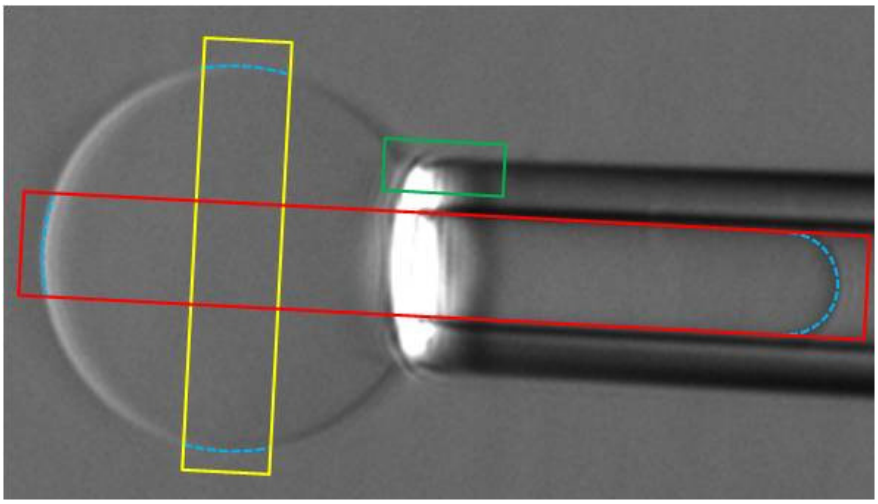


Figure 4.5 The BMM Integration program developed by Dr Brooks uses the LabView and Vision 8.5 software to integrate each frame of the aspiration movie file. Three integration boxes are set to assess five features of each frame. The red box is set as the horizontal integration and is used to track the back edge of the vesicle (exterior to the pipette) and the projection edge (inside the pipette). The vertical integration in yellow, tracks the top and bottom edge of the external section of the vesicle. Finally, the pipette edge is tracked to allow for pipette movement during the experiment, the integration box is shown in green.

The BMM Integration program integrates each frame of the movie based upon the integration region set in this initial frame. The program allows the peaks within the integration profile, which represent each of the edges, to be tracked from one frame to the next (Figure 4.6). The pixel position of the edges, along with the aspiration pressure, is extracted from each frame and used in the last program of the suite.

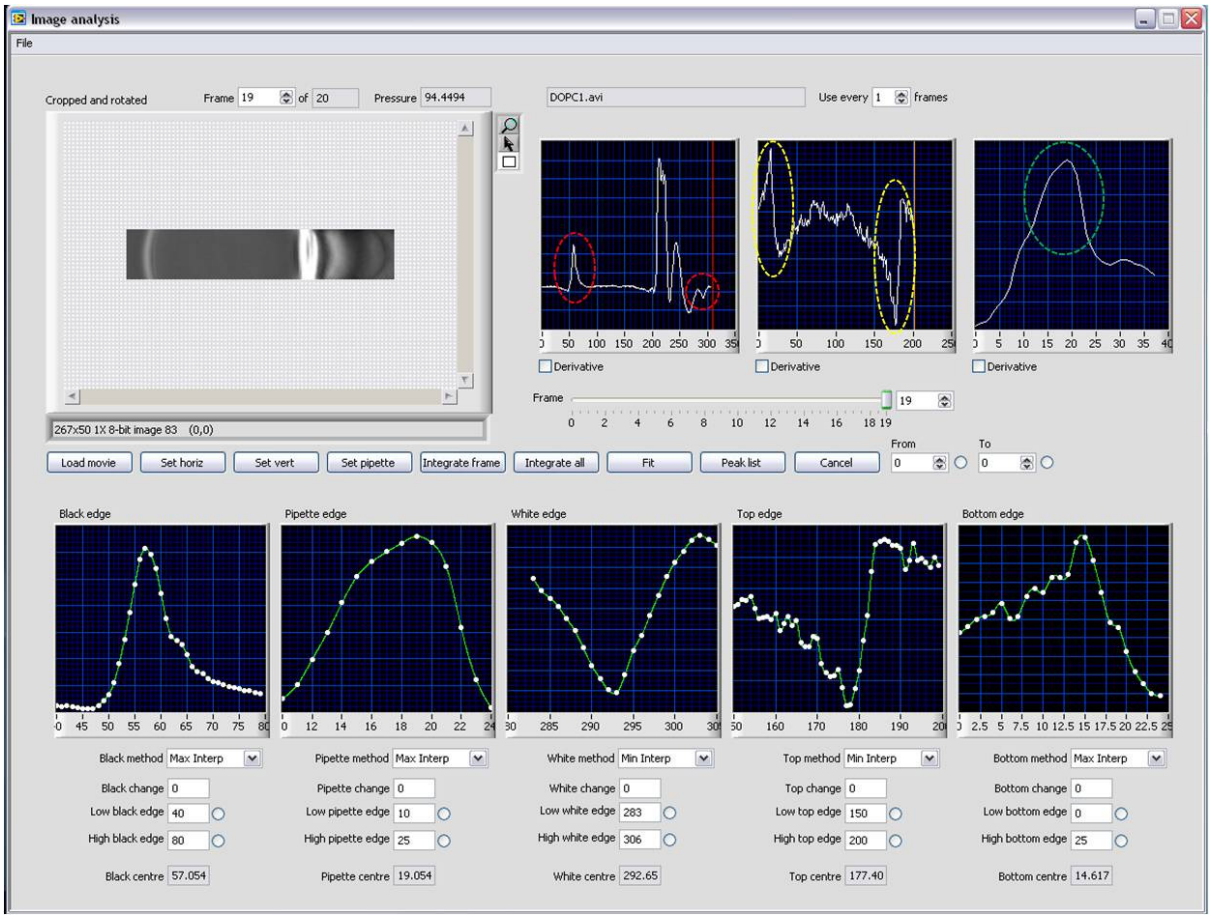


Figure 4.6 This figure shows a screen shot of the BMM Integration program developed by Dr Brooks using the LabView and Vision 8.5 software. In the top left corner is shown the horizontal integration of a movie frame. The frame number, aspiration pressure and movie file name are also shown in this corner. In the top right corner are the three integration profiles of this frame, from the set integration regions. From left to right, the horizontal integration showing the back and projecting edge of the vesicle (circled in red). The next integration profile shows the top and bottom edge of the vesicle, circled in yellow. Finally the pipette edge region is integrated, circled in green. Specific regions of these profiles can be analysed to find peak positions and these are shown in the five windows across the bottom of the program window. Again left to right these are the back edge of the external vesicle section, the pipette edge, the vesicle projection edge, the top and bottom of the external vesicle section.

In the final program (Show Data), the data is presented as a series of pixel vs. pressure plots, one for each of the five edges described above (Figure 4.7). One frame of the movie under analysis is chosen as a reference frame. This is usually the final frame of the movie (before vesicle rupture) as the projection length is at its greatest. Using LabView Vision, the visual position of the projecting edge in this frame is marked. The height and width of the external vesicle section in this frame is then entered into the program. Using the initial image of the vesicle, the radius of the vesicle under zero tension is entered to provide a value for A_p^{in}, and the magnification used during the experiment is entered to allow all of these measurements (which currently have pixel units) to be converted to microns. The relative positions of the edges are used and any variation in the pipette position is taken into account, allowing the projection length and vesicle size to be calculated more accurately. The frame area (A_p) of the vesicle at each pressure is calculated by the program using Equations 4.3 to 4.5, and the frame tension (τ) using Equations 4.5 and 4.9. The program therefore outputs a frame tension (mN/m) vs. frame area (μm^2) plot for the vesicle, over the whole aspiration experiment.

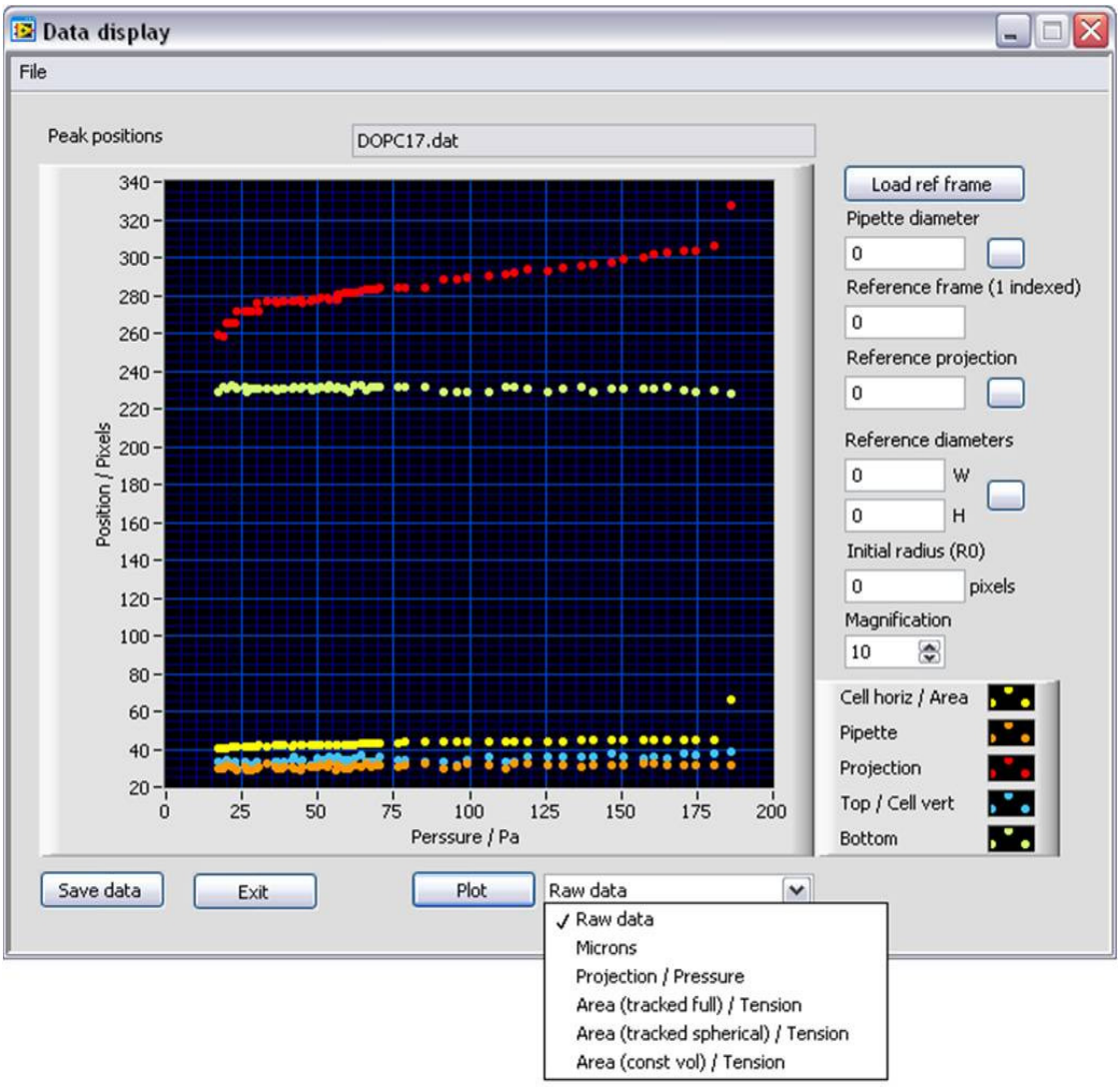


Figure 4.7 Using the BMM Integration program, the peak position of the projection, back, top, bottom and pipette edges were extracted for each movie frame. The screen shot here is of the Show Data program (developed by Dr. Brooks) which presents the position of each edge (in pixels) as a function of pressure (Pa). The program allows one frame of the movie to be selected and used as a reference frame. Once the magnification used is also entered, the program converts the aspiration data into a frame area (μm^2) vs. frame tension (mN/m) plot. This final plot is exported to Microsoft Excel for final analysis.

4.2.4 DATA ANALYSIS

Final data analysis was performed by exporting the frame area vs. frame tension data to Microsoft Excel. In order to evaluate the data, approximate values for both the bending rigidity and area expansion moduli were first found using the flaccid and tense regime equations described in section 4.1.3. In the flaccid regime, using Equations 4.6 and 4.10, it can be seen that A_p varies as a function of $Ln(\tau)$:

$$A_p = A_p^{in}\left[\frac{Ln(\tau)}{8\pi\beta\kappa_A} + 1\right] \qquad \textit{Equation 4.13}$$

Therefore, a linear fit of the first few data points of a $Ln(\tau)$ vs. A_p data plot gives an approximate value for the bending rigidity as the intersect of this line is A_p^{in} and the gradient is $A_p^{in}/8\pi\beta\kappa_A$.

For an initial value of the area expansion modulus, the tense pressure regime equation was used. From Equations 4.6 and 4.11, it can be seen that a linear fit to the high pressure data points of a τ vs. A_p plot gives an axis intersection at A_p^{in} and a gradient of A_p^{in}/K_a :

$$A_p = A_p^{in}\left[\frac{\tau}{K_a} + 1\right] \qquad \textit{Equation 4.14}$$

As already stated in section 4.1.3.3, taking $A_p^{in} = A_0$ allows the frame tension (τ) to be identified with the surface tension (σ). The values of the moduli obtained above were used to calculate a theoretical frame area for each tension value, based upon Equation 4.15 (which comes from substituting Equation 4.6 into Equation 4.12):

$$A_p = A_0\left[\frac{Ln(\sigma)}{8\pi\beta\kappa_{A0}} + \frac{\sigma}{K_a} + 1\right] \qquad \textit{Equation 4.15}$$

The frame area data calculated from Equation 4.15 was plotted against the experimentally obtained data and the data sets compared using a nonlinear least square fit. Using the Solver application of Microsoft Excel, A_0, κ_{A0} and K_a were varied to minimise the sum variance, producing a curve of best fit for the experimental data with known moduli values (Figure 4.8).

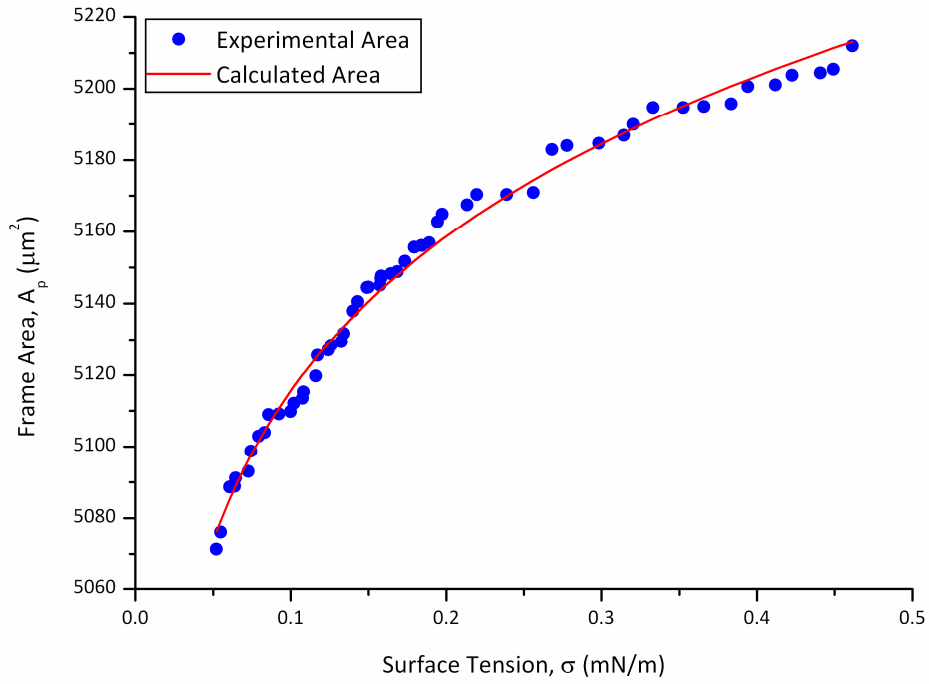


Figure 4.8 An example of the experimental data yielded from micropipette aspiration of a DOPC vesicle is shown in blue. The frame area vs. surface tension relationship was then calculated using Equation 4.15 and approximate values for the bending rigidity and area expansion moduli found. Using a nonlinear least square fit, the moduli and initial area values were altered to improve the fit of the calculated data curve to the experimental data. In this example it was found that the calculated curve best fit the experimental data (sum variance 699.3 (1 d.p)) when A_0 was set at 5250.2 μm^2, K_a at 276.2 mN/m and κ to 3.5 k_BT.

4.3 Results and Discussion

4.3.1 DOPC and Di-Ether PC Micropipette Aspiration Studies

GUVs used for aspiration studies are most commonly formed using a swelling method as some researchers believe that electroformation causes defects in the vesicle bilayer, altering the membrane properties[314]. The ester linkages of DOPC are susceptible to hydrolysis, degrading DOPC into 18:1 lysoPC (1-(9Z-octadecenoyl)-sn-glycero-3-phosphocholine) and oleic acid. It is possible that the application of an electric field to a DOPC film increases the rate of degradation, resulting in the presence of significant amounts of the lysoPC and fatty acid in the GUV bilayer. This action is analogous to the role of the enzyme PLA_2 *in vivo*. Computer simulations[315] of the affects of PLA_2 on the elastic moduli reveal that these moduli decrease in value with increasing enzyme activity. This would therefore suggest that if electroformation does cause lipid degradation, the moduli values found would be lower than the true value for a DOPC bilayer. However, despite numerous attempts, it has not been possible to form giant unilamellar vesicles containing SNARE protein by a swelling method. Despite the possible complications arising from lipid degradation, the aspiration studies discussed in this chapter have therefore been conducted on GUVs formed by electroformation.

In order to assess the possible impact of the use of electroformation, a micropipette aspiration study of DOPC GUVs prepared by this method has been conducted. The membrane moduli values obtained can be compared to the published work of Rawicz and Evans who formed GUVs by a swelling method and found the elastic moduli values using micropipette aspiration[306]. An aspiration study of di-ether PC vesicles (again prepared by electroformation) has also been conducted. Di-ether PC has a similar structure of DOPC but with the ester linkages replaced by ether links (Figure 4.9); it is therefore not able to hydrolyse easily at this position. There is no comparative data for the membrane properties of ether-linked DOPC; however, many studies have been performed on DPPC (1,2-dipalmitoyl-*sn*-glycero-3-phosphocholine) and its ether analogue DHPC (1,2-di-O-hexadecyl-*sn*-glycero-3-phosphocholine). Comparisons of these two lipids show that the bilayers they form have the same membrane thickness, packing and lipid conformation (within experimental error) when in a fluid phase[316]. This may suggest that the elastic moduli values of the two lipids are similar. However, the bending rigidity of DHPC has been found to be lower than that of DPPC at $0.42 \pm 0.07 \times 10^{-19}$ J ($\approx 10\ k_BT$) and $0.67 \pm 0.07 \times 10^{-19}$ J ($\approx 16\ k_BT$) respectively[317].

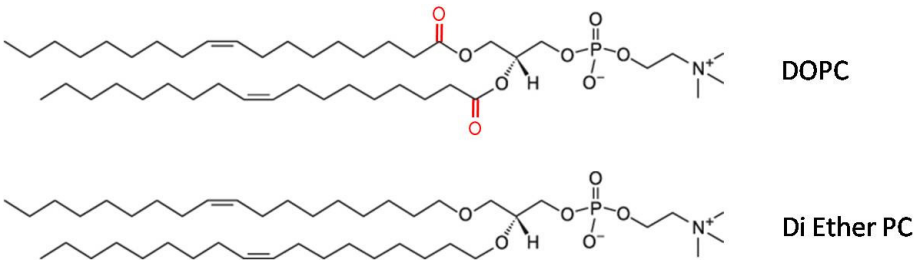


Figure 4.9 Di-ether PC is an ether-linked version of DOPC and the differences between the two structures is highlighted in red. The ester linkages of DOPC make it susceptible to hydrolysis, upon which it breaks down into 18:1 lysoPC and oleic acid. Electroformation may increase the degradation of DOPC, altering the membrane properties compared to vesicles formed by a swelling method. Di-ether PC, with its ether link does not hydrolyse at this position easily and therefore should not degrade readily during electroformation.

The bending rigidity (κ) and area expansion (K_a) moduli values found by the aspiration of 24 vesicles composed of DOPC and prepared by electroformation are shown in Figure 4.10. To best present the data, the area expansion values are shown in ascending order with the bending rigidity of the corresponding vesicle shown directly below. The average moduli values from these vesicles were found to be 13.4 ± 2.00 k_BT (3sf) for the bending rigidity modulus and 147 ± 22.3 mN/m (3sf) for the area expansion modulus (the error quoted in each case is the standard error). Rawicz and Evans[306] micropipette aspiration study found a bending rigidity of 0.85 ±0.10 x10^{-19} J (≈ 21.25 ±2.5 k_BT) and area expansion modulus of 265 ± 18 mN/m for K_a at 18°C.

Focussing on the area expansion data (Figure 4.10A); it appears that the vesicles may belong to as many as four discrete groups with the K_a values stepping up significantly from 19.7 to 46.8, 62.9 to 116 and 119 to 194 mN/m. One of the criteria for choosing a vesicle is that it fluctuates, increasing the probability that the vesicles chosen are unilamellar. However, vesicles can still fluctuate if the number of bilayers is low and aspiration of these vesicles gives rise to moduli values which are multiples of the unilamellar values. If the grouping seen in this study represents results from multiple bilayer vesicles then the lowest value group would represent unilamellar vesicles. Visually, it would appear that this group contains five vesicles (21% of the total studies) and has an average area expansion modulus of 9.71 ± 3.57 mN/m (3sf). The highest value group contains 50% of the vesicles with a group average of 248 ± 9.77 mN/m (3sf). The difference in the average value of these two groups would suggest that the vesicles of the high value group contain approximately 25 bilayers, a number making vesicle fluctuation unlikely. In addition, the bending rigidity data does not suggest the presence of multiple bilayers. As stated above, the literature value is 265 ± 18 mN/m and is therefore consistent with the latter group average. As already stated, hydrolysis of DOPC would be expected to lower the elastic moduli as is seen for the PLA_2 enzyme. Therefore, these lower values are more likely to reflect DOPC degradation, due to the preparation method used.

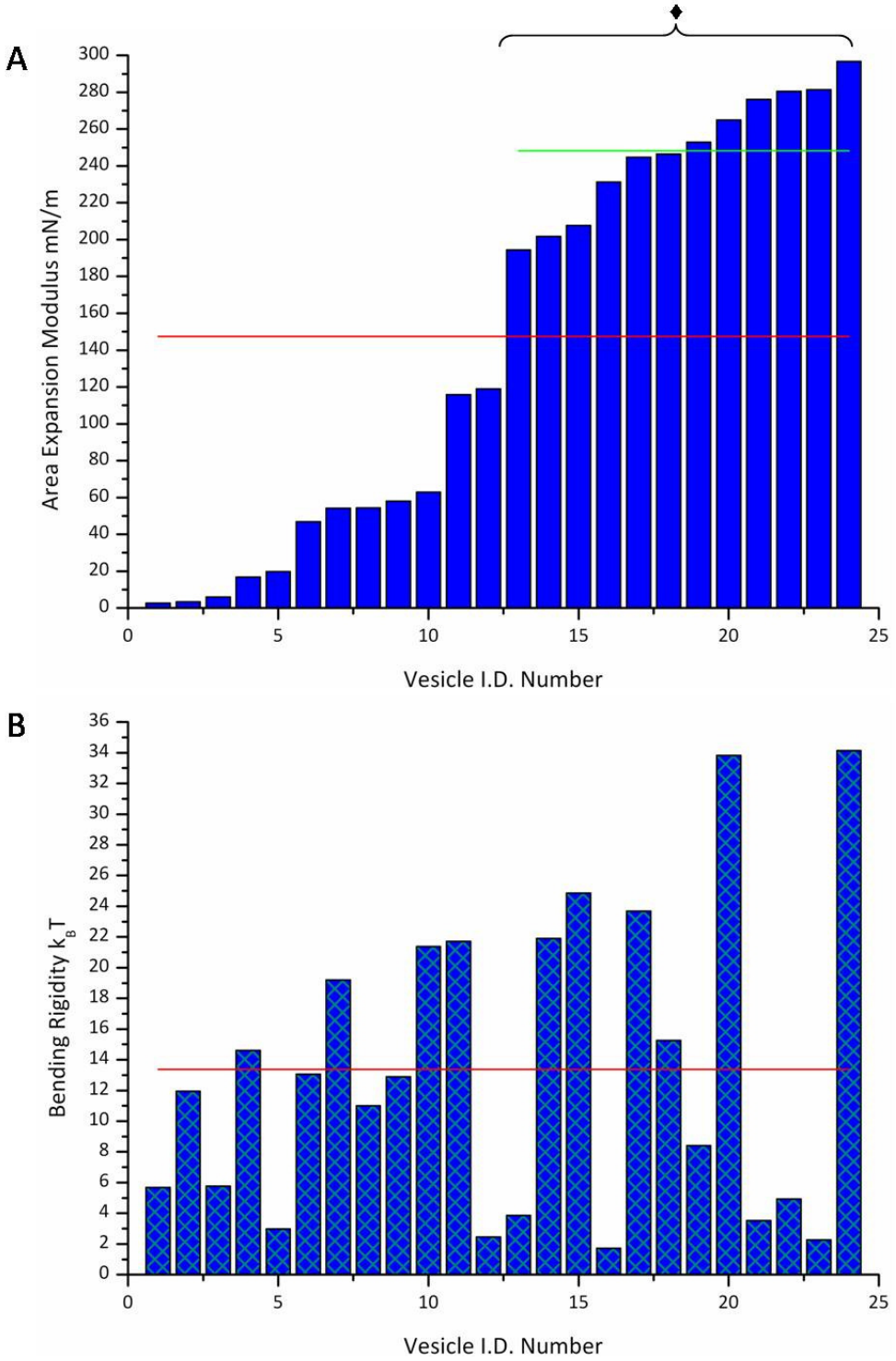


Figure 4.10. The membrane properties of a DOPC bilayer were investigated by the micropipette aspiration of 24 vesicles. Figure A shows the area expansion modulus of each vesicle, in ascending order. The red line shows the overall average value of this modulus; 147 ± 22.3 mN/m (3sf). The group indicated by ♦ represents vesicles without significant lipid degradation and has an average value of 248 ± 9.77 mN/m (3sf); shown by the green line. Figure B shows the bending rigidity of each vesicle (corrsponding to the area expansion modulus above) with the average value line (red) at 13.4 ±2.00 k_BT (3sf). The average value based on only the ♦ group is 14.9 ±3.57 k_BT (3sf). The error quoted is the standard error.

Micropipette aspiration of vesicles composed of di-ether PC gave an average bending rigidity modulus of 14.6 ± 4.68 $_{kB}$T (3sf) and an area expansion modulus of 232 ± 25.5 mN/m (3sf; Figure 4.11). Unlike the K_a data of DOPC, the di-ether PC data shows no extremely low values of this modulus or obvious grouping. This would further suggest that some vesicles in the DOPC study had significant levels of lipid degradation. In order to assess the K_a of DOPC bilayers, the vesicles with extremely low values should therefore be excluded. The largest data group for DOPC also represents the vesicles with the largest K_a values. Here it is hypothesised that this group does not contain significant levels of lipid degradation. Given this hypothesis, the bending rigidity and K_a values for DOPC should be taken from this group giving moduli values of 14.9 ± 3.57 $_{kB}$T (3sf) and 248 ± 9.77 mN/m (3sf) respectively.

From the DOPC and di-ether PC aspiration studies, it is clear that using the electroformation method produces some GUVs with significantly lower K_a. No considerable differences were seen for the value of the bending rigidity. This is unexpected as it too would be expected to be lower. A reduction in this value may be masked by the large experimental error associated with the bending rigidity data. It would be preferable to use a swelling method to form GUVs where possible. As already stated, GUVs containing SNARE proteins could not be produced using swelling. Electroformation has therefore been used for all the aspiration studies discussed in this chapter, allowing data to be directly compared. The influence of lipid degradation on the results however, is also discussed.

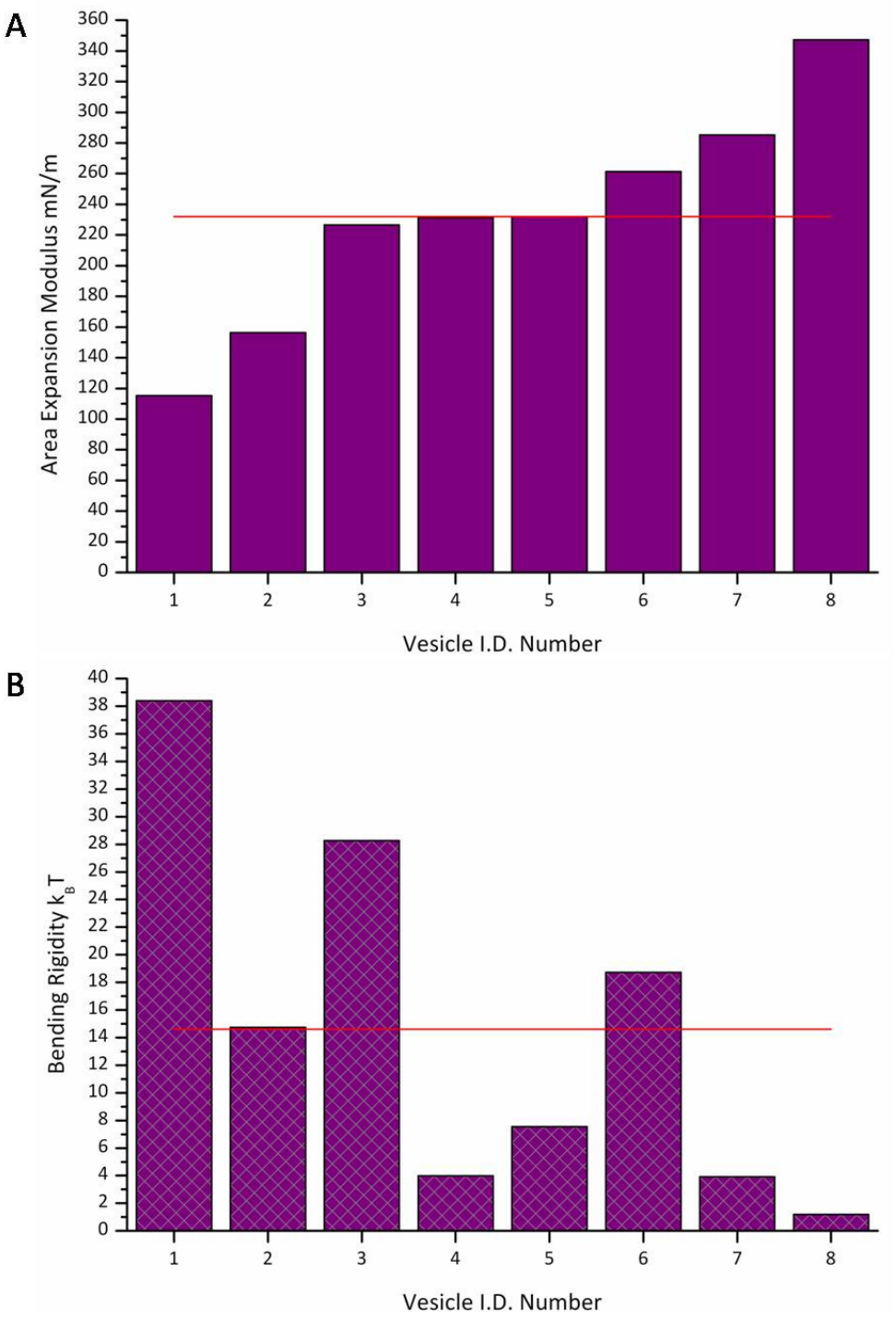


Figure 4.11. The membrane properties of a diether-PC bilayer were investigated by the micropipette aspiration of 8 vesicles. Figure A shows the area expansion modulus of these vesicles, in ascending order. The red line indicates the average value of this modulus; 232 ± 25.5 mN/m (3sf). Figure B shows the bending rigidity of each vesicle (corresponding to the area expansion modulus above) with an average value of 14.6 ± 4.68 k_BT (3sf).

4.3.2 SNARE Protein Micropipette Aspiration Studies

To investigate the impact of inserting the v-SNARE protein VAMP2 into a membrane, a micropipette aspiration study of 19 DOPC vesicles containing VAMP2 (1:300 protein: lipid molar ratio) was conducted. A bending rigidity modulus of 5.32 ± 0.81 k_BT (3sf) and an area expansion modulus of 143 ± 7.06 mN/m (3sf) were found (Figure 4.12). Unlike the K_a data for DOPC, the data for VAMP2 does not appear to form discrete groups or contain low values (the K_a values ranged from 88.1 to 206 mN/m). This would suggest that the GUVs aspirated did not contain significant levels of degradation products.

The aspiration of 33 vesicles composed of DOPC containing the t-SNARE proteins Syntaxin 1A and SNAP-25 (0.5: 0.5: 300 Syx 1A/SNAP-25/DOPC) found κ to be 8.13 ± 1.42 k_BT (3sf) and K_a to be 366 ± 37.1 mN/m (3sf; Figure 4.13). Like the DOPC data, the presence of low values of K_a suggests that some of the aspirated vesicles contained significant amounts of lipid degradation product. The highest values obtained for the K_a were 733 and 799 mN/m (3sf) and the vesicles with these values also had the highest bending rigidity values (30.8 and 37.4 k_BT respectively). As both elastic moduli values are significantly higher than the remaining data, these two vesicles may contain multiple (most likely two) bilayers and were therefore excluded from further analysis. The highest value group of the remaining data contains 18 vesicles (55% of the total studies). Like the DOPC study, this group is hypothesised to represent vesicles without significant lipid hydrolysis. Therefore, the average moduli values for this group are thought to provide values that better represent the effect of t-SNARE insertion on DOPC bilayers compared with the total averages. The K_a average of this group was found to be 493 ± 6.00 mN/m (3sf) and κ to be 8.30 ± 1.15 k_BT (3sf).

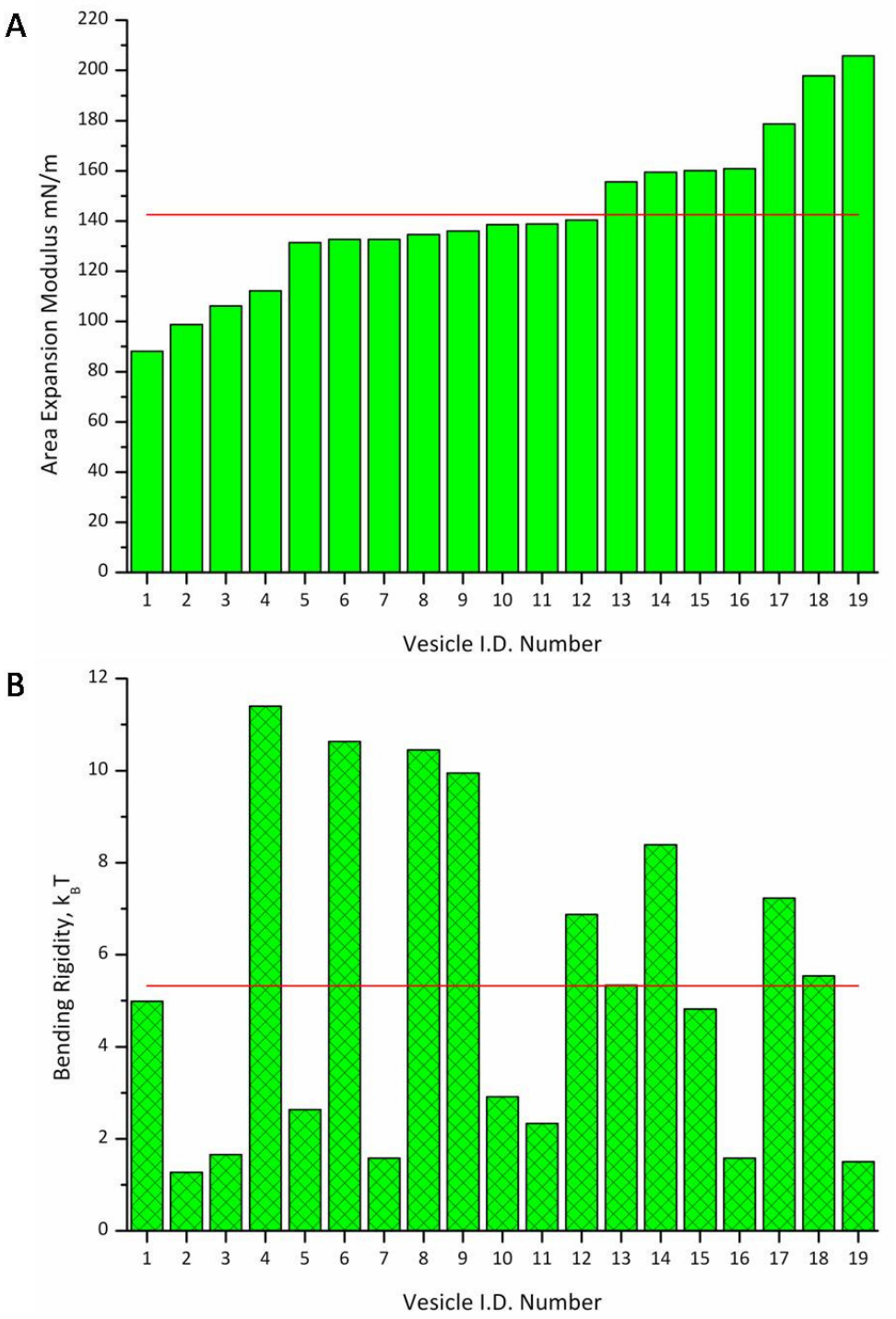


Figure 4.12 The membrane properties of a DOPC bilayer containing the SNARE protein VAMP2 (1:300 protein: lipid molar ratio) was investigated by the micropipette aspiration of 19 vesicles. Figure A shows the area expansion modulus of these vesicles, in ascending order. The red line indicates the average value of this modulus; 143 ± 7.06 mN/m (3sf). Figure B shows the bending rigidity of each vesicle (corresponding to the area expansion modulus above) leading to an average value of 5.32 ± 0.81 k_BT (3sf).

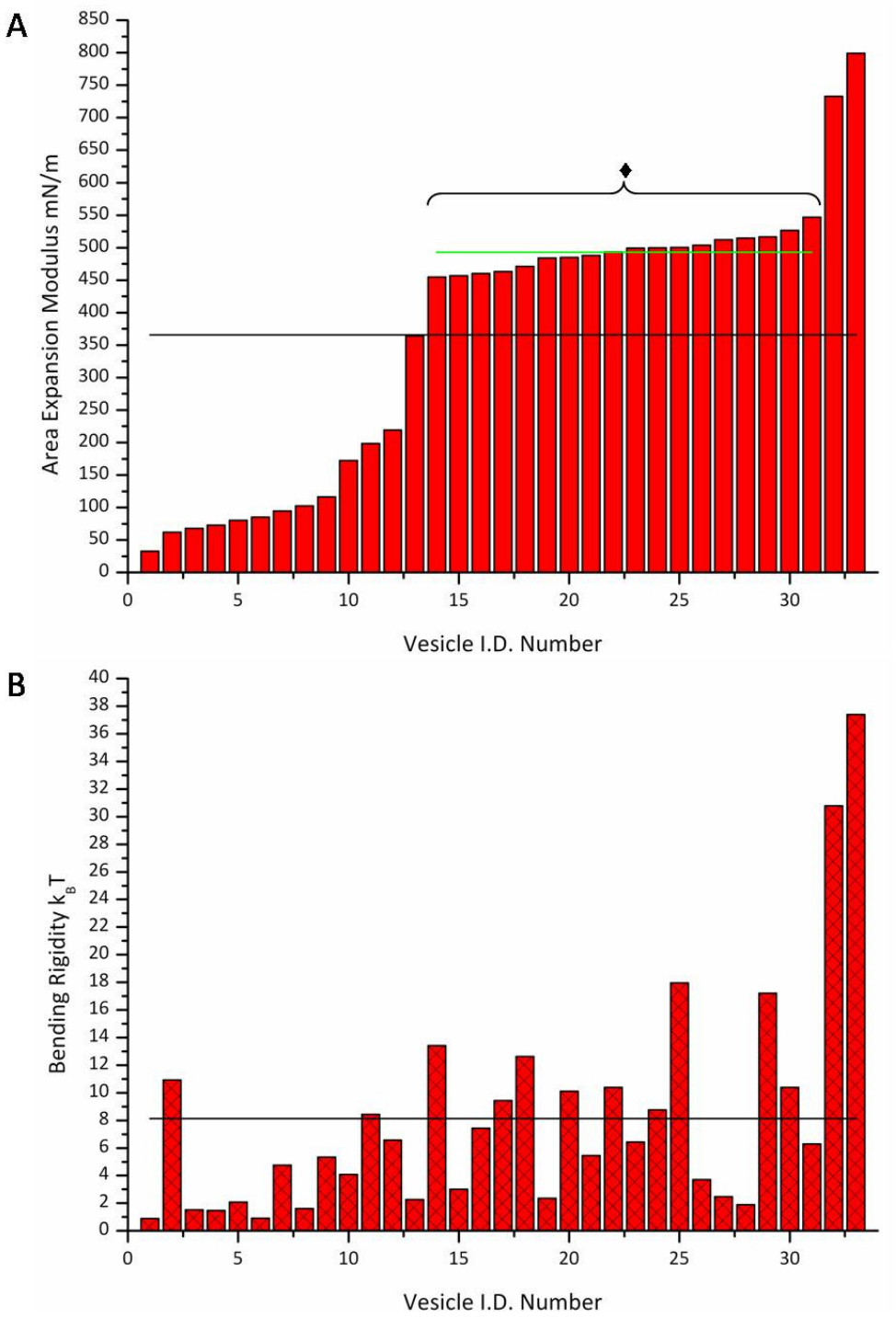


Figure 4.13 The membrane properties of a DOPC bilayer containing the t-SNARE proteins Syntaxin 1A and SNAP-25 (1:1 protein molar ratio, 1:300 total protein: lipid ratio) was investigated by micropipette aspiration of 33 vesicles. Figure A shows the area expansion modulus of each vesicle, in ascending order. The black line shows the overall average value of this modulus; 366 ± 37.1 mN/m (3sf). The group indicated by ♦ represents vesicles which are believed to be unilamellar with no significant levels of lipid degradation; the average value of this group is shown by the green line and is 493 ± 6.00 mN/m (3sf). Figure B shows the bending rigidity of each vesicle (corrsponding to the area expansion modulus above) with the average value line (black) at 8.13 ±1.42 k_BT (3sf). The average value based on only the ♦ group is 8.30 ± 1.15 k_BT (3sf).

4.3.3 Effect of SNARE Protein Incorporation

Table 4.1 shows the moduli values for each vesicle composition. In each case the average of all data obtained is given, however, for the DOPC and t-SNARE samples it is hypothesised that lipid degradation affected the study and therefore a group average value is also given, where the selected vesicle population is not believed to contain significant amounts of these degradation products.

Composition	Total Average		Selective Population Average	
	κ, k_BT (1 d.p.)	K_a mN/m (3sf)	κ, k_BT (1 d.p.)	K_a mN/m (3sf)
DOPC	13.4 ± 2.00	147 ± 22.3	14.9 ± 3.57	248 ± 9.77
Di-ether PC	14.6 ± 4.68	232 ± 25.5	-	-
VAMP2: DOPC (1:300)	5.32 ± 0.81	143 ± 7.06	-	-
t-SNARE: DOPC (1:300)	8.13 ± 1.42	366 ± 37.1	8.30 ± 1.15	493 ± 6.00

Table 4.1

For model lipid systems in a fluid phase, the bending rigidities are expected to be of the order of 10 k_BT[(318)], consistent with the data found in this study. Accurate calculation of the bending rigidity modulus requires small pressure changes at very low aspiration pressures. The micropipette aspiration equipment used, and the error on the aspiration pressure (± 1 Pa), makes this difficult to achieve and a large error is associated with the values found for this elastic modulus. While it cannot be stated conclusively, it is possible that the bending rigidities of membranes containing SNARE proteins are lower than that of the pure lipid bilayer (whether considering the total or selective average values).

In section 1.4.1 membrane dimpling was discussed. As the SNARE complexes form and the membranes are brought closer together the SNARE proteins are forced to bend, applying a force to the membrane; causing it to dimple. This process is thought to be essential in lowering the inter-membrane distance, allowing stalk formation to occur. A reduction in the bending rigidity due to the presence of SNARE proteins would decrease the energy needed to buckle the membranes. In addition, at other stages of the fusion process VAMP resides at the Golgi complex and plasma membrane. At both of these sites VAMP2 is incorporated into budding vesicles. Again, this requires a deformation of the bilayer and a reduction in the bending rigidity would lower the energy required. It would therefore be expected from these findings that VAMP2 would promote vesicle budding and that this protein and the t-SNARE proteins would promote fusion (at least to the hemifusion stage).

It can be seen that the area expansion modulus value of liposomes containing VAMP2 is the same (within error) as the total average for the pure DOPC sample. While lipid degradation cannot be ruled out for the VAMP population, the data suggests that this was not present at significant levels in

the vesicles aspirated. The DOPC study did show lipid degradation and therefore comparing the VAMP2 data with the selective DOPC population data is more appropriate. It can be seen from this comparison that VAMP addition reduced the area expansion modulus. This indicates that the membrane becomes easier to stretch and like the change in the bending rigidity, would be expected to make membrane dimpling easier. It has been shown that the K_a can be approximately related to the bending rigidity and the membrane thickness by the following expression[318]:

$$K_a = \frac{\phi\kappa}{h^2} \qquad \textit{Equation 4.16}$$

Where h is the membrane thickness and ϕ is a numerical constant (this is normally represented by α but has been changed to prevent confusion with its use in this chapter for relative area). The K_a value of liposomes containing VAMP2 is approximately 58% that of the pure lipid vesicles. A rough calculation based upon Equation 4.16 shows that if the fall in K_a was due only to the reduction of the bending rigidity then κ would have to fall to approximately 8.59 k_BT, much higher than the experimental value found. However, in Chapter 3 it was hypothesised that the increase in the relaxed curvature of GUVs containing this protein was caused by thinning of the bilayer due to the hydrophobic mismatch of the protein transmembrane domain and lipid bilayer thickness. It was approximated in section 3.4 that the DOPC bilayer would have to reduce from 35 to 30 Å to accommodate the transmembrane region of a VAMP2 protein molecule. Assuming this to be true, it can be estimated that with a thickness of 30 Å, the bending rigidity of the bilayer would have to be 6.31 k_BT to result in the K_a found. This is only 0.18 k_BT higher than the error range of the experimental value found and suggests that the hypothesis still stands.

For the t-SNARE liposomes a comparison of the selective liposome population data with the selective population data for DOPC shows that the K_a doubles due to presence of the proteins (the t-SNARE value is 199% the DOPC value). An increase is also clearly seen in a comparison of the total data averages. Using the same approach as in the previous paragraph it can be seen that without a change in the bending rigidity, the bilayer would have to thin to ≈25 Å. Without each monolayer curving significantly to enable the headgroups to stay closely packed, the chain splay required to thin the bilayer by such a large amount would likely expose the hydrophobic regions to water. Unlike VAMP2, it is not expected that insertion of the Syntaxin 1A transmembrane domain will cause hydrophobic mismatch. Therefore, assuming no change in the membrane thickness, the bending rigidity would have to increase to ≈29.6 k_BT to account for the increase in the area expansion modulus. This value lies significantly outside the error margin of the result shown in Table 4.1. From the results of this chapter it is suggested that t-SNARE insertion decreases the membrane bending

rigidity. It would appear that the relationship between the K_a and the bending rigidity in this case does not match Equation 4.16.

Another explanation for the results seen due to t-SNARE insertion is that these proteins interact to form interconnected protein complexes. The two SNARE motifs from SNAP-25 and the motif of Syntaxin 1A form a complex *in vivo*, along with a 'place holder' protein such as Tomosyn (see section 1.5.5) which acts as an intermediate structure in the membrane fusion mechanism. The lack of chaperone proteins like Tomosyn in this *in vitro* experiment prevents precise control of t-SNARE complex formation. *In vitro* studies have shown that it is possible to form SNARE complexes composed of only Q-SNARE proteins (section 1.2.3.4) and it can be imagined that the t-SNARE proteins are able to interact in a variety of ways; as illustrated in Figure 4.14. As SNAP-25 has two SNARE motifs, it is possible that one SNAP-25 molecule participates in two separate complexes. This would result in a non-specific aggregated structure which could surround the lipid bilayer and alter the elastic moduli. It is possible that the high curvature found in chapter 3 is also due to this protein structure. The presence of such an aggregate during electroformation would be expected to increase the energy required to form vesicles from the lipid film, reducing the average size of the giant unilamellar vesicles over the time of the growing procedure.

Unfortunately the presence of such aggregates may mean that the protein density is higher in the vesicles than the 1:300 ratio used in preparation. However, it is not thought that the density is vastly greater as electroformation was not possible when a 1:60 ratio was used in the VAMP2 studies of chapter 3. Also, high protein density is associated with leaky vesicles. These would be expected to rupture at lower aspiration pressures due to their instability but no differences were observed between the pressures at which these vesicle ruptured compared with that of the pure DOPC, di-ether PC or VAMP2 containing vesicles. Equally the aggregation may result in lower protein: lipid ratios (as more protein would be left on the glass substrate during electroformation) but if this was the case then the true impact of the t-SNARE proteins on the elastic moduli must be even greater than that observed in this study.

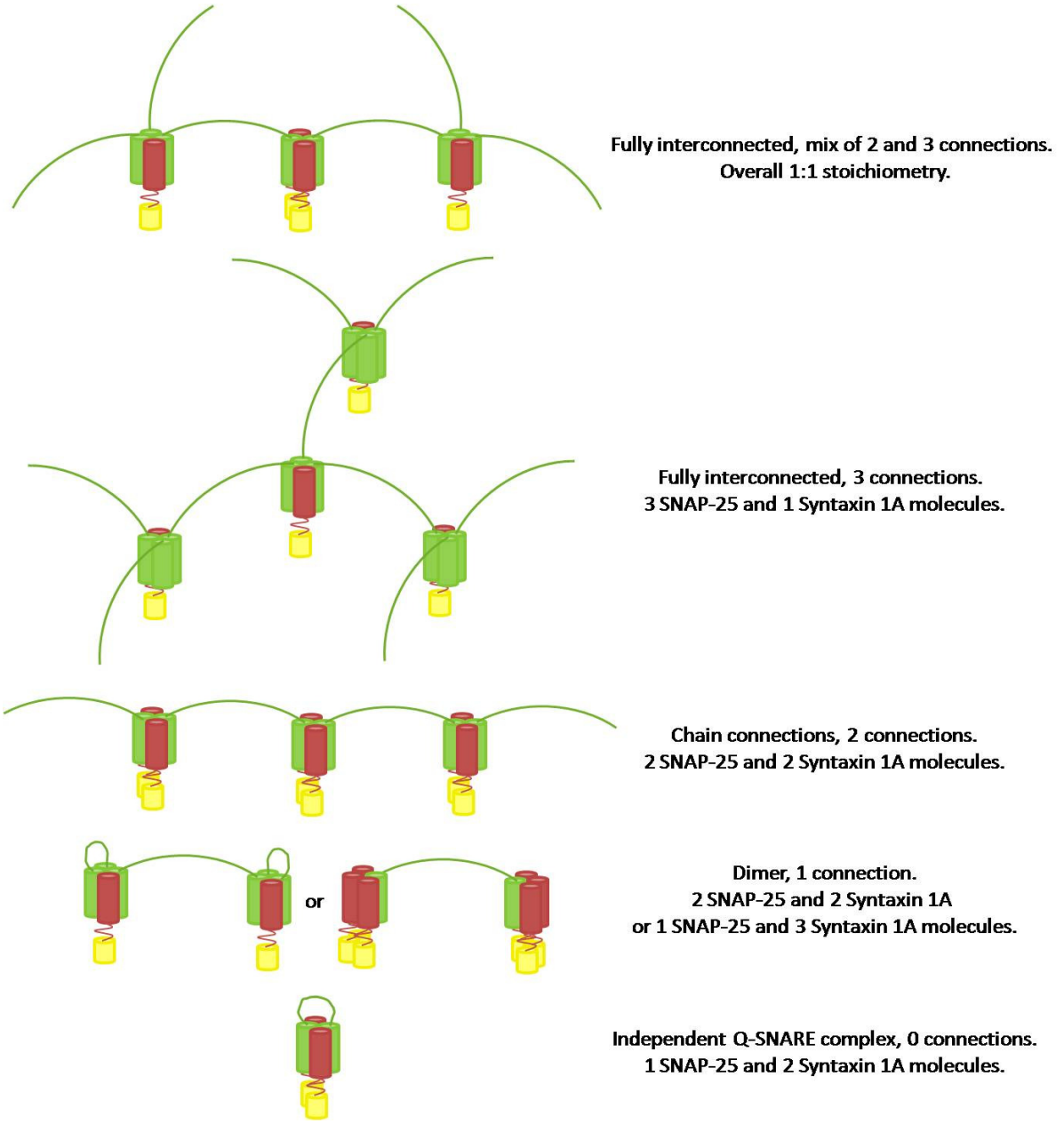


Figure 4.14 The wild-type intermediary complex has a 1:1 stoichiometry of Syntaxin 1A and SNAP-25 with a placeholder protein such as Tomosyn providing the additional amphipathic helix required. Without regulatory proteins such as Tomosyn several t-SNARE complexes could form during in vitro experiments. SNAP-25 (shown in green) contains two SNARE motifs and it can be imagined that one SNAP-25 molecule could participate in two separate complexes, thereby linking them. Depending on the t-SNARE protein ratio and the amount of cross-complex involvement by SNAP-25 it can be seen that complexes could form into lines or even an interconnected structure. Ascending through the figure, the number of interconnected complexes increases and an interconnected aggregate structure can form while preserving the 1:1 SNAP-25: Syntaxin 1A ratio. All of these structures are anchored to the lipid bilayer by the transmembrane domain (yellow) of Syntaxin 1A (red).

The insertion of the t-SNARE proteins may not directly increase the rigidity of the membrane. If the aggregation structure is interconnected and covers the vesicle surface then the K_a would increase as energy would be required to stretch and/or pull apart the proteins in addition to the energy requirements of stretching the lipid bilayer itself. The K_a is therefore an indication of the strength of the protein aggregate. The aggregate formed by the t-SNARE proteins is linked together through the formation of Q-SNARE complexes and therefore it would be these complexes that need to be pulled apart during aspiration. The wild-type SNARE complex (VAMP2, SNAP-25 and Syntaxin 1A) is one of the strongest protein complexes known with a stabilisation energy of 35 k_BT for the partially folded complex[85] but the Q-SNARE complex would not be expected to be as strong. Assuming the area expansion modulus of the lipid bilayer is equal to the pure lipid system this would give a K_a value for the protein aggregate of 245 mN/m (DOPC 248, t-SNARE 493 mN/m). Making a further assumption that the protein: lipid ratio remains 1:300 ratio, as used during preparation, this would equate to a protein density of 1.89 $x10^{20}$ proteins/m^2. From these values, the energy required by break each Q-SNARE complex would be 1.2 k_BT. However, this assumes that it is necessary to break every Q-SNARE complex before the bilayer could stretch, which is unlikely; making the true energy required to break a Q-SNARE complex much higher.

It has been hypothesised that SNARE complexes form a ring surrounding the membrane fusion site and therefore the strength and flexibility of this collar, as well as individual SNARE complexes is an important consideration. While in this study it is thought that SNAP-25 interlinks Q-SNARE complexes, it is unlikely that this occurs to form a ring of complexes *in vivo*. No such structures have ever been observed and there are no known proteins that could orchestrate the formation of such a structure. The complexity of the recycling mechanism by NSF/α-SNAP (see section 1.5.6) would also vastly increase. Some evidence suggests that the transmembrane domains of Syntaxin interact with each other, allowing the ringed structure to form. The strength of the aggregate in this study reflects the known stability of SNARE complexes *in vivo*. However, the bending rigidity found also suggests that the complexes are flexible as otherwise the rigidity in the presence of such an interconnected structure would be expected to be greater, not equal or lower than the rigidity of a pure lipid bilayer. A ringed structure would provide a scaffold that is therefore strong but flexible.

As discussed throughout this thesis, membrane tension is seen as an essential requirement in the formation of fusion pores. Studies using theoretical modelling[113, 130], computer simulations[131] and experimental studies[129] have highlighted its importance in the fusion mechanism. In addition, studies have been conducted on the kinetics of phase transitions in bulk mesophases[319]. Transitions between a fluid lamellar phase (a bulk mesophase in which bilayers are stacked) and a bicontinuous

cubic phase (interconnected sponge-like structures containing two distinct water channels) are thought to proceed via stalk-like structures, making such studies relevant to membrane fusion. It has been shown by such work that tension promotes the phase transition, suggesting that it drives the formation of these stalk-like intermediates. As well as tension, the computer simulations also hypothesise that membranes must be pulled sharply. Several researchers have proposed that the trans-SNARE complex provides a pulling force which induces fusion[114, 320, 321]; though it is still unclear whether this is required for the hemifusion step, fusion pore step or both.

If a ring of SNARE complexes does form around the fusion site then it would be conceived that a reduction in the bending rigidity would allow the membrane to dimple more easily. This would reduce the membrane separation. The interaction of the SNARE transmembrane domains in the formation of this ringed structure would also restrict lipid movement and such dimpling may therefore increase membrane tension. As discussed in the previous paragraph this would promote stalk formation. These affects may be sufficient to allow the bilayers to undergo hemifusion. During these processes, the SNARE complexes must be strong enough to overcome the repulsive forces associated with the close proximity of the membranes.

A pulling force could be applied by a change in the conformation of the complexes. A recent AFM study[322] presented evidence that the formation of the trans-SNARE complex has two distinct energy barriers. The first, which they call the outer barrier, must be overcome for unbound SNARE proteins to form an intermediate complex structure (this may represent partial zipping). The second or inner barrier is much larger and governs the transition from this intermediate state to the fully formed trans-SNARE complex. As discussed above, a partially folded SNAREpin may be sufficient to induce hemifusion. The action potential of neurotransmission (see section 1.1.2) could then trigger a change from a partially folded to fully folded SNAREpin (overcoming the inner energy barrier due to interactions with regulatory proteins such as Synaptotagmin and Complexin; section 1.5.7 and 1.5.8). This could cause the hypothesised ring of complexes to pull on the membrane of the fusion site (possibly in the form of a hemifusion diaphragm) from all directions. As the membrane would already be under tension, this would lead to the formation of a fusion pore. For this to occur the complexes must be strong (to make membrane fusion favourable over complex disassembly) and flexible (so that minimal energy is required to change the complex conformation and allowing it to occur quickly, resulting in a sharp pull). These characteristics are suggested by the high K_a but low bending rigidity values found for the t-SNARE liposome population.

4.4 CHAPTER SUMMARY

In this chapter the effects of SNARE protein insertion on the membrane properties of a DOPC bilayer have been investigated by micropipette aspiration. It has been shown that GUVs produced by electroformation can have lower than expected moduli values and this has been attributed to the hydrolysis of the ester linkages of DOPC. Careful analysis of the vesicle data and the use of selective vesicle populations have allowed comparisons to be made between the membrane properties of pure DOPC vesicles and proteoliposomes. However, it is concluded that a swelling method for GUV formation should be used when possible in preference to electroformation.

The insertion of VAMP2 has been shown to lower the energy of membrane dilation and a reduction in the bending energy is also indicated. The data is consistent with the hypothesis posed in Chapter 3 that the lipid bilayer is forced to thin as a result of hydrophobic mismatch between the length of the transmembrane domain of VAMP2 and the width of the lipid bilayer. The lowering of the elastic moduli suggests that the energy required to deform lipid bilayers is decreased when VAMP2 is present and this may aid both membrane fusion and vesicle budding.

As in Chapter 3, the interpretation of the data of the t-SNARE liposomes is more challenging. It is not thought that hydrophobic mismatch occurs in this case; however, like the insertion of VAMP2, a reduction in the bending rigidity may occur. The K_a was found to be greater than that of the pure lipid vesicles and has been attributed to the presence of an interconnected protein aggregate. The higher energy required to stretch the bilayer is thought to be due to the need to break up this aggregate. The aggregate is thought to form interconnected Q-SNARE complexes and it is hypothesised that the strength and flexibility of the aggregate reflects the nature of wild-type SNARE complexes *in vivo*. It is suggested that these qualities allow a ring of SNARE complexes to put the membrane within the fusion site under tension and may induce hemifusion at this point. A conformational change in the SNARE complexes then applies a pulling force; inducing fusion pore formation.

Chapter 5.

THE EFFECT OF MEMBRANE PROPERTIES ON LIPOSOME FUSION RATES

This chapter presents two studies which investigate the affect of membrane composition on liposome fusion rates. A lipid fusion assay was employed in which two fluorescently labelled lipids which act as FRET (Förster (or Fluorescence) Resonance Energy Transfer) partners were used. These lipid probes were NBD-PE (1- oleoyl- 2- [12- [(7- Nitro- 2- 1,3- benzoxadiazol- 4-yl) amino] dodecanoyl]- *sn*- glycero- 3- phosphoethanolamine) and Rh-PE (1,2- dioleoyl- *sn*- glycero- 3- phosphoethanolamine- N- (lissamine rhodamine B sulphonyl) (ammonium salt)) and were incorporated into the membranes at 0.5 mol% each. A probe dilution technique was used whereby vesicles containing both probes were mixed with non-fluorescent vesicles and the reduction in acceptor emission was monitored.

Two studies were conducted to examine composition affects. The first study investigated the change in fusion rates as a result of DOPE addition to DOPC membranes while the second studied the effect of cholesterol addition, also to DOPC membranes. The kinetic model proposed by Lee and Lentz[(106)] was used to interpret the data and contains three steps within the fusion process. It was found that it was not possible to determine the extent or rate of full-fusion events and a content mixing assay is required to provide additional information for this step. The initial, reversible step of non-fusion lipid transfer was found in both studies to be independent of membrane composition and to also contribute to less than 10% of the acceptor emission reduction. It was found that only the middle step which relates to hemifusion of the liposomes was dependent membrane composition.

The addition of either DOPE or cholesterol resulted in an increase of the rate of hemifusion as well as the amount of hemifusion compared to non-fusion lipid transfer. For the DOPE study the rate of hemifusion rose continually with its addition. The rate of hemifusion for the cholesterol study were higher than those of DOPE but the rate reached a plateau with the addition of approximately 10 mol% cholesterol. The rate increases are thought to be due to changes in both the curvature free energy of the initial vesicles and the energy required to form the intermediate structures i.e. the stalk and hemifusion diaphragm. For DOPE, the spontaneous curvature is the dominating influence and thought to promote fusion by lowering the activation energy. For cholesterol, the spontaneous curvature also promotes fusion. However, at higher mol% the stiffening of the membrane by cholesterol hinders fusion by increasing the amount of energy required to form the intermediate structures.

5.1 INTRODUCTION

Increasingly, the functions of membrane proteins are being explored using *in vitro* assays where the protein is placed in a lipid environment. However, it is now widely accepted that lipids provide more than just a structural framework for proteins to function, with lipid properties affecting protein characteristics such as binding affinity and conformation[70, 323, 324]. This poses an interesting problem whereby the results of these assays are affected not only by the proteins but also the choice of lipids. Commonly, a natural lipid extract is used to provide an environment similar to that of the protein *in vivo*. However, the lipid composition of a particular membrane *in vivo* is dynamic and while perhaps better than using a synthetic mixture, the lipid composition may still skew the assay results compared to actual biological processes.

The exact role of SNARE proteins in the fusion mechanism has been explored by several researchers using lipid mixing assays[38, 216, 325]. These assays usually contain several controls in which protein-free and single protein containing membranes are compared to assays in which mixed membrane populations are used (i.e. v-SNARE liposomes mixed with t-SNARE liposomes). Typically the rate and extent of fusion are monitored, but the results found vary widely with some researchers observing only hemifusion and others recording full fusion events. These and other researchers[326] have also used liposomes to explore the effect of calcium introduction on fusion rates and again the results vary; often with contradiction. The variation seen may result partly because of differences in the lipid environment.

The work presented in Chapter 3 and Chapter 4 found that SNARE proteins significantly alter membrane properties. The changes observed in fusion assays may in part be due to this and it is important to ascertain the proportion of the changes that are due to membrane energetics and the portion contributed by more active protein functions such as SNARE complex formation. Clearly some of this information can be extracted from comparisons of single protein studies with the studies containing the full complement of proteins. But several questions arise when considering the lipid-protein relationship. Firstly, is it actually possible to decouple the effects of altered membrane properties from protein functions? Part of the protein's function may be to alter lipid properties leading to the promotion of a particular event. Have proteins evolved so that they are designed for particular lipid environments (lowering the energy associated with its presence and providing some spatial selectivity) or does the lipid composition alter due to a protein's design? In order to begin answering these questions for the SNARE proteins, the relationship between membrane properties and fusion rates must be explored and the studies presented in this chapter aim to investigate this.

5.1.1 Lipid Mixing Assays

FRET is a widely used technique in both the physical and life sciences. In FRET, energy is transferred from the excited state of one fluorophore (the donor) to another excited state fluorophore (the acceptor) without the appearance of a photon[327]. Providing the spectral overlap integral J(λ) is sufficient, FRET can occur; but it is distance dependent (Figure 5.1).

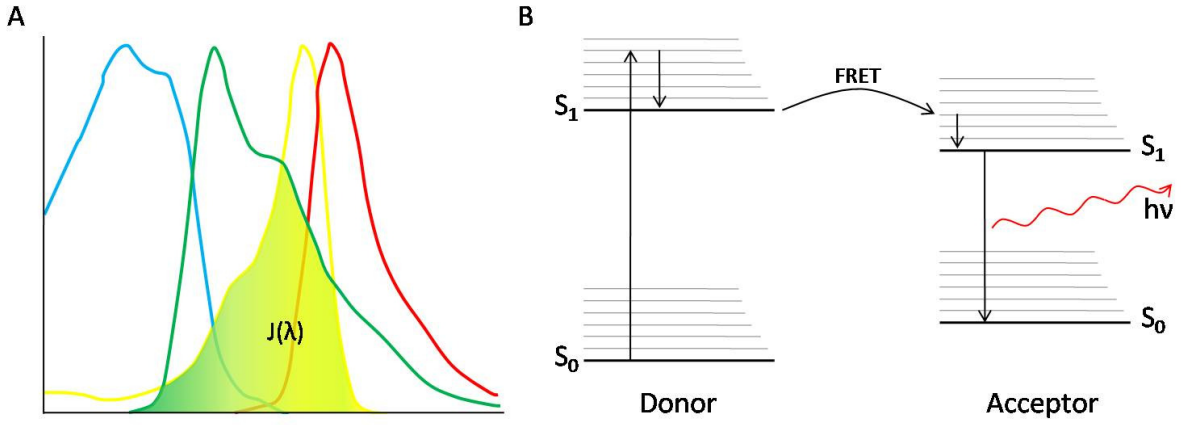


Figure 5.1 When the emission spectrum of one fluorophore overlaps with the excitation spectrum of another, FRET can occur (figure A). The spectral overlap integral J(λ) indicates the degree of spectral overlap and consequently the efficiency of FRET. When the spectra overlap, the energy of the donor fluorophore (in an excited state) can transfer to the excited state of the acceptor fluorophore. Relaxation of the acceptor to the ground state results in the release of a photon. A Jablonsky diagram of this process is shown in figure B.

The rate of FRET, $K_T(r)$ is given by:

$$K_T(r) = \frac{1}{\tau_D}\left(\frac{R_0}{r}\right)^6 \qquad \textit{Equation 5.1}$$

The equation shows that the rate of FRET depends on the Förster distance (R_0), the decay time of the donor in the absence of the acceptor, τ_D, and the distance between the FRET partners, r. The Förster distance of a fluorophore is the distance at which the efficiency of energy transfer is 50%. As well as J(λ), the Förster distance depends on the quantum yield of the donor and the orientation of the fluorophore dipoles with respect to each other. R_0 of a fluorophore is typically 10-100Å and therefore the donor and acceptor dyes must be at a distance below this for FRET to occur efficiently. The Förster distance is characteristic of the FRET pair being used and the decay time of each donor fluorophore is also specific. The FRET efficiency can be expressed as:

$$E = \frac{1}{1 + (r/R_0)^6} \qquad \textit{Equation 5.2}$$

During typical experiments, the only factor to change (and therefore altering the rate and efficiency of FRET) is the distance between the fluorophores. The power six dependence on the dye separation means that acceptor emission rapidly fades as it increases above R_0 and makes the technique highly sensitive to distance variations.

The lipid mixing fusion assay combines two populations of vesicles and monitors fusion through the use of FRET. There are two alternative methods; probe mixing and probe dilution[328]. The former mixes vesicles containing the acceptor probe with vesicles containing the donor probe. As vesicle fusion occurs FRET is seen to increase. The second method is probe dilution and mixes labelled vesicles (which contain both fluorophores) with unlabelled vesicles. As these vesicles fuse, the percentage of lipid probe in a membrane decreases (increasing dye separation) causing a decrease in FRET efficiency (Figure 5.2). Thus, the fusion of vesicles can be monitored by measuring the decrease in emission from the acceptor molecule over time. Alternatively, the increase in donor emission can be monitored. The probe dilution method is preferable to probe mixing as it has been shown that probe mixing is sensitive to vesicle aggregation causing over reporting of fusion events[329]. Probe dilution is affected by probe transfer across the solution but, providing that the fluorescent lipid probes used have sufficiently long hydrocarbon chains (above 16 carbons in length); this type of lipid transfer is negligible[328].

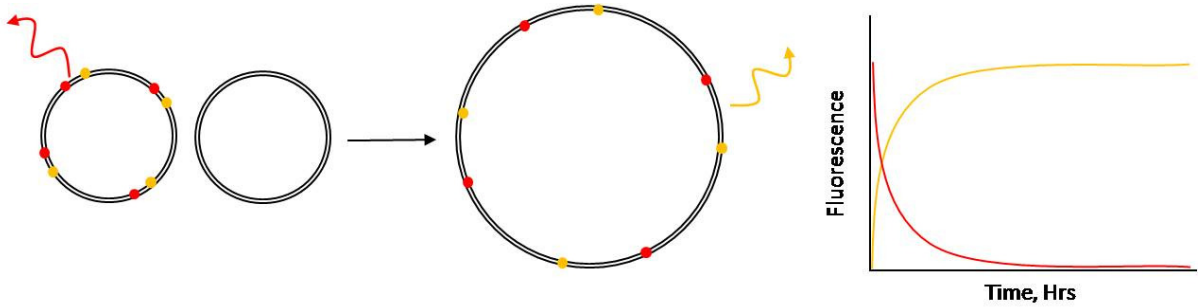


Figure 5.2 Lipid mixing assays can be conducted using probe dilution or probe mixing. This figure shows probe dilution which, unlike probe mixing, is insensitive to vesicle aggregation. The FRET partners are inserted into one vesicle population and mixed with an unlabelled vesicle population. The labelled vesicles initially give rise to high acceptor emission (red). Fusion of vesicles from each population results in increased dye separation, leading to a reduction in FRET and therefore a fall in the accepter emission and an increase in donor emission (yellow).

5.1.2 CONTENT MIXING ASSAYS

While lipid mixing fusion assays can be used to report fusion events, it is not always possible to distinguish adequately between hemi-fusion and full fusion events. In a hemi-fusion event the proximal leaflet of each liposome fuses together, for a probe dilution assay this causes increased dye separation and therefore a reduction in FRET. Full fusion, when the distal monolayers fuse, causes further probe dilution and the content of the vesicles mix. On a single vesicle pair basis it would be possible to distinguish between the two fusion events by monitoring a step-wise reduction in the FRET signal. However, fusion assays are most commonly global experiments which monitor thousands of vesicles at one time. In order to distinguish between these two fusion events it is usually necessary to also use a content mixing reporter either in a combined assay or as separate studies.

There are two principal methods used for content mixing fusion assays[330] (Figure 5.3). The first uses two separate chemicals, each enclosed in a vesicle population. Upon full fusion of a vesicle from each population, the two chemicals mix, resulting in a change in the fluorescence. There are several examples of this assay type but the most rigorously examined (for reliability) are the use of Tb (terbium) with DPA (Dipicolinic Acid) or ANTS (Aminonaphthalenetrisulphonic Acid) with DPX (p-xylylene bis(pyridinium) Bromide). In the first of these assays terbium weakly fluoresces but upon contact with DPA, it forms a chelate complex which has an intense fluorescence. The latter assay monitors the reduction in fluorescence as ANTS has an intense fluorescence but DPX acts as a quencher.

The second method uses self quenching species. During preparation, fluorescent species must be protected from light at all times. One of the advantages of using this technique over those described in the previous paragraph, is that only one fluorescent vesicle population is made. The most commonly used chemicals for this assay are carboxyfluorescein based, such as calcein. According to the manufacturer (Invitrogen) the fluorescence of carboxyfluorescein and calcein is 95% self-quenched above 100mM. Fusion of vesicles containing high concentrations of dye with dye-free liposomes causes a drop in concentration and therefore the fluorescence intensity increases. A disadvantage of this dye is that leakage into the bulk solution also causes an increase in the fluorescence intensity. It is possible to use Co^{2+} in the bulk solution to quench the dye but it is not always suitable to add it.

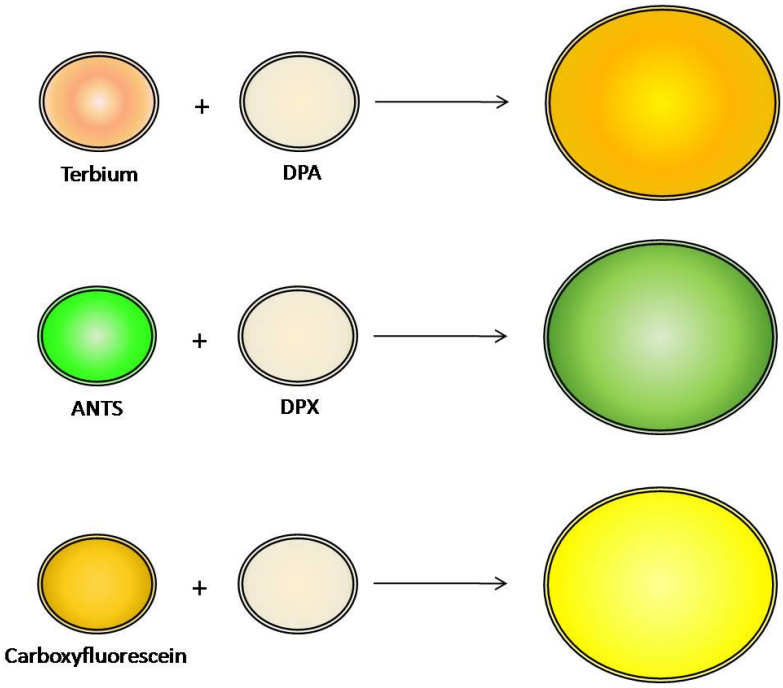


Figure 5.3 Content mixing fusion assays most commonly use one of three methods. The first, shown at the top of this figure is to mix terbium containing vesicles with those containing DPA. Upon fusion and content mixing, the fluorescence intensity increases. Alternatively, mixing ANTS and DPX vesicles causes a decrease in intensity due to quenching of the ANTS fluorescence by DPX. The final method, shown at the bottom of this figure, uses the self-quenching property of carboxyfluorescein. Encapsulated at high concentrations, the dye containing liposomes are mixed with vesicles containing only buffer. Upon fusion, the dye concentration falls below the self-quenching threshold and therefore the fluorescence intensity increases.

5.2 Materials and Methods

5.2.1 Vesicle Preparation

All phospholipids and fluorescent lipid probes were purchased from Avanti Polar Lipids, USA. Cholesterol was purchased from Sigma Aldrich, UK.

5.2.1.1 Unlabelled Vesicles

Low Salt PBS (LS-PBS)	2 mM KH_2PO_4 pH 7.4, 50 mM NaCl, 3 mM KCl, 5 mM Na_2HPO_4

DOPC was dissolved in chloroform at 10 mg/ml and DOPE or cholesterol at 1 mg/ml. The appropriate volumes of these lipid solutions were co-mixed in a 10 ml round bottom flask to give the required lipid composition. The chloroform was removed under a nitrogen stream and the lipid film dried in a vacuum desiccator for one hour. LS-PBS buffer was added to the film to give a total lipid concentration of 3 mM in 1 ml solvent. The flask was allowed to stand for one hour before being agitated with a vortex and allowed to stand for a further 30 minutes. Following this, the sample was freeze-thaw cycled five times using liquid nitrogen and a hair-dryer. The sample was then extruded using a mini-extruder (Avanti Polar Lipids inc., USA) 21 times through a 0.1 μm polycarbonate filter (Avanti Polar Lipids inc., USA) to produce 100 nm LUVs (Large Unilamellar Vesicles).

5.2.1.2 Fluorescent Vesicles

The fluorescent lipid probes NBD-PC (1-oleoyl-2-[12-[(7-nitro-2-1,3-benzoxadiazol-4-yl)amino] dodecanoyl]-sn-glycero-3-phosphocholine), NBD-PE and Rh-PE were purchased pre-dissolved in chloroform at 1 mg/ml. All steps were conducted in the dark and samples wrapped in foil where possible. Vesicles were made as described for unlabelled vesicles but replacing 1 mol% of the DOPC with 1 mol% total lipid probe.

Rh-PE with either NBD-PE or NBD-PC can be used as FRET partners where NBD-PE (or PC) acts as the donor, ex 480 nm, and Rh-PE an acceptor, em 593 nm. The R_0 for these FRET pairs is ~50 Å[328]. The spectra of these dyes supplied by the manufacturer were taken in distilled water at 20°C; the spectra of each probe (Figure 5.4) was therefore analysed for the fusion assay conditions (i.e. at 37°C, in the form of LUVs containing 1 mol% probe in 99% DOPC LUVs and suspended in LS-PBS buffer).

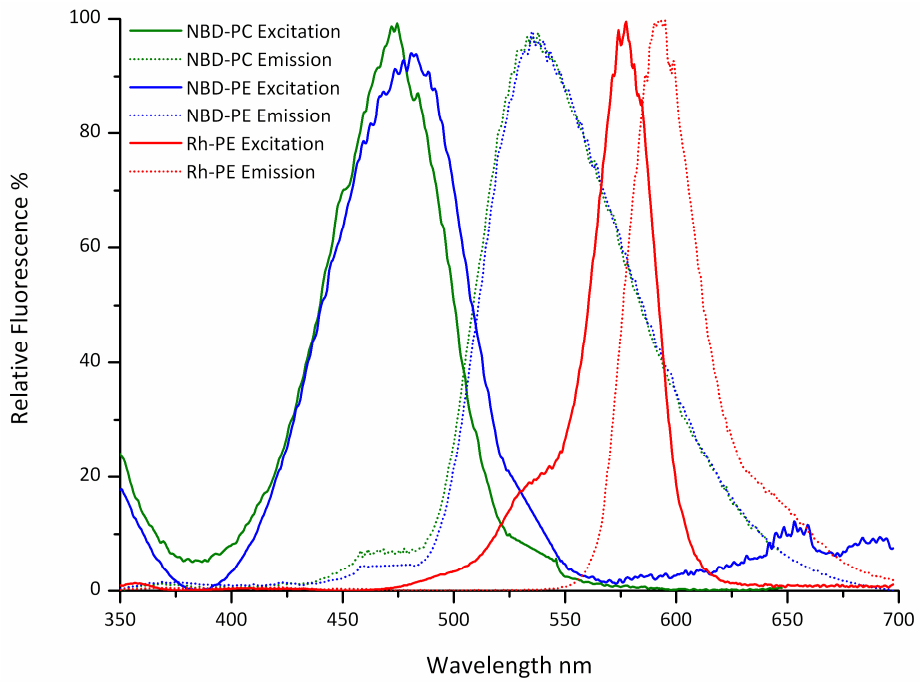


Figure 5.4 The emission and excitation spectra of NBD-PC, NBD-PE and Rh-PE are shown. Sufficient overlap of the emission spectrum of the NBD probes with the excitation spectrum of Rh-PE indicates their ability to be used as FRET partners. From the spectra it was concluded that a wavelength of 480 nm would be used to excite the NBD probes and the emission of Rh-PE monitored at 593 nm.

5.2.2 Fluorimeter Assay

Experiments were conducted using 10 mm light path, UV, 4 clear sided, 4.5 ml cuvettes (Kartell purchased from VWR, UK). A PerkinElmer luminescence spectrometer LS50B was used, heated to 37°C using a water circulator. Excitation was set at 480 nm and emission at 593 nm (slit width 2.5 mm). Background studies were conducted on a 0.33 mM fluorescent vesicle solution (330 µl 3 mM solution made up to 3 ml with LS-PBS). For fusion assays the sample also contained 0.67 mM unlabelled vesicle solution giving a 1 mM total lipid concentration. A ratio of 1 labelled to two unlabelled vesicles was used to increase the probability of labelled vesicles fusing with unlabelled ones.

Individual vesicle populations were first placed in separate vials and equilibrated to the experiment temperature in the water circulator for 30 minutes. For the fusion assay, the populations were then mixed. Readings of the fluorescence were taken every 10 seconds for a minimum of 14 hours overnight. The experiment was calibrated by addition of 30 µl pre-warmed Triton X-100 (1% (v/v) solution). Following Triton X-100 addition the vial was vigorously shaken to lyse the vesicles, the cuvette was then placed back in the fluorimeter and the fluorescence intensity of the sample recorded for two minutes.

5.2.3 Data Analysis

Triton X-100 causes the LUVs to break down and for the fluorescence intensity of the acceptor to fall to its lowest value. Using this final reading, each experimental run was converted from raw fluorescent units (RFU) to relative fluorescence, allowing for variations in concentrations and making the runs comparable (Figure 5.5). The RFU following Triton X-100 addition was set as 0% and the highest recorded RFU to 100%. For each liposome composition a background study was conducted where only fluorescent liposomes were present and therefore no change in FRET should have been observed. This allowed the effects of photo-bleaching to be accounted for over the time-scale of the experiments.

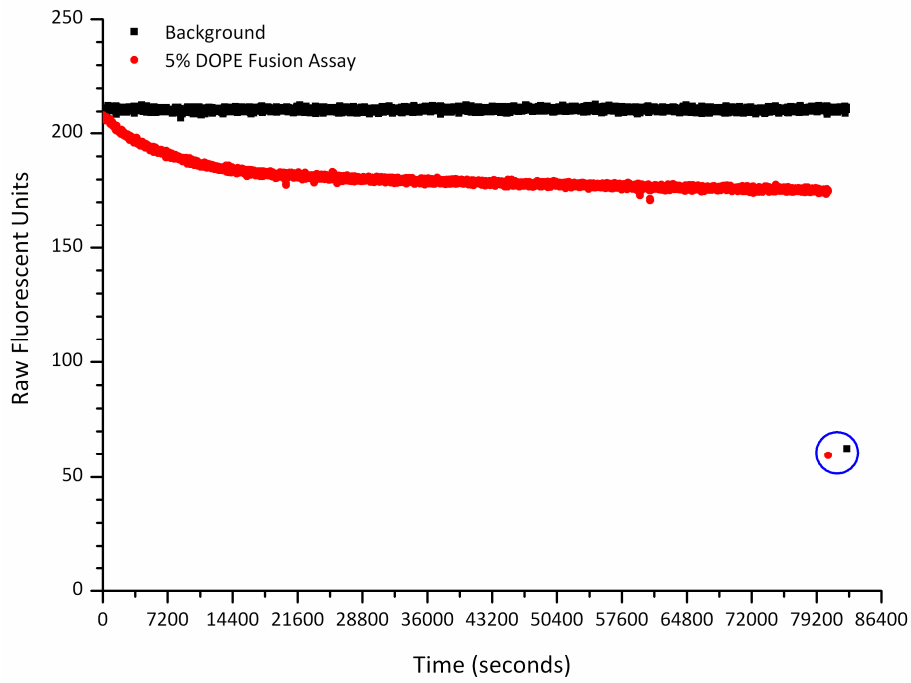


Figure 5.5 The raw data recorded by the fluorimeter is shown. The data in black shows the background study and the red data is the corresponding fusion assay. In order to allow compare experiments the raw data is converted to relative fluorescence using a Triton X-100 calibration. This is achieved by setting the highest raw value to 100% and the average Triton X-100 value (circled in blue) to 0%.

A nonlinear least square fit was used on the relative fluorescence plots for each composition; based upon the kinetic model proposed by Lee and Lentz in 1998[106]. In this model the fusion of two vesicles is hypothesised to occur in three steps (Figure 5.6). First the vesicles form a transient structure which may represent the stalk intermediary structure (see section 1.4.2.2). This structure then develops into a hemifused structure where the proximal leaflets of each vesicle are fused but the distal leaflets remain discrete entities, preventing content mixing. A fusion pore opens when the distal leaflets fuse and the contents mix. In each of these steps lipid exchange occurs and therefore the emission of the acceptor fluorophore decreases in intensity.

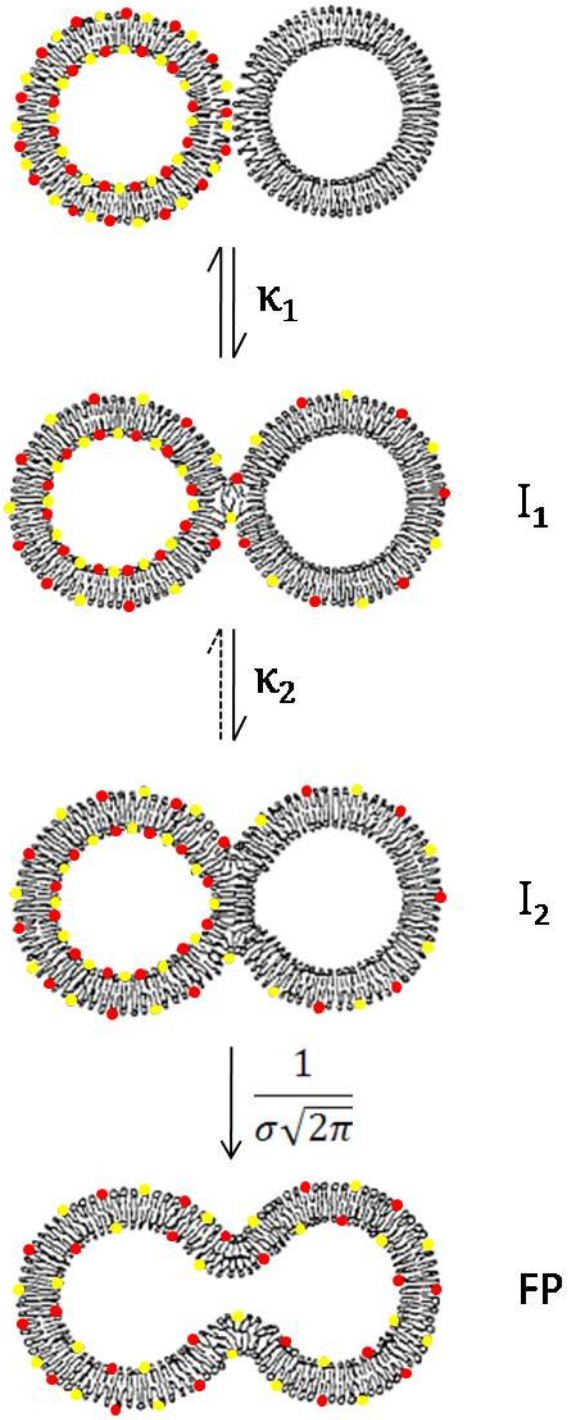


Figure 5.6 Following close contact between two vesicles, the proximal leaflets can form a transient structure allowing lipid content exchange (I_1). This structure may be similar to the stalk intermediary structure proposed in the fusion mechanism. The transient nature of this structure means it is a reversible step. In the second step the vesicles go from the stalk-like structure to a hemifused state (I_2). The backwards step to the stalk structure is thought to be sufficiently slow that it can be neglected. The third and final step is full fusion by generation of a fusion pore (FP). It is assumed that this final stage has a Gaussian distribution due to the global nature of the experiment. The rate of this step therefore relates to the peak height of the distribution where σ is peak width. The figure has been modified from Lee[(106)].

In the Lee Lentz study, the vesicles were triggered to fuse by addition of the dehydrating agent PEG. Due to this trigger, they applied a constraint to the hemifusion step whereby 95% of the vesicles must have first undertaken the first, stalk forming step. A time delay term of $3/k_1$ was therefore imposed on this term. They further assumed that the final full fusion event followed a Gaussian distribution with a mean time of $\bar{t}$. The integration of this distribution gives the probability of fusion pore opening and the peak height gives the frequency. The rate constant for this step is considered to be the frequency and therefore is equal to $1/\sigma\sqrt{2\pi}$. The full equation for this kinetic model is given in Equation 5.3.

$$y = y_0 + Ae^{-k_1 t} + Be^{-k_2(t-3/k_1)} + C\left(1 - \int e^{-\frac{(t-\bar{t})^2}{2\sigma^2}}.dt\right) \qquad \text{Equation 5.3}$$

Where y_0 is the value of y at time zero, k_1 is the rate of formation of the transient stalk structure and k_2 is the rate of formation of the hemifusion structure. As stated above, the full fusion rate constant is determined from the peak height of the Gaussian distribution, $1/\sigma\sqrt{2\pi}$.

The kinetic model was input into the graphing software program Origin 7.0 (OriginLab Corporation, Northampton, USA) with Equation 5.3 rewritten to expand the integral function.

$$y = A1e^{-k_1 t} + A2e^{-k_2(t-\tau)} + A3\left(1 + \frac{S}{t-\bar{t}}\, e^{-\frac{(t-\bar{t})^2}{S}}\right) + A4 \qquad \text{Equation 5.4}$$

As no trigger (like PEG induced dehydration) was used in this study, the $3/k_1$ constraint was altered to an arbitrary time delay τ. To improve iteration times the coefficient S replaced $2\sigma^2$. The coefficient y_0 was replaced by A4 to also include the integration constant of the third term. The experimental data of each fusion assays was fitted to this function to find the rates and amplitudes (A1, A2 and A3) for each fusion step (Figure 5.7).

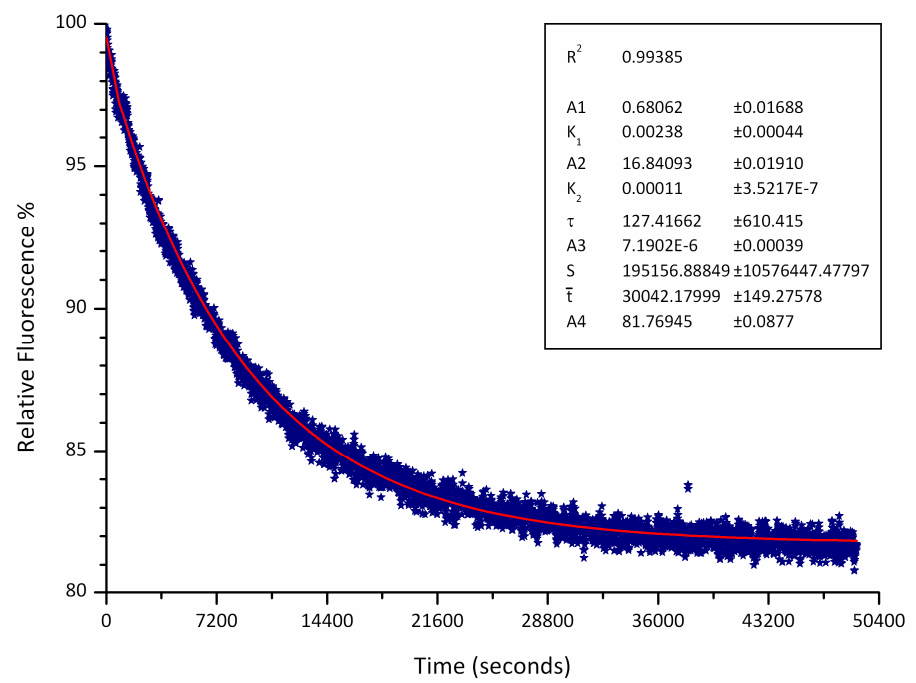


Figure 5.7 In this figure an example of a nonlinear least square fit to experimental data, based upon the kinetic model of Lee and Lentz is shown. This particular fusion assay consists of two vesicle populations; one composed of 90:10 DOPC: DOPE (at 0.67 mM concentration) and the other 90:9:0.5:0.5 DOPC: DOPE: NBD-PE: Rh-PE (0.33 mM concentration). The ratios given are mol%.

5.3 RESULTS

The affect of DOPE or cholesterol addition to DOPC bilayers on liposome fusion rates has been investigated. Fusion assays were performed on liposomes with various compositions and fit to the Lee Lentz fusion model (Equation 5.4). In all cases, the errors displayed are those resulting from the fit of the assay data to the kinetic model. Each data point contained within the graphs presented in this section (figures 5.8-5.13) represents an independent experiment.

The third term of this model describes the full fusion step and the amplitude of this term (A3) was close to zero for all compositions (Figure 5.8). It was found to be several orders of magnitude smaller than the amplitude of the hemifusion (A2) or non-fusion lipid transfer (A1) term, suggesting full fusion accounts for only a small percentage of the FRET reduction monitored. The size of the third term amplitudes and the errors associated with them do not make it possible to determine the relationship between full fusion events and membrane composition. As content mixing assays monitor full fusion events specifically, the use of such an assay should provide this information.

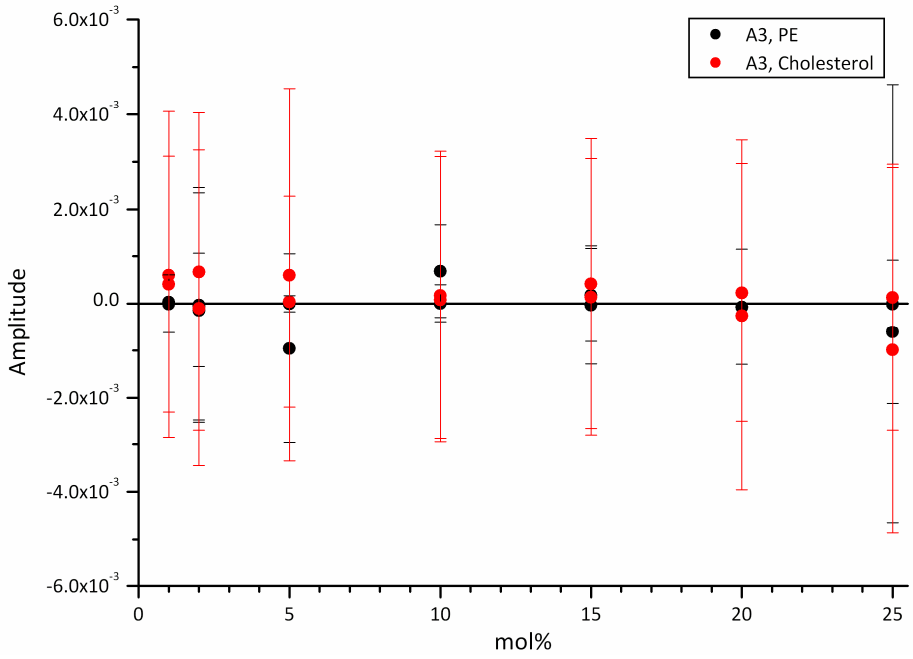


Figure 5.8 The amplitude of the full fusion rate step, A3, is shown as a function of the PE (black) or cholesterol (red) content. Liposomes were composed of DOPC, 0.5 mol% NBD-PE, 0.5 mol% Rh-PE and varying amounts of DOPE or cholesterol. For the PE study the contribution of the lipid probes is included in the x-axis. From the plots it can be seen that the amplitude is small in both cases and for all compositions. The error associated with each data point does not allow a relationship between composition and the amount of full fusion to be determined.

The time delay (τ) of the hemifusion step was found to be less than 360 seconds for each assay and the delay was not dependent on liposome composition in either study. Given the small time delay (the time scale of the experiment was 50400 seconds (14 hours)) and the error associated with it, this parameter can be considered to be zero. Along with the tiny contribution to FRET reduction by full fusion events, the Lee Lentz model effectively simplifies to a second order exponential curve (Equation 5.5). The remaining analysis will be discussed based on this premise.

$$y = y_0 + A1e^{-k_1 t} + A2e^{-k_2 t} \qquad \textit{Equation 5.5}$$

The y_0 term is theoretically the lowest relative fluorescence achievable by a given sample (Figure 5.9). The data for the PE study clearly shows that this value decreases inversely with DOPE addition. In the cholesterol study it is less clear; it is possible that there is also a decrease but that the values quickly plateau. As well as cholesterol, the vesicles of this study also contain 1 mol% PE probe and therefore the comparison of the 1 mol% samples from each study allows the effect of just cholesterol addition to be assessed. It can be seen that the y_0 value of the 1% cholesterol sample is considerably lower than the corresponding PE sample, suggesting that even at this low concentration cholesterol has a significant affect on the DOPC bilayer. The values of y_0 obtained suggest that in both studies, the addition of these components promotes liposome fusion.

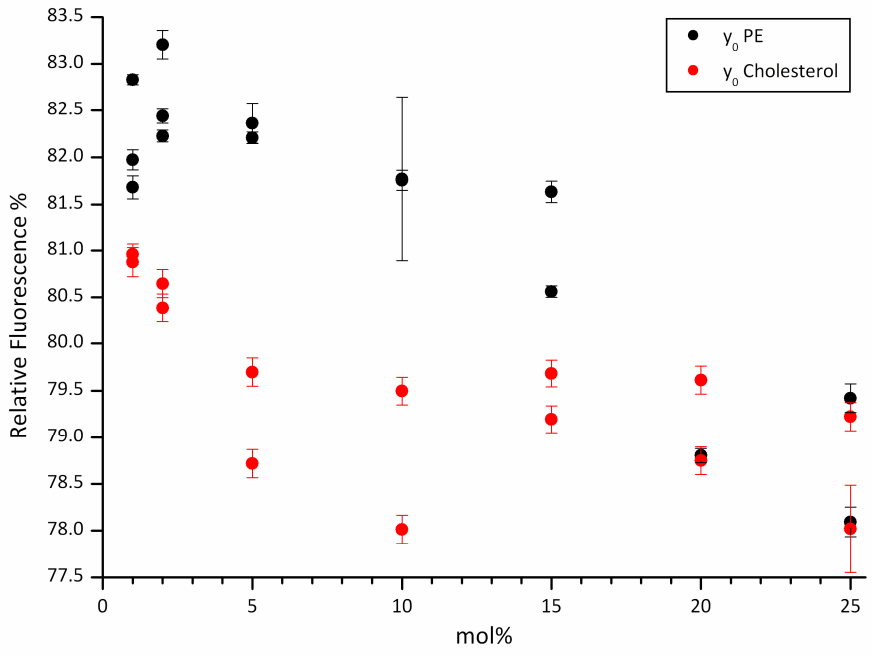


Figure 5.9 The fusion of vesicles composed of x mol% DOPE or cholesterol (plus 1 mol% lipid probe with the remainder DOPC) was assessed by lipid mixing and the data fit to the Lee Lentz kinetic model[106]. The y_0 values, which represent the lowest theoretical fluorescence value, are shown as a function of PE (black) or cholesterol (red). A clear reduction in the value of y_0 is observed for increasing PE content (where the PE contribution of the lipid probes is included). It is less clear for cholesterol addition but may show an initial reduction in y_0 which reaches a plateau. These studies indicate that DOPE and cholesterol promote liposome fusion.

The first rate term of the Lee Lentz model takes account of non-fusion lipid transfer (referred to from now on as NFLT). The amplitude (A1) and rate (k_1) of this step for both the PE and cholesterol study are shown in Figure 5.10 and Figure 5.11 respectively. The data suggests that the amount or rate of NFLT is not affected by the liposome composition. From these findings (and the very small contribution by full fusion events) it would therefore appear that the decrease in y_0 values is predominantly due to the second term of the kinetic model; hemifusion.

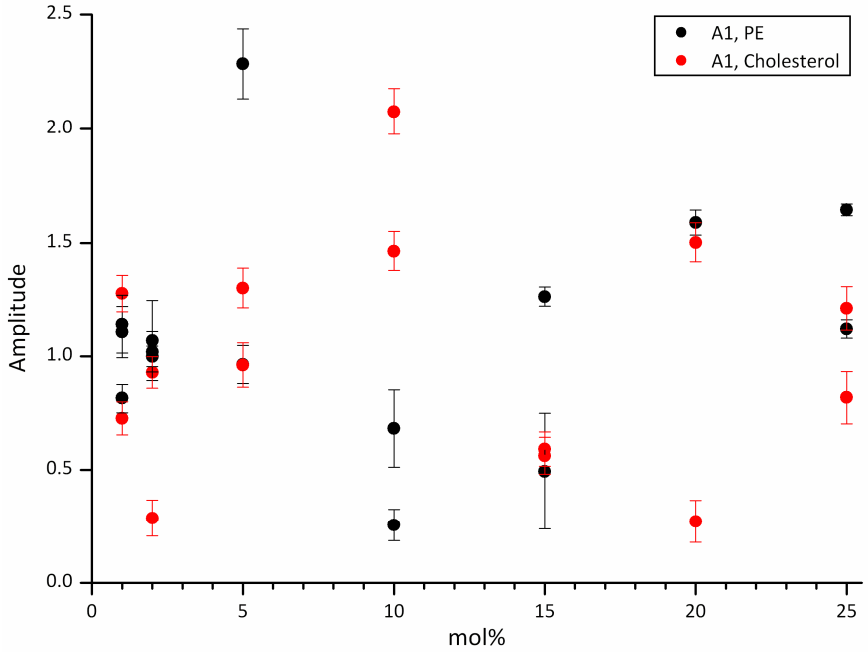


Figure 5.10 The amplitude of the rate step for non-fusion lipid transfer (A1) is shown as a function of PE (black) or cholesterol (red) content. Liposomes were composed of x mol% DOPE or cholesterol (plus 1 mol% lipid probe with the remainder DOPC). For the PE study the contribution of the lipid probes is included in the x-axis. From this data there appears to be no relationship between the amplitude of NFLT and the liposome composition.

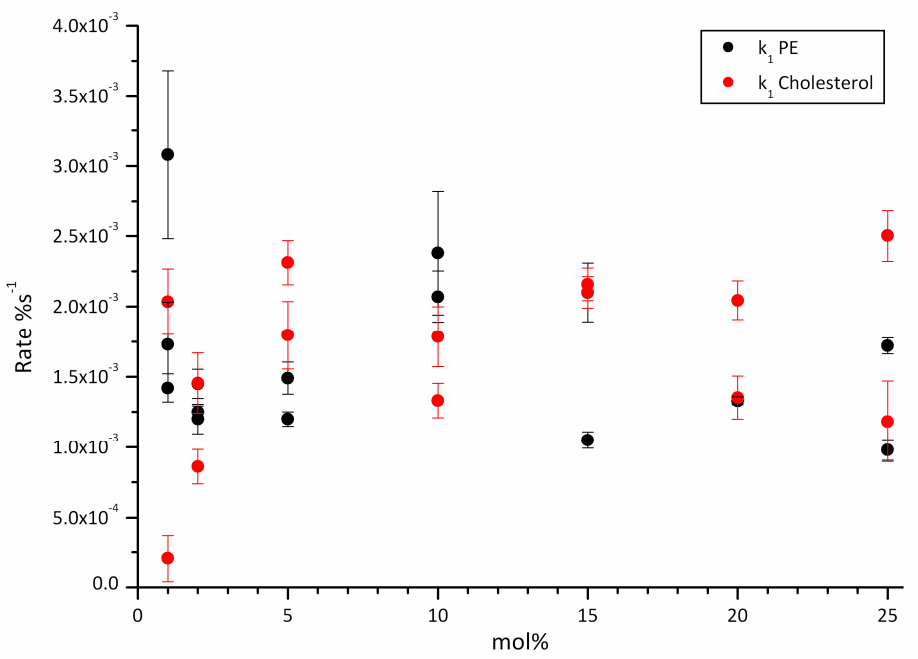


Figure 5.11 The rate of non-fusion lipid transfer (k_1) is shown as a function of PE (black) or cholesterol (red) content. Liposomes were composed of x mol% DOPE or cholesterol (plus 1 mol% lipid probe with the remainder DOPC). For the PE study the contribution of the lipid probes is included in the x-axis. From this data there appears to be no relationship between the rate of NFLT and the liposome composition.

As stated above, it would appear from the findings relating to A1, k_1, τ and A3 that the reduction in y0 can be attributed to the alteration of the second term of the kinetic model i.e. the effect of DOPE or cholesterol addition on the hemifusion stage of liposome fusion. From plotting the values found for the amplitude (A2, Figure 5.12) it can be seen that in both cases the amount of hemifusion occurring increases with the amount of DOPE or cholesterol. By comparing these values with those of NFLT it can be seen that the amount of hemifusion is an order of magnitude higher, suggesting that the majority of vesicles undergo this fusion event once the transient stalk-like structure associated with NFLT is formed. The results also indicate that while cholesterol has a greater affect than DOPE on this amplitude initially, the amplitude for cholesterol plateaus at higher concentrations unlike that of the DOPE study which continues to rise. This would suggest that above a certain level cholesterol is no longer able to promote hemifusion.

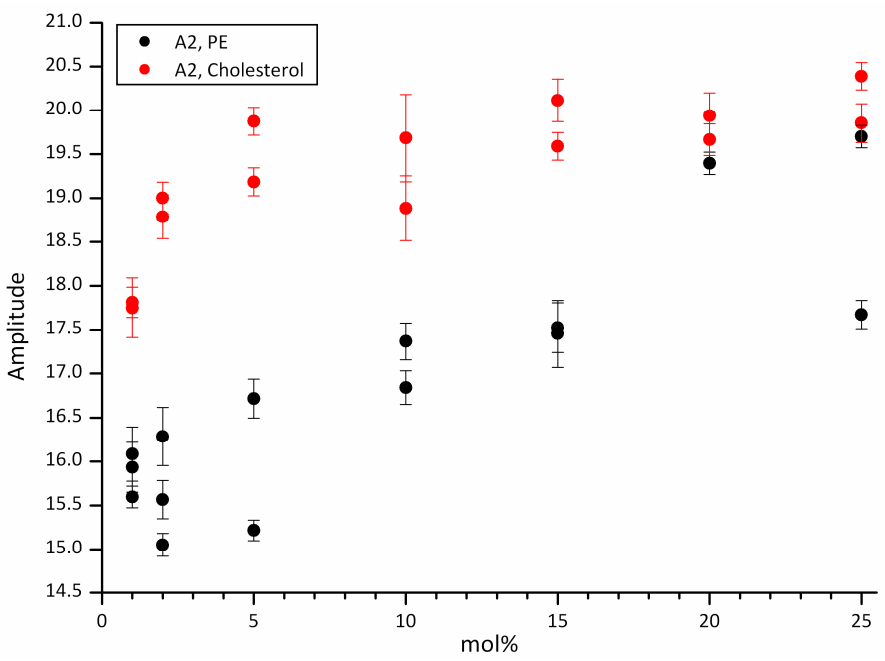


Figure 5.12 The amplitude of the hemifusion rate step (A2) is shown as a function of PE (black) or cholesterol (red) content. Liposomes were composed of x mol% DOPE or cholesterol (plus 1 mol% lipid probe with the remainder DOPC). For the PE study the contribution of the lipid probes is included in the x-axis. A comparison of these values with the amplitude of non-fusion lipid transfer indicates that the majority of vesicles, once in close enough proximity, undergo a fusion event rather than undergo the reversible NFLT step. A comparison between the two studies shows cholesterol to have a larger affect on the amplitude initially, which plateaus between 10 and 15 mol%. The amplitude of hemifusion in the PE study continues to increase with its addition.

The rate of hemifusion (k_2, Figure 5.13) in both studies is also seen to increase, though once again the data for cholesterol suggests a plateau is reached above 10 mol%. The exact relationship between the DOPE content and the hemifusion rate is less clear as the data could be interpreted as either a linear or a curve such as an exponential association. It is therefore possible that the DOPE hemifusion rates also plateau. Additional data points would be required to assess this, but if the relationship is the same as that for the amplitude it would be expected to be linear.

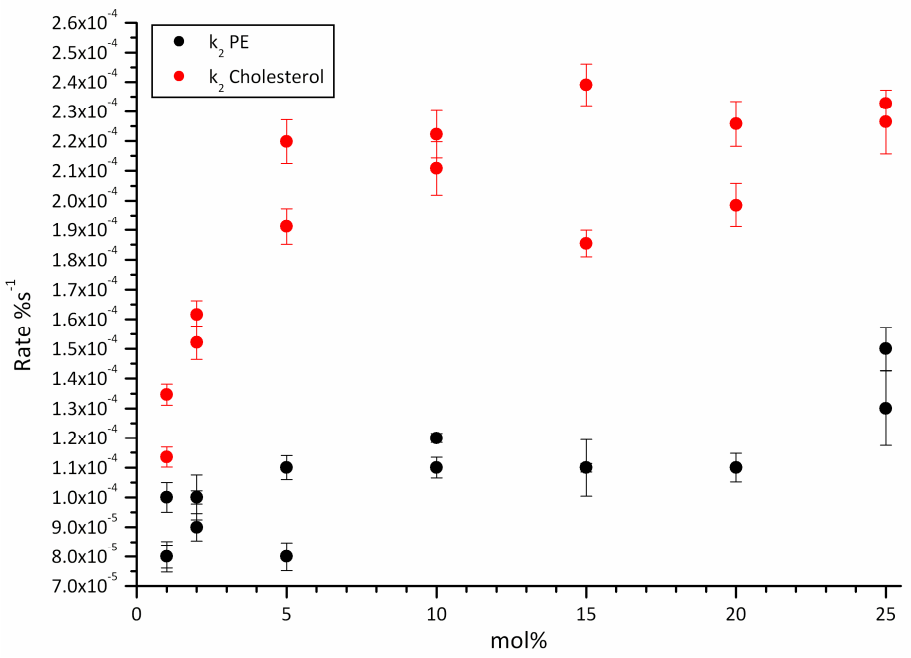


Figure 5.13 The rate of hemifusion (k_2) is shown as a function of either PE (black) or cholesterol (red) content. Liposomes were composed of x mol% DOPE or cholesterol (plus 1 mol% lipid probe with the remainder DOPC). For the PE study the contribution of the lipid probes is included in the x-axis. The addition of either DOPE or cholesterol results in an increase in the rate of hemifusion. The effect of DOPE addition is smaller than for cholesterol but the rate reaches a platues in the latter case. It is not clear whether this is also true for the DOPE study or if the rate continues to increase.

The evidence gathered from lipid mixing probe dilution fusion assays suggests that the addition of either PE or cholesterol promotes at least the hemifusion stage of vesicle fusion. In order to assess the impact of their addition on full fusion a content mixing assay is required. Initial experiments have been conducted (using a self quenching content mixing assay) but are yet to be completed and are therefore not presented in this thesis.

5.4 DISCUSSION

The Helfrich equation (Equation 1.3) is an expression of the curvature free energy of a membrane.

$$g_c = \frac{1}{2}\kappa(c_1 + c_2 - 2c_0)^2 + \kappa_G c_1 c_2 \qquad \textit{Equation 1.3}$$

As discussed in section 1.3.2, a symmetrical bilayer (like those of the liposomes in this study) has a relaxed curvature equal to zero. If we take two vesicles (spherical, radius = r) and fuse them together to form a single larger spherical vesicle, the final vesicle will have a radius of √2r (from the assumption that the surface area doubles). Assuming the composition of the initial vesicles to be equal, the elastic moduli of the initial and final states will be the same so that a change in the curvature free energy will be dependent only on the decrease of the principal curvatures c_1 and c_2 (which are equal in a sphere). From this it can be seen that the decrease in curvature through fusion lowers the curvature free energy of the system, making it a favourable process.

Another consideration is the stored curvature elastic stress. The bilayer relaxed curvature may be zero for a symmetric system but this is not true of the monolayers. The constraint on the monolayers to couple back to back results in a higher system energy compared to the relaxed curvature of the monolayers. If we apply Equation 1.3 to a flat monolayer surface then the free energy is equal to $2\kappa^{(m)}c_0^2$ where $\kappa^{(m)}$ is the monolayer bending rigidity ($\kappa^{(b)} = 2\kappa^{(m)}$) and c_0 is the spontaneous curvature of the monolayer[331]. From this it can be seen that bilayers with higher elastic moduli and spontaneous curvatures will have greater stored energy; these systems may be more driven to fuse in order to lower this stored energy.

5.4.1.1 DOPE

The bending rigidity of a DOPE bilayer at 0.94 $x10^{-19}$ J[331, 332] is only 10% higher than that of a DOPC bilayer which has a bending rigidity of 0.85 $x10^{-19}$ J[306]. The spontaneous curvature however is significantly different with a value of -1/3 nm^{-1} for DOPE[333] and -1/8.7 nm^{-1} for DOPC[332, 334]. Considering the free energy term for a flat monolayer ($2\kappa^{(m)}c_0^2$, previous paragraph), the addition of DOPE would increase the stored stress; predominantly due to the changes in the spontaneous curvature. The additional frustration of the monolayers would promote fusion as the system tries to lower its energy.

PE has been shown by several researchers to promote fusion[121, 335-338] and the findings of this study (a continual rise in liposome fusion rates with its addition) are consistent with this. During fusion intermediate structures are formed such as the stalk and hemifusion diaphragm and the energy of

these states depends on the membrane properties. As discussed briefly in section 1.4.2.2, it is believed that membrane fusion occurs via the stalk and hemifusion structures. Type II lipids (such as DOPE) have a negative spontaneous curvature and the energy required for them to form these structures is lower than lipids of less negative or positive curvature. Calculations on the energy of the stalk structure when composed of DOPC or DOPE have shown that the difference in spontaneous curvature results in a change from 45 k_BT for DOPC to -30 k_BT for DOPE[108]. The fall in the energy of the stalk structure can be thought of as a lowering of the transition state energy; this would reduce the activation energy of the fusion 'reaction'. The drop in stalk structure energy is known to allow DOPE to undergo spontaneous fusion[71]. The structure of the hemifusion diaphragm is also favourable for type II lipids and the energy of this structure will fall as PE concentration increases. The combined effects of these energies changes would be a promotion of hemifusion (Figure 5.14).

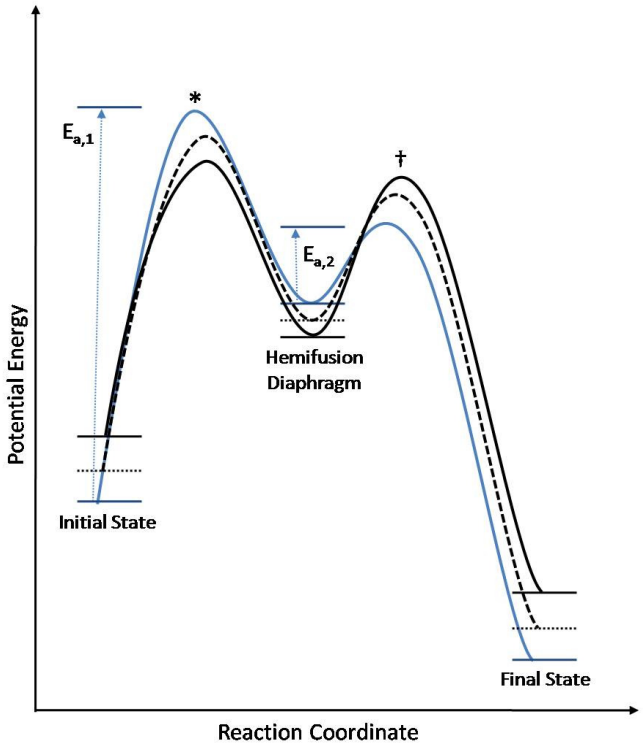


*Figure 5.14 The figure shows a fusion reaction profile to illustrate the effects that DOPE addition has on a DOPC bilayer. The profile of pure DOPC liposomes is shown in blue with the consequence of increasing DOPE concentration shown in black (concentration increases from dashed to solid line). The free energy and stored curvature elastic stress of the membrane becomes raised and the energy required to form the stalk structure (transition state *) is reduced. This results in an overall decrease in the activation energy ($E_{a,1}$) and the promotion of hemifusion. The energy of the hemifusion diaphragm would be expected to remain approximately the same as the distal monolayers would show an energy increase and the proximal leaflets an energy decrease. For the full fusion event another energy barrier must be overcome ($E_{a,2}$). DOPE would be expected to hinder such a step due to increasing the energy of the second transition state (†).*

The final stage (that of fusion pore formation) however, is thought to be inhibited by type II lipids as the fusion pore is modelled to have positive curvature[71]. The lower energy of the hemifusion diaphragm and the larger energy of the second transition state (the fusion pore) would raise the activation energy of the second step. Unfortunately, the data from the PE study which relates to this final step is too small to assess this theory.

5.4.1.2 Cholesterol

The spontaneous curvature of cholesterol[332] is between -1/2.9 and -1/2.3 nm^{-1} and would be expected to have a similar affect on fusion rates as DOPE. In 2006 Tenchov and Siegel[339] presented work examining the effects of cholesterol addition on bulk mesophases. Adding cholesterol to DOPC led to the formation of inverse bicontinuous cubic phases. As discussed briefly in chapter 4, phosphatidylcholine lipids such as DOPC form lamellar phases (stacked bilayers). The bicontinuous cubics are believed to form from these lamellar phases through the formation of stalk-like structures. Therefore, the ability of these systems to form the cubics is seen as an indication that the additional component can promote fusion. From this work, Siegel suggested that cholesterol is a fusogen. Haque[338] also found cholesterol to increase rates of fusion using liposome assays. While this was true with or without the presence of sphingomyelin he believed that without sphingomyelin, cholesterol made the vesicles leaky; increasing the rupture rather than fusion of vesicles. The lipid mixing study presented here indicates that cholesterol acts as a fusogen. If vesicles ruptured without a fusion event occurring it would be expected that the NFLT rates would also be affected by composition, which was not the case. It is not possible to assess conclusively whether the vesicles became leakier, as this would require a content mixing assay. If the vesicles do become leakier then it is suprising that a plateau in the hemifusion rates was reached at relatively low cholesterol concentration. It would be expected that increasing the cholesterol content would make them increasingly leaky, further increasing the rates observed.

The hemifusion rates of cholesterol are higher compared with the DOPE sample of the same concentration. If we assume that these rates do indicate promotion of hemifusion then what causes cholesterol to be more fusogenic than DOPE? As already stated, the spontaneous curvature of these two components is similar and therefore the first consideration should be the affect that cholesterol has on the bending rigidity of the bilayer. The value for this modulus is not known for pure cholesterol but studies have shown that its addition to some phospholipid bilayers increases the bending rigidity[299, 332, 340-342]. It would appear however that the consequences of cholesterol addition are not universal and that the saturation of the phospholipid is an important factor. The rigidity of bilayers composed of saturated lipids such as DMPC[342] (dimyristoyl phosphocholine) and DPPC[343,

[344] (dipalmitoyl phosphocholine) were shown to increase upon cholesterol addition. This is also true of SOPC[345] (1-stearoyl, 2-oleoyl-*sn*-glycero-3-phosphocholine) and POPC[299] (1-palmitoyl, 2-oleoyl-*sn*-glycero-3-phosphocholine) which contain one saturated and one monounsaturated hydrocarbon chain. However, the bending rigidity of a lipid bilayer where both hydrocarbon chains are unsaturated (such as DOPC) seems to be less affected[346].

If we imagine for a moment that adding cholesterol does increase the bending rigidity of the liposomes then this membrane property (along with the change in spontaneous curvature of the monolayers) would increase the stored curvature elastic stress. This energy increase would drive the system to fuse and may initially lower the activation energy. However, increasing the bending rigidity would also mean that the energy required to deform/remodel the membrane would be greater, making the energy needed to form the intermediate structures higher. This would result in the activation energy rising as more cholesterol was added, inhibiting fusion. The plateau seen in the hemifusion rates of this study would be consistent with this theory.

If the bending rigidity does not change significantly then what other affect could cholesterol have? Rawicz and Evans[347] have recently shown that cholesterol increases the area expansion modulus of a DOPC bilayer and an earlier study[343] showed this to occur for cholesterol addition to DPPC bilayers. This modulus is a measure of the energy required to stretch the membrane and as such shows how elastic the membrane is. Like the bending rigidity, an increase in this modulus raises the energy required to deform the membrane and the energy needed to form the stalk and hemifusion structures. So while the bending rigidity modulus may not be affected, it would appear that the membrane does become more rigid upon cholesterol addition and therefore the arguments of the previous paragraph stand. It can be predicted from this theory that further cholesterol addition would result in a reduction in the hemifusion rates.

The addition of cholesterol to a DOPC bilayer also increases the orientational order and bilayer thickness[346]. This indicates that the presence of cholesterol restricts the movement of the DOPC hydrocarbon chains, causing them to stretch. Both of these events would increase the stored curvature elastic stress of the bilayer. As previously discussed, this would increase the drive for fusion to occur and raise the initial state energy; lowering the activation energy at first. At higher concentrations the increase in the transition state energy would work to increase the activation energy, slowing hemifusion rates and causing the plateau in hemifusion rates observed. Like DOPE, it is predicted that cholesterol would inhibit the final fusion step, that of fusion pore formation. This would result from the higher energy required to deform the membrane, increasing the second transition state energy (Figure 5.15).

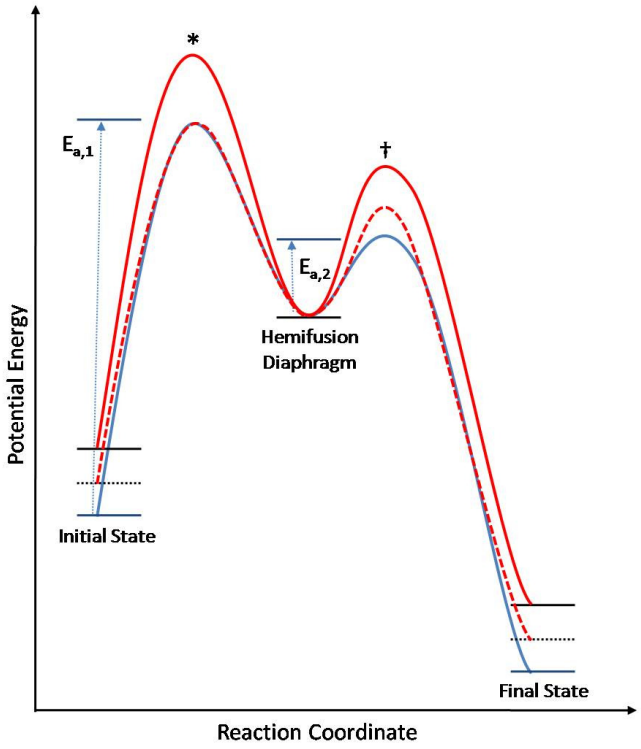


Figure 5.15 The figure shows a fusion reaction profile to illustrate the effects that cholesterol addition has on a DOPC bilayer. The profile of pure DOPC liposomes is shown in blue with the consequences of increasing cholesterol concentration shown in red (concentration increases from dashed to solid line). The free energy and stored curvature elastic stress of the membrane becomes raised due to cholesterol increasing the order and thickness of the bilayer, as well as the monolayer spontaneous curvature; driving fusion forward. To begin with, the rise in the initial state energy reduces the activation energy ($E_{a,1}$), increasing the rate of hemifusion. As the concentration of cholesterol increases, the energy required to form the transition state (, stalk structure) rises; inhibiting hemifusion. For the full fusion event another energy barrier must be overcome ($E_{a,2}$). Cholesterol would be expected to hinder this step due to an increase in energy required to deform the membrane. This stiffening and the influence of the negative spontaneous curvature would increase the energy of the second transition state (†).*

5.5 SUMMARY

In this chapter, lipid mixing assays have been used to investigate the affect of membrane properties on the fusion rates of liposomes. Fluorescent lipid probes that act as FRET partners were used and the reduction in acceptor emission monitored. It was not possible assess the impact on full fusion using these assays and therefore the studies should be extended to include content mixing assays. The rate of non-fusion lipid transfer was seen in both the DOPE and cholesterol study to be independent of bilayer composition and accounted for less than 10% of the reduction in acceptor emission monitored. The addition of DOPE to DOPC membranes has been shown to increase the rate of hemifusion and is thought to result from a lowering of the activation energy, predominantly due to the more negative spontaneous curvature. The addition of cholesterol to the bilayers has also been shown to promote fusion with an increase in hemifusion rates shown. However, the rate quickly reached a plateau (at approximately 10 mol% cholesterol) and this has been attributed to cholesterol stiffening the membrane, increasing the energy of formation for the intermediate structures. This raises the activation energy of the fusion process, hindering fusion at higher cholesterol content.

5.6 Implications for SNARE-Mediated Membrane Fusion

Both lipid and content mixing assays have been performed with bilayers containing SNARE proteins[38, 216, 218, 221, 224, 348-350] and show that these proteins increase the rate of fusion (either hemifusion or full fusion). The increase in the fusion rate has been attributed to the formation of the SNARE complex but how this (and the protein insertion itself) might influence membrane properties to promote such an event has rarely been considered. A study by Lui in 2008[102] investigated the effect of adding DOPE to SNARE proteoliposomes. In this study v-SNARE vesicles were prepared containing 0-60 mol% DOPE (plus 15 mol% DOPS, 1mol% fluorescent lipid and the remainder made up with POPC) and their fusion with t-SNARE planar bilayers containing 0 or 20 mol% DOPE (plus 15 mol% DOPS and the remainder POPC) monitored. The study showed that PE inhibited full fusion and promoted hemifusion but as has been seen from the results of this chapter (and other studies), the promotion of hemifusion by DOPE is true whether proteins are present or not. However, the findings do add to the evidence that SNARE-mediated fusion follows the same fusion mechanism as protein-free systems, albeit from an *in vitro* assay. Unfortunately, a protein-free assay was not performed by Lui to allow a direct comparison of the results. It would be interesting to know if the change in fusion rates he observed could not be explained by PE addition alone. Some proteins change conformation in different lipid environments[324] and so an additional contribution may come from changes in the structure of the SNARE proteins (most likely in the transmembrane and linker regions).

Considering the effect of protein insertion itself, the liposome studies of Chapter 3 showed that VAMP2 or t-SNARE incorporation increased the relaxed curvature of the bilayer and the aspiration studies in Chapter 4 showed that their insertion potentially reduces the bending rigidity (for VAMP2 a reduction in the area expansion modulus was also found). In view of the findings of this chapter, the modification of the membrane properties due to SNARE protein insertion is expected to promote fusion. The increase in curvature will work to raise fusion rates by increasing the free energy and stored curvature elastic energy of the initial state. This competes directly with the effect of changing the bending rigidity which will initially reduce both of these energies. However, at higher protein concentrations the reduction in the bending rigidity will make it easier to deform/remodel membranes and therefore the activation energy will be lowered. This can be considered to be the opposite effect to that seen by cholesterol addition. *In vivo*, it has been hypothesised that several SNARE complexes form a ring around the fusion site and therefore the local concentration of SNARE proteins would be high.

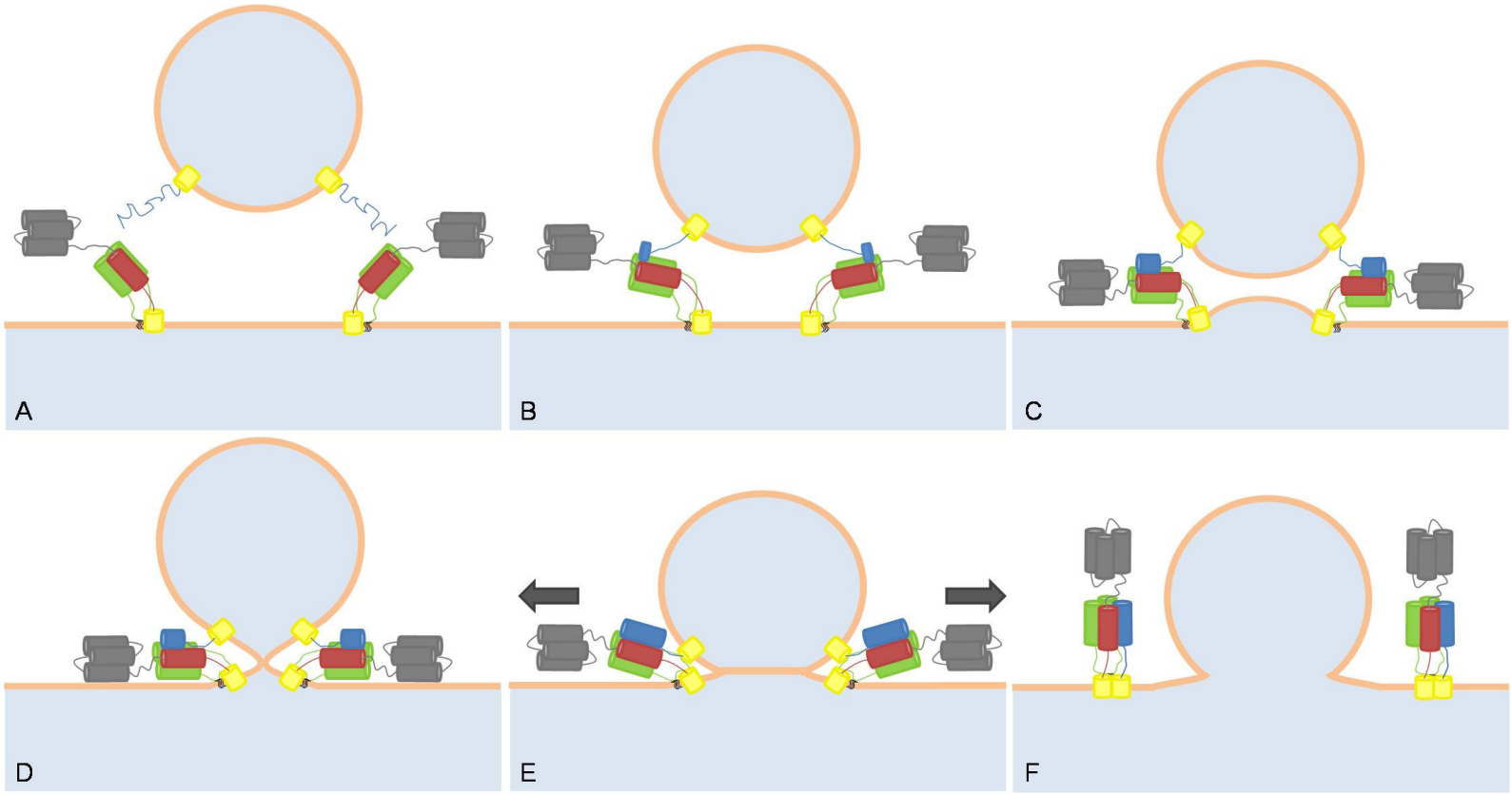


Figure 5.16 This figure shows the fusion model for SNARE-mediated membrane fusion. Unfolded VAMP2 interacts with a t-SNARE intermediary complex (A), undergoing N-terminal zipping to bring the vesicle and target membrane closer together (B). A ring of partially folded complexes surrounds the fusion site and the high concentration of SNARE proteins softens the membrane and increases the relaxed curvature. As the trans-SNARE complexes begin to form, a torque is applied causing the bilayers to buckle and the membrane tension to increase (C). Lipid protrusions from the bilayers lead to the formation of stalk structures (D) which then expand into a hemifusion diaphragm. The increase in the membrane tension and raised relaxed curvature promote the formation of these intermediate structures. The trans-SNARE complexes fully fold following a calcium influx, pulling on the hemifusion diaphragm (E) and inducing fusion pore formation. With the membranes fully merged the trans-SNARE complexes can now rearrange into the most stable form, the cis-complex (F).

By applying the theory of the previous paragraph to membrane fusion *in vivo*, it can be seen that the SNARE proteins may assist the merger of two bilayers in several ways (Figure 5.16). As discussed in section 3.4, the higher relaxed curvature in the presence of VAMP2 may aid vesicle budding as well as VAMP2 recruitment to synaptic vesicles. In the fusion mechanism itself, this higher curvature may promote the dimpling of both the synaptic vesicle bilayer and plasma membrane; reducing the inter-membrane distance. The lower bending rigidity (and area expansion modulus in the case of VAMP2) would decrease the energy required to form such dimples. In section 4.3.3 the necessity of membrane tension was discussed, where both kinetic studies of bulk mesophases and computer simulations suggested tension promotes stalk formation. As well as decreasing the membrane separation, dimpling of the bilayers by the SNARE proteins would be expected to increase the membrane tension. It is therefore hypothesised that the manipulation of the bilayers by SNARE proteins should be sufficient to induce the proximal leaflets of the membranes to merge, forming the hemifusion diaphragm.

The computer simulations investigating the need for membrane tension[131] also found tension was necessary for a full fusion rather than hemifusion event to occur. The strength and flexibility of a t-SNARE protein aggregate structure (Chapter 4) is believed to reflect these qualities in native SNARE complexes. Following hemifusion the SNARE complexes would influence the hemifusion diaphragm. As with dimpling, the complexes may exert a torque force on the diaphragm and along with the transmembrane domains around the rim, may further increase the tension. If the *trans*-complexes folded further this would also increase the tension. As the complexes then fully fold into the *trans* state, they would pull on the hemifusion diaphragm causing it to rupture and forming a fusion pore. This conformational change could be triggered by the action potential of the neuron (causing changes in regulatory proteins).

5.7 CONCLUSIONS

Membrane fusion *in vivo* is a highly regulated process utilising a myriad components. Despite the SNAREs being identified as fusion proteins 16 years ago, the intricacies of the fusion mechanism mean that there is still much to be discovered about how they truly function. The properties of the lipid bilayer itself have been shown to be important for the competency and efficiency of fusion and links between proteins (such as Synaptotagmin) and certain lipids have been made. It is only now however, that the influence of the SNARE proteins on lipid bilayer properties has been explored.

Studies showing increases in fusion rates due to the presence of SNARE proteins have attributed this to the formation of the SNARE complex (see section 5.6). However, fusion via a stalk structure is the most favoured model; suggesting that fusion does not involve proteins directly. As discussed throughout this thesis, speculations have been made using theoretical modelling and computer simulations of how SNARE proteins might influence lipid bilayers; but little experimental evidence has been produced. This project has used *in vitro* assays to investigate this aspect of SNARE protein function. The SNARE complex certainly brings membranes into close proximity, but this is unlikely to be sufficient for full fusion events to occur[351]. The SNARE proteins have not been found to bind directly to lipids but the results of this project show that they nonetheless influence the properties of bilayers; suggesting their role goes beyond simply bringing (and holding) membranes together.

The neuronal SNARE proteins have been purified and incorporated into model membrane systems. In Chapter 3, the SNARE proteins were shown to increase the relaxed curvature of the lipid bilayer. The micropipette aspiration studies of Chapter 4 suggested the bending rigidity of membranes was reduced upon SNARE protein insertion and changes in the area expansion modulus were also found. In Chapter 5, the addition of DOPE to DOPC bilayers was shown to promote hemifusion; consistent with previously published works (for references see section 5.4.1.1). Cholesterol addition was also shown to promote fusion but raising the concentration inhibited hemifusion due to increasing membrane stiffness. Combining the findings of all these studies it is hypothesised that the SNARE proteins promote the fusion process, achieving this through bringing membranes into close proximity and altering the membrane properties; driving the fusion process forward, reducing the energy required to form intermediate structures and increasing membrane tension.

5.8 FUTURE WORK

The changes in the membrane properties of a DOPC bilayer due to the insertion of VAMP2 has been attributed to a hydrophobic mismatch between the preferred bilayer thickness and the length of the transmembrane domain of the protein. While these changes are expected to promote fusion, it is important to establish if these changes are a universal effect of VAMP2 incorporation or whether it is only due to the choice of lipid for the model. For this reason it would be prudent to expand the studies of chapters 3 and 4 to include vesicles composed of a more complex mixture of lipids. Studies have shown the lipid content of synaptic vesicles to be 36-40 mol% PC, 23-32 mol% PE, 12 mol% PS, 5 mol% PI and 10-40 mol% cholesterol[325, 352]. The remainder is made up primarily of sphingomyelin and ceramide. The most commonly used composition in the literature[325] is PC/PE/PS/cholesterol at 48:20:12:20 and therefore the most logical composition to study initially.

The dependence of fusion rates on membrane properties was studied in chapter 5. No information could be gained from the lipid mixing assays on the final, full fusion step. As mentioned in the discussion of that chapter, the use of content mixing assays (in addition to the lipid mixing assays) would provide useful information, improving the interpretation of the data. Also related to the studies of chapter 5, the effects of PE addition to PC are fairly well understood but the effect of cholesterol addition appears to depend on the type of phospholipid bilayer to which it is added. It has been found that cholesterol has a greater affect on raising the bending rigidity of bilayers composed of saturated phospholipids compared to bilayers of unsaturated lipids such as DOPC. The membrane properties of the compositions used in the studies of chapter 5 should therefore be explored quantitatively; perhaps using micropipette aspiration. This data would provide additional information on how fusion rates are affected by membrane properties. Benefits would also be gained by evaluating fusion rates of more complex mixtures.

Studies of fusion rates of vesicles containing SNARE protein have shown that the rates obtained depend on the vesicle composition and it is known that the conformation of some proteins is affected by the lipid environment. The transmembrane domains of the SNARE proteins appear to be instrumental for the function of these proteins in the fusion mechanism. It would be interesting to establish whether the structure of these domains is also composition dependent and what membrane properties this corresponds to.

For the *in vitro* assays performed in which t-SNARE proteins were inserted, it was suggested that the results were affected by the formation of large, interconnected protein aggregates. Conducting micropipette aspiration studies using just the transmembrane domain of Syntaxin would provide

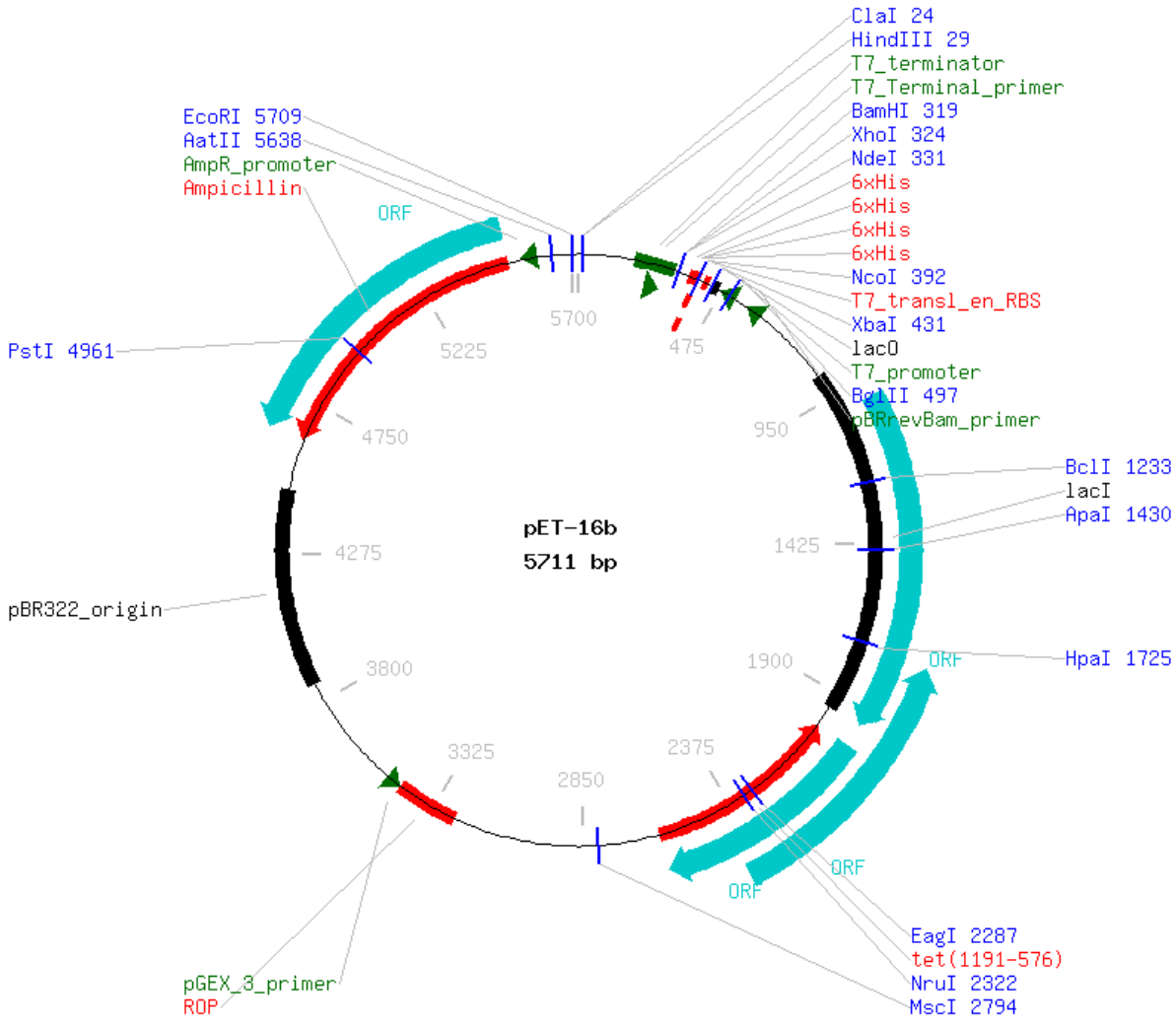
greater clarity to results from this study. In addition, expressing SNAP-25 in a mammalian cell line would allow purified protein to be produced containing the palmitoyl lipid anchors. Repeating the studies of chapters 3 and 4 with membrane-associated SNAP-25 would provide further insights.

The role of the SNARE proteins in the membrane fusion mechanism is fairly well established, but many questions remain as to how this is achieved. This project has investigated how these proteins may alter the local lipid environment to aid the fusion process. As illustrated above however, there is much scope for the project to be developed further. It is hoped that the work of this thesis highlights the importance of the interplay between proteins and lipids and that it (along with the raft of literature previously published) will encourage researchers not to consider either of these elements in isolation.

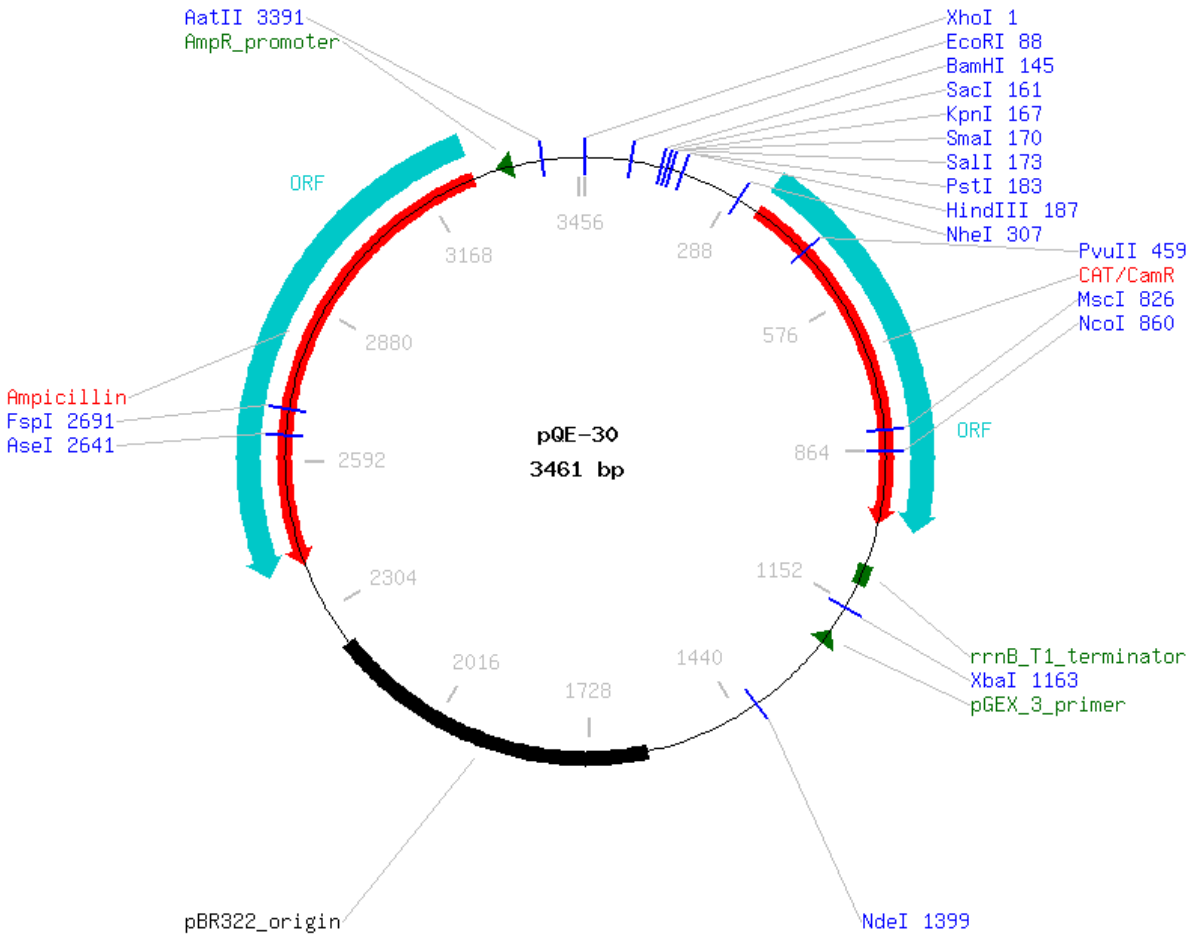
APPENDICES

Vector Maps

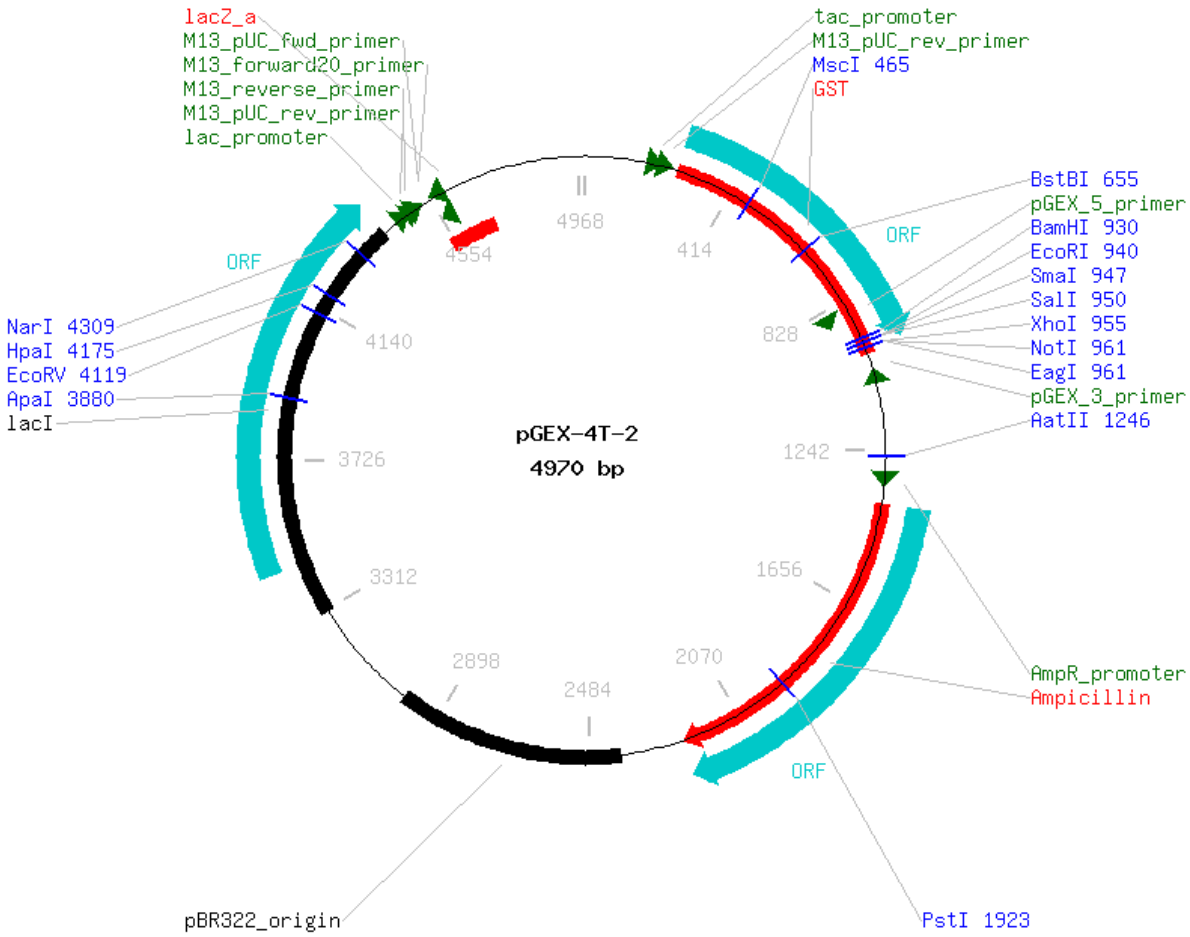
pET-16b



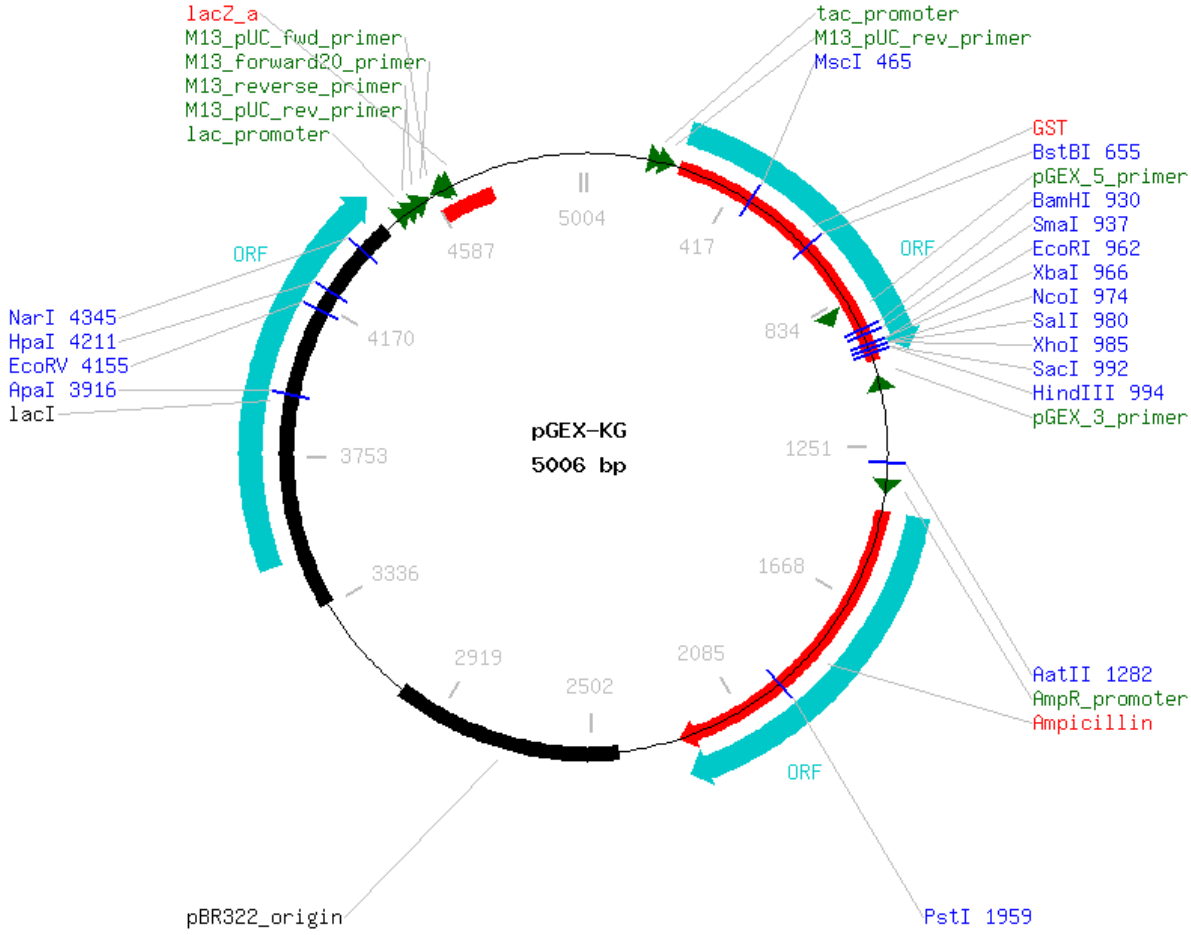
pQE-30


AatII 3391
AmpR_promoter
ORF
3456
288
576
864
1152
1440
1728
2016
2304
2592
2880
3168
XhoI 1
EcoRI 88
BamHI 145
SacI 161
KpnI 167
SmaI 170
SalI 173
PstI 183
HindIII 187
NheI 307
PvuII 459
CAT/CamR
MscI 826
NcoI 860
ORF
rrnB_T1_terminator
XbaI 1163
pGEX_3_primer
NdeI 1399
pBR322_origin
Ampicillin
FspI 2691
AseI 2641
pQE-30
3461 bp

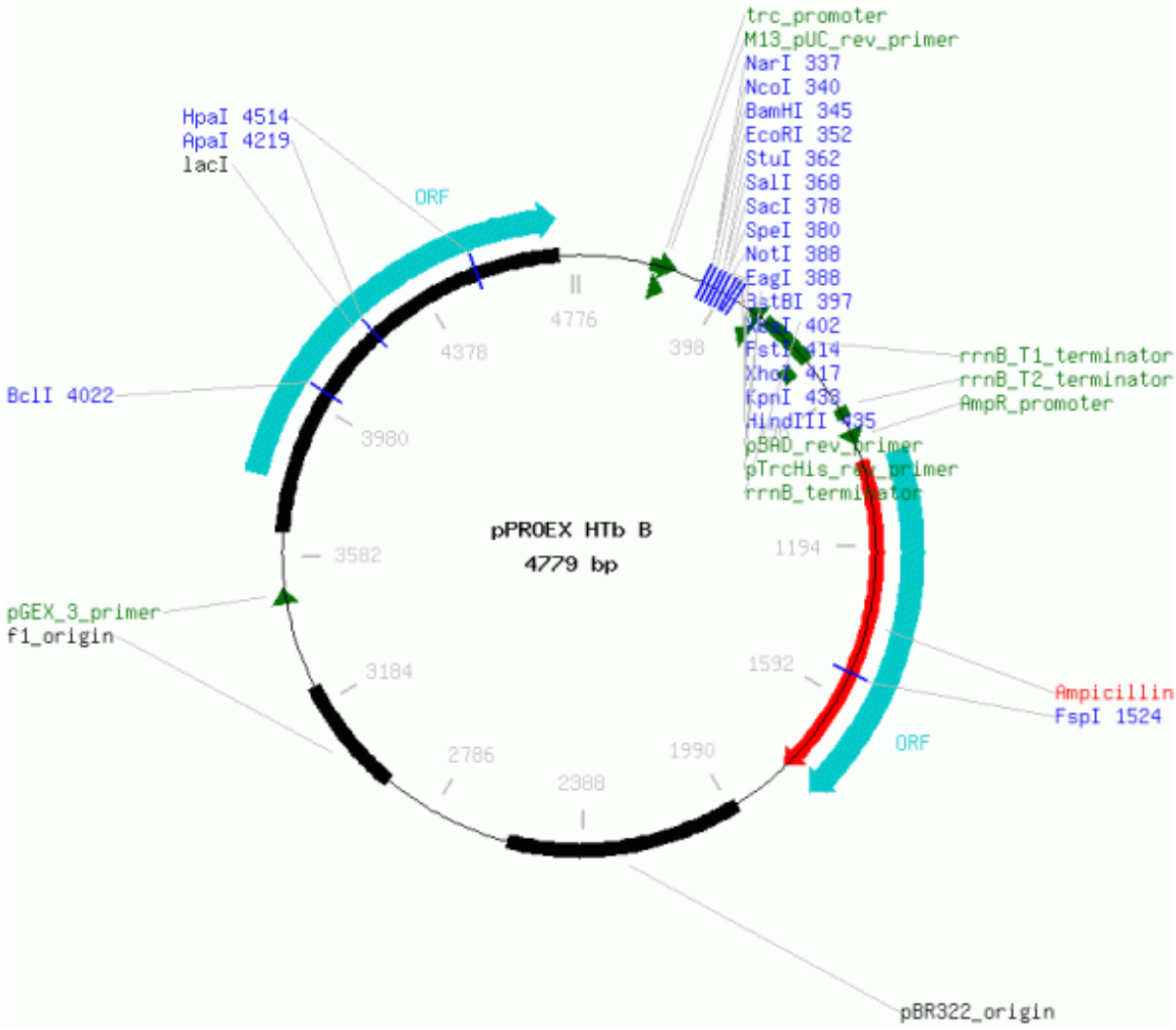
pGEX-4T-2


lacZ_a
M13_pUC_fwd_primer
M13_forward20_primer
M13_reverse_primer
M13_pUC_rev_primer
lac_promoter
tac_promoter
M13_pUC_rev_primer
MscI 465
GST
BstBI 655
pGEX_5_primer
BamHI 930
EcoRI 940
SmaI 947
SalI 950
XhoI 955
NotI 961
EagI 961
pGEX_3_primer
AatII 1246
ORF
ORF
NarI 4309
HpaI 4175
EcoRV 4119
ApaI 3880
lacI
pGEX-4T-2
4970 bp
4968
414
828
1242
1656
2070
2484
2898
3312
3726
4140
4554
AmpR_promoter
Ampicillin
ORF
pBR322_origin
PstI 1923

pGEX KG


lacZ_a
M13_pUC_fwd_primer
M13_forward20_primer
M13_reverse_primer
M13_pUC_rev_primer
lac_promoter
tac_promoter
M13_pUC_rev_primer
MscI 465
GST
BstBI 655
pGEX_5_primer
BamHI 930
SmaI 937
EcoRI 962
XbaI 966
NcoI 974
SalI 980
XhoI 985
SacI 992
HindIII 994
pGEX_3_primer
NarI 4345
HpaI 4211
EcoRV 4155
ApaI 3916
lacI
ORF
ORF
ORF
5004
417
834
1251
1668
2085
2502
2919
3336
3753
4170
4587
pGEX-KG
5006 bp
AatII 1282
AmpR_promoter
Ampicillin
pBR322_origin
PstI 1959

pPROEX-HTb


trc_promoter
M13_pUC_rev_primer
NarI 337
NcoI 340
BamHI 345
EcoRI 352
StuI 362
SalI 368
SacI 378
SpeI 380
NotI 388
EagI 388
BstBI 397
XbaI 402
FstI 414
XhoI 417
KpnI 438
HindIII 435
pBAD_rev_primer
pTrcHis_rev_primer
rrnB_terminator
rrnB_T1_terminator
rrnB_T2_terminator
AmpR_promoter
HpaI 4514
ApaI 4219
lacI
ORF
BclI 4022
pGEX_3_primer
f1_origin
pPROEX HTb B
4779 bp
Ampicillin
FspI 1524
ORF
pBR322_origin
4776
398
4378
3980
3582
1194
1592
3184
2786
1990
2388

Protein Sequences

SYNTAXIN 1A SEQUENCES

Full Length, Wild-Type Syntaxin 1A (Rattus norvegicus)

Amino Acid Sequence

```
  1  MKDRTQELRT  AKDSDDDDDV  TVTVDRDRFM  DEFFEQVEEI  RGFIDKIAEN  VEEVKRKHSA
 61  ILASPNPDEK  TKEELEELMS  DIKKTANKVR  SKLKSIEQSI  EQEEGLNRSS  ADLRIRKTQH
121  STLSRKFVEV  MSEYNATQSD  YRERCKGRIQ  RQLEITGRTT  TSEELEDMLE  SGNPAIFASG
181  IIMDSSISKQ  ALSEIETRHS  EIIKLENSIR  ELHDMFMDMA  MLVESQGEMI  DRIEYNVEHA
241  VDYVERAVSD  TKKAVKYQSK  ARRKKIMIII  CCVILGIIIA  STIGGIFG
```

DNA Sequence

```
   1  atgaaggacc  gaacccagga  gctccgcacg  gccaaggaca  gcgatgacga  cgatgatgtc
  61  actgtcactg  tggaccgaga  ccgcttcatg  gatgagttct  ttgaacaggt  ggaagagatc
 121  cggggcttta  ttgacaagat  tgctgaaaac  gtggaggagg  tgaagaggaa  acacagcgcc
 181  atcctggcct  ccccgaaccc  cgatgagaag  accaaggagg  aactggagga  gctcatgtcg
 241  gacattaaga  agacagcgaa  caaagttcgc  tccaagctaa  agagcatcga  gcagagcatc
 301  gagcaggagg  aaggtctgaa  ccgctcgtcg  gcggacctga  ggatccggaa  gacgcagcat
 361  tccacgctgt  cccgaaagtt  tgtggaggtc  atgtccgagt  acaacgccac  tcagtcagac
 421  taccgagaac  gctgcaaagg  gcgcatccag  aggcagctgg  agatcactgg  ccggaccacg
 481  accagtgagg  agttggaaga  catgctggag  agtgggaatc  ccgccatctt  tgcctctggg
 541  atcatcatgg  actccagcat  ctcgaagcag  gccctcagtg  agatcgagac  caggcacagt
 601  gagatcatca  agttggagaa  cagcatccgg  gagctacacg  atatgttcat  ggacatggcc
 661  atgctggtgg  agagccaggg  ggagatgatt  gacaggatcg  agtacaatgt  ggaacacgct
 721  gtggactacg  tggagagggc  cgtgtctgac  accaagaagg  ccgtcaagta  ccagagcaag
 781  gcacgcagga  agaagatcat  gatcatcatt  tgctgtgtga  ttctgggcat  catcatcgcc
 841  tccaccatcg  ggggcatctt  tggatag
```

ΔN-Syntaxin 1A

Amino Acid Sequence: 181-288 of full length Syntaxin 1A; *DNA Sequence:* 541-867 of full length Syntaxin 1A

ΔN-Syntaxin 1A Cysteine Mutant

Amino Acid Sequence (residues 1-108 correspond to residues 181-288 of the full length Syntaxin 1A sequence)

```
  1  IIMDSSISKQ  ALSEIETRHS  EIIKLENSIR  ELHDMFMDMA  MLVESQGEMI  DRIEYNVEHA
 61  VDYVERAVSD  TKKAVKYQSK  ARRKKIMIII  CCVILGIIIA  STIGGIFGCC
```

DNA Sequence

```
   1  atcatcatgg  actccagcat  ctcgaagcag  gccctcagtg  agatcgagac  caggcacagt
  61  gagatcatca  agttggagaa  cagcatccgg  gagctacacg  atatgttcat  ggacatggcc
 121  atgctggtgg  agagccaggg  ggagatgatt  gacaggatcg  agtacaatgt  ggaacacgct
 181  gtggactacg  tggagagggc  cgtgtctgac  accaagaagg  ccgtcaagta  ccagagcaag
 241  gcacgcagga  agaagatcat  gatcatcatt  tgctgtgtga  ttctgggcat  catcatcgcc
 301  tccaccatcg  ggggcatctt  tggatgctgt  tag
```

SNAP-25B SEQUENCE

Full Length, Wild-Type SNAP-25b (Rattus norvegicus)

```
  1  MAEDADMRNE  LEEMQRRADQ  LADESLESTR  RMLQLVEESK  DAGIRTLVML  DEQGEQLERI
 61  EEGMDQINKD  MKEAEKNLTD  LGKFCGLCVC  PCNKLKSSDA  YKKAWGNNQD  GVVASQPARV
121  VDEREQMAIS  GGFIRRVTND  ARENEMDENL  EQVSGIIGNL  RHMALDMGNE  IDTQNRQIDR
181  IMEKADSNKT  RIDEANQRAT  KMLGSG
```

VAMP2 SEQUENCES

Full Length, Wild-Type VAMP2 (Rattus norvegicus)

Amino Acid Sequence

```
  1  MSATAATVPP  AAPAGEGGPP  APPPNLTSNR  RLQQTQAQVD  EVVDIMRVNV  DKVLERDQKL
 61  SELDDRADAL  QAGASQFETS  AAKLKRKYWW  KNLKMMIILG  VICAIILIII  IVYFST
```

DNA Sequence

```
  1  atgtcggcta  ccgctgccac  cgtcccgcct  gccgccccgg  ccggcgaggg  tggcccccct
 61  gcacctcctc  caaatcttac  cagtaacagg  agactgcagc  agacccaggc  ccaggtggat
121  gaggtggtgg  acatcatgag  ggtgaatgtg  gacaaggtcc  tggagcggga  ccagaagcta
181  tcggaactgg  atgatcgcgc  agatgccctc  caggcagggg  cctcccagtt  tgaaacaagt
241  gcagccaagc  tcaagcgcaa  atactggtgg  aaaaacctca  agatgatgat  catcttggga
301  gtgatttgcg  ccatcatcct  catcatcatc  atcgtttact  tcagcactta  a
```

VAMP2 Cysteine Mutant

Amino Acid Sequence

```
  1  MSATAATVPP  AAPAGEGGPP  APPPNLTSNR  RLQQTQAQVD  EVVDIMRVNV  DKVLERDQKL
 61  SELDDRADAL  QAGASQFETS  AAKLKRKYWW  KNLKMMIILG  VICAIILIII  IVYFSTC
```

DNA Sequence

```
  1  atgtcggcta  ccgctgccac  cgtcccgcct  gccgccccgg  ccggcgaggg  tggcccccct
 61  gcacctcctc  caaatcttac  cagtaacagg  agactgcagc  agacccaggc  ccaggtggat
121  gaggtggtgg  acatcatgag  ggtgaatgtg  gacaaggtcc  tggagcggga  ccagaagcta
181  tcggaactgg  atgatcgcgc  agatgccctc  caggcagggg  cctcccagtt  tgaaacaagt
241  gcagccaagc  tcaagcgcaa  atactggtgg  aaaaacctca  agatgatgat  catcttggga
301  gtgatttgcg  ccatcatcct  catcatcatc  atcgtttact  tcagcacttg  ctaa
```

BIBLIOGRAPHY

1. J. S. Bonifacino and B. S. Glick, *Cell*, 2004, **116**, 153-166.
2. S. Martens and H. T. McMahon, *Nat. Rev. Mol. Cell Biol.*, 2008, **9**, 543-556.
3. S. L. Schmid, *Annu. Rev. Biochem.*, 1997, **66**, 511-548.
4. J. S. Bonifacino and J. Lippincott-Schwartz, *Nat. Rev. Mol. Cell Biol.*, 2003, **4**, 409-414.
5. S. R. Pfeffer, *Nat. Cell Biol.*, 1999, **1**, E17-22.
6. M. G. Waters and S. R. Pfeffer, *Curr. Opin. Cell Biol.*, 1999, **11**, 453-459.
7. M. G. Waters and F. M. Hughson, *Traffic*, 2000, **1**, 588-597.
8. S. Pfeffer, *Mol. Cell*, 2001, **8**, 729-730.
9. J. R. Whyte and S. Munro, *J. Cell Sci.*, 2002, **115**, 2627-2637.
10. H. Q. Cai, K. Reinisch and S. Ferro-Novick, *Developmental Cell*, 2007, **12**, 671-682.
11. D. Fasshauer, W. Antonin, M. Margittai, S. Pabst and R. Jahn, *J. Biol. Chem.*, 1999, **274**, 15440-15446.
12. T. Sollner, S. W. Whiteheart, M. Brunner, H. Erdjument-Bromage, S. Geromanos, P. Tempst and J. E. Rothman, *Nature*, 1993, **362**, 318-324.
13. A. Mayer, *Annu. Rev. Cell Dev. Biol.*, 2002, **18**, 289-314.
14. J. A. Szule and J. R. Coorssen, *Biochim. Biophys. Acta*, 2003, **1641**, 121-135.
15. T. H. Sollner, *Curr. Opin. Cell Biol.*, 2004, **16**, 429-435.
16. R. Jahn and R. H. Scheller, *Nat. Rev. Mol. Cell Biol.*, 2006, **7**, 631-643.
17. J. Rizo and C. Rosenmund, *Nat. Struct. Mol. Biol.*, 2008, **15**, 665-674.
18. Y. A. Chen and R. H. Scheller, *Nat. Rev. Mol. Cell Biol.*, 2001, **2**, 98-106.
19. B. Alberts, A. Johnson, J. Lewis, M. Raff, K. Roberts and P. Walter, *Molecular Biology of The Cell*, 4th edn., Garland Science Publishing, New York, 2002.
20. B. L. Sabatini and W. G. Regehr, *Annu. Rev. Physiol.*, 1999, **61**, 521-542.
21. S. O. Rizzoli and W. J. Betz, *Nat. Rev. Neurosci.*, 2005, **6**, 57-69.
22. G. A. Oyler, G. A. Higgins, R. A. Hart, E. Battenberg, M. Billingsley, F. E. Bloom and M. C. Wilson, *J. Cell Biol.*, 1989, **109**, 3039-3052.
23. W. S. Trimble, D. M. Cowan and R. H. Scheller, *Proc. Natl. Acad. Sci. U. S. A.*, 1988, **85**, 4538-4542.
24. M. Baumert, P. R. Maycox, F. Navone, P. Decamilli and R. Jahn, *EMBO J.*, 1989, **8**, 379-384.
25. M. K. Bennett, N. Calakos and R. H. Scheller, *Science*, 1992, **257**, 255-259.

26. W. Hong, *Biochim. Biophys. Acta*, 2005, **1744**, 120-144.

27. J. C. Hay, J. Klumperman, V. Oorschot, M. Steegmaier, C. S. Kuo and R. H. Scheller, *J. Cell Biol.*, 1998, **141**, 1489-1502.

28. J. A. McNew, F. Parlati, R. Fukuda, R. J. Johnston, K. Paz, F. Paumet, T. H. Sollner and J. E. Rothman, *Nature*, 2000, **407**, 153-159.

29. S. J. Scales, Y. A. Chen, B. Y. Yoo, S. M. Patel, Y. C. Doung and R. H. Scheller, *Neuron*, 2000, **26**, 457-464.

30. J. C. Hay and R. H. Scheller, *Curr. Opin. Cell Biol.*, 1997, **9**, 505-512.

31. T. Sollner, M. K. Bennett, S. W. Whiteheart, R. H. Scheller and J. E. Rothman, *Cell*, 1993, **75**, 409-418.

32. D. Fasshauer, R. B. Sutton, A. T. Brunger and R. Jahn, *Proc. Natl. Acad. Sci. U. S. A.*, 1998, **95**, 15781-15786.

33. T. Weimbs, K. Mostov, S. H. Low and K. Hofmann, *Trends Cell Biol.*, 1998, **8**, 260-262.

34. R. B. Sutton, D. Fasshauer, R. Jahn and A. T. Brunger, *Nature*, 1998, **395**, 347-353.

35. W. Antonin, D. Fasshauer, S. Becker, R. Jahn and T. R. Schneider, *Nat. Struct. Biol.*, 2002, **9**, 107-111.

36. M. A. Poirier, W. Xiao, J. C. Macosko, C. Chan, Y. K. Shin and M. K. Bennett, *Nat. Struct. Biol.*, 1998, **5**, 765-769.

37. J. J. Skehel and D. C. Wiley, *Cell*, 1998, **95**, 871-874.

38. T. Weber, B. V. Zemelman, J. A. McNew, B. Westermann, M. Gmachl, F. Parlati, T. H. Sollner and J. E. Rothman, *Cell*, 1998, **92**, 759-772.

39. P. I. Hanson, R. Roth, H. Morisaki, R. Jahn and J. E. Heuser, *Cell*, 1997, **90**, 523-535.

40. R. C. Lin and R. H. Scheller, *Neuron*, 1997, **19**, 1087-1094.

41. L. Katz and P. Brennwald, *Mol. Biol. Cell*, 2000, **11**, 3849-3858.

42. R. Ossig, H. D. Schmitt, B. de Groot, D. Riedel, S. Keranen, H. Ronne, H. Grubmuller and R. Jahn, *EMBO J.*, 2000, **19**, 6000-6010.

43. I. Fernandez, J. Ubach, I. Dulubova, X. Zhang, T. C. Sudhof and J. Rizo, *Cell*, 1998, **94**, 841-849.

44. J. C. Lerman, J. Robblee, R. Fairman and F. M. Hughson, *Biochem.*, 2000, **39**, 8470-8479.

45. M. Margittai, D. Fasshauer, R. Jahn and R. Langen, *Biochem.*, 2003, **42**, 4009-4014.

46. K. M. Misura, R. H. Scheller and W. I. Weis, *J. Biol. Chem.*, 2001, **276**, 13273-13282.

47. J. E. Richmond, R. M. Weimer and E. M. Jorgensen, *Nature*, 2001, **412**, 338-341.

48. D. Hess, T. Slater, M. Wilson and J. Skene, *J. Neurosci.*, 1992, **12**, 4634-4641.

49. M. Veit, T. H. Sollner and J. E. Rothman, *FEBS Lett.*, 1996, **385**, 119-123.

50. K. Vogel and P. A. Roche, *Biochem. Biophys. Res. Commun.*, 1999, **258**, 407-410.

51. P. G. Woodman, *Biochim. Biophys. Acta*, 1997, **1357**, 155-172.

52. M. Veit, A. Becher and G. Ahnert-Hilger, *Mol. Cell. Neurosci.*, 2000, **15**, 408-416.

53. T. Lang, N. D. Halemani and B. Rammner, *Prog. Lipid Res.*, 2008, **47**, 461-469.

54. A. P. May, K. M. Misura, S. W. Whiteheart and W. I. Weis, *Nat. Cell Biol.*, 1999, **1**, 175-182.

55. A. P. May, S. W. Whiteheart and W. I. Weis, *J. Biol. Chem.*, 2001, **276**, 21991-21994.

56. R. C. Yu, R. Jahn and A. T. Brunger, *Mol. Cell*, 1999, **4**, 97-107.

57. R. Duden, *Trends Cell Biol.*, 2001, **11**, 56.

58. A. Lupas, M. Van Dyke and J. Stock, *Science*, 1991, **252**, 1162-1164.

59. D. Fasshauer, W. K. Eliason, A. T. Brunger and R. Jahn, *Biochem.*, 1998, **37**, 10354-10362.

60. B. Yang, L. C. J. Gonzalez, R. Prekeris, M. Steegmaier, R. J. Advani and R. H. Scheller, *J. Biol. Chem.*, 1999, **274**, 5649-5653.

61. M. A. Poirier, et. al., *J. Biol. Chem.*, 1998, **273**, 11370-11377.

62. T. Hayashi et. al., *EMBO J.*, 1994, **13**, 5051-5061.

63. O. Rossetto, G. Schiavo, C. Montecucco, B. Poulain, F. Deloye, L. Lozzi and C. C. Shone, *Nature*, 1994, **372**, 415-416.

64. A. Stein, G. Weber, M. C. Wahl and R. Jahn, *Nature*, 2009, **460**, 525-528.

65. S. T. Hyde, *Handbook of Applied Surface and Colloid Chemistry*, John Wiley & Sons, Ltd., 2001.

66. W. Helfrich, *Z.Naturforsch.(C)*, 1973, **C 28**, 693-703.

67. D. Marsh, *Biochim. Biophys. Acta*, 1996, **1279**, 119-123.

68. R. S. Cantor, *J. Phys. Chem. B*, 1997, **101**, 1723-1725.

69. R. H. Templer, S. J. Castle, A. R. Curran, G. Rumbles and D. R. Klug, *Faraday Discuss.*, 1999, **111**, 41-53.

70. G. S. Attard, R. H. Templer, W. S. Smith, A. N. Hunt and S. Jackowski, *Proc. Natl. Acad. Sci. U. S. A.*, 2000, **97**, 9032-9036.

71. L. V. Chernomordik and M. M. Kozlov, *Annu. Rev. Biochem.*, 2003, **72**, 175-207.

72. W. Helfrich, in *Physics of Defects*, eds. R. Balian, M. Kleman and J. P. Poirier, North-Holland, Amsterdam, Editon edn., 1981, pp. 715-755.

73. R. H. Templer, B. J. Khoo and J. M. Seddon, *Langmuir*, 1998, **14**, 7427-7434.

74. C. Nielsen and O. S. Andersen, *Biophys. J.*, 2000, **79**, 2583-2604.

75. G. C. Shearman, O. Ces, R. H. Templer and J. M. Seddon, *J. Phys. Condens. Matter*, 2006, **18**, S1105-S1124.

76. R. P. Rand and V. A. Parsegian, *Biochim. Biophys. Acta*, 1989, **988**, 351-376.

77. Y. Kozlovsky, A. Efrat, D. A. Siegel and M. M. Kozlov, *Biophys. J.*, 2004, **87**, 2508-2521.

78. B. R. Lentz, *Eur. Biophys. J. Biophys.*, 2007, **36**, 315-326.

79. B. R. Lentz and J. Lee, *Mol. Membr. Biol.*, 1999, **16**, 279-296.

80. D. Fasshauer and M. Margittai, *J. Biol. Chem.*, 2004, **279**, 7613-7621.

81. A. T. Brunger, *Q. Rev. Biophys.*, 2005, **38**, 1-47.

82. A. V. Pobbati, A. Stein and D. Fasshauer, *Science*, 2006, **313**, 673-676.

83. K. M. Fiebig, L. M. Rice, E. Pollock and A. T. Brunger, *Nat. Struct. Biol.*, 1999, **6**, 117-123.

84. R. C. Lin and R. H. Scheller, *Annu. Rev. Cell Dev. Biol.*, 2000, **16**, 19-49.

85. F. Li, F. Pincet, E. Perez, W. S. Eng, T. J. Melia, J. E. Rothman and D. Tareste, *Nat. Struct. Mol. Biol.*, 2007, **14**, 890-896.

86. C. Montecucco, G. Schiavo and S. Pantano, *Trends Biochem. Sci.*, 2005, **30**, 367-372.

87. X. Lu, Y. Zhang and Y.-K. Shin, *Nat. Struct. Mol. Biol.*, 2008, **15**, 700-706.

88. Y. Hua and R. H. Scheller, *Proc. Natl. Acad. Sci. U. S. A.*, 2001, **98**, 8065-8070.

89. D. H. Kweon, C. S. Kim and Y. K. Shin, *J. Biol. Chem.*, 2003, **278**, 12367-12373.

90. J. A. McNew, T. Weber, D. M. Engelman, T. H. Sollner and J. E. Rothman, *Mol. Cell*, 1999, **4**, 415-421.

91. M. Bowen and A. T. Brunger, *Proc. Natl. Acad. Sci. U. S. A.*, 2006, **103**, 8378-8383.

92. D. H. Kweon, C. S. Kim and Y. K. Shin, *Biochem.*, 2002, **41**, 9264-9268.

93. A. D. Lam, P. Tryoen-Toth, B. Tsai, N. Vitale and E. L. Stuenkel, *Mol. Biol. Cell*, 2008, **19**, 485-497.

94. V. Knecht and H. Grubmuller, *Biophys. J.*, 2003, **84**, 1527-1547.

95. M. M. Kozlov and L. V. Chernomordik, *Biophys. J.*, 1998, **75**, 1384-1396.

96. S. G. Peisajovich and Y. Shai, *Trends Biochem. Sci.*, 2002, **27**, 183-190.

97. L. Chernomordik, A. Chanturiya, J. Green and J. Zimmerberg, *Biophys. J.*, 1995, **69**, 922-929.

98. M. Lindau and W. Almers, *Curr. Opin. Cell Biol.*, 1995, **7**, 509-517.

99. C. Peters, M. J. Bayer, S. Buhler, J. S. Andersen, M. Mann and A. Mayer, *Nature*, 2001, **409**, 581-588.

100. R. M. Markosyan, F. S. Cohen and G. B. Melikyan, *Mol. Biol. Cell*, 2005, **16**, 5502-5513.

101. G. B. Melikyan, R. J. Barnard, L. G. Abrahamyan, W. Mothes and J. A. Young, *Proc. Natl. Acad. Sci. U. S. A.*, 2005, **102**, 8728-8733.

102. T. Liu, T. Wang, E. R. Chapman and J. C. Weisshaar, *Biophys. J.*, 2008, **94**, 1303-1314.

103. T. Y. Yoon, B. Okumus, F. Zhang, Y. K. Shin and T. Ha, *Proc. Natl. Acad. Sci. U. S. A.*, 2006, **103**, 19731-19736.

104. J. Zimmerberg, *Trends Cell Biol.*, 2001, **11**, 233-235.

105. L. V. Chernomordik, J. Zimmerberg and M. M. Kozlov, *J. Cell Biol.*, 2006, **175**, 201-207.

106. J. Lee and B. R. Lentz, *Proc. Natl. Acad. Sci. U. S. A.*, 1998, **95**, 9274-9279.

107. P. I. Kuzmin, J. Zimmerberg, Y. A. Chizmadzhev and F. S. Cohen, *Proc. Natl. Acad. Sci. U. S. A.*, 2001, **98**, 7235-7240.

108. Y. Kozlovsky and M. M. Kozlov, *Biophys. J.*, 2002, **82**, 882-895.

109. L. Chernomordik, M. M. Kozlov and J. Zimmerberg, *J. Membr. Biol.*, 1995, **146**, 1-14.

110. D. P. Siegel, *Biophys. J.*, 1993, **65**, 2124-2140.

111. D. P. Siegel, *Biophys. J.*, 1999, **76**, 291-313.

112. A. Efrat, L. V. Chernomordik and M. M. Kozlov, *Biophys. J.*, 2007, **92**, L61-L63.

113. L. V. Chernomordik, G. B. Melikyan and Y. A. Chizmadzhev, *Biochim. Biophys. Acta*, 1987, **906**, 309-352.

114. J. Rizo and H. Dai, *Nat. Struct. Mol. Biol.*, 2007, **14**, 880-882.

115. L. V. Chernomordik and M. M. Kozlov, *Cell*, 2005, **123**, 375-382.

116. L. V. Chernomordik, S. S. Vogel, A. Sokoloff, H. O. Onaran, E. A. Leikina and J. Zimmerberg, *FEBS Lett.*, 1993, **318**, 71-76.

117. G. B. Melikyan, R. M. Markosyan, H. Hemmati, M. K. Delmedico, D. M. Lambert and F. S. Cohen, *J. Cell Biol.*, 2000, **151**, 413-423.

118. P. L. Yeagle, F. T. Smith, J. E. Young and T. D. Flanagan, *Biochem.*, 1994, **33**, 1820-1827.

119. Y. Gaudin, *J. Cell Biol.*, 2000, **150**, 601-612.

120. C. J. Russell, T. S. Jardetzky and R. A. Lamb, *EMBO J.*, 2001, **20**, 4024-4034.

121. L. Chernomordik, *Chem. Phys. Lipids*, 1996, **81**, 203-213.

122. X. Han, C.-T. Wang, J. Bai, E. R. Chapman and M. B. Jackson, *Science*, 2004, **304**, 289-292.

123. S. J. Cho, M. Kelly, K. T. Rognlien, J. A. Cho, J. K. Horber and B. P. Jena, *Biophys. J.*, 2002, **83**, 2522-2527.

124. G. B. Melikyan, S. Lin, M. G. Roth and F. S. Cohen, *Mol. Biol. Cell*, 1999, **10**, 1821-1836.

125. G. B. Melikyan, S. A. Brener, D. C. Ok and F. S. Cohen, *J. Cell Biol.*, 1997, **136**, 995-1005.

126. L. V. Chernomordik, V. A. Frolov, E. Leikina, P. Bronk and J. Zimmerberg, *J. Cell Biol.*, 1998, **140**, 1369-1382.

127. V. I. Razinkov, G. B. Melikyan, R. M. Epand, R. F. Epand and F. S. Cohen, *J. Gen. Physiol.*, 1998, **112**, 409-422.

128. E. Grote, C. M. Carr and P. J. Novick, *J. Cell Biol.*, 2000, **151**, 439-452.

129. O. Sandre, L. Moreaux and F. Brochard-Wyart, *Proc. Natl. Acad. Sci. U. S. A.*, 1999, **96**, 10591-10596.

130. Y. Kozlovsky, L. V. Chernomordik and M. M. Kozlov, *Biophys. J.*, 2002, **83**, 2634-2651.

131. L. Gao, R. Lipowsky and J. Shillcock, *Soft Matter*, 2008, **4**, 1208-1214.

132. C. K. Haluska, K. A. Riske, V. Marchi-Artzner, J.-M. Lehn, R. Lipowsky and R. Dimova, *Proc. Natl. Acad. Sci. U. S. A.*, 2006, **103**, 15841-15846.

133. D. Langosch, M. Hofmann and C. Ungermann, *Cell. Mol. Life Sci.*, 2007, **64**, 850-864.

134. D. Langosch, J. M. Crane, B. Brosig, A. Hellwig, L. K. Tamm and J. Reed, *J. Mol. Biol.*, 2001, **311**, 709-721.

135. T. C. Sudhof, *Annu. Rev. Neurosci.*, 2004, **27**, 509-547.

136. J. Malsam, S. Kreye and T. Sollner, *Cell. Mol. Life Sci.*, 2008, **65**, 2814-2832.

137. R. Jahn and T. C. Sudhof, *Annu. Rev. Biochem.*, 1999, **68**, 863-911.

138. T. Ohya, M. Miaczynska, U. Coskun, B. Lommer, A. Runge, D. Drechsel, Y. Kalaidzidis and M. Zerial, *Nature*, 2009, **459**, 1091-1097.

139. F. Valtorta, M. Pennuto, D. Bonanomi and F. Benfenati, *Bioessays*, 2004, **26**, 445-453.

140. M. V. Khvotchev and T. C. Sudhof, *Biochem.*, 2004, **43**, 15037-15043.

141. L. Edelmann, *EMBO J.*, 1995, **14**, 224-231.

142. P. Washbourne, G. Schiavo and C. Montecucco, *Biochem. J.*, 1995, **305**, 721-724.

143. M. Pennuto, D. Bonanomi, F. Benfenati and F. Valtorta, *Mol. Biol. Cell*, 2003, **14**, 4909-4919.

144. D. Mitter, C. Reisinger, B. Hinz, S. Hollmann, S. V. Yelamanchili, S. Treiber-Held, T. G. Ohm, A. Herrmann and G. Ahnert-Hilger, *J. Neurochem.*, 2003, **84**, 35-42.

145. H. T. McMahon, V. Y. Bolshakov, R. Janz, R. E. Hammer, S. A. Siegelbaum and T. C. Sudhof, *Proc. Natl. Acad. Sci. U. S. A.*, 1996, **93**, 4760-4764.

146. R. Janz, T. C. Sudhof, R. E. Hammer, V. Unni, S. A. Siegelbaum and V. Y. Bolshakov, *Neuron*, 1999, **24**, 687-700.

147. L. Thomas, K. Hartung, D. Langosch, H. Rehm, E. Bamberg, W. Franke and H. Betz, *Science*, 1988, **242**, 1050-1053.

148. E. P. Garcia, E. Gatti, M. Butler, J. Burton and P. De Camilli, *Proc. Natl. Acad. Sci. U. S. A.*, 1994, **91**, 2003-2007.

149. Y. Hata, C. A. Slaughter and T. C. Sudhof, *Nature*, 1993, **366**, 347-351.

150. D. Schutz, F. Zilly, T. Lang, R. Jahn and D. Bruns, *Eur. J. Neurosci.*, 2005, **21**, 2419-2432.

151. M. Verhage, A. S. Maia, J. J. Plomp, A. B. Brussaard, J. H. Heeroma, H. Vermeer, R. F. Toonen, R. E. Hammer, T. K. van den Berg, M. Missler, H. J. Geuze and T. C. Sudhof, *Science*, 2000, **287**, 864-869.

152. W. Guo, D. Roth, C. Walch-Solimena and P. Novick, *EMBO J.*, 1999, **18**, 1071-1080.

153. B. L. Scott, J. S. Van Komen, H. Irshad, S. Liu, K. A. Wilson and J. A. McNew, *J. Cell Biol.*, 2004, **167**, 75-85.

154. J. Shen, D. C. Tareste, F. Paumet, J. E. Rothman and T. J. Melia, *Cell*, 2007, **128**, 183-195.

155. F. Varoqueaux, A. Sigler, J. S. Rhee, N. Brose, C. Enk, K. Reim and C. Rosenmund, *Proc. Natl. Acad. Sci. U. S. A.*, 2002, **99**, 9037-9042.

156. J. S. Rhee, A. Betz, S. Pyott, K. Reim, F. Varoqueaux, I. Augustin, D. Hesse, T. C. Sudhof, M. Takahashi, C. Rosenmund and N. Brose, *Cell*, 2002, **108**, 121-133.

157. A. Betz, M. Okamoto, F. Benseler and N. Brose, *J. Biol. Chem.*, 1997, **272**, 2520-2526.

158. R. Guan, H. Dai and J. Rizo, *Biochem.*, 2008, **47**, 1474-1481.

159. I. Dulubova, S. Sugita, S. Hill, M. Hosaka, I. Fernandez, T. C. Sudhof and J. Rizo, *EMBO J.*, 1999, **18**, 4372-4382.

160. I. Dulubova, X. Lou, J. Lu, I. Huryeva, A. Alam, R. Schneggenburger, T. C. Sudhof and J. Rizo, *EMBO J.*, 2005, **24**, 2839-2850.

161. Y. Fujita, H. Shirataki, T. Sakisaka, T. Asakura, T. Ohya, H. Kotani, S. Yokoyama, H. Nishioka, Y. Matsuura, A. Mizoguchi, R. H. Scheller and Y. Takai, *Neuron*, 1998, **20**, 905-915.

162. E. S. Masuda, B. C. Huang, J. M. Fisher, Y. Luo and R. H. Scheller, *Neuron*, 1998, **21**, 479-480.

163. T. Baba, T. Sakisaka, S. Mochida and Y. Takai, *J. Cell Biol.*, 2005, **170**, 1113-1125.

164. T. Sakisaka, T. Baba, S. Tanaka, G. Izumi, M. Yasumi and Y. Takai, *J. Cell Biol.*, 2004, **166**, 17-25.

165. S. J. Scales, B. A. Hesser, E. S. Masuda and R. H. Scheller, *J. Biol. Chem.*, 2002, **277**, 28271-28279.

166. B. S. Glick and J. E. Rothman, *Nature*, 1987, **326**, 309-312.

167. V. Malhotra, I. Orci, B. S. Glick, M. R. Block and J. E. Rothman, *Cell*, 1988, **54**, 221-227.

168. M. R. Block, B. S. Glick, C. A. Wilcox, F. T. Wieland and J. E. Rothman, *Proc. Natl. Acad. Sci. U. S. A.*, 1988, **85**, 7852-7856.

169. P. J. Weidman, P. Melancon, M. R. Block and J. E. Rothman, *J. Cell Biol.*, 1989, **108**, 1589-1596.

170. D. O. Clary, I. Griff and J. E. Rothman, *Cell*, 1990, **61**, 709-721.

171. S. W. Whiteheart, M. Brunner, D. W. Wilson, M. Weidman and J. E. Rothman, *J. Biol. Chem.*, 1992, **267**, 12239-12243.

172. C. Wimmer, T. M. Hohl, C. A. Hughes, S. A. Muller, T. H. Sollner, A. Engel and J. E. Rothman, *J. Biol. Chem.*, 2001, **276**, 29091-29097.

173. A. Mayer, W. Wickner and A. Haas, *Cell*, 1996, **85**, 83-94.

174. S. J. Scales, B. Y. Yoo and R. H. Scheller, *Proc. Natl. Acad. Sci. U. S. A.*, 2001, **98**, 14262-14267.

175. P. L. Hanson, O. H, J. Barton and R. Jahn, *J. Biol. Chem.*, 1995, **270**, 16955-16961.

176. E. A. Matveeva, S. W. Whiteheart, T. C. Vanaman and J. T. Slevin, *J. Biol. Chem.*, 2001, **276**, 12174-12181.

177. K. Matsushita, C. N. Morrell, B. Cambien, S. X. Yang, M. Yamakuchi, C. Bao, M. R. Hara, R. A. Quick, W. Cao, B. O'Rourke, J. M. Lowenstein, J. Pevsner, D. D. Wagner and C. J. Lowenstein, *Cell*, 2003, **115**, 139-150.

178. C. Zhao, J. T. Slevin and S. W. Whiteheart, *FEBS Lett.*, 2007, **581**, 2140-2149.

179. A. W. Sudlow, B. W. McFerran, H. Bodill, R. J. Barnard, A. Morgan and R. D. Burgoyne, *FEBS Lett.*, 1996, **393**, 185-188.

180. J. Xu, Y. Xu, G. C. Ellis-Davies, G. J. Augustine and F. W. Tse, *J. Neurosci.*, 2002, **22**, 53-61.

181. K. Tani, M. Shibata, K. Kawase, H. Kawashima, K. Hatsuzawa, M. Nagahama and M. Tagaya, *J. Biol. Chem.*, 2003, **278**, 13531-13538.

182. K. Reim, M. Mansour, F. Varoqueaux, H. T. McMahon, T. C. Sudhof, N. Brose and C. Rosenmund, *Cell*, 2001, **104**, 71-81.

183. S. Huntwork and J. T. Littleton, *Nat. Neurosci.*, 2007, **10**, 1235-1237.

184. X. Chen, D. R. Tomchick, E. Kovrigin, D. Arac, M. Machius, T. C. Sudhof and J. Rizo, *Neuron*, 2002, **33**, 397-409.

185. A. V. Pobbati, A. Razeto, M. Boddener, S. Becker and D. Fasshauer, *J. Biol. Chem.*, 2004, **279**, 47192-47200.

186. C. G. Giraudo, W. S. Eng, T. J. Melia and J. E. Rothman, *Science*, 2006, **313**, 676-680.

187. K. Hu, J. Carroll, C. Rickman and B. Davletov, *J. Biol. Chem.*, 2002, **277**, 41652-41656.

188. W. D. Matthew, L. Tsavaler and L. F. Reichardt, *J. Cell Biol.*, 1981, **91**, 257-269.

189. S. Takamori, M. Holt, K. Stenius, E. A. Lemke, M. Gronborg, D. Riedel, H. Urlaub, S. Schenck, B. Brugger, P. Ringler, S. A. Muller, B. Rammner, F. Grater, J. S. Hub, B. L. De Groot, G. Mieskes, Y. Moriyama, J. Klingauf, H. Grubmuller, J. Heuser, F. Wieland and R. Jahn, *Cell*, 2006, **127**, 831-846.

190. M. Perin, *Nature*, 1990, **345**, 260-263.

191. M. Craxton, *BMC Genomics*, 2004, **5**, 43.

192. N. Charvin, C. L'Eveque, D. Walker, F. Berton, C. Raymond, M. Kataoka, Y. Shoji-Kasai, M. Takahashi, M. De Waard and M. J. Seagar, *EMBO J.*, 1997, **16**, 4591-4596.

193. D. K. Kim and W. A. Catterall, *Proc. Natl. Acad. Sci. U. S. A.*, 1997, **94**, 14782-14786.

194. R. Llinas, M. Sugimori and R. B. Silver, *Science*, 1992, **256**, 677-679.

195. M. Geppert, B. Ullrich, D. G. Green, K. Takei, L. Daniels, P. De Camilli, T. C. Sudhof and R. E. Hammer, *EMBO J.*, 1994, **13**, 3720-3727.

196. E. R. Chapman, P. I. Hanson, S. An and R. Jahn, *J. Biol. Chem.*, 1995, **270**, 23667-23671.

197. Y. Kee and R. H. Scheller, *J. Neurosci.*, 1996, **16**, 1975-1981.

198. G. Schiavo, G. Stenbeck, J. E. Rothman and T. H. Sollner, *Proc. Natl. Acad. Sci. U. S. A.*, 1997, **94**, 997-1001.

199. J. A. Ernst and A. T. Brunger, *J. Biol. Chem.*, 2003, **278**, 8630-8636.

200. C. Rickman and B. Davletov, *J. Biol. Chem.*, 2003, **278**, 5501-5504.

201. E. Ales, L. Tabares, J. M. Poyato, V. Valero, M. Lindau and G. Alvarez de Toledo, *Nat. Cell Biol.*, 1999, **1**, 40-44.

202. C. T. Wang, J. Bai, P. Y. Chang, E. R. Chapman and M. B. Jackson, *J. Physiol.*, 2006, **570**, 295-307.

203. C. T. Wang, R. Grishanin, C. A. Earles, P. Y. Chang, T. F. Martin, E. R. Chapman and M. B. Jackson, *Science*, 2001, **294**, 1111-1115.

204. C. T. Wang, J. C. Lu, J. Bai, P. Y. Chang, T. F. Martin, E. R. Chapman and M. B. Jackson, *Nature*, 2003, **424**, 943-947.

205. N. Brose, A. G. Petrenko, T. C. Sudhof and R. Jahn, *Science*, 1992, **256**, 1021-1025.

206. B. A. Davletov and T. C. Sudhof, *J. Biol. Chem.*, 1993, **268**, 26386-26390.

207. E. R. Chapman and R. Jahn, *J. Biol. Chem.*, 1994, **269**, 5735-5741.

208. I. Fernandez, D. Arac, J. Ubach, S. H. Gerber, O. Shin, Y. Gao, R. G. Anderson, T. C. Sudhof and J. Rizo, *Neuron*, 2001, **32**, 1057-1069.

209. J. Bai, W. C. Tucker and E. R. Chapman, *Nat Struct Mol Biol*, 2004, **11**, 36-44.

210. K. Aoyagi, T. Sugaya, M. Umeda, S. Yamamoto, S. Terakawa and M. Takahashi, *J. Biol. Chem.*, 2005, **280**, 17346-17352.

211. S. Martens, M. M. Kozlov and H. T. McMahon, *Science*, 2007, **316**, 1205-1208.

212. D. Arac, T. Murphy and J. Rizo, *Biochem.*, 2003, **42**, 2774-2780.

213. W. Nickel, T. Weber, J. A. McNew, F. Parlati, T. H. Sollner and J. E. Rothman, *Proc. Natl. Acad. Sci. U. S. A.*, 1999, **96**, 12571-12576.

214. R. M. Weimer and E. M. Jorgensen, *J. Cell Sci.*, 2003, **116**, 3661-3666.

215. T. C. Sudhof, *Proc. Natl. Acad. Sci. U. S. A.*, 2007, **104**, 13541-13542.

216. X. B. Lu, F. Zhang, J. A. McNew and Y. K. Shin, *J. Biol. Chem.*, 2005, **280**, 30538-30541.

217. M. J. Janiak, D. M. Small and G. G. Shipley, *J. Biol. Chem.*, 1979, **254**, 6068-6078.

218. T. T. Liu, W. C. Tucker, A. Bhalla, E. R. Chapman and J. C. Weisshaar, *Biophys. J.*, 2005, **89**, 2458-2472.

219. M. E. Bowen, K. Weninger, A. T. Brunger and S. Chu, *Biophys. J.*, 2004, **87**, 3569-3584.

220. K. L. Nicholson, M. Munson, R. B. Miller, T. J. Filip, R. Fairman and F. M. Hughson, *Nat. Struct. Biol.*, 1998, **5**, 793-802.

221. Y. Jun and W. Wickner, *Proc. Natl. Acad. Sci. U. S. A.*, 2007, **104**, 13010-13015.

222. S. M. Dennison, M. E. Bowen, A. T. Brunger and B. R. Lentz, *Biophys. J.*, 2006, **90**, 1661-1675.

223. Y. B. Xu, F. Zhang, Z. L. Su, J. A. McNew and Y. K. Shin, *Nat. Struct. Mol. Biol.*, 2005, **12**, 417-422.

224. C. Reese, F. Heise and A. Mayer, *Nature*, 2005, **436**, 410-414.

225. C. G. Giraudo, C. Hu, D. Q. You, A. M. Slovic, E. V. Mosharov, D. Sulzer, T. J. Melia and J. E. Rothman, *J. Cell Biol.*, 2005, **170**, 249-260.

226. M. E. Graham, P. Washbourne, M. C. Wilson and R. D. Burgoyne, *Ann. N. Y. Acad. Sci.*, 2002, **971**, 210-221.

227. P. Washbourne, P. M. Thompson, M. Carta, E. T. Costa, J. R. Mathews, G. Lopez-Bendito, Z. Molnar, M. W. Becher, C. F. Valenzuela, L. D. Partridge and M. C. Wilson, *Nat. Neurosci.*, 2002, **5**, 19-26.

228. T. Sakaba, A. Stein, R. Jahn and E. Neher, *Science*, 2005, **309**, 491-494.

229. G. Schiavo, M. Matteoli and C. Montecucco, *Physiol. Rev.*, 2000, **80**, 717-766.

230. J. Rizo, X. C. Chen and D. Arac, *Trends Cell Biol.*, 2006, **16**, 339-350.

231. S. Schoch, F. Deak, A. Konigstorfer, M. Mozhayeva, Y. Sara, T. C. Sudhof and E. T. Kavalali, *Science*, 2001, **294**, 1117-1122.

232. F. Deak, S. Schoch, X. Liu, T. C. Sudhof and E. T. Kavalali, *Nat. Cell Biol.*, 2004, **6**, 1102-1108.

233. S. Springer and R. Schekman, *Science*, 1998, **281**, 698-700.

234. M. L. Nonet, A. M. Holgado, F. Brewer, C. J. Serpe, B. A. Norbeck, J. Holleran, L. Wei, E. Hartwieg, E. M. Jorgensen and A. Alfonso, *Mol. Biol. Cell*, 1999, **10**, 2343-2360.

235. B. Zhang, Y. H. Koh, R. B. Beckstead, V. Budnik, B. Ganetzky and H. J. Bellen, *Neuron*, 1998, **21**, 1465-1475.

236. W. C. Tucker, T. Weber and E. R. Chapman, *Science*, 2004, **304**, 435-438.

237. L. K. Mahal, S. M. Sequeira, J. M. Gureasko and T. H. Sollner, *J. Cell Biol.*, 2002, **158**, 273-282.

238. L. V. Chernomordik and K. Melikov, *Biophys. J.*, 2006, **90**, 2657-2658.

239. J. Zimmerberg and M. M. Kozlov, *Nat. Rev. Mol. Cell Biol.*, 2006, **7**, 9-19.

240. K. Farsad, N. Ringstad, K. Takei, S. R. Floyd, K. Rose and P. De Camilli, *J. Cell Biol.*, 2001, **155**, 193-200.

241. B. J. Peter, H. M. Kent, I. G. Mills, Y. Vallis, P. J. Butler, P. R. Evans and H. T. McMahon, *Science*, 2004, **303**, 495-499.

242. J. Zimmerberg and S. McLaughlin, *Curr. Biol.*, 2004, **14**, R250-252.

243. K. Farsad and P. De Camilli, *Curr. Opin. Cell Biol.*, 2003, **15**, 372-381.

244. M. G. Ford, I. G. Mills, B. J. Peter, Y. Vallis, G. J. Praefcke, P. R. Evans and H. T. McMahon, *Nature*, 2002, **419**, 361-366.

245. R. V. Stahelin, F. Long, B. J. Peter, D. Murray, P. De Camilli, H. T. McMahon and W. Cho, *J. Biol. Chem.*, 2003, **278**, 28993-28999.

246. M. C. Lee, L. Orci, S. Hamamoto, E. Futai, M. Ravazzola and R. Schekman, *Cell*, 2005, **122**, 605-617.

247. T. Lang, *J. Physiol.-London*, 2007, **585**, 693-698.

248. E. Teissier and E. I. Pecheur, *Eur. Biophys. J. Biophys.*, 2007, **36**, 887-899.

249. K. Bacia, P. Schwille and T. Kurzchalia, *Proc. Natl. Acad. Sci. U. S. A.*, 2005, **102**, 3272-3277.

250. T. Lang, D. Bruns, D. Wenzel, D. Riedel, P. Holroyd, C. Thiele and R. Jahn, *EMBO J.*, 2001, **20**, 2202-2213.

251. J. J. Sieber, K. I. Willig, R. Heintzmann, S. W. Hell and T. Lang, *Biophys. J.*, 2006, **90**, 2843-2851.

252. M. Ohara-Imaizumi, C. Nishiwaki, T. Kikuta, K. Kumakura, Y. Nakamichi and S. Nagamatsu, *J. Biol. Chem.*, 2004, **279**, 8403-8408.

253. J. J. Sieber, K. I. Willig, C. Kutzner, C. Gerding-Reimers, B. Harke, G. Donnert, B. Rammner, C. Eggeling, S. W. Hell, H. Grubmuller and T. Lang, *Science*, 2007, **317**, 1072-1076.

254. C. Gil, A. Soler-Jover, J. Blasi and J. Aguilera, *Biochem. Biophys. Res. Commun.*, 2005, **329**, 117-124.

255. L. H. Chamberlain, R. D. Burgoyne and G. W. Gould, *Proc. Natl. Acad. Sci. U. S. A.*, 2001, **98**, 5619-5624.

256. K. Bacia, C. G. Schuette, N. Kahya, R. Jahn and P. Schwille, *J. Biol. Chem.*, 2004, **279**, 37951-37955.

257. D. E. Saslowsky, J. C. Lawrence, R. M. Henderson and J. M. Edwardson, *J. Membr. Biol.*, 2003, **194**, 153-164.

258. J. Valdez-Taubas and H. Pelham, *EMBO J.*, 2005, **24**, 2524-2532.

259. I. C. Bark, K. M. Hahn, A. E. Ryabinin and M. C. Wilson, *Proc. Natl. Acad. Sci. U. S. A.*, 1995, **92**, 1510-1514.

260. G. Nagy, I. Milosevic, D. Fasshauer, E. M. Muller, B. L. de Groot, T. Lang, M. C. Wilson and J. B. Sorensen, *Mol. Biol. Cell*, 2005, **16**, 5675-5685.

261. C. Bark, F. P. Bellinger, A. Kaushal, J. R. Mathews, L. D. Partridge and M. C. Wilson, *J. Neurosci.*, 2004, **24**, 8796-8805.

262. G. A. Oyler, J. W. Polli, M. C. Wilson and M. L. Billingsley, *Proc. Natl. Acad. Sci. U. S. A.*, 1991, **88**, 5247-5251.

263. J. B. Sorensen, G. Nagy, F. Varoqueaux, R. B. Nehring, N. Brose, M. C. Wilson and E. Neher, *Cell*, 2003, **114**, 75-86.

264. D. K. Koticha, E. E. McCarthy and G. Baldini, *J. Cell Sci.*, 2002, **115**, 3341-3351.

265. B. Davletov, E. Connell and F. Darios, *Cell. Mol. Life Sci.*, 2007, **64**, 1597-1608.

266. D. Arac, X. Chen, H. A. Khant, J. Ubach, S. J. Ludtke, M. Kikkawa, A. E. Johnson, W. Chiu, T. C. Sudhof and J. Rizo, *Nat Struct Mol Biol*, 2006, **13**, 209-217.

267. G. Schiavo, Q. M. Gu, G. D. Prestwich, T. H. Sollner and J. E. Rothman, *Proc. Natl. Acad. Sci. U. S. A.*, 1996, **93**, 13327-13332.

268. I. Milosevic, J. B. Sorensen, T. Lang, M. Krauss, G. Nagy, V. Haucke, R. Jahn and E. Neher, *J. Neurosci.*, 2005, **25**, 2557-2565.

269. D. J. James, C. Khodthong, J. A. Kowalchyk and T. F. J. Martin, *J. Cell Biol.*, 2008, jcb.200801056.

270. T. F. Martin, *Curr. Opin. Cell Biol.*, 2001, **13**, 493-499.

271. M. R. Wenk and P. De Camilli, *Proc. Natl. Acad. Sci. U. S. A.*, 2004, **101**, 8262-8269.

272. S. L. Osborne, P. J. Wen and F. A. Meunier, *J. Neurochem.*, 2006, **98**, 336-342.

273. X. Mulet, R. H. Templer, R. Woscholski and O. Ces, *Langmuir*, 2008, **24**, 8443-8447.

274. C. Ho, S. J. Slater, B. Stagliano and C. D. Stubbs, *Biochem.*, 2001, **40**, 10334-10341.

275. F. D. Huang, E. Woodruff, R. Mohrmann and K. Broadie, *J. Neurosci.*, 2006, **26**, 2369-2379.

276. N. Vijayakrishnan and K. Broadie, *Biochem. Soc. Trans.*, 2006, **34**, 81-87.

277. A. R. Brash, *J. Clin. Invest.*, 2001, **107**, 1339-1345.

278. B. A. Davletov, F. A. Meunier, A. C. Ashton, H. Matsushita, W. D. Hirst, V. G. Lelianova, G. P. Wilkin, J. O. Dolly and Y. A. Ushkaryov, *EMBO J.*, 1998, **17**, 3909-3920.

279. L. Sheu, E. A. Pasyk, J. Ji, X. Huang, X. Gao, F. Varoqueaux, N. Brose and H. Y. Gaisano, *J. Biol. Chem.*, 2003, **278**, 27556-27563.

280. O. Rossetto, L. Morbiato, P. Caccin, M. Rigoni and C. Montecucco, *J. Neurochem.*, 2006, **97**, 1534-1545.

281. N. G. Bazan, *Mol. Neurobiol.*, 2005, **32**, 89-103.

282. H. Y. Kim, L. Edsall, M. Garcia and H. Zhang, *Adv. Exp. Med. Biol.*, 1999, **447**, 75-85.

283. W. C. Chang, C. Nelson and A. B. Parekh, *Faseb J*, 2006, **20**, 2381-2383.

284. S. Prasarnpun, J. Walsh and J. B. Harris, *Neuropharmacology*, 2004, **47**, 304-314.

285. M. Rigoni, P. Caccin, S. Gschmeissner, G. Koster, A. D. Postle, O. Rossetto, G. Schiavo and C. Montecucco, *Science*, 2005, **310**, 1678-1680.

286. G. M. Lesa, M. Palfreyman, D. H. Hall, M. T. Clandinin, C. Rudolph, E. M. Jorgensen and G. Schiavo, *J. Cell Sci.*, 2003, **116**, 4965-4975.

287. E. Marza and G. M. Lesa, *Biochem. Soc. Trans.*, 2006, **34**, 77-80.

288. J. L. Watts, E. Phillips, K. R. Griffing and J. Browse, *Genetics*, 2003, **163**, 581-589.

289. C. Rickman and B. Davletov, *Chem. Biol.*, 2005, **12**, 545-553.

290. G. Barcelo-Coblijn, K. Kitajka, L. G. Puskas, E. Hogyes, A. Zvara, L. Hackler, Jr. and T. Farkas, *Biochim. Biophys. Acta*, 2003, **1632**, 72-79.

291. E. Connell, F. Darios, K. Broersen, N. Gatsby, S. Y. Peak-Chew, C. Rickman and B. Davletov, *EMBO Rep.*, 2007, **8**, 414-419.

292. C. E. Turner, MRes Final Report, Imperial College London, 2005.

293. J. Kreuter, *Colloidal Drug Delivery Systems*, CRC Press, New York, 1994.

294. A. Jesorka and O. Orwar, *Annu. Rev. Anal. Chem.*, 2008, **1**, 801-832.

295. M. I. Angelova and D. S. Dimitrov, *Mol. Crys. Liq. Crys.*, 1987, **152**, 89-104.

296. M. Angelova and D. Dimitrov, *Trends in Colloid and Interface Science II*, Springer Berlin / Heidelberg, 1988.

297. E. M. A. Pereira, D. F. S. Petri and A. M. Carmona-Ribeiro, *J. Phys. Chem. B*, 2002, **106**, 8762-8767.

298. D. J. Estes and M. Mayer, *Colloid Surf. B*, 2005, **42**, 115-123.

299. J. Henriksen, A. C. Rowat and J. H. Ipsen, *Eur. Biophys. J.*, 2004, **33**, 732-741.

300. J. R. Henriksen and J. H. Ipsen, *Eur. Phys. J. E*, 2004, **14**, 149-167.

301. M. D. Abramoff, P. J. Magelhaes and S. J. Ram, in *Biophotonics International*, Editon edn., 2004, vol. 11, pp. 36-42.

302. S. C. Costigan, P. J. Booth and R. H. Templer, *Biochim. Biophys. Acta*, 2000, **1468**, 41-54.

303. J. A. Killian, *Biochim. Biophys. Acta*, 1998, **1376**, 401-415.

304. S. H. Park and S. J. Opella, *J. Mol. Biol.*, 2005, **350**, 310-318.

305. J. Kyte and R. F. Doolittle, *J. Mol. Biol.*, 1982, **157**, 105-132.

306. W. Rawicz, K. C. Olbrich, T. McIntosh, D. Needham and E. Evans, *Biophys. J.*, 2000, **79**, 328-339.

307. F. Brochard and J. F. Lennon, *J. Phys.-Paris*, 1975, **36**, 1035-1047.

308. H. Engelhardt, H. P. Duwe and E. Sackmann, *J. Phys. Lett.-Paris* 1985, **46**, 395-400.

309. J. F. Faucon, M. D. Mitov, P. Méléard, I. Bivas and P. Bothorel, *J. Phys.-Paris*, 1989, **50**, 2389-2414.

310. A. Zilker, H. Engelhardt and E. Sackmann, *J. Phys.-Paris*, 1987, **48**, 2139-2151.

311. E. Evans and W. Rawicz, *Phys. Rev. Lett.*, 1997, **79**, 2379 LP - 2382.

312. G. J. Evans, A. Morgan and R. D. Burgoyne, *Traffic*, 2003, **4**, 653-659.

313. V. Heinrich and W. Rawicz, *Langmuir*, 2005, **21**, 1962-1971.

314. X. Mulet, PhD, Imperial College London, 2007.

315. A. F. Jakobsen, O. G. Mouritsen and M. Weiss, *J. Phys. Condens. Matter*, 2005, **17**, S4015-S4024.

316. K. Shinoda, W. Shinoda, T. Baba and M. Mikami, *The Journal of Chemical Physics*, 2004, **121**, 9648-9654.

317. S. D. Guler, D. D. Ghosh, J. Pan, J. C. Mathai, M. L. Zeidel, J. F. Nagle and S. Tristram-Nagle, *Chem. Phys. Lipids*, 2009, **106**, 33-44.

318. R. Dimova, S. Aranda, N. Bezlyepkina, V. Nikolov, K. A. Riske and R. Lipowsky, *J. Phys. Condens. Matter*, 2006, **18**, S1151-S1176.

319. C. E. Conn, O. Ces, X. Mulet, S. Finet, R. Winter, J. M. Seddon and R. H. Templer, *Phys. Rev. Lett.*, 2006, **96**, 108102-108104.

320. P. I. Hanson, J. E. Heuser and R. Jahn, *Curr. Opin. Neurobiol.*, 1997, **7**, 310-315.

321. K. Wiederhold and D. Fasshauer, *J. Biol. Chem.*, 2009, **284**, 13143-13152.

322. M. H. Abdulreda, *Integr. Biol.*, 2009, **1**, 301-310.

323. A. Valiakhmetov, *Biochem. (Moscow)*, 2008, **2**, 83-95.

324. R. Phillips, T. Ursell, P. Wiggins and P. Sens, *Nature*, 2009, **459**, 379-385.

325. X. Chen, D. Arac, T.-M. Wang, C. J. Gilpin, J. Zimmerberg and J. Rizo, *Biophys. J.*, 2006, **90**, 2062-2074.

326. A. Jeremic, M. Kelly, J. A. Cho, S. J. Cho, J. K. Horber and B. P. Jena, *Cell Biol. Int.*, 2004, **28**, 19-31.

327. J. R. Lakowicz, *Principles of Fluorescence Spectroscopy*, 3rd edn., Springer US, New York, 2006.

328. D. Hoekstra and N. Duzgunes, *Methods Enzymol*, 1993, **220**, 15-32.

329. N. Duzgunes, T. M. Allen, J. Fedor and D. Papahadjopoulos, *Biochem.*, 1987, **26**, 8435-8442.

330. N. Duzgunes and J. Wilschut, *Methods Enzymol*, 1993, **220**, 3-14.

331. D. Marsh, *Chem. Phys. Lipids*, 2006, **144**, 146-159.

332. Z. Chen and R. P. Rand, *Biophys. J.*, 1997, **73**, 267-276.

333. S. Leikin, M. M. Kozlov, N. L. Fuller and R. P. Rand, *Biophys. J.*, 1996, **71**, 2623-2632.

334. J. A. Szule, N. L. Fuller and R. P. Rand, *Biophys. J.*, 2002, **83**, 977-984.

335. D. Alford, H. Ellens and J. Bentz, *Biochem.*, 1994, **33**, 1977-1987.

336. P. Moreau, H. Juguelin, C. Cassagne and D. J. Morre, *FEBS Lett.*, 1992, **310**, 223-228.

337. M. Vidal and D. Hoekstra, *J. Biol. Chem.*, 1995, **270**, 17823-17829.

338. M. E. Haque, T. J. McIntosh and B. R. Lentz, *Biochem.*, 2001, **40**, 4340-4348.

339. B. G. Tenchov, R. C. MacDonald and D. P. Siegel, *Biophys. J.*, 2006, **91**, 2508-2516.

340. H. P. Duwe, J. Kaes and E. Sackmann, *J. Phys.-Paris*, 1990, **51**, 945-962.

341. J. Song and R. E. Waugh, *Biophys. J.*, 1993, **64**, 1967-1970.

342. P. Meleard, C. Gerbeaud, T. Pott, L. Fernandez-Puente, I. Bivas, M. D. Mitov, J. Dufourcq and P. Bothorel, *Biophys. J.*, 1997, **72**, 2616-2629.

343. E. Endress, S. Bayerl, K. Prechtel, C. Maier, R. Merkel and T. M. Bayerl, *Langmuir*, 2002, **18**, 3293-3299.

344. C. Hofsäß, E. Lindahl and O. Edholm, *Biophys. J.*, 2003, **84**, 2192-2206.

345. E. Evans and W. Rawicz, *Phys. Rev. Lett.*, 1990, **64**, 2094-2097.

346. J. Pan, T. T. Mills, S. Tristram-Nagle and J. F. Nagle, *Phys. Rev. Lett.*, 2008, **100**, 198103-198104.

347. W. Rawicz, B. A. Smith, T. J. McIntosh, S. A. Simon and E. Evans, *Biophys. J.*, 2008, **94**, 4725-4736.

348. F. Parlati, T. Weber, J. A. McNew, B. Westermann, T. H. Sollner and J. E. Rothman, *Proc. Natl. Acad. Sci. U. S. A.*, 1999, **96**, 12565-12570.

349. M. Fix, T. J. Melia, J. K. Jaiswal, J. Z. Rappoport, D. You, T. H. Sollner, J. E. Rothman and S. M. Simon, *Proc. Natl. Acad. Sci. U. S. A.*, 2004, **101**, 7311-7316.

350. C. G. Schuette, K. Hatsuzawa, M. Margittai, A. Stein, D. Riedel, P. Kuster, M. Konig, C. Seidel and R. Jahn, *Proc. Natl. Acad. Sci. U. S. A.*, 2004, **101**, 2858-2863.

351. J. A. McNew, T. Weber, F. Parlati, R. J. Johnston, T. J. Melia, T. H. Sollner and J. E. Rothman, *J. Cell Biol.*, 2000, **150**, 105-117.

352. F. Benfenati, P. Greengard and J. Brunner, *J. Cell Biol.*, 1989, **108**, 1851-1862.